Detailed Core and Log Analysis of a Producing Viola Dolomite Well in Comanche County, Kansas

by

William Kitchell Hagood, Jr.

B.S., University of Louisiana at Lafayette, 2013

A THESIS

submitted in partial fulfillment of the requirements for the degree

MASTER OF SCIENCE

Department of Geology
College of Arts and Sciences

KANSAS STATE UNIVERSITY
Manhattan, Kansas

2019

Approved by:

Major Professor
Dr. Matthew Totten

Copyright

Abstract

The Ordovician-aged Viola Limestone of southwestern Kansas is a developing carbonate resource play with significant accumulations of hydrocarbons. The Viola surface is an unconformity, and production comes from regions of preserved dolomite on paleo-topographic highs. Evaluation of a cored interval of the upper Viola recognized several distinct facies, which were examined in conjunction with detailed well log analysis and X-Ray Fluorescence analysis to recognize facies control on Viola production. Five major facies were determined by petrographic analysis and core examination, labeled cherty dolomite, intraclastic breccia, intraclastic rudstone, bioclastic grainstone, and muddy dolostone. The depositional environments of the facies were interpreted to be a shallow marine environment, ranging from low to high energy, with the cherty dolomite and muddy dolostone facies being classified as low energy, and intraclastic breccia, intraclastic rudstone, and bioclastic grainstone facies classified as high energy. The Viola formation has been divided into zones, based on well log signatures and are named the "A", "B", and "C" zones. The cherty dolomite is the only observed reservoir quality facies in the core, due to the "A" zone not being recovered from coring and comprises the majority of the "B" zone. The cherty dolomite has density porosity (DPHI) values up to 34% and only appears once in the cored section, with a thickness of roughly 8ft (2.4m). The "A" and "B" zones are the chief producers of the Viola Limestone in south-central Kansas. In the core of the study well, from Rich C #7 of the Herd field in Comanche County, Kansas, the "B" zone is capped by alternating thin beds of rudstone and breccia petrofacies, along with a thin layer of breccia near the bottom of the "B" zone. Muddy dolostone with thin layers of rudstone mainly comprise the area between the "B" and "C" zone and below the "C" zone. The "C" zone well log facies is non-productive, and consists mainly of muddy dolostone, with a thin layer of rudstone marking the top of the zone in the Rich C #7 core. An almost two-foot-thick layer of rudstone is located a couple feet below the top of the "C" zone. Wire-line log signatures differentiated the "A", "B", and "C" zones and cherty dolomite facies in Rich C #7 and correlate easily with other Viola-producing wells in south-central Kansas, like Herd 1. The productive well log facies can be identified from neutron porosity (NPHI), DPHI, and sonic log (DT) signatures and are discriminated by cross plots of NPHI, DPHI, and DT. The chemical data from the handheld XRF machine was able to partly discriminate well log facies and some described facies using specific elemental signatures and ratios. All of the well log facies and the cherty dolomite, rudstone, and muddy dolostone petrofacies were discriminated from plotting Si versus Al, Si/Al versus Ti, Si/Al versus Zr. The Zr vs Ti cross plot was only able to discriminate the "B" zone and cherty dolomite petrofacies. P-Wave velocity measurements exhibited correlations to the NPHI, DPHI, and sonic log values of Rich C #7. The "B" zone correlates exactly with the P-Wave velocities, with the cherty dolomite facies being discriminated by the velocities. This study illustrates the advantages of correlating depositional facies with reservoir quality and linking specific reservoir petrofacies with well log signatures, ultimately to create a greater understanding of the controls on reservoir quality to aid in predicting new areas of exploration.

Table of Contents

List of Figures

List of Tables

Acknowledgements

Foremost, I would like to thank my thesis advisor, Dr. Matthew Totten and my committee members, Dr. Abdelmoneam Raef and Dr. Saugata Datta for their guidance during my time at Kansas State University and throughout my graduate research. They were readily willing to give me assistance when needed to complete this research. I would like to thank Dr. Karin Goldberg for her assistance with my thesis, and I would also like to thank Dr. Pamela Kempton for her generous support during my graduate career.

I would like to thank Kansas Geological Society for allowing me to borrow multiple sets of cores from their core library in Lawrence, Kansas for research. The KGS was very flexible with keeping, picking up, and returning cores, which helped make this research go smoother.

I would also like to thank the Kansas Geological Foundation for their generous research grant. This helped tremendously with keeping my research expenses down to a minimum.

Finally, I would like to give a special thanks to my family for all their support during my academic career. Their guidance and support throughout my life helped in finishing my education.

Dedication

I would like to dedicate this thesis to my family, for supporting my goals and endeavors in life and academia.

Chapter 1 - Introduction

1.1 Introduction

Shallow epicontinental seas covered most of Kansas during the Ordovician period (Figure 1.1). This resulted in a sequence of shallow-marine limestones, dolomites, and cherty dolomites that comprise the Viola Formation (Bornemann et al., 1982). The Viola Formation has developed into a modern oil and gas play containing numerous hydrocarbon reservoirs. The dolomite zones in the upper Viola are ideal reservoir rocks, unlike most of the limestone in the Viola, which does not typically produce (Richardson, 2013).

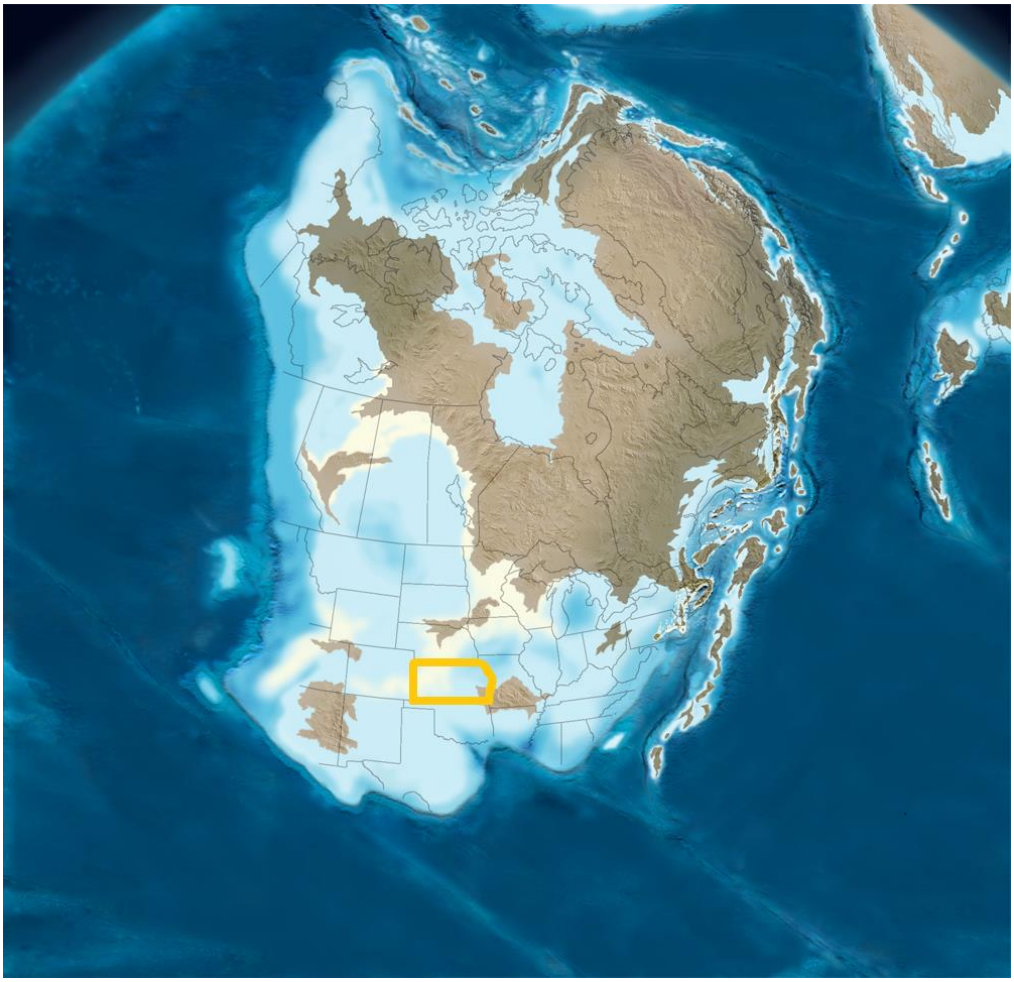

Figure 1.1: Paleogeographic reconstruction of the Middle Ordovician, illustrating the inundation of Kansas (Blakey, 2016).

There is an important erosional unconformity between the Viola and the overlying Maqouketa/Kinderhook section (Adkison, 1972). Areas where the Maqouketa is thinnest typically have the thicker dolomitic sections of Viola beneath, which have the potential to produce hydrocarbons (Richardson, 2013). It is not known whether the hiatus between the Middle Ordovician when the Viola formation was deposited, and the Late Ordovician, when the Maquoketa shale was deposited, was primarily due to a period of non-deposition or erosion (Zeller, 1968). Significant erosion did occur, resulting in paleo-topographic high areas of the Viola which can trap significant amounts of hydrocarbons in southwestern Kansas (Richardson, 2013). For example, the Herd Viola trend in Comanche county (where one of the wells in this study is located) has produced over 1.1 million barrels of oil (MMBO) along with over 3.2 billion cubic feet of gas (BCFG) from the Viola, Mississippian, and Marmaton (Richardson, 2013; KGS, 2018).

1.2 Geologic Setting

The Midcontinent region was prone to periodic flooding from epicontinental seaways during the Paleozoic and Mesozoic eras, due to its relatively flat low-relief topography (Harries, 2009). Transgressing and regressing epeiric seas reoccurred in the Midcontinent region throughout, leaving behind carbonate sediment deposits during times of high eustatic sea levels, and exposed topography during the lowest sea levels (Harries, 2009). An epeiric sea inundated most of North America during the Middle Ordovician (Figure 1.2). The Viola Limestone was possibly deposited during the high stand of this sea as a basal limestone along the paleoshoreline (Bornemann et al., 1982).

Much of the Viola Limestone was initially deposited in a relatively static, flat environment, but nearby geologic provinces such as the Pratt Anticline, underwent periods of repeated uplift and faulting. These tectonics, in combination with global sea level changes, could explain the hiatus between the Viola and the overlying Maquoketa formation **(**Merriam, 1963; Zeller**,** 1968). During the Ordovician, the Pratt Anticline in southcentral Kansas was overlain by deposits of Viola sediment (Figure 1.3), indicating the present-day region of the Pratt Anticline was a submarine environment at one time (Bornemann et al., 1982). Lithologic evidence from the geologic region of the Pratt Anticline indicates it existed as a submerged high during the latter part of the deposition of the Viola in the Middle Ordovician (Bornemann et al., 1982). The Viola Limestone in the south-central Kansas region was significantly affected by an additional tectonic event, uplift of the Central Kansas Arch, during the Middle Ordovician to the Middle Pennsylvanian. This event affected Viola deposition by restricting marine circulation. The uplift of these Viola sediments was subjected to extensive dolomitization from meteoric diagenesis in the mixed marine zone (Bornemann et al., 1982).

It is important to note that the Viola formation in southwestern Kansas has gone through periods of sea level changes and erosion, and its surface is an unconformity, with the overlying Late Ordovician-aged Maquoketa Shale/Early Mississippian-aged Kinderhook Shale section (Bornemann et al., 1982; Richardson, 2013) (Figure 1.4). With a non-porous formation overlying the unconformable surface of the Middle Ordovician-aged Viola formation, it is possible for paleotopographic traps to have formed in the preserved erosional high surfaces of the Viola dolomite, which can accumulate hydrocarbons in these porous dolomite (Figure 1.5). The paleotopographic traps of the Viola dolomite have been located where the overlying Maquoketa section is thinner (Richardson, 2013).

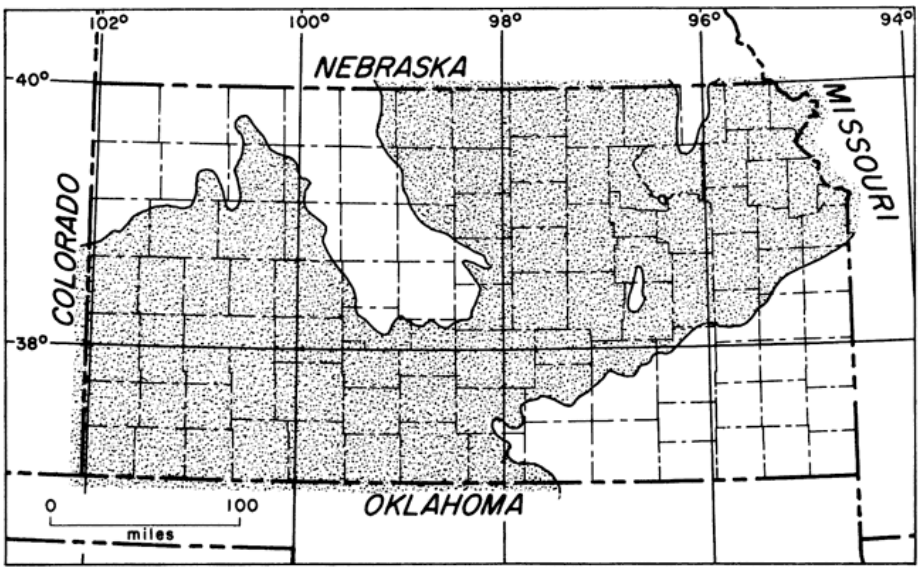

Figure 1.2: Geologic map displaying the lateral extension of the Viola Limestone across Kansas (KGS, 1963).

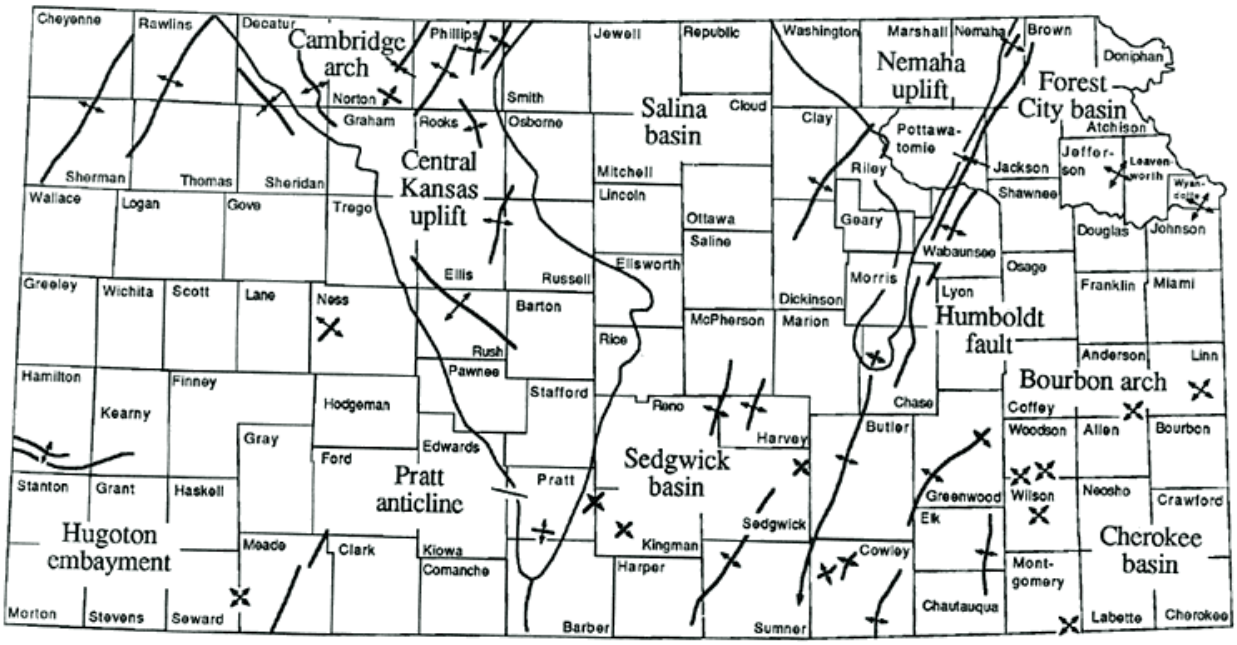

Figure 1.3: Map displaying the prominent structural features of Kansas (Newell et al., 1987).

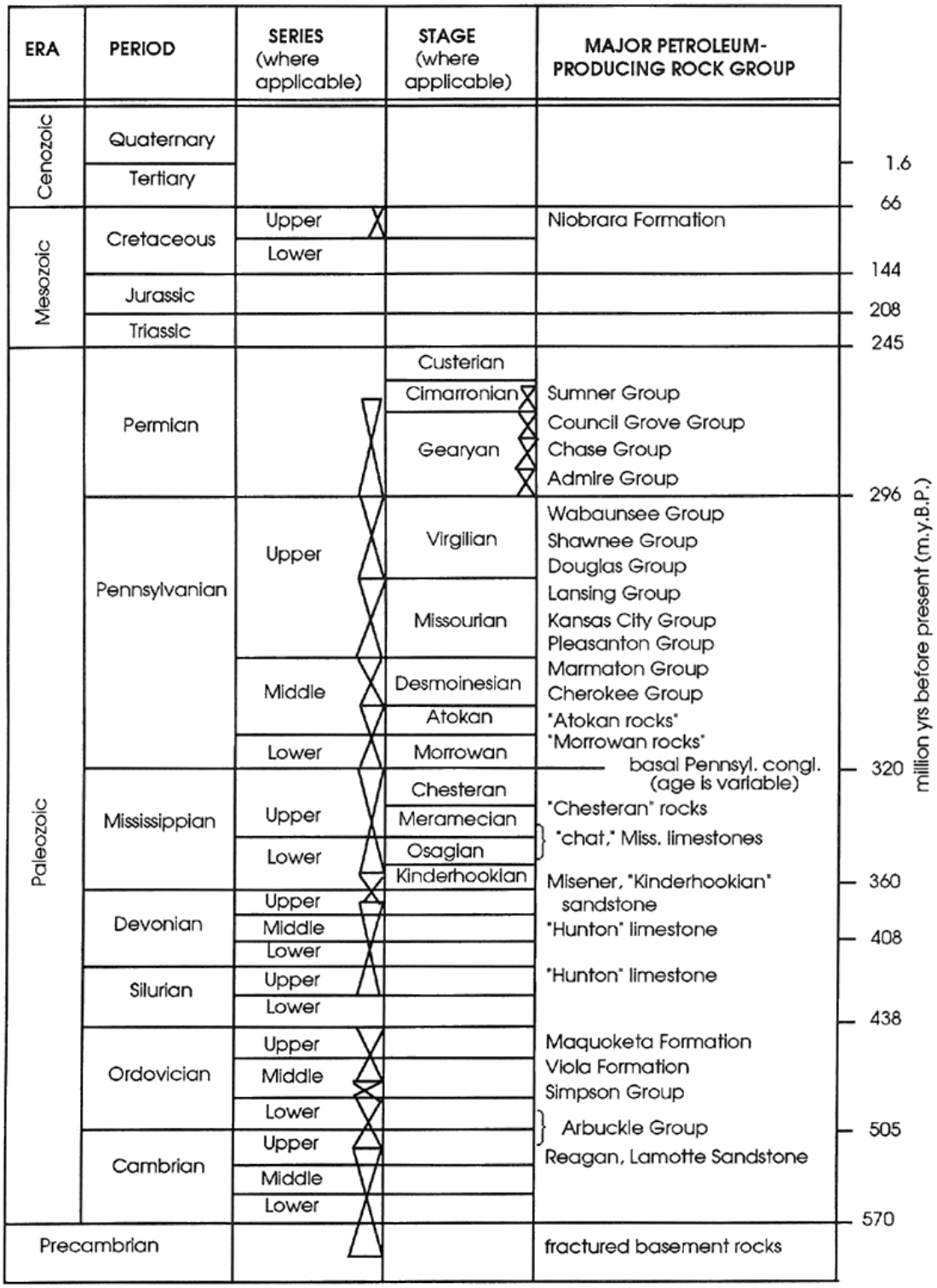

Figure 1.4: Geologic timetable showing various producing formations in Kansas (Newell et al., 1987).

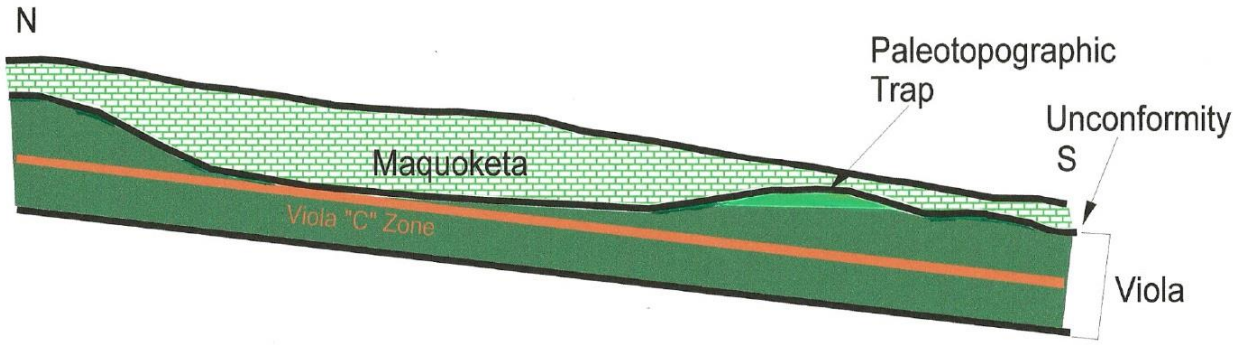

Figure 1.5: Illustration of the unconformity present between the Viola formation and Maquoketa shale. The overlying Maquoketa shale sealing the top of the Viola formation resulted in a paleotopographic trap being formed (Richardson, 2013).

1.3 Study Area

The focus of research is the Middle Ordovician (470-440 My) Viola Limestone Formation. The study area is the Herd Field of Comanche County (Figure 1.6). The Rich C #7 well is the only well in Comanche and Clark Counties where significant core (60 feet) through most of the upper Viola was retrieved. Several additional earlier drilled wells report core from the Viola, but these were found to be misidentified as Viola, and actually were from the lowermost Maquoketa. The Herd field in Comanche county lies between the Hugoton Embayment to the west and the Central Kansas Uplift and Pratt anticline to the east (Figure 1.7).

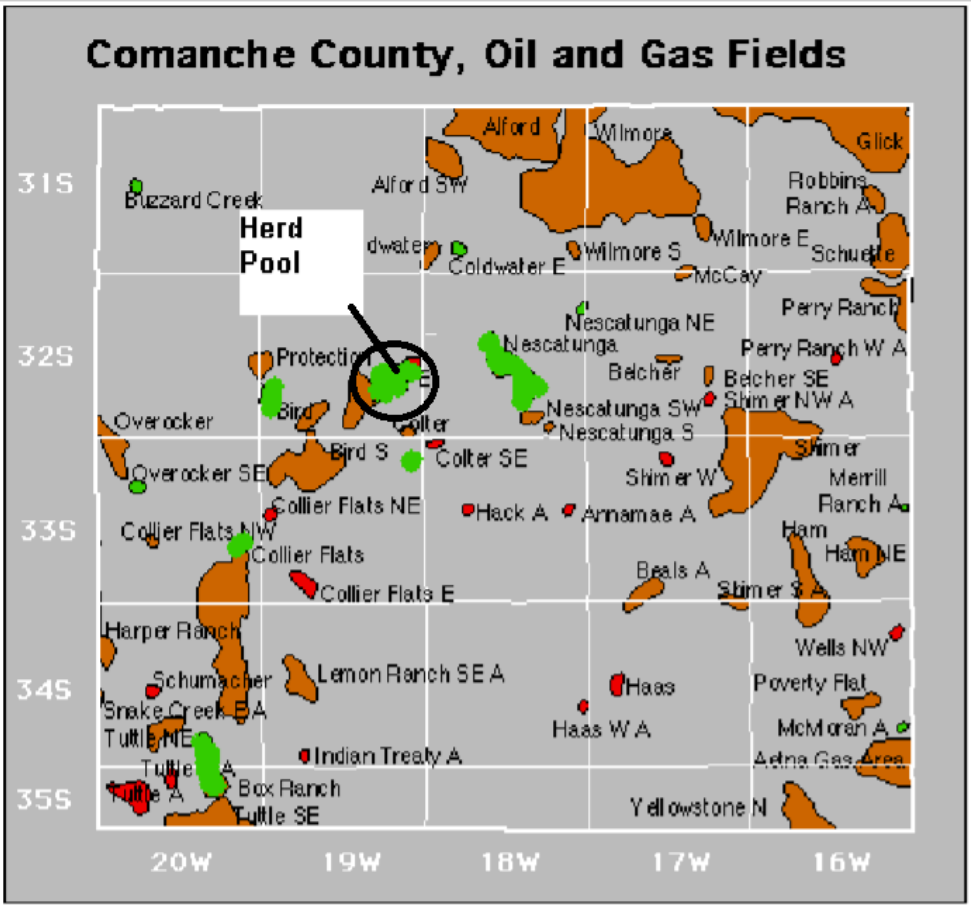

Figure 1.6: Location of the Herd field (circled) where the study well, Rich C #7, is located (Richardson, 2013).

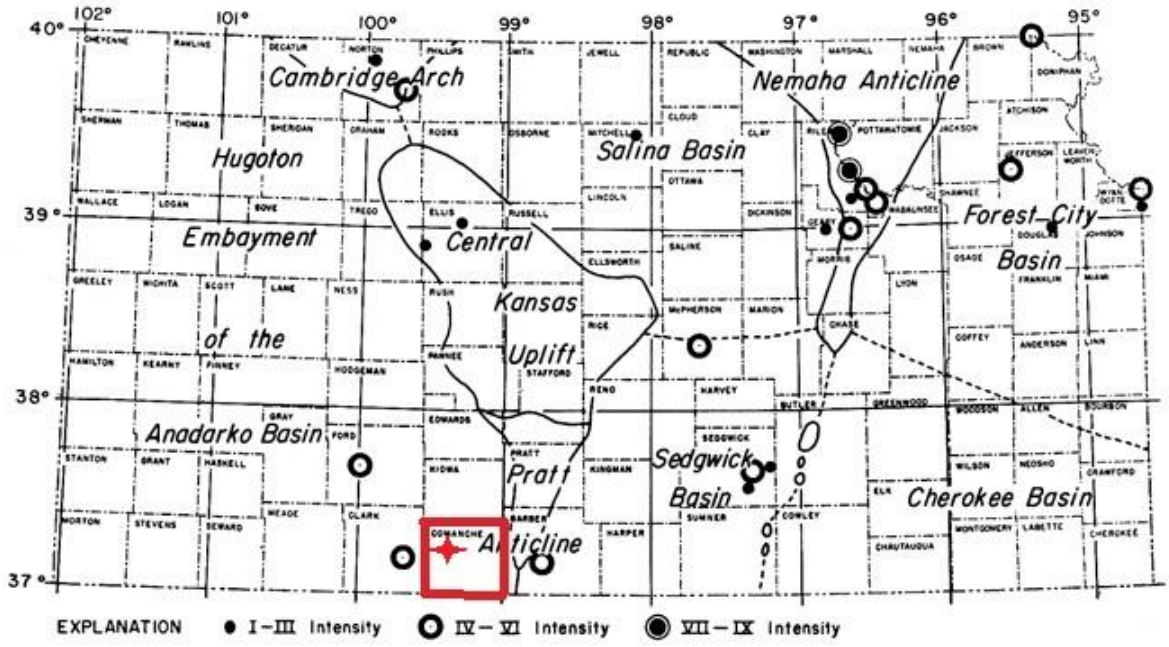

Figure 1.7: Location of the study area (red star) in Comanche county (outlined in red) (Merriam, 1963).

1.4 Viola Production in South-central Kansas

The Viola production of the Herd field where the study core from Rich C #7 was drilled totals 1.16 MMBO and 3.2 BCFG (KGS, 2018). Rich C #7, located at S22-T32S-R19W (Table 1.1), has produced over 360,000 barrels of oil (BO) (KGS, 2018). Oil accounts for the majority of production, but oil and gas can both be produced on the Pratt anticline (Newell et al., 1987). The Upper Viola Formation can trap hydrocarbon accumulations in dolomitic reservoirs that were paleotopographic highs preserved during the erosional event before deposition of the Maquoketa shale (Richardson, 2013). The Upper Viola has been categorized into different zones for this region. They are commonly labeled the "A", "B", and "C" zones, as seen in log cross-section (Figure 1.8). Production typically does not happen below the "C" zone, due to the lack of porous dolomite (Richardson, 2013). The zones are not all present throughout this region, most likely due to variation in erosion, as seen in log cross-section (Figure 1.9). A map displaying

both cross-section lines can be seen, below (Figure 1.10). Rich C #7 was perforated at 5807'-5811' in the "A" zone and at 5819'-5822' in the "B" zone, while another productive well in the same field, Herd 1, was perforated at 5806'-5811' in the "A" zone. Older wells targeted the Mississippian, above the Viola formation, and typically stopped drilling short of the oil/water contact in the Mississippian. Utilizing new exploration techniques and re-evaluating older wells could provide an efficient way to exploit the Viola Limestone.

Location	API#	Well Name	County	Field Name	Type-Status	KB	Cored Interval in Viola LS (ft)			Perf. Intvl.
							Top	Btm	Total	
S22-T32S-R19W	15-033-21305	Rich C#7	Comanche	Herd	O&G-Producing	1,992	5,808	5,868	60	5807-5811 5819-5822

Table 1.1: Information on the Rich C #7 study well (KGS, 2019).

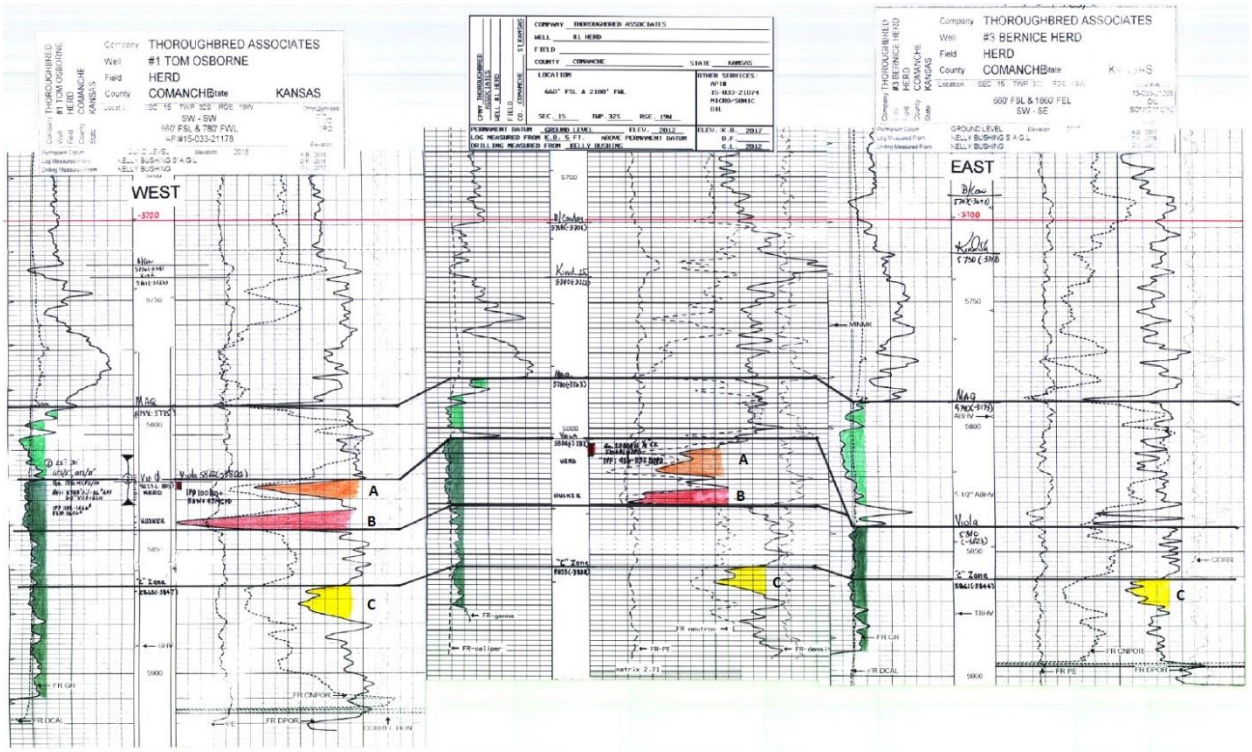

Figure 1.8: A well log correlation, going eastward from left to right, of the "A", "B", and "C" zones of the Upper Viola in the Herd field in Comanche county. The Tom Osborne 1 well is on the left, Herd 1 in the middle, and the Bernice Herd 3 well is on the right. The zones are colored inside the solid-black density curve. The "A" zone is colored orange, "B" is red, and "C" is yellow. The "A" and "B" zone is not present in the Bernice Herd 3 well. Note the density and neutron porosity signatures of the zones (Richardson, 2013).

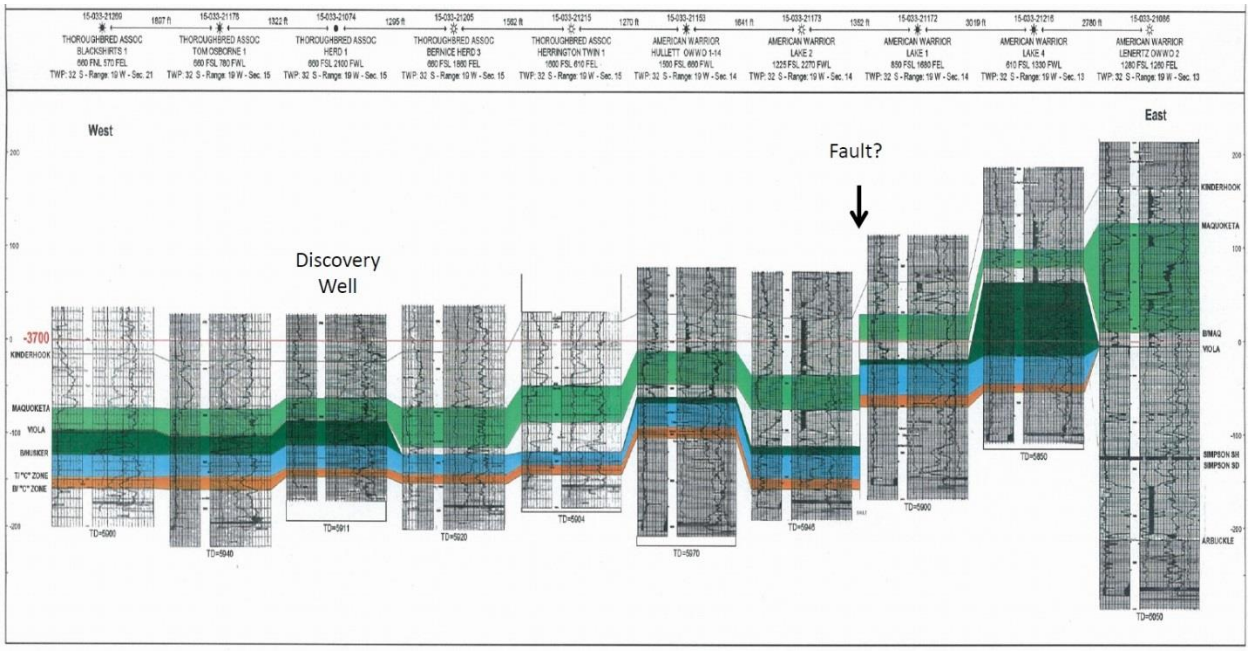

Figure 1.9: A well log correlation of the overlying Maquoketa, "A", "B", and "C" zones of the Upper Viola going west to east across the Herd Field, Comanche County. The signature zones are not present in all the wells, most likely due to variation in erosion (Richardson, 2013).

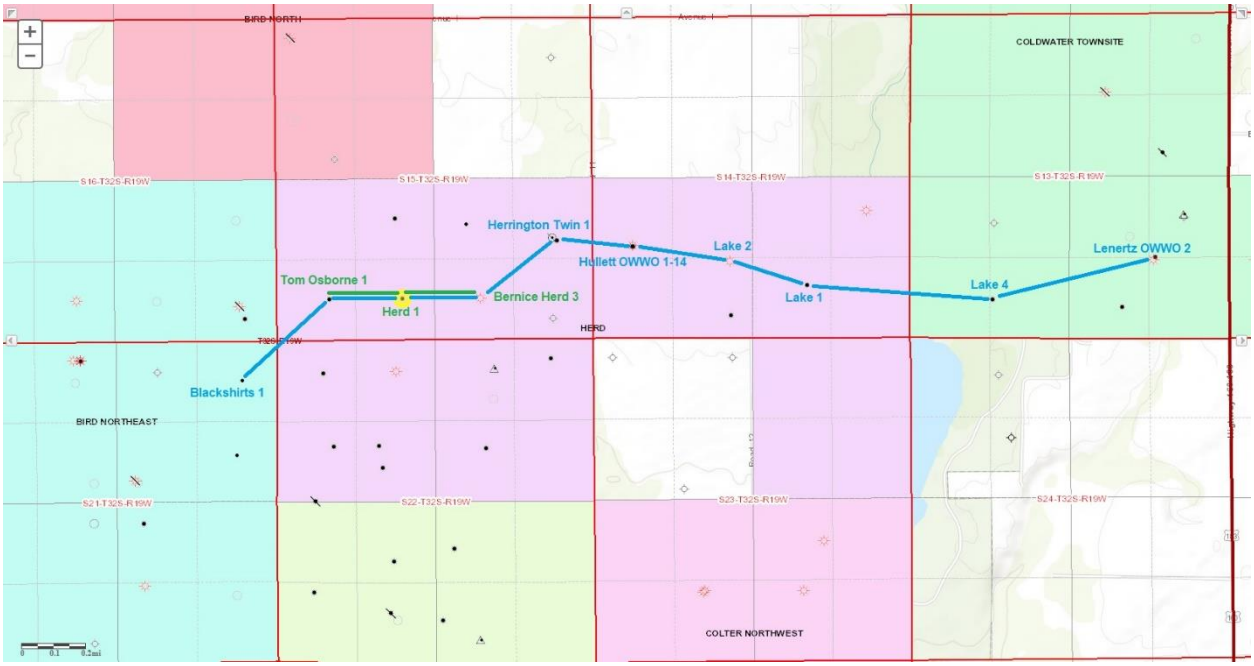

Figure 1.10: A map displaying the cross-section lines, from above. The green line displays the cross-section from Figure 1.8, and the blue line displays the cross-section from Figure 1.9 (KGS, 2019).

1.5 Lithofacies of the Viola in Clark and Comanche Counties

Detailed analyses of slabbed Viola core and thin sections were made from wells in Barber and Pratt counties to study the petrography, lithofacies, and diagenetic processes in the Viola Limestone (St. Clair, 1985). A generalized stratigraphic section of the Viola formation was made (Figure 1.11), along with unit names. Wireline log analysis recognized two basic end-member facies, consisting of a low-porosity limestone of crinoidal packstones and grainstones, and a moderately porous cherty dolomitic limestone representing dolomitized wackestones and mudstones. Fourier analysis of log-derived mineralogy suggests that facies migration was cyclic, influenced by eustatic or tectonic processes (Bornemann et al., 1982).

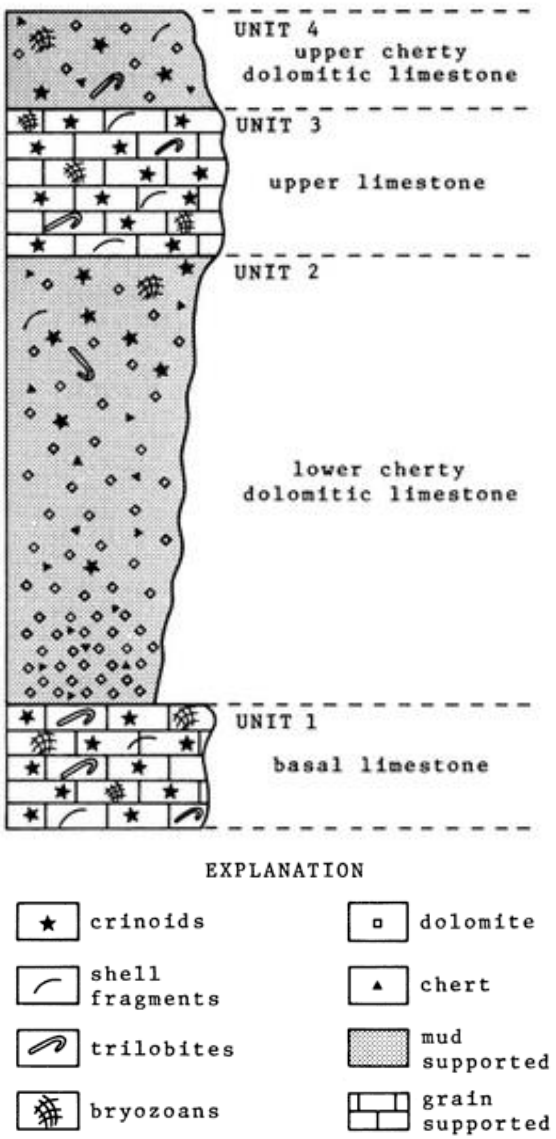

Figure 1.11: The four facies within the stratigraphic section of the Viola Limestone in south-central Kansas exhibit a cyclic pattern (St. Clair, 1985).

Structural control is important for hydrocarbon production, but in the case of the Viola formation, preservation of the upper Viola which contains productive dolomite porosity is key. Preserved sections of porous dolomite lie underneath an erosional unconformity between the Viola formation and the overlying Maquoketa/Kinderhook section as paleotopographic traps (Richardson, 2013). These producing paleotopgraphic traps typically have well log signatures

and are divided into the well log facies named the “A”, “B”, and “C” zones. Production typically does not happen below the “C” zone, due to the lack of porous dolomite, and the zones are not all present throughout this region, most likely due to erosion (Richardson, 2013). Cuttings from the Stephens Ranch lease in Clark County, Kansas, were analyzed in a previous study to determine the control for ideal Viola formation reservoir conditions. The best reservoir conditions did not coincide with structural position but were dependent on the dolomitization processes occurring between the adjacent “A” and “B” zones, combined with preferential erosion at the time of the uppermost Viola unconformity (Linares, 2016). A 3D seismic attribute analysis determined the same producing wells with a preserved “A” zone facies in the Stephens Ranch lease are represented as diagnostic thin beds with anomalously low amplitude tuning effects. In contrast, the non-producing Stephens Ranch wells correlate to an increase in the normalized amplitude and diminished instantaneous frequency. These applied 3D attributes have been able to delineate stratigraphic heterogeneities and define the limits of where the top dolomitized “A” or “B” zone facies in the Viola limestone is the most productive (Vohs, 2016). Ultrasonic velocity measurements were taken from the cored section of Rich C #7 in Comanche County, Kansas, to investigate if whether elastic properties can correlate to the Viola formation well log facies and described facies. P-wave velocities correlated with productive well log facies and one of the described productive facies. Elastic properties discriminate each zone respectfully, indicating changes in lithology and porosity (Hagood et al, 2018).

1.6 Objectives

The objectives of this research include the following:

1. Refine the lithofacies distribution within the Rich C #7 core

2. Determine what the environmental setting was during deposition of the Upper Viola in this region
3. Correlate well log signatures with each respective lithofacies to determine whether wire-line logs can discriminate zones of differing reservoir quality.
4. Correlate hand-held X-ray fluorescence data taken from intact core with each respective facies to determine whether X-ray fluorescence can discriminate zones of differing reservoir quality or indicate relationships in environment of deposition.

Chapter 2 - Methods

The methods employed for this study included: 1) core analysis, 2) Hand-held X-ray fluorescence (HHXRF) analysis, 3) petrographic analysis, 4) Scanning Electron Microscopy (SEM) analysis, and 5) well log analysis with Petrel and Petra software.

2.1 Core Analysis

The Rich C #7 well in Comanche County was chosen based on it being the only cored well through the Viola formation in southwestern and south-central Kansas with modern gamma ray and neutron/density logs. A lithological log was constructed for the core, bearing the detailed facies description. Different lithofacies were grouped into facies associations to interpret their depositional environments. Core description guided sampling for textural and compositional changes that ultimately were noted, cut into billets, made into thin sections, and analyzed under the petrographic microscope. The entirety of the core was photographed, along with the thin section billets and core pieces where they originated.

2.2 X-Ray Fluorescence Analysis

The Rich C #7 core was examined with a handheld Bruker X-Ray Fluorescence (HHXRF) in attempt to relate chemical data with log data and described lithofacies. The XRF releases high-energy X-rays that penetrate the core, which will excite the atoms and displace the electrons within the atomic orbital (Bruker, 2015). Characteristic X-rays are released as the atoms relax to ground state. These characteristic X-rays are produced in proportion to the abundance of each element, and when compared to a known standard may be converted to elemental concentration (Bruker, 2015). The Bruker handheld XRF recorded values for the following major elements: magnesium (Mg), aluminum (Al), silicon (Si), phosphorous (P), sulfur (S), potassium (K), calcium (Ca), titanium (Ti), manganese (Mn), iron (Fe), and also

recorded values for the following trace elements: cobalt (Co), nickel (Ni), copper (Cu), zinc (Zn), gallium (Ga), arsenic (As), lead (Pb), thorium (Th), rubidium (Rb), uranium (U), strontium (Sr), yttrium (Y), zirconium (Zr), niobium (Nb), and molybdenum (Mo).

The core from the Rich C #7 well was examined with the HHXRF device while laid out on a table (Figure 2.1). Readings were taken across regular intervals of two inches for major elements and six inches for trace elements. Major elements were examined on power settings 15kV and 25μA with an analysis time of 180 seconds per sample, and trace elements were examined on power settings 40kV and 1.2 μA with an analysis time of 120 seconds per sample. Readings from a metallic standard, Bruker Duplex 2205, and a shale standard, RTC-W-220, were taken regular intervals of once per day for the metallic standard, and every 15-20 samples for the shale standard. This was done to observe potential drift of the HHXRF readings, for evaluating the data precision (Table 2.1). Based on the drift values, the precision of the HHXRF readings is acceptable. The HHXRF data was used to develop an elemental log of the Rich C #7 core. Measurements were made from the top to bottom by measuring from depth markers written on the core, to verify the depths on the core box labels.

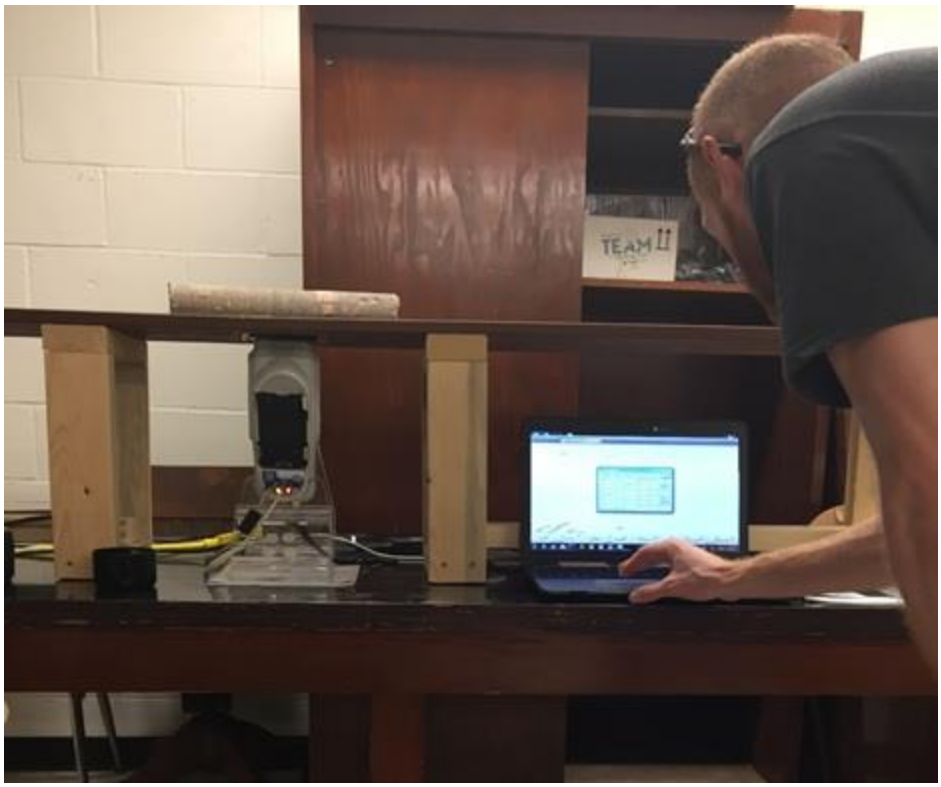

Figure 2.1: The setup that was used for the XRF analysis. The core sits on top of the table and over the handheld XRF machine.

Major	AVG	STD		Trace	AVG	STD
Mg	0.9	0.1		**Co**	14.53	1.26
Al	5.2	0.1		**Ni**	144.55	2.39
Si	31.5	0.6		**Cu**	114.01	2.30
P	0.1	0.0		**Zn**	815.25	14.79
S	2.4	0.1		**Ga**	17.05	0.88
K	2.4	0.0		**As**	21.44	1.53
Ca	0.1	0.0		**Pb**	17.65	0.47
Ti	0.3	0.0		**Th**	11.16	0.15
Mn	0.0	0.0		**Rb**	133.78	2.85

Fe	2.7	0.0		**U**	18.56	3.04
				Sr	63.10	5.52
				Y	32.57	0.93
				Zr	113.05	1.08
				Nb	12.302	0.41
				Mo	73.79	3.44

Table 2.1: Table of major elemental and trace elemental values taken from the RTC-W-220 shale standard. Based on the standard deviations of the drift values, the precision of readings is acceptable.

2.3 Petrographic Analysis

Thin section sample locations were selected from the following criteria: 1) distinct color changes, 2) changes in grain size, roundness, and degree of sorting, 3) changes in fossil material (high or low concentrations), 4) distinct variations in the wire-line log signatures, and 5) distinct variations or anomalies in the XRF chemical signatures. The thin sections had been attempted to be impregnated with blue epoxy, to aid in estimating the visible porosity of the thin section, but the vast majority of the thin sections failed to be impregnated. The majority of the thin sections were not dyed with alizarin red S, which helps differentiate carbonate mineralogy, due to the potential to compromise the elemental signature data from the Energy-dispersive X-ray spectroscopy (EDS) instrument inside the Scanning Electron Microscope (SEM). The thin sections were not covered, to allow them to be further analyzed with SEM.

Each thin section was examined using a petrographic microscope to describe the sample, which then modified the original description of the core. The thin sections were classified according to depositional texture and followed the Dunham (Figure 2.2) and Modified Dunham's

classification scheme (Figure 2.3). Thin sections were examined to aid in determining the depositional environments, fossil identification, and diagenetic processes that may influence reservoir quality.

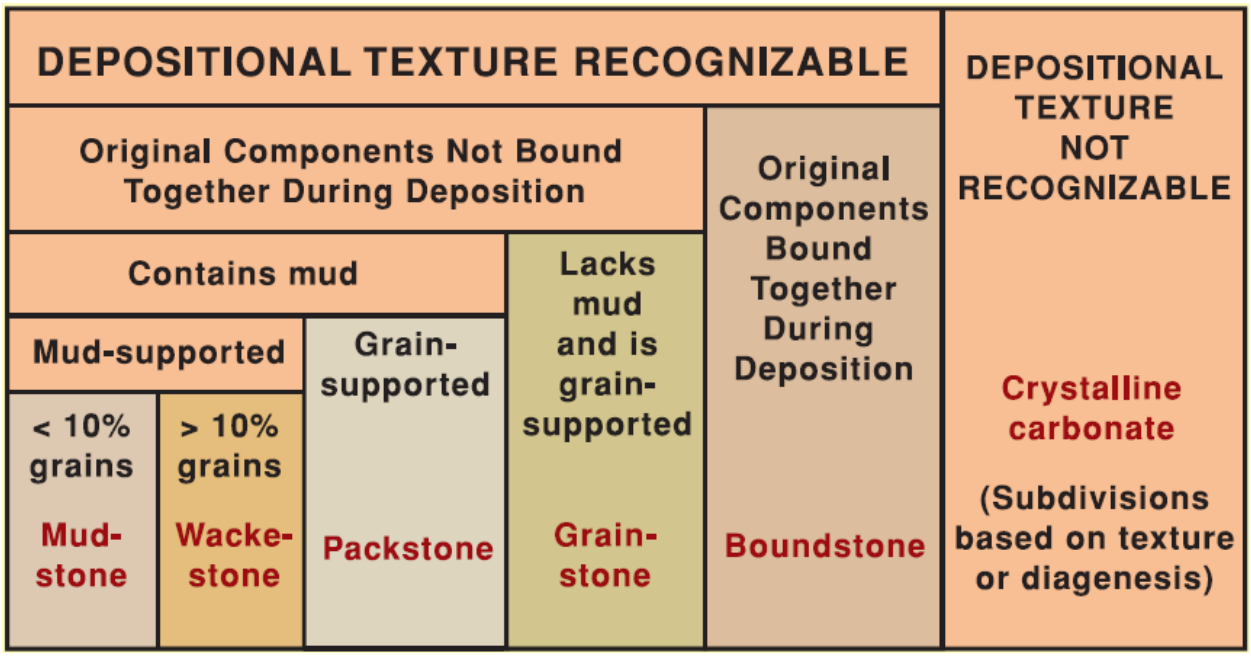

Figure 2.2: Dunham's classification scheme for carbonate rocks (Scholle, 2003).

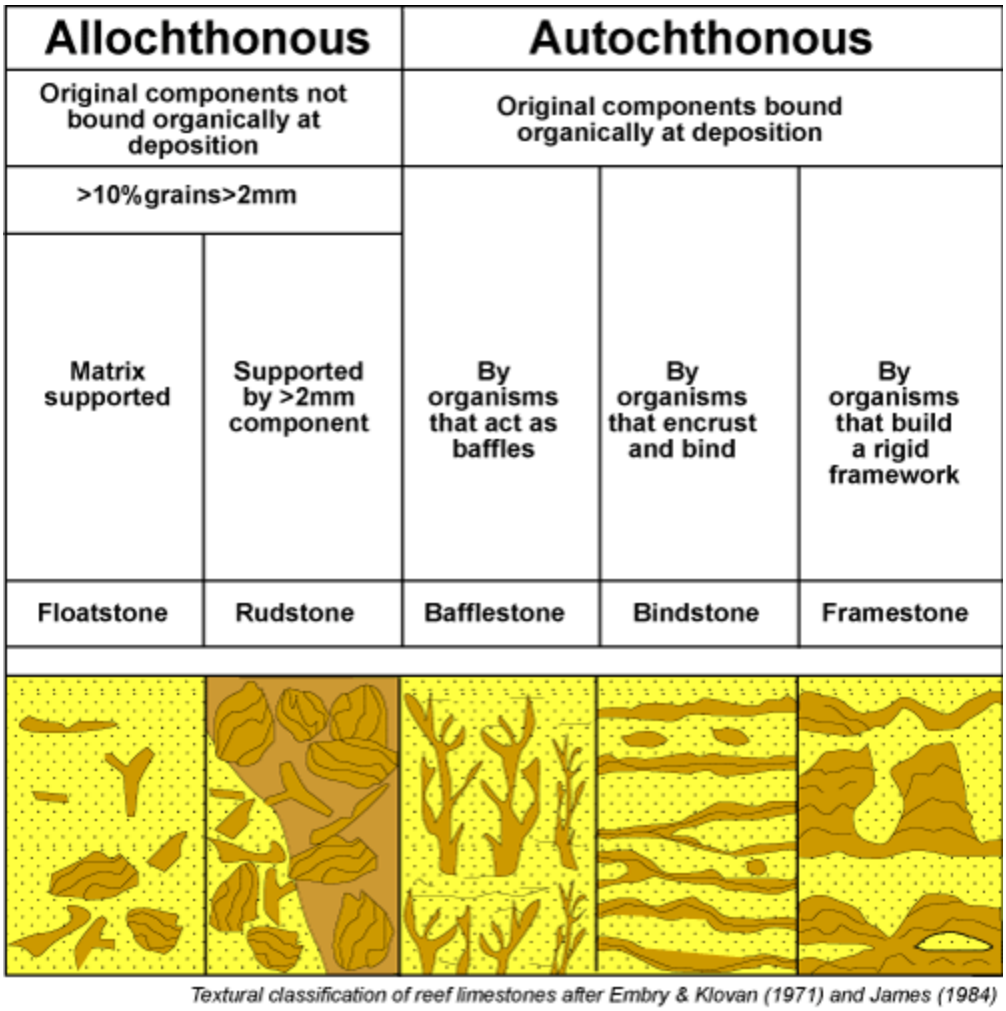

Figure 2.3: Modification of Dunham's classification scheme by Embry and Klovan (1971) and James (1984).

2.4 Scanning Electron Microscopy Analysis

A subset of seven polished thin sections was selected for Scanning Electron Microscopy (SEM) analysis based up the following criteria: 1) well log facies of thin section, 2) depositional facies of thin section, 3) DPHI/NPHI log signatures, and 4) variety of dolomitic crystal sizes and shapes contained within thin section. The polished thin sections were taken to the University of Kansas' Microscopy and Analytical Imaging Laboratory to be examined with the SEM and Energy Dispersive X-ray Spectroscopy (EDS). Each thin section was then analyzed using the

facility's FEI Versa 3D Dual Beam machine. For SEM imaging, a HiVac detector, Everhard-Thornley detector was used, and the EDS attachment was used to produce an elemental map of a selected portion of the thin section. Only seven representative thin sections were imaged due to the high cost of operating the FEI Versa 3D Dual Beam. SEM allows for the imaging of rock cements, texture, and distribution of the pore space, to determine paragenetic relations which will aid in evaluating diagenetic effects (Cone and Kersey, 1992). EDS analysis will produce an elemental map which may aid in identifying specific facies and interpreting diagenetic relations.

In order for the Dual Beam to penetrate the thin section slide, a spraying machine was used to coat the majority of the selected slides with conductive material. The thin sections were sprayed with a 10 nm-thick conductive coating of gold to prevent charging during electron bombardment of the sample, yielding higher-order quantitative results. After the thin sections were coated with the conductive gold material, one thin section at a time was loaded, with nitrile gloves, into the Dual Beam sample chamber and evacuated to 5 mbar. The Dual Beam operates on the xT Microscope Server Software. Once the software was operational, the chamber had to be closed for the vent process to initiate. When the vent procedure was confirmed to be finished, the thin section was centered on a highly precise stage to ensure fixed beam penetration. After the slide was loaded, the chamber was closed, and pump was turned on to produce a vacuum inside the chamber. Once the chamber had become a vacuum, an image of the thin section was displayed, which was modified by adjusting beam focus and alignment to improve image resolution. After the desired image was acquired, the EDS detector was activated. The EDS then focused a beam of electrons that bombarded the thin section to produce a series of X-Rays. These X-Rays emit characteristically high-energy particles from the sample, which yield

diagnostic elemental peaks. The Aztec software was then used to view the elemental peaks, which were displayed as elemental maps of the selected image from the thin section.

2.5 Well Log Analysis

Once the depositional and diagenetic facies were determined, well logs were used to relate reservoir quality with well log facies, interpreted facies, and correlations to the Herd 1 well in the Herd field of Comanche, County. Depositional facies as determined during petrographic examination were attempted to be correlated to specific log signatures. These well log signatures were attempted to be correlated to data found in this study from core description, petrography, and XRF analysis. This could potentially expand the facies distribution beyond the area of core availability and would be helpful when exploring new areas or re-evaluating old areas where only well log data is available. Petrel and Excel were used to make cross plots to discriminate sequences, and Petra was used to correlate well log signatures and well log facies to interpreted facies.

In the Rich C #7 logs, there is a four-foot discrepancy between the reported total depths (TD) of the driller and logger. “Driller Depth” utilizes the total length of downhole tools and drill pipe stands to calculate TD, while wireline tools go down the mud-filled hole after it has already been drilled and utilize the length of tools and cable downhole to calculate the “Logger Depth” TD (Figure 2.4). Variations between reported TD’s often occur due to these different methods of measurement. There is no way to determine which measurement is the correct depth, but the actual TD must be the same point in space. To account for this difference in measurements, the measured core depths had four feet added to their depths. The adjustment to the core depths was more easily accomplished because of the imbedded depth scale on the wireline logs. This was

arbitrary, as either could have been adjusted. The result is a normalizing of depths to the same total depth.

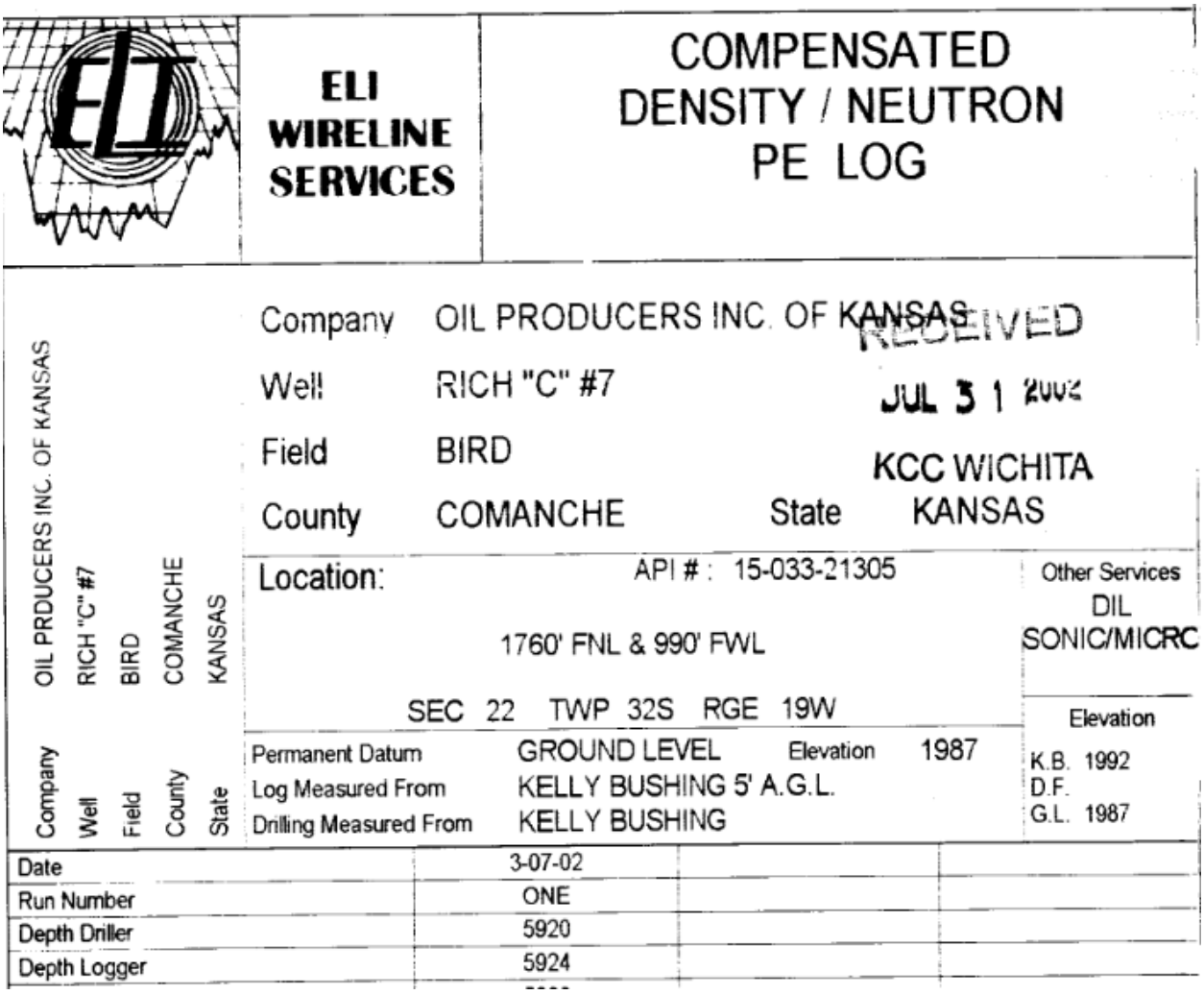

ELI WIRELINE SERVICES

COMPENSATED DENSITY / NEUTRON PE LOG

Company OIL PRODUCERS INC. OF KANSAS

Well RICH "C" #7

Field BIRD

County COMANCHE State KANSAS

RECEIVED
JUL 31 2002
KCC WICHITA

Location: API # : 15-033-21305

1760' FNL & 990' FWL

SEC 22 TWP 32S RGE 19W

Other Services
DIL
SONIC/MICRC

Elevation
K.B. 1992
D.F.
G.L. 1987

Permanent Datum GROUND LEVEL Elevation 1987
Log Measured From KELLY BUSHING 5' A.G.L.
Drilling Measured From KELLY BUSHING

OIL PRDUCERS INC. OF KANSAS
Company
RICH "C" #7
Well
BIRD
Field
COMANCHE
County
KANSAS
State

Date	3-07-02		
Run Number	ONE		
Depth Driller	5920		
Depth Logger	5924		

Figure 2.4: Log header from Rich C #7 displaying the difference of logged depth between "Depth Driller" and "Depth Logger" (KGS, 2018).

Chapter 3 - Results

3.1 Core Description Summary

The cored interval of the Viola Limestone in Rich C #7 is comprised mainly of muddy dolostone (Figure 3.1), with cherty dolomite being the reservoir rock inside the "B" zone. The "A" zone section of this core was not recovered, so the particular reservoir rock of the "A" zone in Rich C #7 was not described. Intraclastic rudstones and breccias can be seen, in thin layers, underneath the "A" and "B" zones, with rudstones appearing sporadically throughout the rest of the core. The bioclastic grainstone only appears twice in the cored section, in two to three-inch layers. Original macro-description of the core can be viewed below (Figure 3.2). Refer to Appendix B to view pictures of the entire core, thin section descriptions, SEM images, and EDS maps.

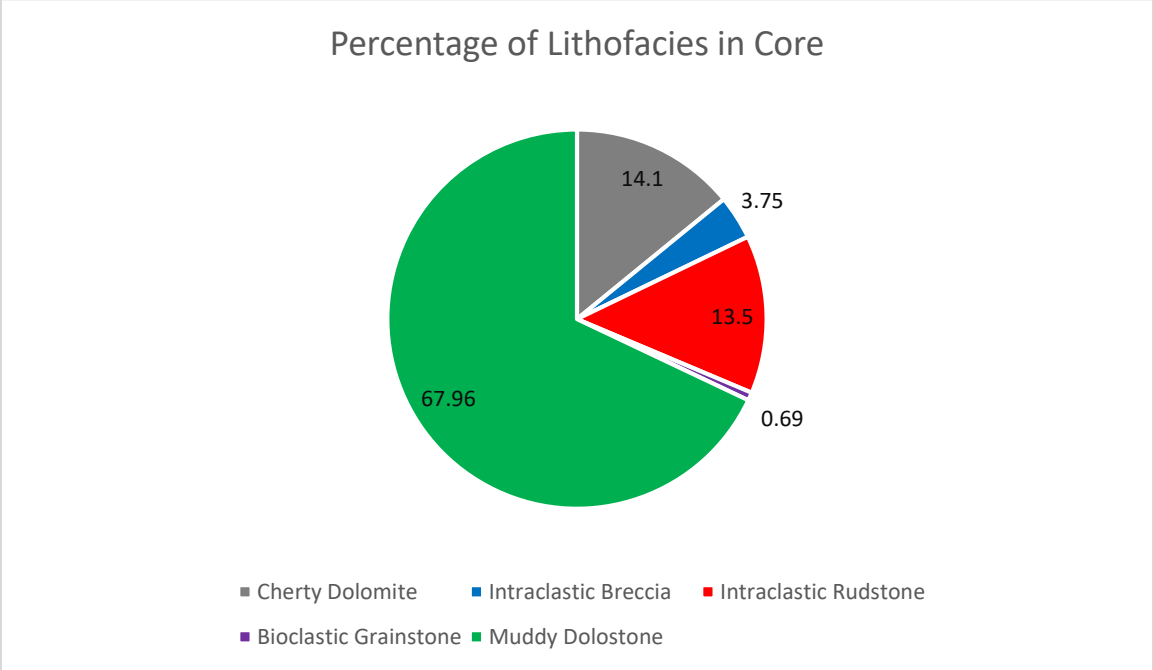

Figure 3.1: Percentage of different lithofacies inside the Rich C #7 core.

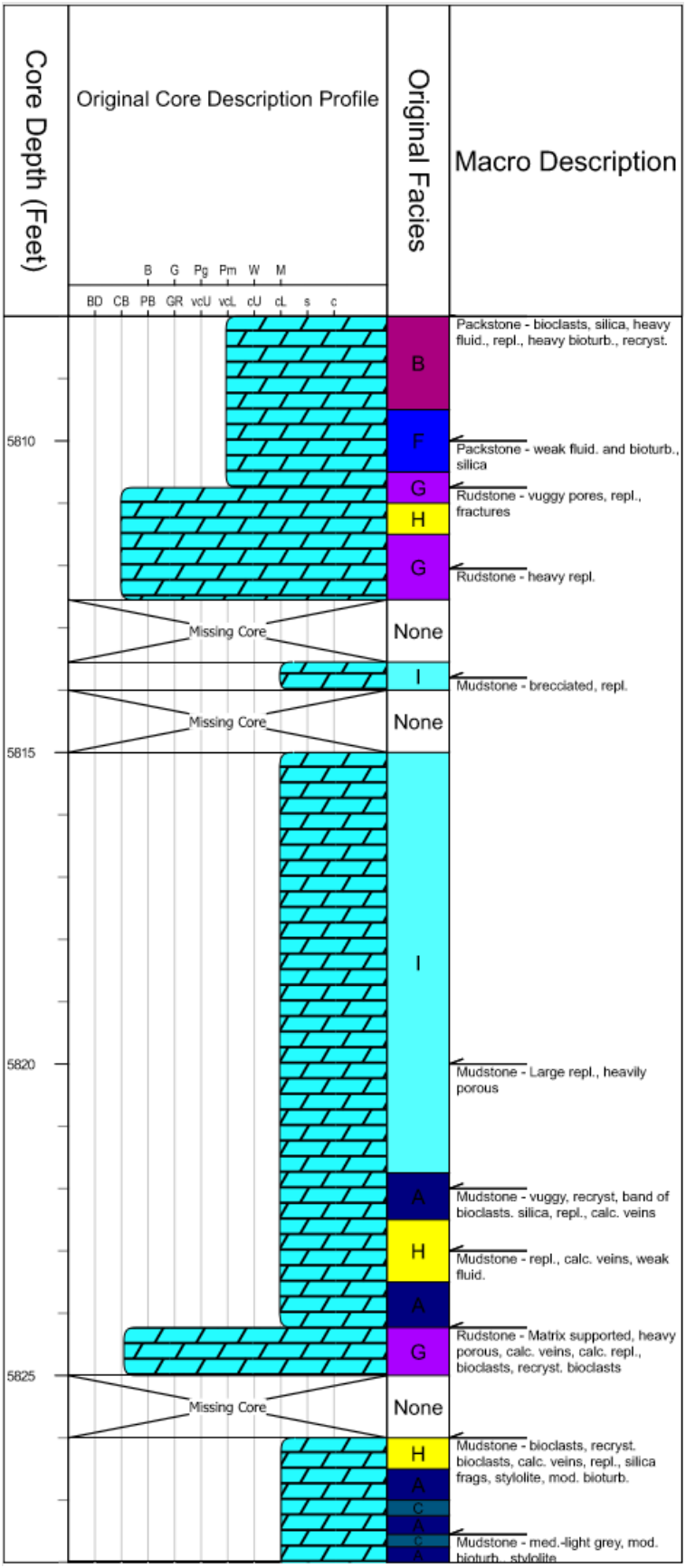
Core Depth (Feet)
Original Core Description Profile
B G Pg Pm W M
BD CB PB GR vcU vcL cU cL s c
Original Facies
Macro Description
5810
5815
5820
5825
B
F
G
H
G
None
I
None
I
A
H
A
G
None
H
A
C
A
C
A
Packstone - bioclasts, silica, heavy fluid., repl., heavy bioturb., recryst.
Packstone - weak fluid. and bioturb., silica
Rudstone - vuggy pores, repl., fractures
Rudstone - heavy repl.
Missing Core
Mudstone - brecciated, repl.
Missing Core
Mudstone - Large repl., heavily porous
Mudstone - vuggy, recryst, band of bioclasts. silica, repl., calc. veins
Mudstone - repl., calc. veins, weak fluid.
Rudstone - Matrix supported, heavy porous, calc. veins, calc. repl., bioclasts, recryst. bioclasts
Missing Core
Mudstone - bioclasts, recryst. bioclasts, calc. veins, repl., silica frags, stylolite, mod. bioturb.
Mudstone - med.-light grey, mod. bioturb., stylolite

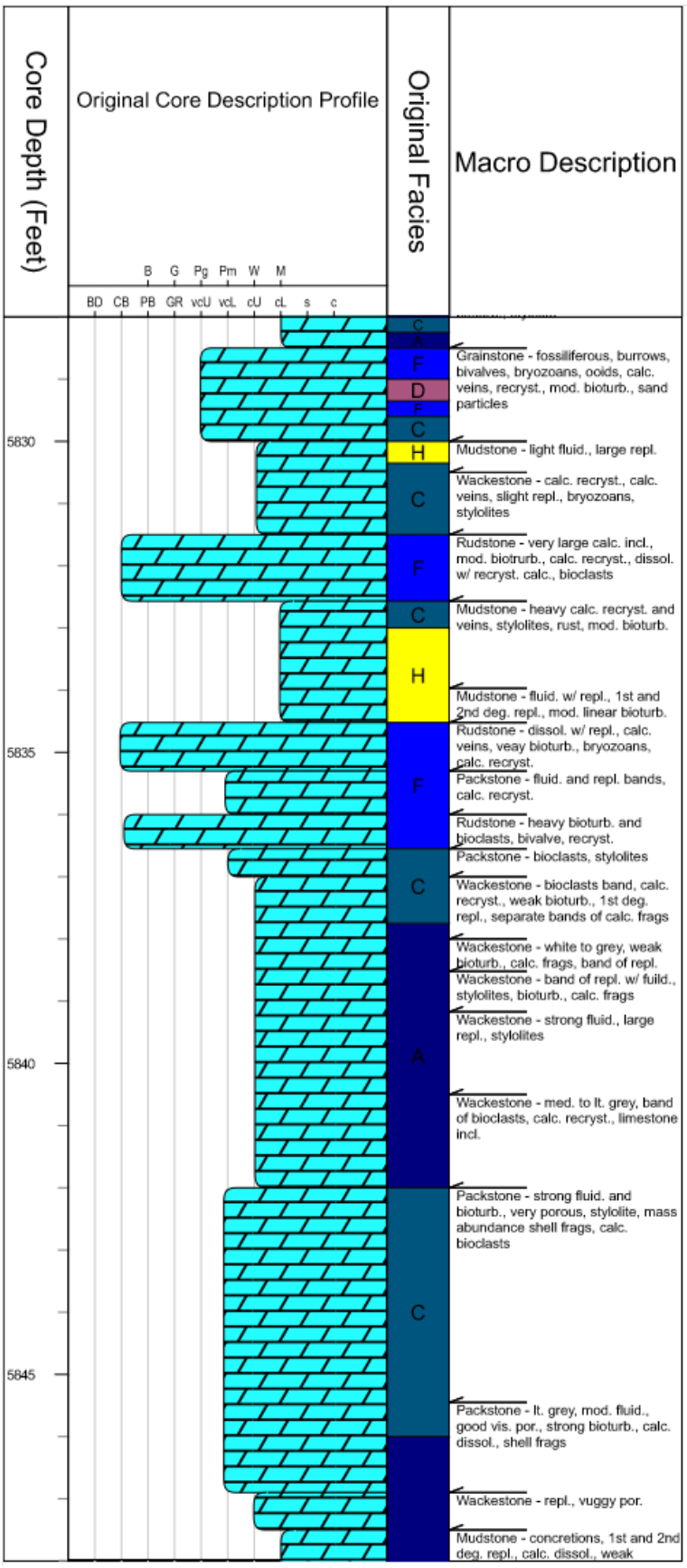
Core Depth (Feet)
Original Core Description Profile
B G Pg Pm W M
BD CB PB GR vcU vcL cU cL s c
Original Facies
Macro Description
5830
5835
5840
5845
Grainstone - fossiliferous, burrows, bivalves, bryozoans, ooids, calc. veins, recryst., mod. bioturb., sand particles
Mudstone - light fluid., large repl.
Wackestone - calc. recryst., calc. veins, slight repl., bryozoans, stylolites
Rudstone - very large calc. incl., mod. biotrurb., calc. recryst., dissol. w/ recryst. calc., bioclasts
Mudstone - heavy calc. recryst. and veins, stylolites, rust, mod. bioturb.
Mudstone - fluid. w/ repl., 1st and 2nd deg. repl., mod. linear bioturb.
Rudstone - dissol. w/ repl., calc. veins, veay bioturb., bryozoans, calc. recryst.
Packstone - fluid. and repl. bands, calc. recryst.
Rudstone - heavy bioturb. and bioclasts, bivalve, recryst.
Packstone - bioclasts, stylolites
Wackestone - bioclasts band, calc. recryst., weak bioturb., 1st deg. repl., separate bands of calc. frags
Wackestone - white to grey, weak bioturb., calc. frags, band of repl.
Wackestone - band of repl. w/ fuild., stylolites, bioturb., calc. frags
Wackestone - strong fluid., large repl., stylolites
Wackestone - med. to lt. grey, band of bioclasts, calc. recryst., limestone incl.
Packstone - strong fluid. and bioturb., very porous, stylolite, mass abundance shell frags, calc. bioclasts
Packstone - lt. grey, mod. fluid., good vis. por., strong bioturb., calc. dissol., shell frags
Wackestone - repl., vuggy por.
Mudstone - concretions, 1st and 2nd deg. repl., calc. dissol., weak

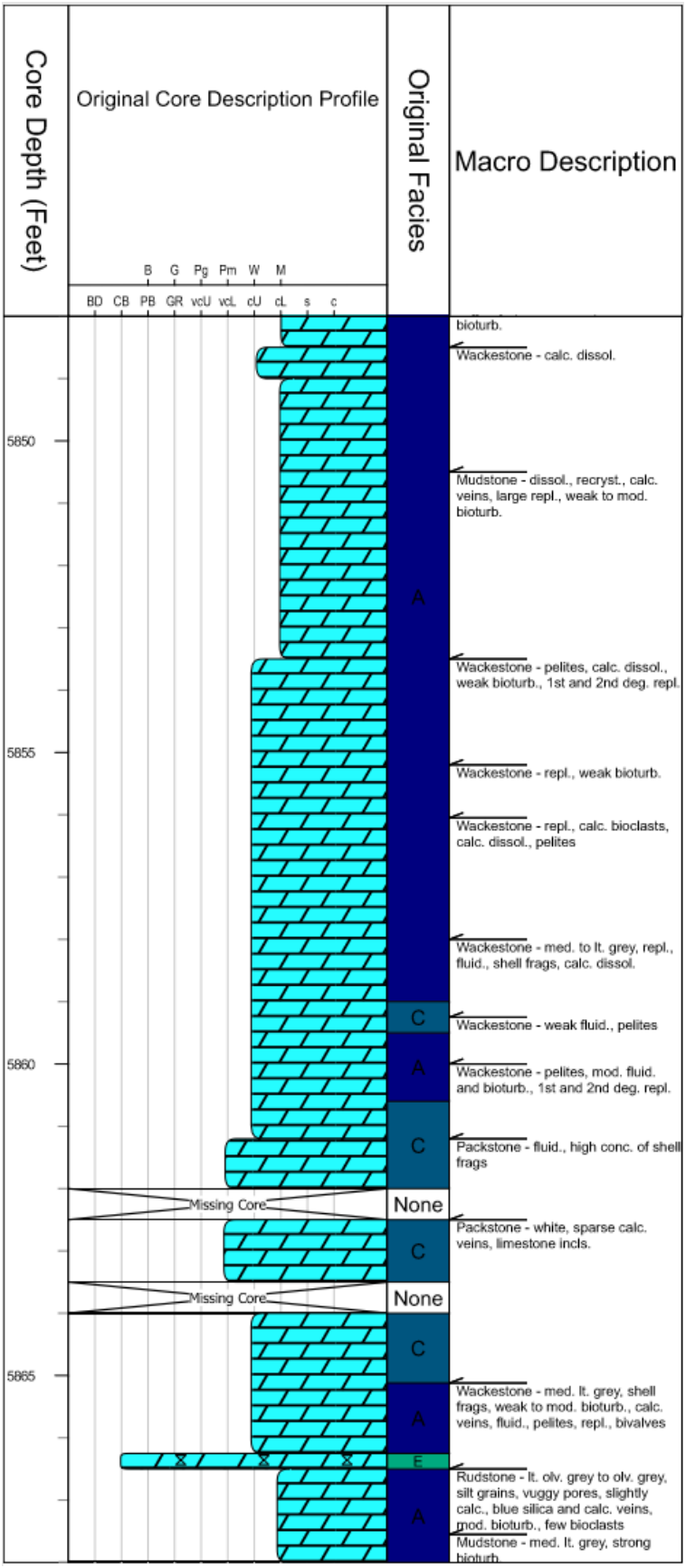
Core Depth (Feet)
Original Core Description Profile
B G Pg Pm W M
BD CB PB GR vcU vcL cU cL s c
Original Facies
Macro Description
5850
5855
5860
5865
bioturb.
Wackestone - calc. dissol.
Mudstone - dissol., recryst., calc. veins, large repl., weak to mod. bioturb.
Wackestone - pelites, calc. dissol., weak bioturb., 1st and 2nd deg. repl.
Wackestone - repl., weak bioturb.
Wackestone - repl., calc. bioclasts, calc. dissol., pelites
Wackestone - med. to lt. grey, repl., fluid., shell frags, calc. dissol.
Wackestone - weak fluid., pelites
Wackestone - pelites, mod. fluid. and bioturb., 1st and 2nd deg. repl.
Packstone - fluid., high conc. of shell frags
Missing Core
None
Packstone - white, sparse calc. veins, limestone incls.
Missing Core
None
Wackestone - med. lt. grey, shell frags, weak to mod. bioturb., calc. veins, fluid., pelites, repl., bivalves
Rudstone - lt. olv. grey to olv. grey, silt grains, vuggy pores, slightly calc., blue silica and calc. veins, mod. bioturb., few bioclasts
Mudstone - med. lt. grey, strong bioturb.
A
C
A
C
None
C
None
C
A
E
A

Figure 3.2: Macro description of core facies labels and descriptions. Rock units on the column were categorized by the Dunham and Modified Dunham classification profiles in the "Original Core Description Profile" column. Abbreviations for the classification are the following: B (boundstone), G (grainstone), Pg/Pm (packstone), W (wackestone), M (mudstone).

3.2 Lithofacies

Cherty Dolomite

The cherty dolomite is one of the main reservoir facies in the Viola Limestone, observed in the "B" zone of the Rich C #7 well. The other potential reservoir facies, located in the "A" zone, was not recovered from coring. The cherty dolomite is characterized as white to light gray chert composed of sponge spicules exhibiting laminations and moderate bioturbation. The chert component is very porous with vuggy porosity, and gray dolomite has extensively replaced the chert in parts (Figure 3.3). Dolomite partially fills some of the vugs formed from the dissolution of chert. Hydrocarbon fills the porosity between chert grains and dolomite rhombs (Figure 3.4). Moldic porosity is displayed from SEM images (Figure 3.5), and dolomite can be seen replacing siliceous material in the EDS elemental maps (Figure 3.6). The cherty dolomite has a thickness of roughly 8ft (2.4m) in the Rich C #7 core, occupying roughly 14% of the cored interval.

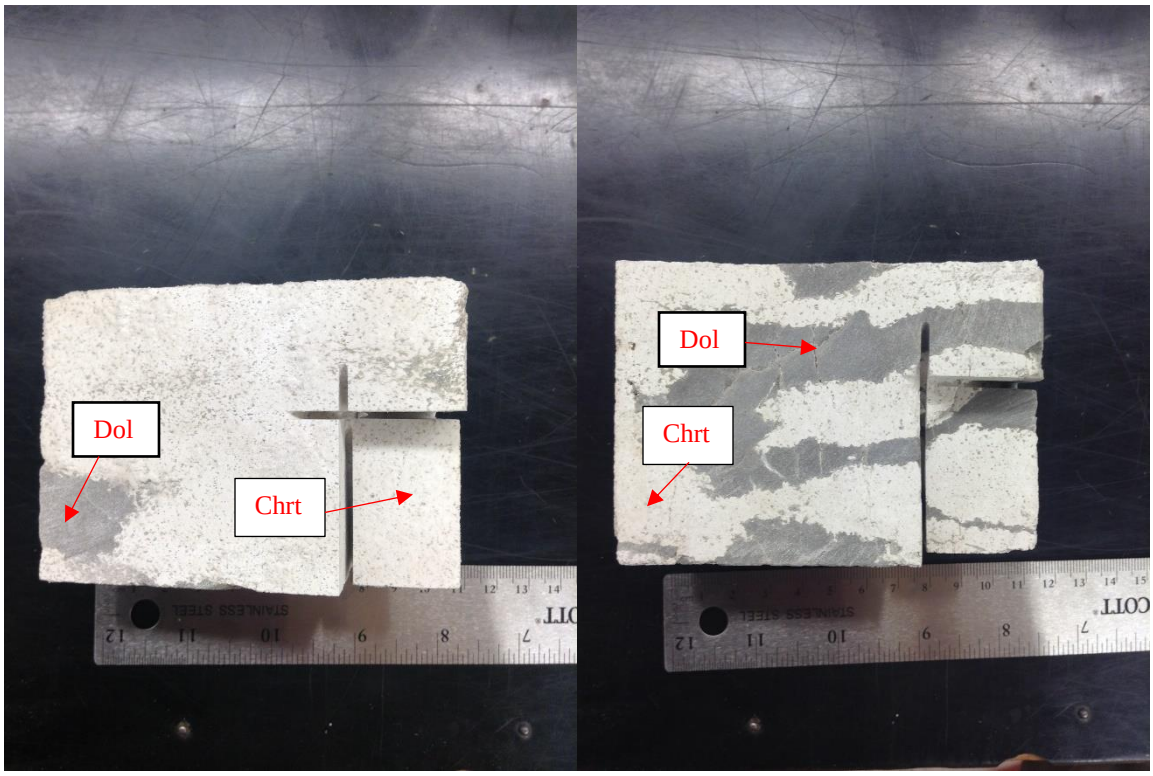

Figure 3.3: Cored section of cherty dolomite in the Viola Ls. from Rich C #7 at depths 5818.5' (left) and 5822' (right). Dolomite can be seen replacing the chert. Abbreviations: Dol (dolomite), Chrt (chert).

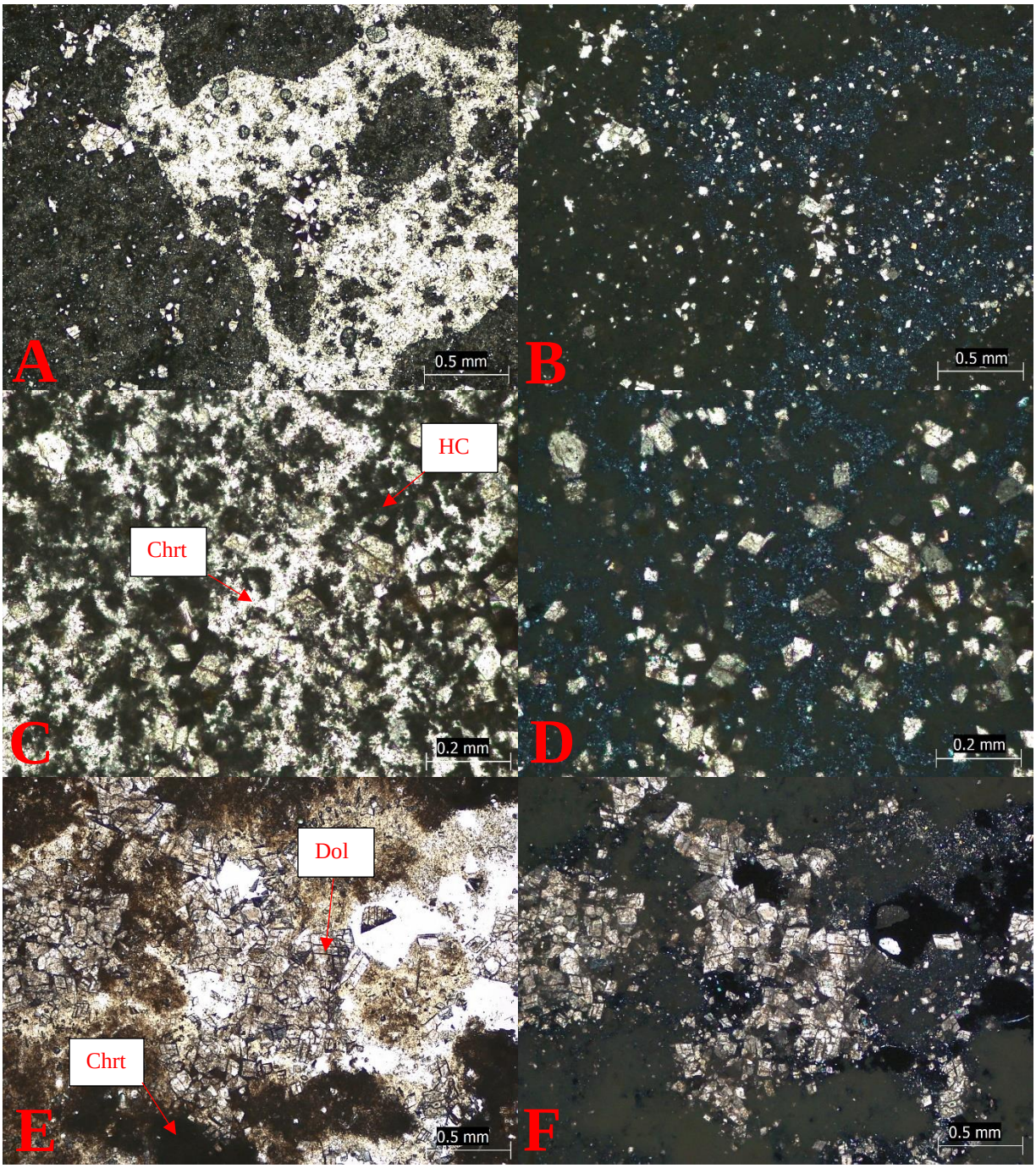

Figure 3.4: Thin section photomicrographs of cherty dolomite. A) plain polarized light (PPL) and B) cross polarized light (XPL) image at 5818.5'. C) PPL and D) XPL image at 5818.5' displaying hydrocarbons inside porosity of siliceous grains. E) PPL and F) XPL

image at 5822' displaying the replacement of chert with dolomite. Abbreviations: Dol (dolomite), Chrt (chert), HC (hydrocarbon).

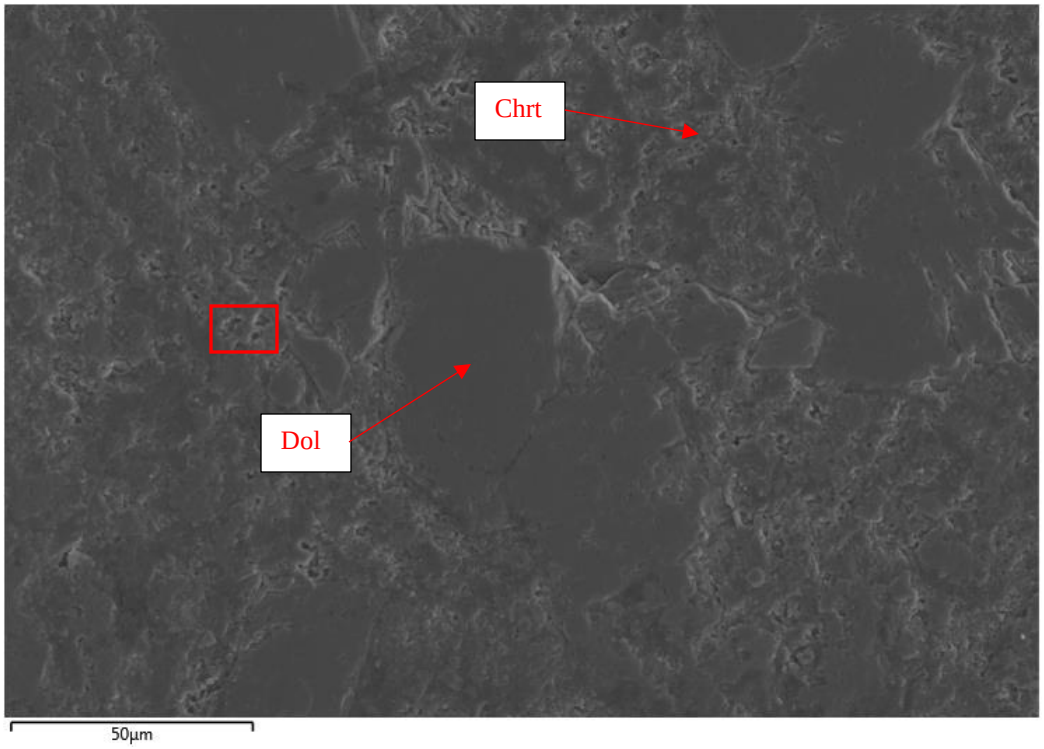

Figure 3.5: SEM image at 50µm of the Cherty dolomite thin section at 5818.5' from the Rich C #7 well. Moldic porosity (highlighted by red square) can be seen throughout the chert in this image. This thin section was coated with a 10 nm thick gold coating. Abbreviations: Dol (dolomite), Chrt (chert).

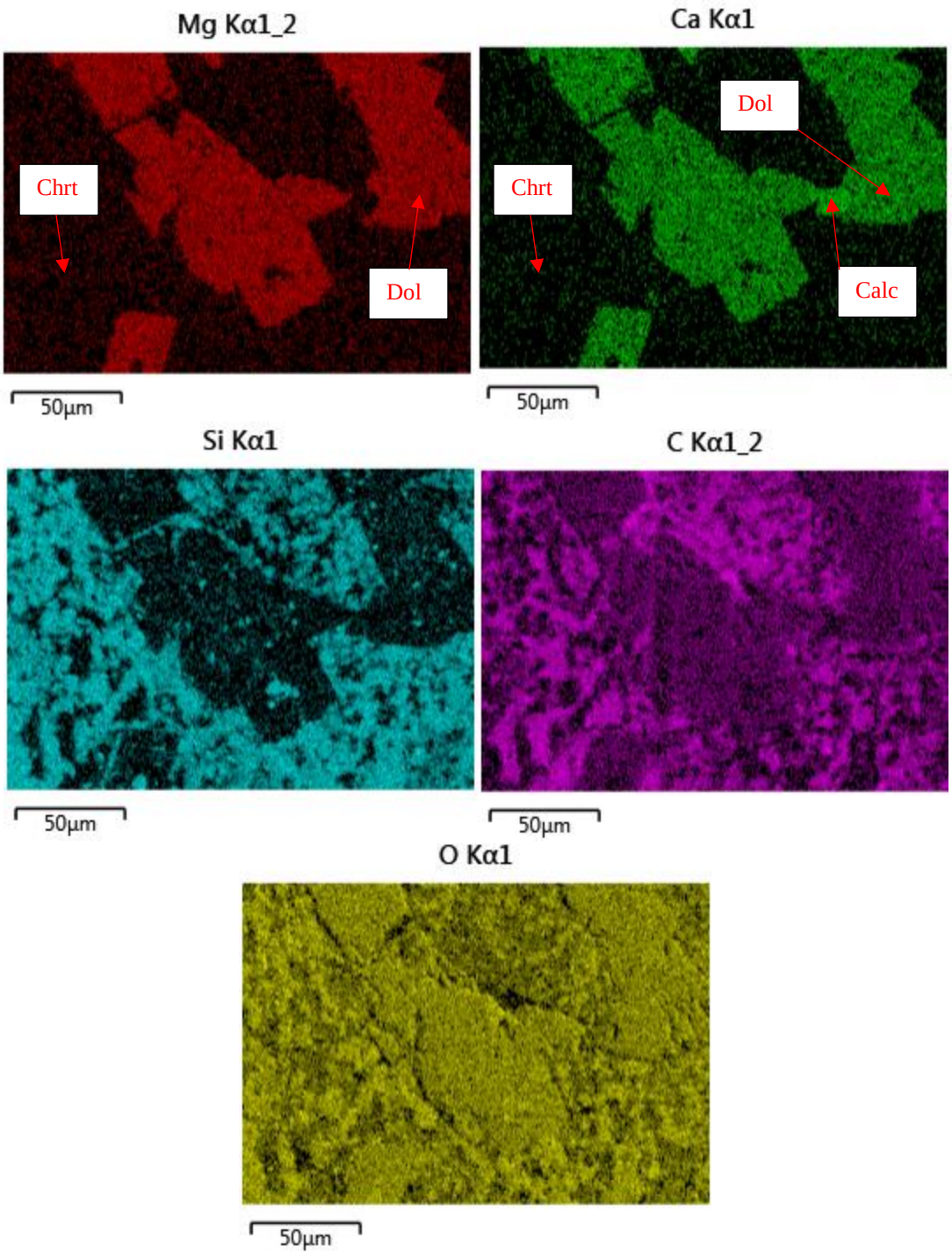

Figure 3.6: From left to right, EDS map images showing the distribution of dolomite (Mg), calcite (Ca), silicates (Si), carbon, and oxygen from the previous SEM image at 5818.5'. The Si EDS map approximates the distribution of chert, the combination of the Ca and Mg EDS maps approximates the distribution of dolomite, and the Ca EDS map by itself

approximates the distribution of calcite. The replacement of chert by dolomite can be observed in the Mg elemental map. Abbreviations: Dol (dolomite), Chrt (chert), Calc (calcite).

Intraclastic Breccia

The intraclastic breccia facies is observed in parts below the "A" zone and near the top and bottom of the "B" zone in the Viola Limestone from the Rich C #7 well. It is characterized as white to gray breccia composed of angular intraclasts of dolomite and chert, ranging from two to six cm in length, with a mud matrix which later became dolomitized (Figure 3.7). The breccia has good intergranular porosity, and coarsely-crystalline calcite fills vugs and fractures, in parts. Chert fragments with sponge spicules and fragments of silicified bioclastic grainstone can be seen in the breccia (Figure 3.8). The bryozoans and bivalves inside the grainstone fragments are cemented by chert and quartz. The breccia facies in Rich C #7 ranges in thickness from a few inches to a foot (0.3m), occupying roughly 4% of the cored interval.

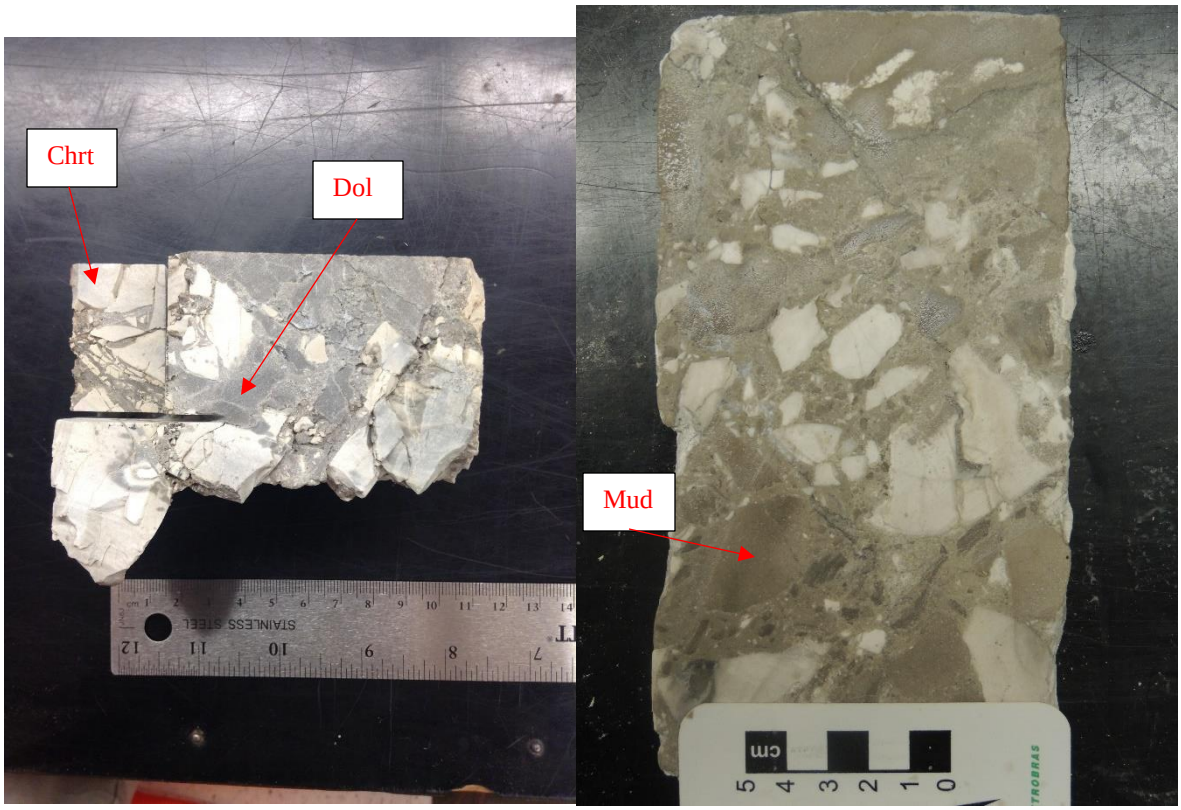

Figure 3.7: Cored section of intraclastic breccia in the Viola Ls. from Rich C #7 at depths 5811.66' (left) and 5812' (right). Dolomite, chert, and mud intraclasts can be seen in the cored sections. Abbreviations: Dol (dolomite), Chrt (chert), Mud, (mud).

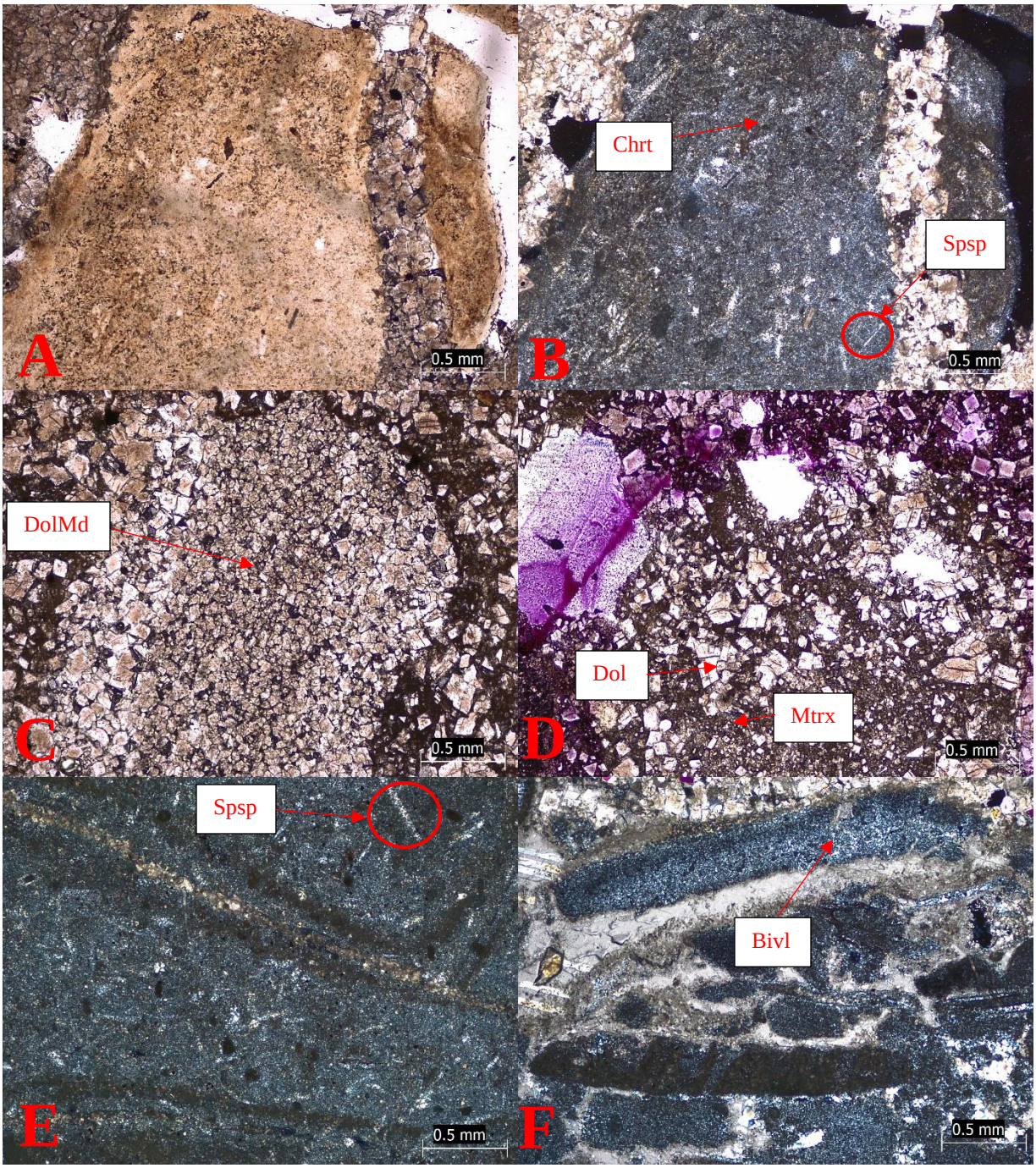

Figure 3.8: Thin section photomicrographs of intraclastic breccia. A) PPL and B) XPL image displaying chert intraclast composed of sponge spicules at 5811.66'. C), D) PPL images displaying mud intraclasts and matrix replaced by dolomite at 5812'. E) XPL image displaying chert intraclast composed of sponge spicules at 5824.66'. F) XPL image

displaying intraclast of bioclastic grainstone with bivalve at 5824.66'. Abbreviations: Chrt (chert), Spsp (sponge spicule), DolMd (dolomitic mud), Dol (dolomite), Mtrx (matrix), Bivl (bivalve).

Intraclastic Rudstone

The intraclastic rudstone facies is observed between the "A" and "B" zone and sporadically throughout the rest of the Rich C #7 core, below the "B" zone. It is characterized as light to olive gray rudstone with dolomite, mud, and/or chert intraclasts, varying from 0.1-1.5cm in size, and bioclasts, which are predominately echinoderms (Figure 3.9). The rudstone is locally fluidized, as seen with the wavy and mixed texture, with weak to heavy bioturbation. It predominately exhibits interparticle and vuggy porosity, with the vuggy porosity locally replaced by silica and dolomite nodules (Figure 3.10). The rudstones contain calcite veins, which can be seen in the SEM image (Figure 3.11) and EDS elemental maps (Figure 3.12) below. The rudstone facies in Rich C #7 ranges in thickness from a few inches to two feet (0.61m), occupying roughly 13% of the cored interval.

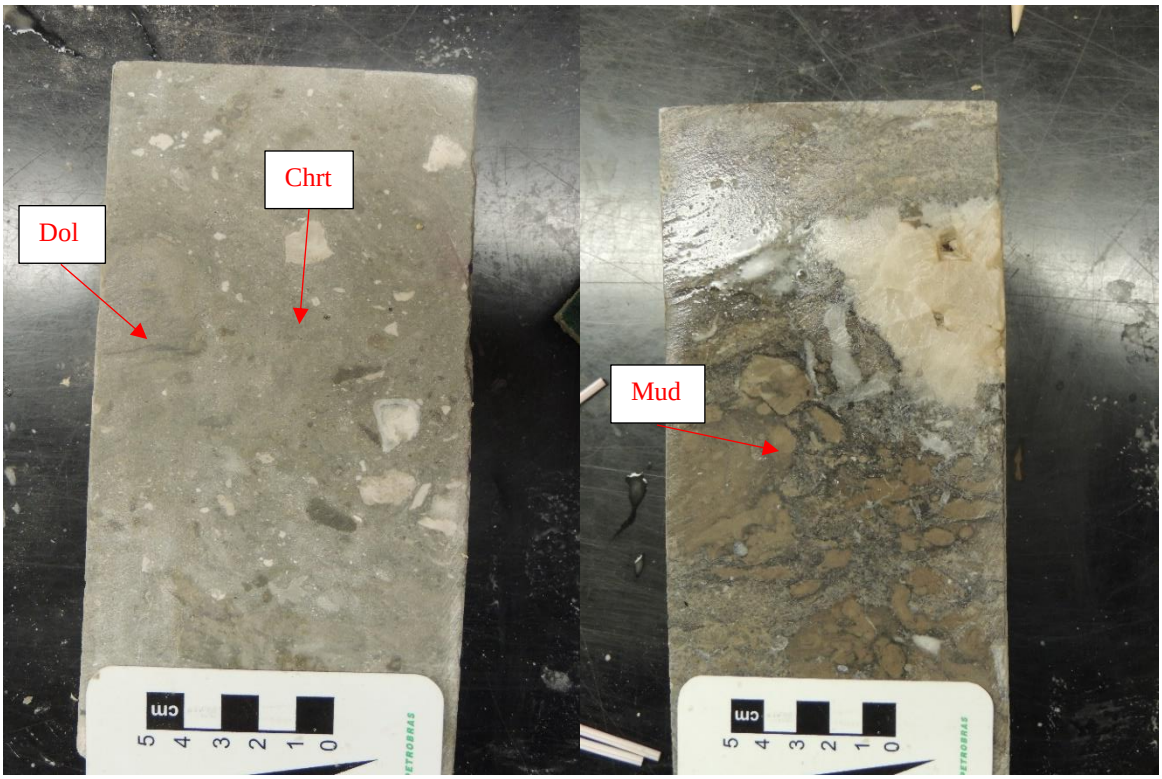

Figure 3.9: Cored section of intraclastic rudstone in the Viola Ls. from Rich C #7 at depths 5808' (left) and 5831.5' (right). Dolomite, chert, and mud intraclasts can be seen in the cored sections. Abbreviations: Chrt (chert), Dol (dolomite), Mud (mud).

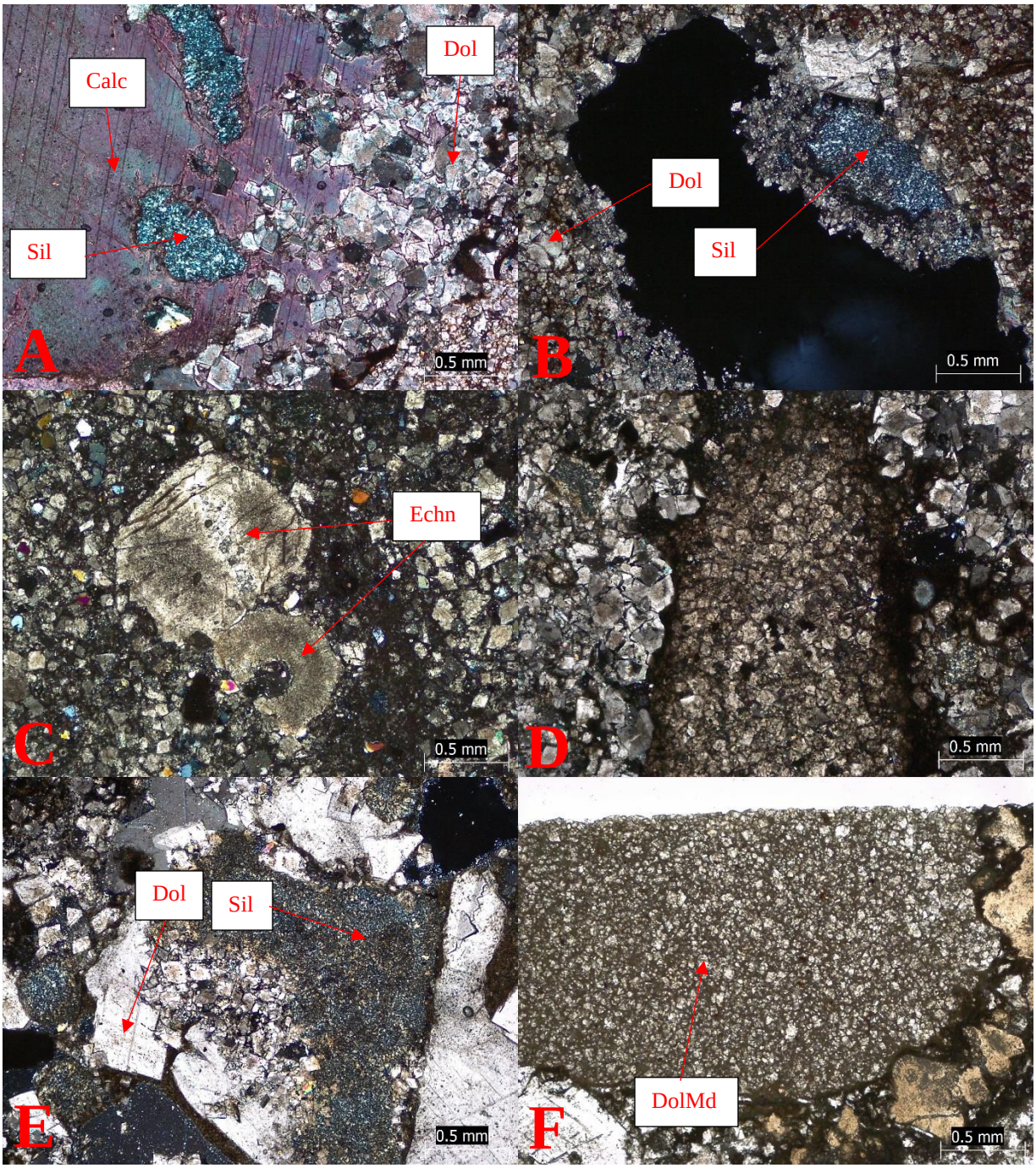

Figure 3.10: Thin section photomicrographs of intraclastic rudstone. A) XPL image displaying calcite (seen by red dye) cementing dolomitic and siliceous intraclasts at 5835.33'. B) XPL image displaying dolomitic intraclast with silica inside vug at 5841.33'. C) XPL image displaying echinoderms at 5808'. D) XPL image displaying dolomitic mud

intraclast at 5828.6'. E) XPL image displaying siliceous intraclasts and coarse dolomite at 5831.5'. F) PPL image displaying dolomitic mud intraclast at 5831.5'. Abbreviations: Calc (calcite), Dol (dolomite), Sil (silica), Echn (echinoderm), DolMd (dolomitic mud).

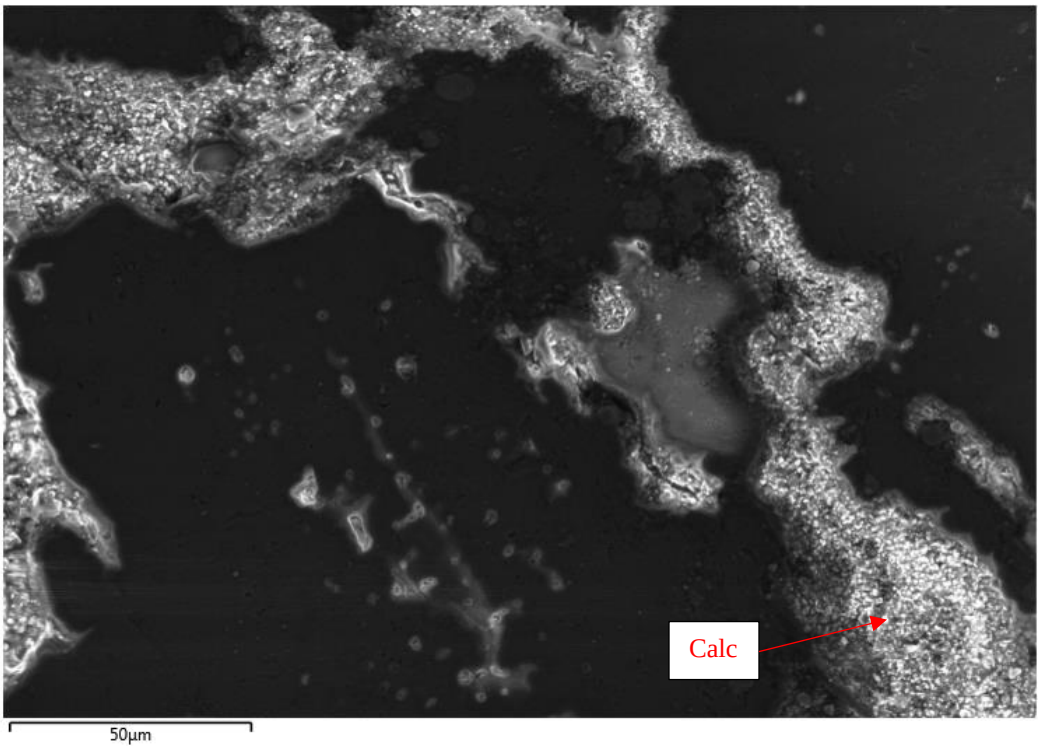

Figure 3.11: SEM image at 50µm of the intraclastic rudstone thin section at 5835.33' from the Rich C #7 well. A vein of calcite can be seen. This thin section was coated with a 10 nm thick gold coating. Abbreviation: Calc (calcite).

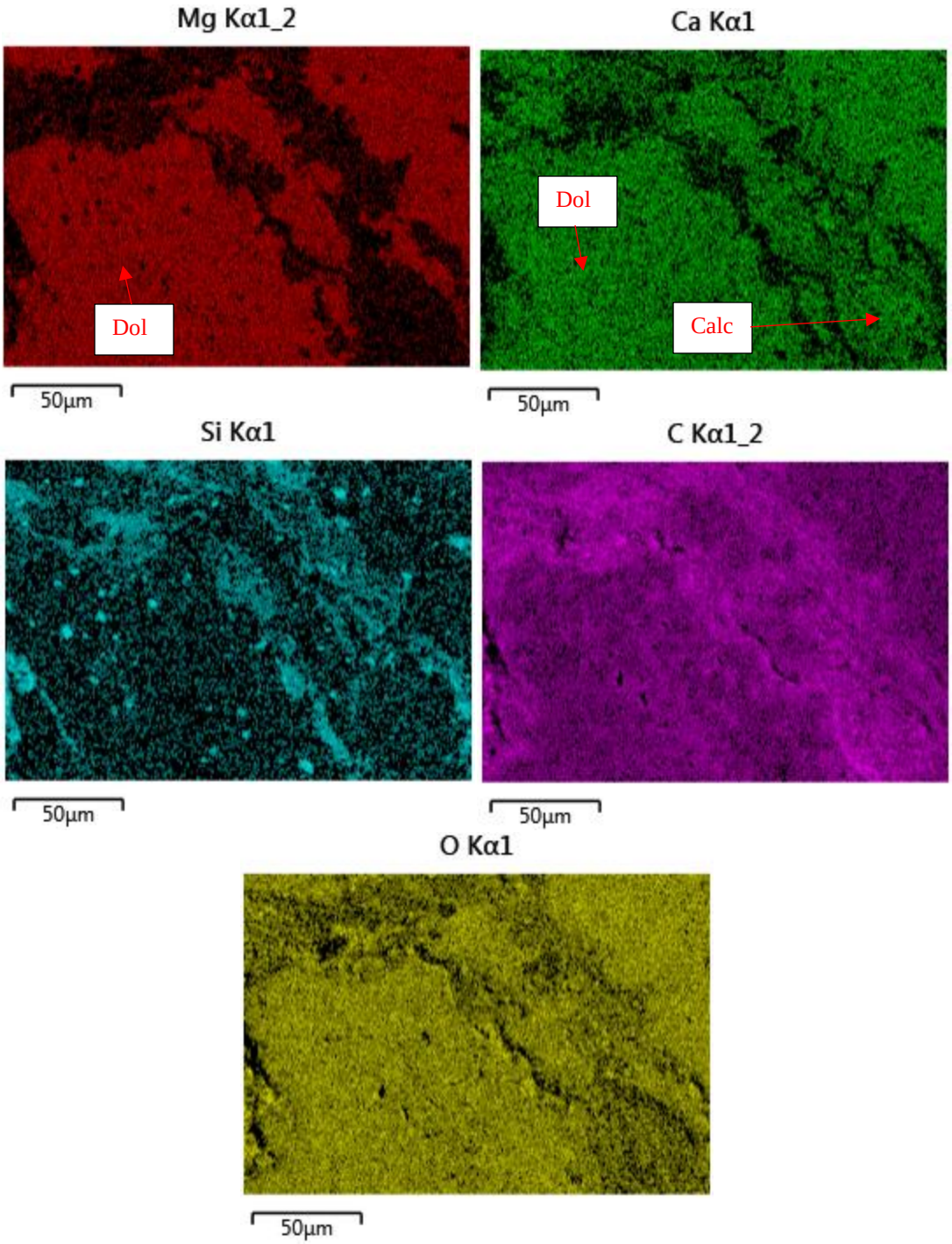

Figure 3.12: From left to right, EDS map images showing the distribution of dolomite (Mg), calcite (Ca), silicates (Si), carbon, and oxygen from the previous SEM image at 5835.33'. The Si EDS map approximates the distribution of chert and/or silica, the combination of the Ca and Mg EDS maps approximates the distribution of dolomite, and the Ca EDS map

by itself approximates the distribution of calcite. A calcite vein can be seen when comparing the Mg and Ca elemental maps. Abbreviations: Dol (dolomite), Calc (calcite).

Bioclastic Grainstone

The bioclastic grainstone facies is observed only in two spots throughout the whole Rich C #7 core, right below the "B" zone and another six and a half feet down from that point. The facies occurs as two to three-inch-thick bands, which are too small to appear on log resolution, but could mark a sequence boundary right below the "B" zone (Figure 3.13). It is characterized as a white to light gray, horizontally laminated grainstone with silicified bryozoans, echinoderms, crinoids, ooids, and siliceous and dolomitic intraclasts (Figure 3.14). Interparticle pores are filled with microcrystalline quartz in parts, and coarse calcite has filled rock fracture porosity. The bioclastic grainstone facies in Rich C #7 occupies less than one percent of the cored interval.

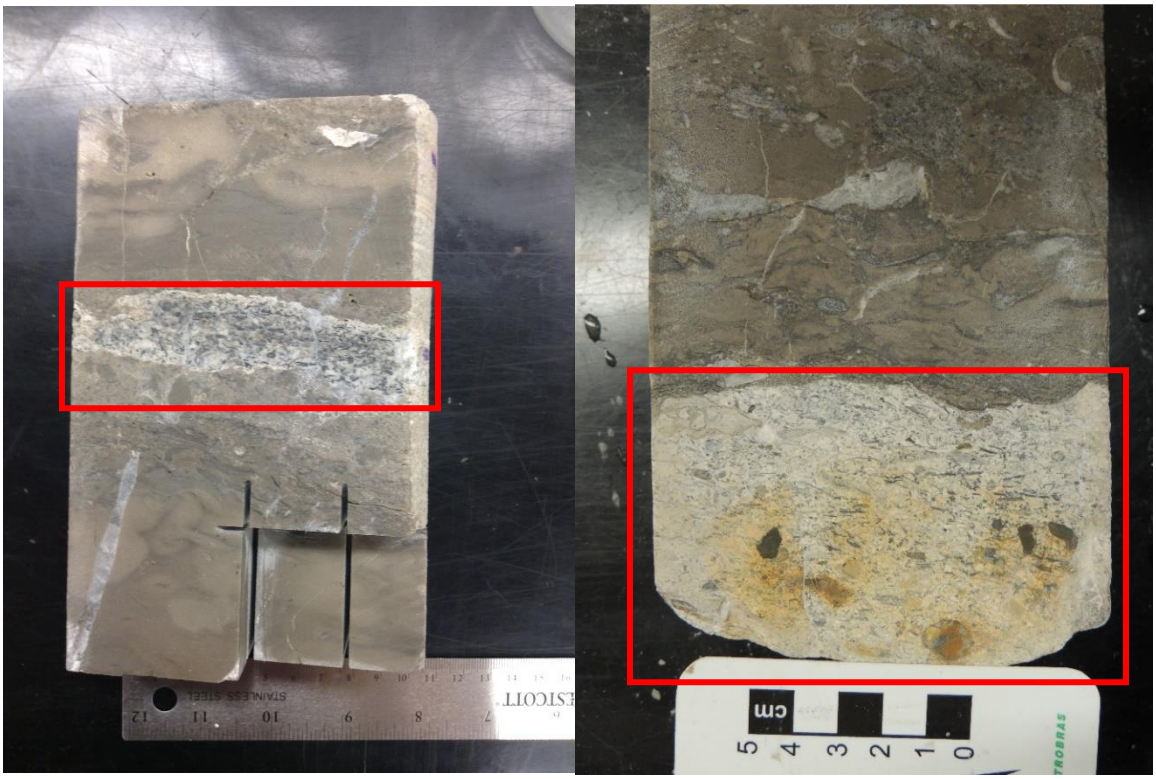

Figure 3.13: Cored section featuring bioclastic grainstone in the Viola Ls. from Rich C #7 at depths 5822' (left) and 5828.5' (right). The grainstone is highlighted by the red square.

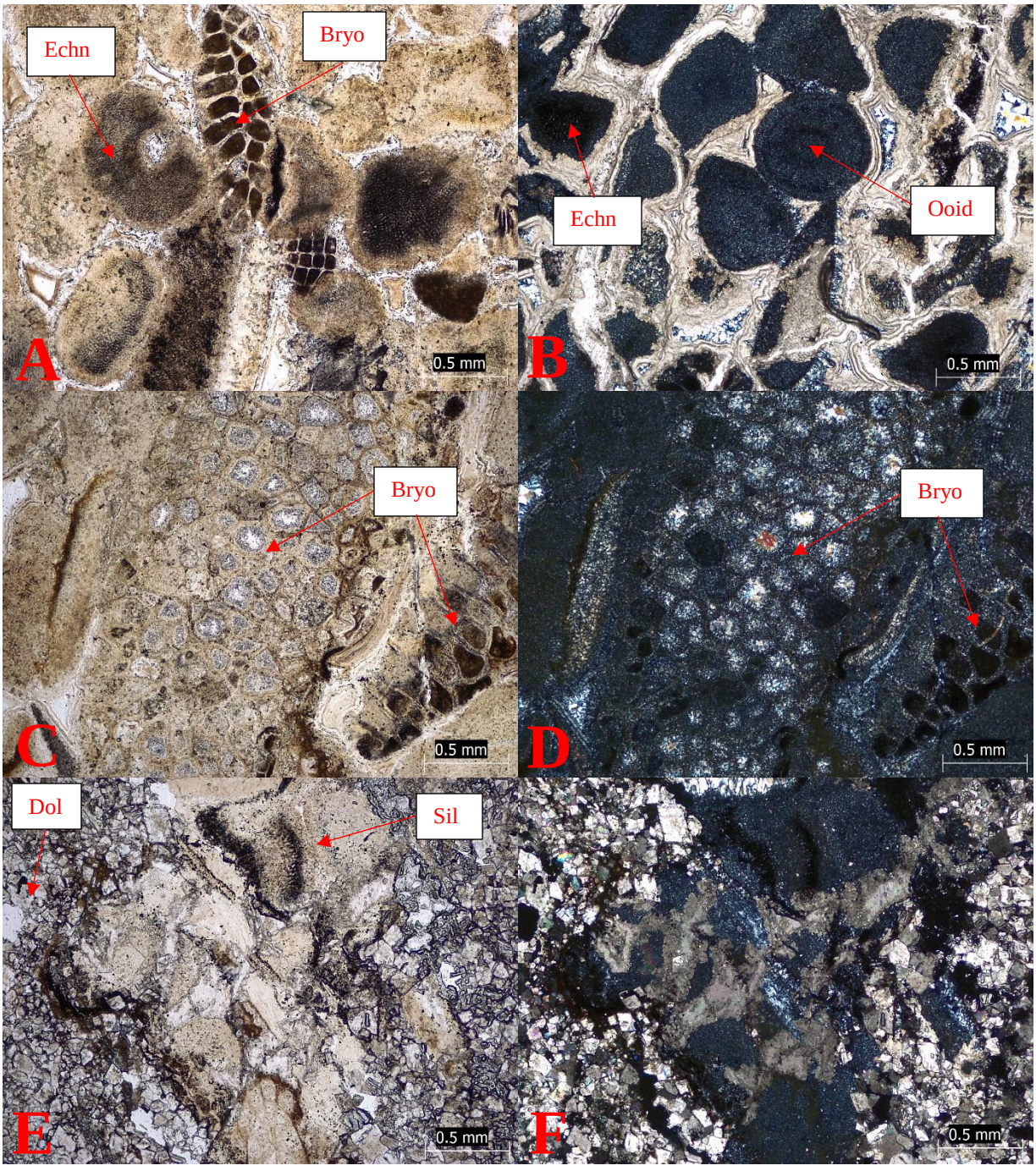

Figure 3.14: Thin section photomicrographs of bioclastic grainstone at 5828.5'. A) PPL image displaying silicified echinoderms and bryozoans. B) XPL image displaying silicified

ooids and echinoderms. C) PPL and D) XPL images displaying silicified bryozoans. E) PPL and F) XPL images displaying siliceous and dolomitic intraclasts. Abbreviations: Echn (echinoderm), Bryo (bryozoan), Ooid (ooid), Dol (dolomite), Sil (silica).

Muddy Dolostone

The muddy dolostone facies is observed throughout most of the cored interval in the Rich C #7 well. It is characterized as a medium-light gray dolostone with fine to medium-crystalline dolomite replacing micritic mud. The dolostone has moderate bioturbation, local fluidization, and scattered biolclasts (Figure 3.16). The dolostone's vuggy porosity can be vacant or filled by calcite (Figure 3.18), coarse dolomite, or silica (Figure 3.17), and the dolostone is also extensively replaced by silica in parts (Figure 3.15) and locally with calcite veins. The muddy dolostone facies in Rich C #7 ranges in thickness from a couple inches to almost 17 feet (5.18m), occupying almost 68% of the cored interval.

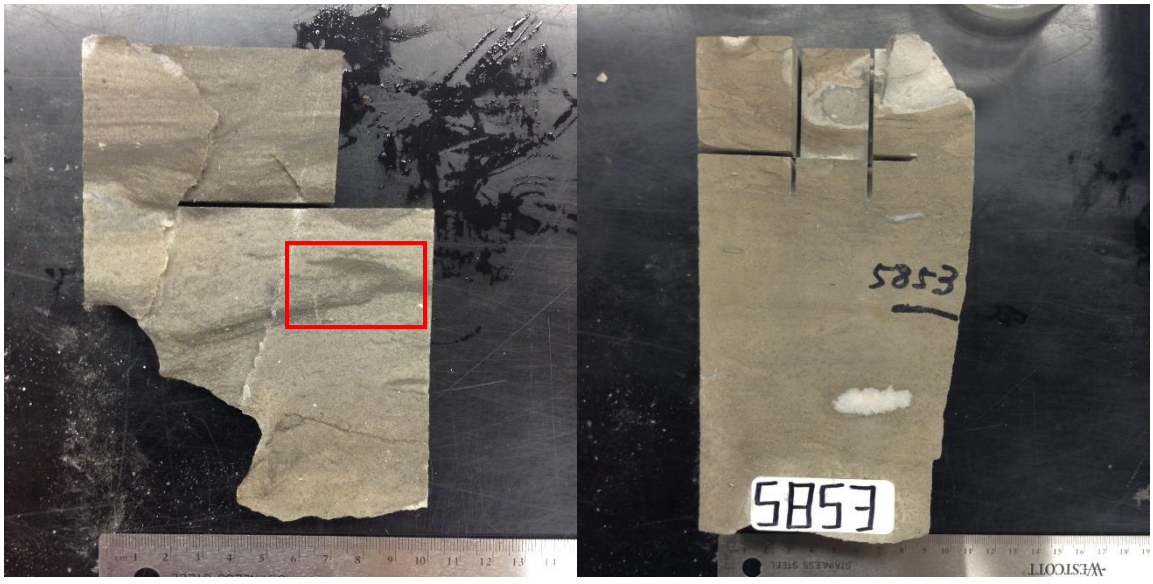

Figure 3.15: Cored section featuring muddy dolostone in the Viola Ls. from Rich C #7 at depths 5841.83' (left) and 5852.66' (right). Fluidization (highlighted by red square) and

laminations can be seen in the section on the left, and silica replacement can be seen at the top of the section on the right.

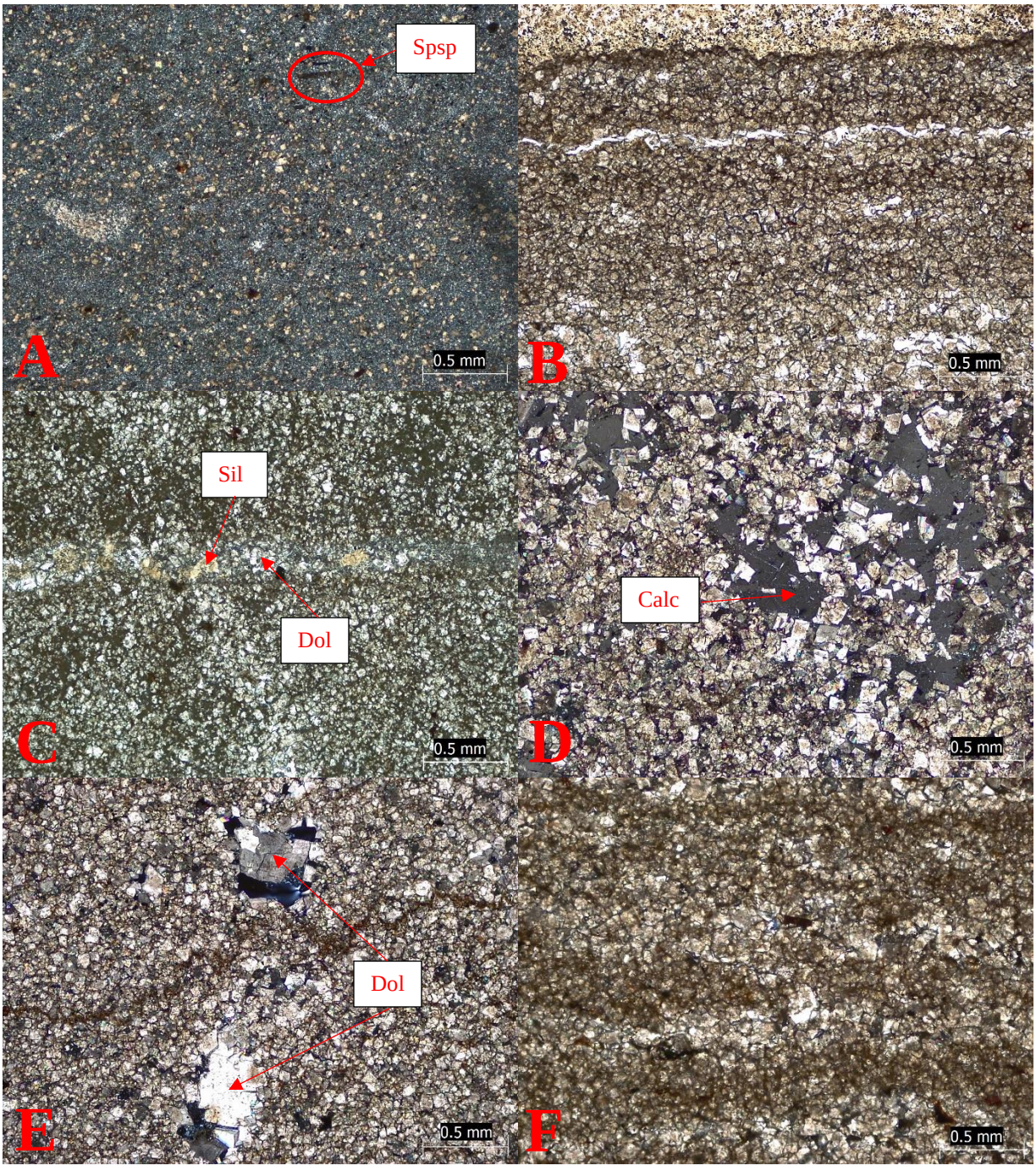

Figure 3.16: Thin section photomicrographs of muddy dolostone. A) XPL image of chert, containing sponge spicules, at 5834'. B) PPL image displaying laminations at 5834'. C) PPL

displaying silica and dolomite rhombs inside fracture at 5857.66'. D) XPL image displaying coarse calcite filling vugs at 5860.5'. E) XPL image displaying coarse dolomite filling vugs at 5837'. F) XPL image displaying laminations at 5841.83'. Abbreviations: Spsp (sponge spicule), Sil (silica), Dol (dolomite), Calc (calcite).

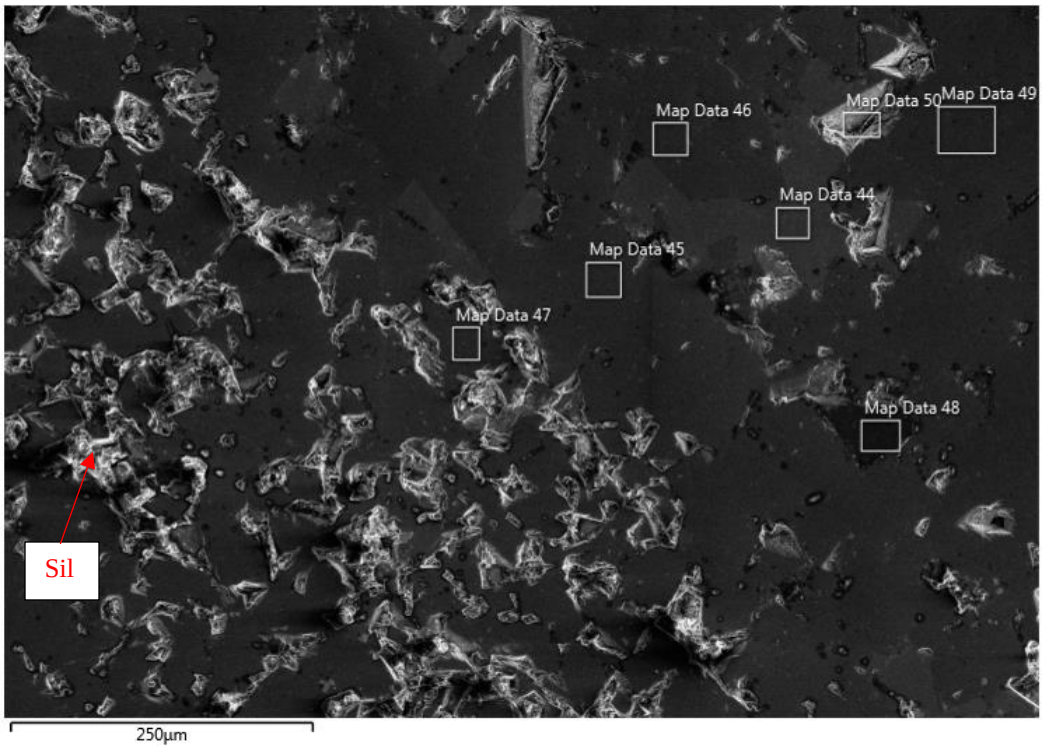

Figure 3.17: Large-field-of-view SEM image at 250µm of the muddy dolostone thin section at 5860.5' from the Rich C #7 well. Siliceous material is noted above. This thin section was coated with a 10 nm thick gold coating. Abbreviation: Sil (silica).

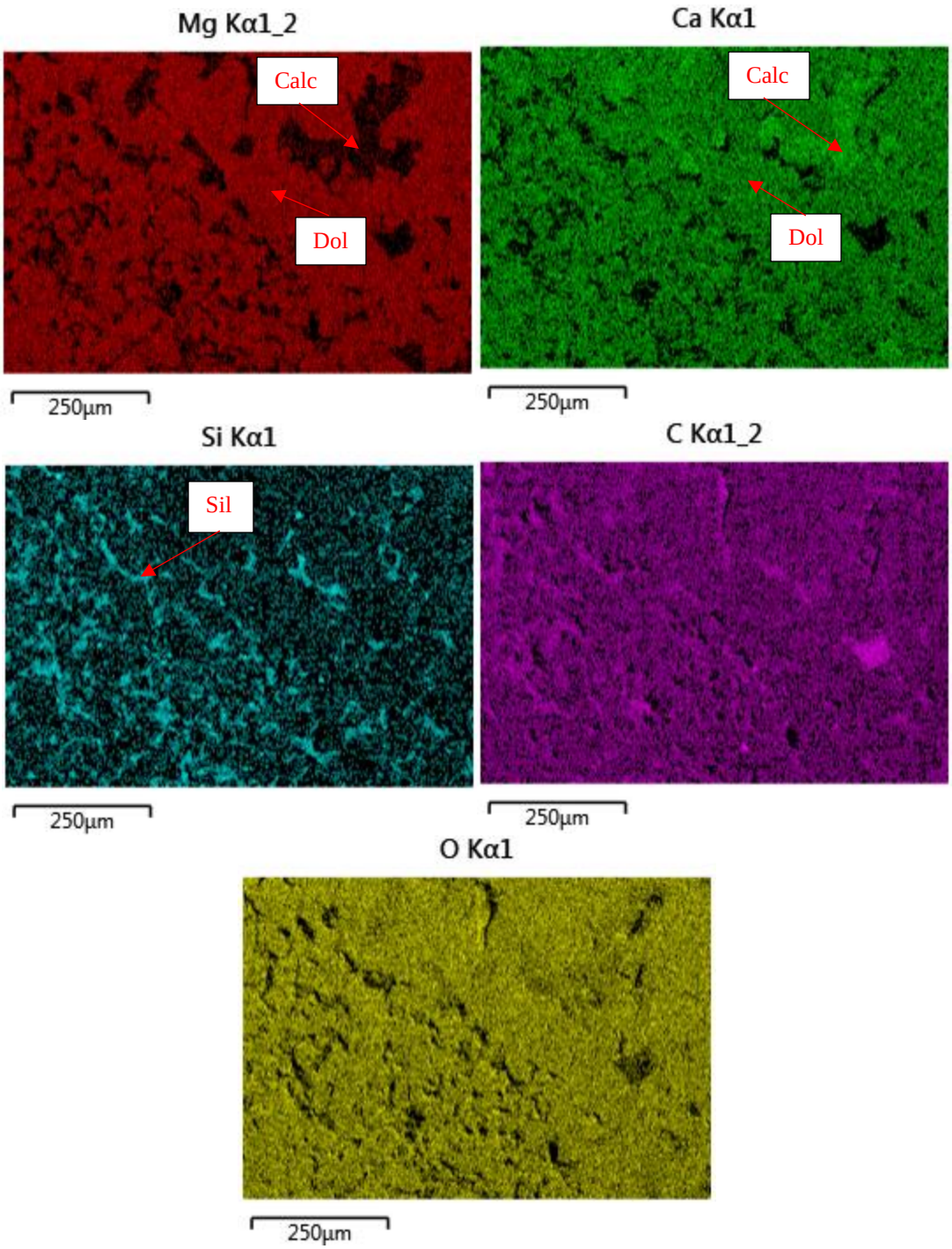

Figure 3.18: From left to right, EDS map images showing the distribution of dolomite (Mg), calcite (Ca), silicates (Si), carbon, and oxygen from the previous SEM image at 5860.5'. The Si EDS map approximates the distribution of chert and/or silica, the combination of the Ca and Mg EDS maps approximates the distribution of dolomite, and the Ca EDS map by

itself approximates the distribution of calcite. Silica can be seen potentially filling moldic porosity and/or replacing dolomite from the "Si" map. Calcite can also be seen filling moldic porosity. Abbreviations: Sil (silica), Dol (dolomite), Calc (calcite).

After petrographic examination, the original macro-description of the core was modified into the current core description profile and facies names (Figure 3.19). The thin sections were classified according to depositional texture and followed the Dunham and Modified Dunham's classification scheme.

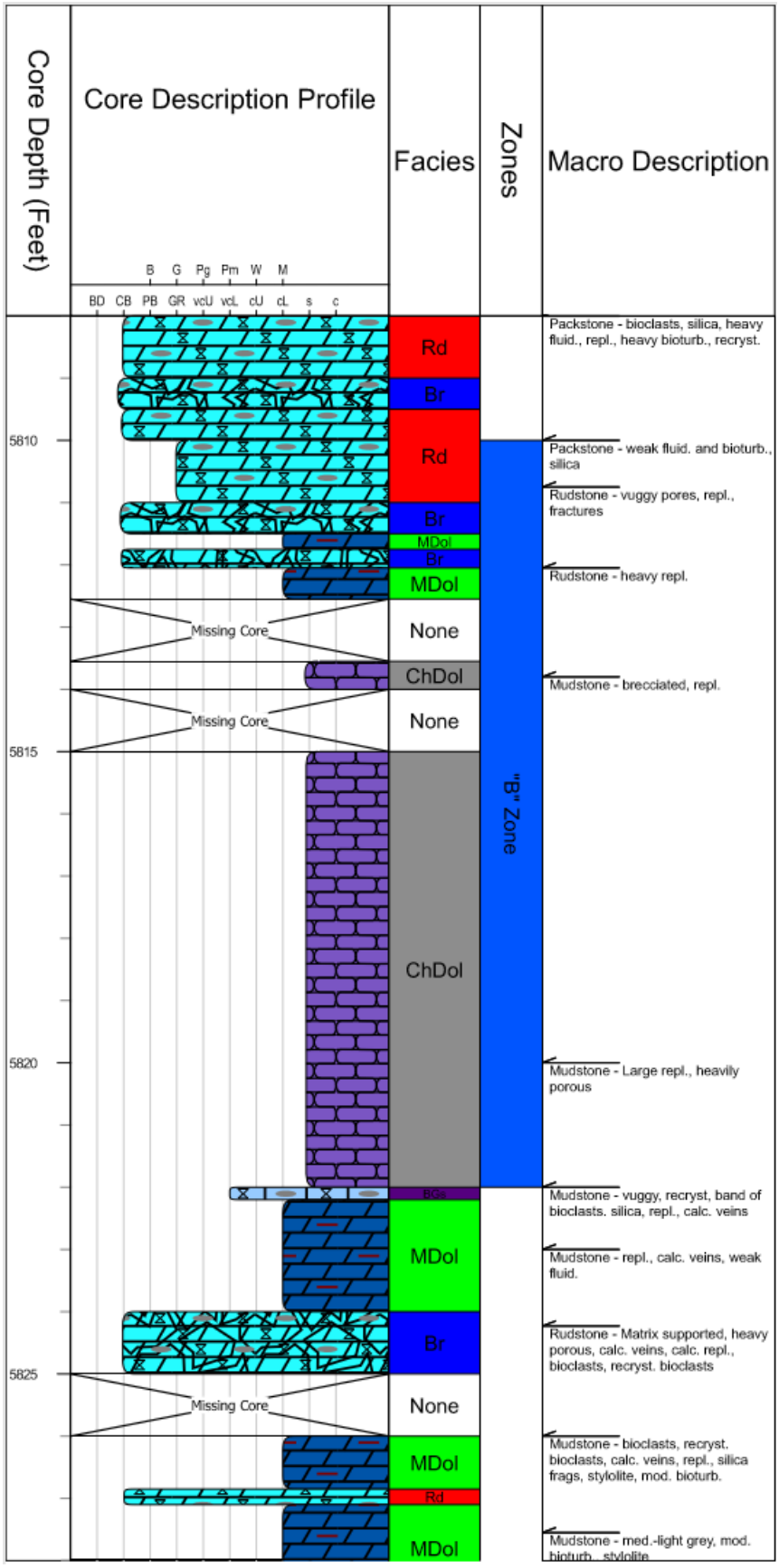
Core Depth (Feet)
Core Description Profile
B G Pg Pm W M
BD CB PB GR vcU vcL cU cL s c
Facies
Zones
Macro Description
5810
5815
5820
5825
Rd
Br
Rd
Br
MDol
Br
MDol
None
ChDol
None
ChDol
BGs
MDol
Br
None
MDol
Rd
MDol
Missing Core
Missing Core
Missing Core
"B" Zone
Packstone - bioclasts, silica, heavy fluid., repl., heavy bioturb., recryst.
Packstone - weak fluid. and bioturb., silica
Rudstone - vuggy pores, repl., fractures
Rudstone - heavy repl.
Mudstone - brecciated, repl.
Mudstone - Large repl., heavily porous
Mudstone - vuggy, recryst, band of bioclasts. silica, repl., calc. veins
Mudstone - repl., calc. veins, weak fluid.
Rudstone - Matrix supported, heavy porous, calc. veins, calc. repl., bioclasts, recryst. bioclasts
Mudstone - bioclasts, recryst. bioclasts, calc. veins, repl., silica frags, stylolite, mod. bioturb.
Mudstone - med.-light grey, mod. bioturb., stylolite

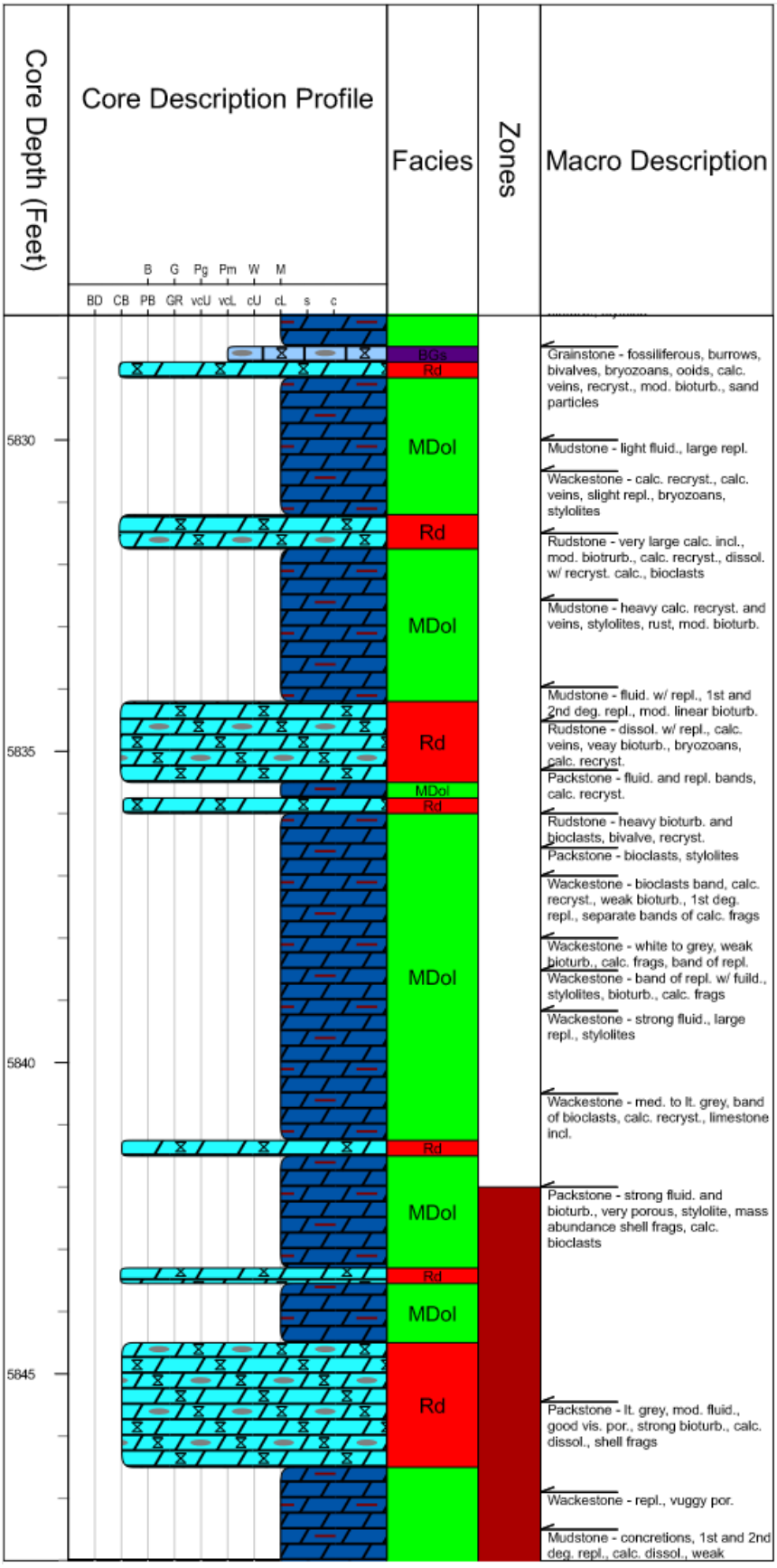
Core Depth (Feet)
Core Description Profile
B G Pg Pm W M
BD CB PB GR vcU vcL cU cL s c
Facies
Zones
Macro Description
5830
5835
5840
5845
BGs
Rd
MDol
Rd
MDol
Rd
MDol
Rd
MDol
Rd
MDol
Rd
Grainstone - fossiliferous, burrows, bivalves, bryozoans, ooids, calc. veins, recryst., mod. bioturb., sand particles
Mudstone - light fluid., large repl.
Wackestone - calc. recryst., calc. veins, slight repl., bryozoans, stylolites
Rudstone - very large calc. incl., mod. biotrurb., calc. recryst., dissol. w/ recryst. calc., bioclasts
Mudstone - heavy calc. recryst. and veins, stylolites, rust, mod. bioturb.
Mudstone - fluid. w/ repl., 1st and 2nd deg. repl., mod. linear bioturb.
Rudstone - dissol. w/ repl., calc. veins, veay bioturb., bryozoans, calc. recryst.
Packstone - fluid. and repl. bands, calc. recryst.
Rudstone - heavy bioturb. and bioclasts, bivalve, recryst.
Packstone - bioclasts, stylolites
Wackestone - bioclasts band, calc. recryst., weak bioturb., 1st deg. repl., separate bands of calc. frags
Wackestone - white to grey, weak bioturb., calc. frags, band of repl.
Wackestone - band of repl. w/ fuild., stylolites, bioturb., calc. frags
Wackestone - strong fluid., large repl., stylolites
Wackestone - med. to lt. grey, band of bioclasts, calc. recryst., limestone incl.
Packstone - strong fluid. and bioturb., very porous, stylolite, mass abundance shell frags, calc. bioclasts
Packstone - lt. grey, mod. fluid., good vis. por., strong bioturb., calc. dissol., shell frags
Wackestone - repl., vuggy por.
Mudstone - concretions, 1st and 2nd deg. repl., calc. dissol., weak

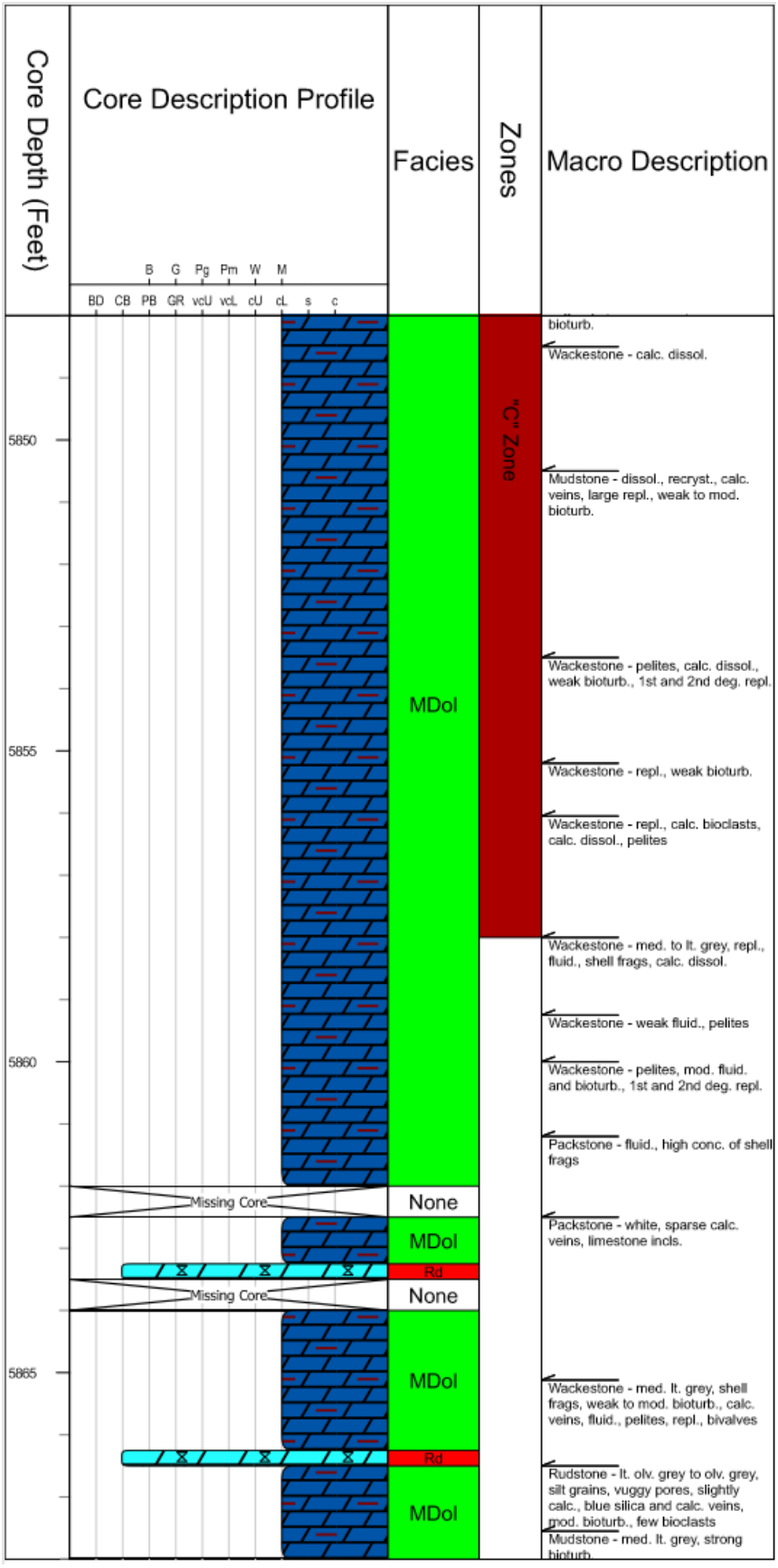
Core Depth (Feet)
Core Description Profile
B G Pg Pm W M
BD CB PB GR vcU vcL cU cL s c
Facies
Zones
Macro Description
5850
5855
5860
5865
"C" Zone
MDol
None
MDol
Rd
None
MDol
Rd
MDol
Missing Core
Missing Core
bioturb.
Wackestone - calc. dissol.
Mudstone - dissol., recryst., calc. veins, large repl., weak to mod. bioturb.
Wackestone - pelites, calc. dissol., weak bioturb., 1st and 2nd deg. repl.
Wackestone - repl., weak bioturb.
Wackestone - repl., calc. bioclasts, calc. dissol., pelites
Wackestone - med. to lt. grey, repl., fluid., shell frags, calc. dissol.
Wackestone - weak fluid., pelites
Wackestone - pelites, mod. fluid. and bioturb., 1st and 2nd deg. repl.
Packstone - fluid., high conc. of shell frags
Packstone - white, sparse calc. veins, limestone incls.
Wackestone - med. lt. grey, shell frags, weak to mod. bioturb., calc. veins, fluid., pelites, repl., bivalves
Rudstone - lt. olv. grey to olv. grey, silt grains, vuggy pores, slightly calc., blue silica and calc. veins, mod. bioturb., few bioclasts
Mudstone - med. lt. grey, strong bioturb.

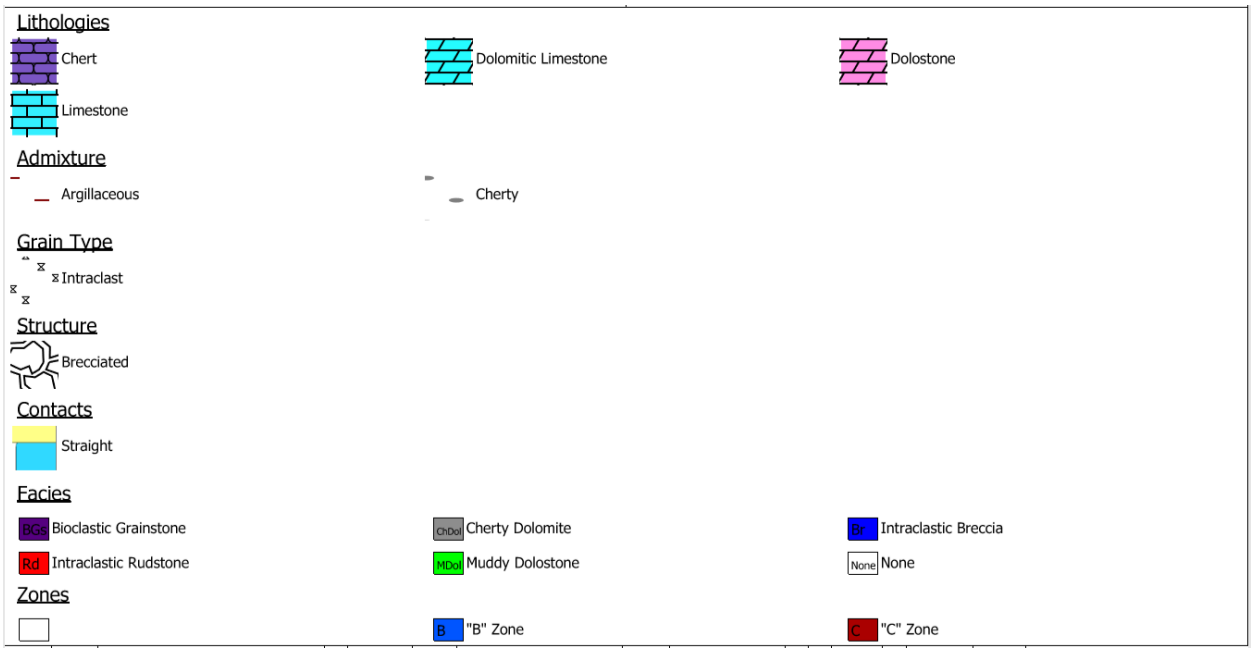

Figure 3.19: Revised description of core displaying revised facies names, well log facies, and original macro-descriptions. Original macro-facies were modified into the current facies names using the Dunham and Modified Dunham classification scheme after petrographic analysis. Rocks units on the column were categorized by grain size using the Wentworth scale in the "Original Core Description Profile" column. Abbreviations for the Wentworth scale are the following: BD (boulder), CB (cobble), PB (pebble), GR (granule), vcU (very coarse-upper), vcL (very coarse-lower), cU (coarse-upper), cL (coarse-lower), s (silt), c (clay). Facies name abbreviations are the following: Rd (rudstone), Br (breccia), ChDol (cherty dolomite), MDol (muddy dolostone), and BGs (grainstone).

3.7 Elemental concentrations

Elemental concentrations were recorded at two-inch intervals for major elements and six-inch intervals for trace elements. The elements in the major table are reported in weight percent (Table 3.1), and the elements in the trace table are reported in ppm (Table 3.2). Elemental concentrations were plotted along depth to display variations in concentrations (Figure 3.20).

Readings were taken at two-inch intervals along the core, but only the readings taken at six-inch intervals were used to compare to the core description and log data, due to wireline data being taken in six-inch intervals.

DEPTH	Mg	Al	Si	P	S	K	Ca	Ti	Mn	Fe
5808.00	1.7	0.2	4.5	0.0	0.2	0.0	8.6	0.0	0.0	1.0
5808.17	4.9	0.6	6.6	0.1	0.2	0.4	19.0	0.0	0.0	0.7
5808.33	6.5	0.5	4.8	0.1	0.3	0.3	20.9	0.0	0.0	0.8
5808.50	5.6	0.3	3.8	0.0	0.2	0.2	20.6	0.0	0.0	0.8
5808.67	4.6	0.3	2.7	0.1	0.2	0.2	20.8	0.0	0.0	0.7
5808.83	2.1	0.3	3.6	0.0	0.3	0.1	14.4	0.0	0.0	0.8
5809.00	2.6	0.2	4.0	0.1	0.2	0.2	16.0	0.0	0.0	0.8
5809.17	3.4	0.4	5.0	0.5	0.3	0.3	15.8	0.0	0.0	0.9
5809.33	4.0	0.3	4.0	0.3	0.5	0.2	19.5	0.0	0.0	1.0
5809.50	4.6	0.5	4.8	0.1	0.2	0.2	20.9	0.0	0.0	0.6
5809.67	6.1	0.4	3.3	0.0	0.4	0.1	23.9	0.0	0.0	0.9
5809.83	6.4	0.1	3.8	0.1	0.3	0.1	25.2	0.0	0.0	0.6
5810.00	3.8	0.0	3.3	0.1	0.2	0.1	21.4	0.0	0.0	0.7
5810.17	4.3	0.3	2.6	0.0	0.8	0.1	23.3	0.0	0.0	1.1
5810.33	4.6	0.0	1.9	0.0	0.3	0.0	24.0	0.0	0.0	0.5
5810.67	6.9	0.0	1.7	0.0	0.2	0.0	24.2	0.0	0.0	0.5
5810.83	5.7	0.0	1.9	0.0	0.2	0.0	23.6	0.0	0.0	0.6
5811.00	4.3	0.0	2.7	0.0	0.2	0.0	19.6	0.0	0.0	0.6
5811.17	4.1	0.0	3.3	0.0	0.3	0.0	21.4	0.0	0.0	0.6
5811.33	2.8	0.2	3.6	0.1	2.8	0.0	20.5	0.0	0.0	2.8
5811.50	0.0	0.0	6.4	0.0	0.8	0.0	0.9	0.0	0.0	0.7
5811.67	3.1	0.1	7.0	0.0	0.7	0.0	17.4	0.0	0.0	0.8
5811.83	0.1	0.3	13.1	0.0	0.9	0.0	2.0	0.0	0.0	0.5
5812.00	8.8	0.0	1.7	0.0	0.3	0.0	23.5	0.0	0.0	0.5
5812.25	2.0	0.0	2.0	0.0	0.2	0.0	17.1	0.0	0.0	0.6
5812.42	1.8	0.1	8.7	0.0	0.2	0.0	15.2	0.0	0.0	0.4
5812.58	2.1	0.2	20.5	0.1	0.2	0.0	7.8	0.0	0.0	0.1
5812.75	4.2	0.3	8.9	0.0	0.3	0.1	18.8	0.0	0.0	0.3
5812.92	2.3	0.8	5.8	0.0	0.4	0.2	14.9	0.0	0.0	0.6
5813.08	0.9	0.1	2.9	0.0	0.3	0.0	15.4	0.0	0.0	0.5
5813.17	0.6	1.2	13.4	0.0	0.9	0.0	1.5	0.0	0.0	0.4
5813.33	0.9	0.7	21.3	0.1	0.2	0.3	5.8	0.0	0.0	0.2
5813.50	0.0	0.2	35.1	0.0	0.2	0.0	1.0	0.0	0.0	0.0
5813.67	0.0	0.2	37.2	0.1	0.2	0.0	0.8	0.0	0.0	0.0
5813.83	0.9	1.3	6.7	0.1	0.3	0.4	8.3	0.0	0.0	0.9
5814.00	0.0	0.2	2.9	0.0	0.3	0.0	0.2	0.0	0.0	1.1
5814.17	3.8	0.7	6.6	0.2	0.2	0.3	18.2	0.0	0.0	0.7
5814.33	5.8	0.2	3.8	0.0	0.3	0.1	21.3	0.0	0.0	0.6
5814.50	3.0	0.3	2.8	0.0	0.3	0.0	13.2	0.0	0.0	0.7
5814.67	5.5	0.2	2.3	0.0	0.2	0.1	18.7	0.0	0.0	0.6
5814.83	5.0	0.3	2.5	0.0	0.3	0.0	18.6	0.0	0.0	0.7
5815.08	0.1	0.3	3.2	0.0	0.3	0.0	0.8	0.0	0.0	1.1
5815.25	7.8	0.2	7.4	0.1	0.2	0.1	22.0	0.0	0.0	0.4
5815.42	0.8	0.3	14.9	0.1	0.3	0.0	3.8	0.0	0.0	0.4
5815.58	1.5	0.2	15.2	0.1	0.2	0.1	8.3	0.0	0.0	0.1
5815.75	4.8	0.4	13.7	0.1	0.2	0.2	19.1	0.0	0.0	0.5
5815.92	1.4	0.4	28.1	0.1	0.2	0.0	3.4	0.0	0.0	0.0
5816.08	3.1	0.3	17.8	0.2	0.2	0.1	12.3	0.0	0.0	0.2
5816.25	0.7	0.5	18.2	0.1	0.3	0.0	2.9	0.0	0.0	0.3
5816.42	0.7	0.5	18.6	0.1	0.4	0.0	2.8	0.0	0.0	0.4
5816.58	1.0	0.4	17.1	0.1	0.4	0.0	4.6	0.0	0.0	0.5
5816.75	4.7	0.0	3.5	0.0	0.2	0.1	20.9	0.0	0.0	0.6
5818.50	0.7	0.3	18.4	0.1	0.5	0.0	4.1	0.0	0.0	0.3
5818.67	1.5	0.4	24.5	0.1	0.7	0.0	5.3	0.0	0.0	0.1
5818.83	0.5	0.2	14.5	0.0	0.2	0.0	2.8	0.0	0.0	0.6
5819.00	2.2	0.1	15.7	0.1	0.2	0.0	7.1	0.0	0.0	0.3
5819.17	2.7	0.2	22.6	0.1	0.2	0.0	9.4	0.0	0.0	0.0
5819.33	0.5	0.2	15.6	0.1	0.2	0.0	5.4	0.0	0.0	0.5
5819.50	0.6	0.3	12.8	0.0	0.3	0.0	3.1	0.0	0.0	0.7
5819.67	0.6	0.2	14.0	0.0	0.3	0.0	4.6	0.0	0.0	0.4
5819.83	0.9	0.3	22.6	0.1	0.3	0.0	4.3	0.0	0.0	0.1
5820.00	0.0	0.4	4.6	0.0	0.3	0.0	0.6	0.0	0.0	1.1
5820.17	9.1	0.0	2.9	0.0	0.2	0.0	25.2	0.0	0.0	0.5
5820.83	5.8	0.1	6.4	0.0	0.3	0.0	21.3	0.0	0.0	0.4
5821.00	1.3	0.3	16.5	0.1	0.3	0.0	4.3	0.0	0.0	0.3
5821.17	5.3	0.0	4.3	0.0	0.2	0.1	23.5	0.0	0.0	0.5
5821.33	0.7	0.3	20.1	0.1	0.3	0.0	2.7	0.0	0.0	0.2
5821.50	1.2	0.2	32.6	0.1	0.2	0.0	4.1	0.0	0.0	0.0
5821.67	1.3	0.2	20.9	0.1	0.2	0.0	6.6	0.0	0.0	0.0
5821.83	1.7	0.5	30.0	0.2	0.2	0.1	4.9	0.0	0.0	0.0
5822.00	0.7	0.3	20.0	0.1	0.2	0.1	6.6	0.0	0.0	0.1
5822.17	9.1	0.4	3.3	0.0	0.2	0.2	25.8	0.0	0.0	0.4

5822.33	0.5	0.0	40.5	0.1	0.2	0.0	0.5	0.0	0.0	0.0
5822.50	8.4	0.3	3.0	0.0	0.3	0.3	25.5	0.0	0.0	0.5
5822.67	5.8	0.2	2.9	0.0	0.3	0.2	23.2	0.0	0.0	0.6
5822.83	7.4	0.4	4.7	0.0	0.2	0.2	24.3	0.0	0.0	0.5
5823.00	3.5	0.5	19.3	0.1	0.2	0.2	11.1	0.0	0.0	0.1
5823.17	5.1	0.7	12.2	0.1	0.2	0.3	16.7	0.1	0.0	0.2
5823.33	1.6	0.3	2.6	0.0	0.4	0.0	11.4	0.0	0.0	0.9
5823.50	4.1	0.4	9.1	0.1	0.3	0.1	13.7	0.0	0.0	0.5
5823.67	6.0	0.5	4.1	0.2	0.4	0.2	20.0	0.0	0.0	0.7
5823.83	7.9	0.6	3.9	0.1	0.3	0.4	25.3	0.1	0.0	0.5
5824.00	0.7	0.7	28.6	0.1	0.5	0.1	1.7	0.0	0.0	0.0
5824.17	8.5	0.3	2.9	0.0	0.3	0.2	25.8	0.0	0.0	0.4
5824.33	8.2	0.4	3.1	0.0	0.3	0.2	24.8	0.0	0.0	0.5
5824.50	5.6	0.8	11.3	0.2	0.3	0.4	18.5	0.0	0.0	0.5
5824.67	4.2	1.2	14.7	0.2	0.3	0.7	14.9	0.1	0.0	0.5
5824.83	2.1	0.6	2.7	0.0	0.2	0.1	42.3	0.0	0.0	0.7
5825.00	1.8	0.7	27.7	0.2	0.7	0.1	10.7	0.0	0.0	0.0
5825.17	8.8	0.9	4.6	0.1	0.3	0.4	25.4	0.1	0.0	0.5
5825.33	7.0	0.6	3.7	0.0	0.3	0.3	25.9	0.0	0.0	0.5
5825.50	2.8	0.6	5.9	0.1	0.3	0.1	11.5	0.0	0.0	0.8
5825.83	8.0	0.4	3.2	0.0	0.3	0.3	25.0	0.0	0.0	0.6
5826.00	1.3	0.7	19.5	0.1	0.9	0.1	5.4	0.0	0.0	0.4
5826.08	4.9	0.7	5.9	0.1	0.4	0.4	22.3	0.1	0.0	0.6
5826.17	5.4	0.6	5.7	0.1	0.5	0.3	21.7	0.0	0.0	0.8
5826.33	4.8	0.4	3.2	0.0	0.3	0.2	26.9	0.0	0.0	0.7
5826.50	6.4	0.3	5.1	7.6	1.9	0.5	23.2	0.1	0.0	1.4
5826.67	5.7	1.1	5.6	0.4	0.6	0.5	24.9	0.1	0.0	0.8
5826.83	7.2	0.4	3.3	0.4	0.4	0.3	25.9	0.0	0.0	0.7
5827.00	5.7	1.5	11.6	0.1	0.7	0.6	15.7	0.1	0.0	0.7
5827.17	9.0	0.9	4.3	0.1	0.6	0.5	26.0	0.1	0.0	0.6
5827.33	7.3	1.0	4.6	0.0	0.6	0.5	24.3	0.1	0.0	0.7
5827.50	7.3	0.9	4.7	0.1	0.4	0.5	24.0	0.1	0.0	0.6
5827.67	0.9	0.4	3.4	0.0	0.7	0.3	15.4	0.3	0.0	0.5
5827.83	7.3	1.1	5.5	0.1	1.1	0.6	23.2	0.1	0.0	0.7
5828.00	2.7	0.4	2.8	0.0	0.3	0.2	36.8	0.0	0.0	0.7
5828.17	4.8	0.8	4.9	0.1	0.5	0.4	28.6	0.1	0.0	0.6
5828.33	0.6	0.7	28.5	0.1	1.3	0.0	1.2	0.0	0.0	0.3
5828.50	4.4	0.2	2.9	0.1	0.6	0.2	23.9	0.0	0.0	0.7
5828.67	3.7	0.6	3.8	0.0	0.8	0.4	21.0	0.1	0.0	0.6
5828.83	3.9	0.4	3.5	0.1	0.3	0.3	22.3	0.0	0.0	0.6
5829.00	7.2	0.7	4.1	0.0	0.3	0.4	25.9	0.1	0.0	0.5
5829.17	9.0	0.8	4.3	0.0	0.4	0.4	24.7	0.1	0.0	0.7
5829.33	5.7	0.7	4.1	0.0	0.4	0.4	22.8	0.1	0.0	0.6
5829.50	4.3	0.5	4.1	0.0	0.3	0.3	21.2	0.0	0.0	0.6
5829.67	5.2	0.4	3.8	0.0	0.4	0.2	20.1	0.0	0.0	0.6
5829.83	6.3	0.5	3.5	0.1	0.4	0.2	27.5	0.0	0.0	0.6
5830.00	5.0	0.5	4.0	0.1	0.4	0.3	23.4	0.0	0.0	0.7
5830.17	6.4	0.6	4.0	0.1	0.4	0.2	28.5	0.0	0.0	0.7
5830.33	9.6	1.2	5.2	0.0	0.4	0.5	25.1	0.1	0.0	0.6
5830.50	1.8	0.1	2.9	0.0	0.4	0.2	15.4	0.0	0.0	0.6
5830.67	5.5	0.2	3.0	0.0	0.3	0.1	23.3	0.0	0.0	0.8
5830.83	6.6	0.3	3.1	0.0	0.3	0.3	24.1	0.0	0.0	0.6
5831.00	7.0	0.3	4.3	0.1	0.4	0.1	23.6	0.0	0.0	0.7
5831.17	6.9	0.5	4.0	0.8	0.9	0.2	26.7	0.0	0.0	1.0
5831.33	7.8	0.6	5.4	0.2	0.6	0.3	24.0	0.0	0.0	0.9
5831.50	7.5	0.8	4.4	0.0	0.4	0.4	24.2	0.1	0.0	0.6
5831.67	5.5	0.7	4.2	0.0	0.4	0.3	22.2	0.0	0.0	0.7
5831.83	6.3	0.7	4.5	0.1	1.2	0.3	23.2	0.1	0.0	0.6
5832.00	6.2	1.0	5.3	0.1	0.4	0.5	22.3	0.1	0.0	0.7
5832.17	5.6	0.6	4.6	0.1	0.3	0.4	23.1	0.1	0.0	0.7
5832.33	5.6	0.7	5.0	0.1	0.3	0.4	22.2	0.1	0.0	0.7
5832.50	6.5	0.8	5.0	0.1	0.3	0.4	22.9	0.1	0.0	0.6
5832.67	3.0	1.1	17.1	0.1	0.7	0.4	10.3	0.1	0.0	0.4
5832.83	4.9	0.8	9.5	0.1	0.5	0.3	20.1	0.0	0.0	0.6
5833.00	4.1	0.8	17.8	0.1	0.5	0.3	14.4	0.0	0.0	0.3
5833.17	7.2	1.0	5.3	0.1	0.4	0.5	23.5	0.1	0.0	0.6
5833.33	4.9	0.9	4.8	0.1	0.3	0.4	24.8	0.1	0.0	0.6
5833.50	0.4	0.6	33.0	0.1	0.4	0.1	1.0	0.0	0.0	0.0
5833.67	2.5	0.8	16.1	0.1	0.6	0.3	11.1	0.0	0.0	0.5
5833.83	7.4	1.0	5.0	0.1	0.4	0.5	23.7	0.1	0.0	0.6
5834.00	0.2	0.3	38.4	0.1	0.4	0.0	0.4	0.0	0.0	0.0
5834.08	0.6	0.7	34.5	0.1	0.9	0.1	1.2	0.0	0.0	0.1
5834.17	7.4	0.9	4.6	0.1	0.4	0.5	24.3	0.1	0.0	0.6

5834.33	3.5	0.8	4.2	0.2	0.4	0.3	34.2	0.1	0.0	0.7
5834.50	7.6	0.9	4.4	0.1	0.5	0.4	25.4	0.1	0.0	0.8
5834.67	3.3	0.3	3.3	0.1	0.3	0.3	21.8	0.0	0.0	0.6
5834.83	6.0	1.1	5.5	0.1	0.5	0.6	22.4	0.1	0.0	0.7
5835.00	5.6	1.1	5.7	0.1	0.5	0.6	22.2	0.1	0.0	0.7
5835.17	5.7	0.9	4.7	0.1	0.3	0.4	25.3	0.1	0.0	0.6
5835.33	4.4	0.9	5.1	0.0	0.3	0.5	20.4	0.1	0.0	0.6
5835.50	0.9	0.9	28.8	0.1	0.6	0.3	3.6	0.0	0.0	0.2
5835.67	4.1	0.6	4.2	0.4	0.3	0.4	22.6	0.0	0.0	0.6
5835.83	3.6	0.5	4.0	0.1	0.3	0.2	31.4	0.0	0.0	0.8
5836.00	5.9	0.5	3.6	0.0	0.3	0.3	26.3	0.0	0.0	0.6
5836.17	5.5	2.0	6.9	0.1	0.7	1.1	19.7	0.2	0.0	1.4
5836.33	4.8	0.8	4.7	0.2	0.4	0.4	26.9	0.1	0.0	0.7
5836.50	4.8	0.7	4.6	0.0	0.5	0.4	20.5	0.1	0.0	0.8
5836.67	3.0	0.3	5.6	0.0	0.3	0.2	30.5	0.0	0.0	0.6
5836.83	4.5	0.6	4.5	0.1	0.6	0.3	29.4	0.0	0.0	0.7
5837.00	5.2	0.8	4.7	0.0	0.7	0.4	21.4	0.1	0.0	0.9
5837.17	6.0	0.8	4.8	0.1	0.6	0.5	22.6	0.1	0.0	0.7
5837.33	4.9	0.6	5.7	0.3	0.9	0.3	26.1	0.0	0.0	1.0
5837.50	4.8	0.6	4.1	0.2	0.4	0.3	23.7	0.0	0.0	0.9
5837.58	6.2	0.9	4.8	0.1	0.5	0.4	21.7	0.1	0.0	0.7
5837.75	5.2	0.7	4.6	0.1	0.4	0.3	26.7	0.0	0.0	0.5
5837.83	6.4	0.7	4.6	0.1	0.4	0.4	22.8	0.1	0.0	0.7
5838.00	6.1	0.9	4.9	0.1	0.6	0.4	22.5	0.1	0.0	0.8
5838.17	5.6	0.6	5.1	0.1	0.4	0.2	26.3	0.0	0.0	0.6
5838.33	5.2	1.2	5.6	0.1	1.2	0.6	21.0	0.1	0.0	0.8
5838.50	0.3	0.2	17.6	0.1	0.4	0.1	7.5	0.0	0.0	0.3
5838.67	5.2	1.1	9.9	0.2	0.8	0.4	18.0	0.1	0.0	0.7
5838.83	5.9	1.1	5.2	0.1	0.6	0.5	22.3	0.1	0.0	0.8
5839.00	4.2	0.7	9.3	1.7	0.7	0.3	25.5	0.1	0.0	1.0
5839.17	5.4	2.5	7.8	0.2	1.1	1.4	18.3	0.3	0.0	1.6
5839.33	2.3	0.3	3.0	0.1	1.1	0.2	13.9	0.0	0.0	0.9
5839.50	7.3	0.5	3.9	0.2	0.6	0.3	24.1	0.0	0.0	0.7
5839.67	7.7	0.5	4.2	0.5	0.5	0.3	23.9	0.0	0.0	0.8
5839.83	5.7	0.8	4.4	0.1	0.6	0.5	21.3	0.1	0.0	0.8
5840.00	2.0	0.6	26.3	0.3	0.5	0.2	6.0	0.0	0.0	0.2
5840.17	7.1	0.7	4.9	0.4	0.6	0.4	23.9	0.1	0.0	0.8
5840.33	7.0	1.4	5.9	0.6	0.9	0.6	21.5	0.1	0.0	1.3
5840.50	7.8	0.9	4.7	0.1	0.5	0.4	24.4	0.1	0.0	0.7
5840.67	5.7	1.3	5.8	0.1	1.5	0.7	21.0	0.1	0.0	1.0
5840.83	5.3	1.2	5.4	0.1	0.9	0.6	21.6	0.1	0.0	0.9
5841.00	5.9	0.4	3.7	0.3	0.5	0.4	22.4	0.1	0.0	0.9
5841.17	7.3	0.0	2.6	0.1	0.4	0.1	24.4	0.0	0.0	0.7
5841.33	6.0	0.2	3.1	0.2	0.4	0.2	23.2	0.0	0.0	0.7
5841.50	8.8	0.1	2.4	0.0	0.4	0.2	25.9	0.0	0.0	0.6
5841.67	7.9	0.0	2.2	0.0	0.4	0.1	24.7	0.0	0.0	0.6
5841.83	7.5	0.0	2.1	0.0	0.4	0.1	24.9	0.0	0.0	0.6
5842.00	0.5	0.0	35.5	0.1	0.3	0.0	1.4	0.0	0.0	0.0
5842.17	5.4	0.1	3.4	1.2	1.2	0.2	21.5	0.0	0.0	0.7
5842.33	6.7	0.3	3.7	0.4	0.3	0.2	23.1	0.0	0.0	0.7
5842.50	6.0	0.1	3.7	0.7	0.3	0.2	23.1	0.0	0.0	0.8
5842.67	4.8	0.3	4.2	0.3	0.4	0.2	22.1	0.0	0.0	1.0
5842.83	8.1	0.7	4.2	0.2	0.4	0.4	23.9	0.1	0.0	0.7
5843.00	5.8	0.1	3.0	0.3	0.4	0.2	22.9	0.0	0.0	0.8
5843.17	7.0	0.2	3.4	0.6	0.5	0.2	22.9	0.0	0.0	0.9
5843.42	5.0	0.2	3.7	0.1	0.3	0.2	22.8	0.0	0.0	0.9
5843.50	4.3	0.2	3.2	0.0	0.4	0.2	19.9	0.0	0.0	1.0
5843.67	6.7	0.4	4.1	0.3	0.4	0.2	24.0	0.0	0.0	0.9
5843.83	6.4	0.6	4.1	0.1	0.4	0.3	23.3	0.1	0.0	0.8
5844.00	6.1	0.9	5.2	0.1	0.4	0.5	21.5	0.1	0.0	0.8
5844.17	4.2	0.5	4.6	0.3	0.4	0.3	21.7	0.0	0.0	0.7
5844.33	5.5	0.5	4.9	0.1	0.4	0.3	21.9	0.0	0.0	0.7
5844.50	6.5	0.4	4.0	0.1	0.4	0.2	22.9	0.0	0.0	0.7
5844.67	4.3	0.2	4.6	0.1	0.3	0.1	20.2	0.0	0.0	0.6
5844.83	5.4	0.3	3.9	0.1	0.3	0.2	21.7	0.0	0.0	0.7
5845.00	3.6	0.4	4.2	0.0	0.5	0.3	17.7	0.0	0.0	0.7
5845.17	4.0	0.5	5.2	0.3	0.6	0.3	19.4	0.0	0.0	0.9
5845.33	7.1	0.6	5.1	0.2	0.5	0.3	22.7	0.0	0.0	0.7
5845.50	5.4	0.5	4.6	0.4	0.7	0.3	21.7	0.0	0.0	0.6
5845.67	6.1	0.4	4.3	0.1	0.4	0.2	23.1	0.0	0.0	0.7
5845.83	7.0	0.7	4.9	0.1	0.3	0.4	23.0	0.1	0.0	0.7
5846.00	6.4	0.6	5.5	0.1	0.4	0.3	22.8	0.0	0.0	0.7
5846.17	3.3	0.4	5.3	0.1	0.3	0.2	19.4	0.0	0.0	0.9

5846.33	6.0	0.7	4.8	0.0	0.5	0.4	22.1	0.1	0.0	0.7
5846.50	5.7	0.6	5.6	0.1	0.3	0.3	21.1	0.0	0.0	0.7
5846.67	7.0	1.0	6.1	0.1	0.4	0.5	22.3	0.1	0.0	0.7
5846.83	5.2	0.7	5.0	0.0	0.4	0.4	21.1	0.1	0.0	0.7
5847.00	5.5	0.7	5.4	0.1	0.3	0.4	22.3	0.1	0.0	0.6
5847.17	0.4	0.5	25.5	0.1	0.5	0.0	1.5	0.0	0.0	0.1
5847.33	6.6	0.8	5.3	0.0	0.2	0.4	22.9	0.1	0.0	0.5
5847.50	0.6	0.3	30.9	0.1	0.2	0.0	2.1	0.0	0.0	0.0
5847.67	6.1	0.7	4.9	0.1	0.2	0.4	22.7	0.0	0.0	0.5
5847.83	3.8	0.2	3.9	0.0	0.2	0.2	19.3	0.0	0.0	0.7
5848.00	5.7	0.5	4.3	0.0	0.2	0.4	22.4	0.0	0.0	0.5
5848.17	5.6	0.8	5.3	0.0	0.3	0.4	22.2	0.1	0.0	0.5
5848.33	3.7	0.4	4.3	0.0	0.2	0.3	21.5	0.0	0.0	0.5
5848.50	1.0	0.6	24.8	0.1	0.3	0.1	4.3	0.0	0.0	0.0
5848.67	6.6	0.5	4.3	0.0	0.2	0.3	23.4	0.0	0.0	0.5
5848.83	5.7	0.6	5.3	0.1	0.2	0.3	21.9	0.0	0.0	0.7
5849.00	5.5	0.6	4.5	0.0	0.2	0.3	22.2	0.0	0.0	0.5
5852.17	3.4	0.3	4.5	0.0	0.3	0.2	19.5	0.0	0.0	0.6
5852.33	5.9	0.7	5.8	0.1	0.3	0.3	21.6	0.0	0.0	0.6
5852.50	6.1	0.6	5.6	0.0	0.3	0.3	21.8	0.0	0.0	0.6
5852.67	5.4	0.6	6.1	0.0	0.3	0.3	20.4	0.0	0.0	0.6
5852.83	3.4	0.5	5.4	0.0	0.4	0.4	19.0	0.0	0.0	0.6
5853.00	3.4	0.6	5.6	0.0	0.3	0.3	19.4	0.1	0.0	0.6
5853.17	4.8	0.8	6.7	0.1	0.5	0.4	19.8	0.1	0.0	0.6
5853.33	0.1	0.1	25.3	0.0	0.4	0.0	1.2	0.0	0.0	0.0
5853.50	5.0	0.6	6.2	0.0	0.6	0.4	20.2	0.1	0.0	0.5
5853.67	7.2	0.8	6.8	0.0	0.5	0.4	21.6	0.1	0.0	0.6
5853.83	4.9	0.4	5.3	0.0	0.5	0.3	20.6	0.0	0.0	0.6
5854.00	3.9	0.5	5.6	0.1	0.4	0.4	19.7	0.0	0.0	0.6
5854.17	6.9	0.8	6.2	0.1	0.5	0.4	20.6	0.1	0.0	0.7
5854.33	5.7	0.8	6.1	0.0	0.5	0.4	20.9	0.1	0.0	0.6
5854.50	2.1	0.4	8.6	0.0	0.4	0.2	12.3	0.0	0.0	0.6
5856.17	5.1	0.7	5.9	0.1	0.7	0.4	18.6	0.1	0.0	0.9
5856.33	6.5	0.9	10.3	0.1	0.5	0.4	18.2	0.1	0.0	0.6
5856.50	6.4	0.9	6.3	0.1	0.9	0.5	20.3	0.1	0.0	0.7
5856.67	6.6	0.9	6.2	0.1	0.6	0.4	21.4	0.1	0.0	0.6
5856.83	5.3	0.8	5.8	0.1	0.8	0.4	20.5	0.1	0.0	0.7
5857.00	6.2	0.8	5.5	0.1	0.8	0.4	21.1	0.1	0.0	0.7
5857.17	4.4	0.8	5.7	0.1	0.7	0.5	19.3	0.1	0.0	0.8
5857.33	3.8	0.6	5.8	0.1	0.4	0.3	18.2	0.0	0.0	0.8
5857.50	6.6	0.7	5.1	0.1	0.6	0.4	21.4	0.1	0.0	0.7
5857.67	6.5	0.8	5.1	0.1	0.7	0.4	21.7	0.1	0.0	0.8
5857.83	5.9	0.7	4.9	0.1	0.4	0.4	20.5	0.0	0.0	0.7
5858.00	6.5	0.7	5.1	0.4	0.4	0.4	20.3	0.1	0.0	0.7
5858.17	5.9	0.8	5.2	0.1	0.4	0.4	19.8	0.0	0.0	0.7
5858.33	2.5	0.3	9.9	0.0	0.3	0.2	15.3	0.0	0.0	0.6
5858.50	5.6	1.0	6.4	0.3	0.5	0.5	21.1	0.1	0.0	0.8
5858.67	6.2	1.2	6.1	0.1	0.9	0.6	20.0	0.1	0.0	0.8
5858.83	3.9	0.7	5.2	0.1	0.5	0.4	19.2	0.1	0.0	0.7
5859.00	4.5	0.7	5.1	0.1	0.9	0.4	20.5	0.1	0.0	0.7
5859.17	0.7	0.4	32.9	0.1	0.8	0.0	2.0	0.0	0.0	0.0
5859.33	3.7	0.4	7.3	0.0	0.4	0.2	16.9	0.0	0.0	0.6
5859.50	6.5	1.0	5.9	0.1	0.5	0.4	22.3	0.1	0.0	0.7
5859.67	5.2	1.1	5.9	0.1	0.5	0.6	20.2	0.1	0.0	0.7
5859.83	2.6	1.0	5.4	0.0	0.4	0.5	16.9	0.1	0.0	0.7
5860.00	5.1	1.8	5.2	0.2	1.7	0.7	23.8	0.2	0.0	1.1
5860.17	5.7	0.9	4.6	0.1	0.5	0.5	22.1	0.1	0.0	0.7
5860.33	2.5	0.4	3.8	0.0	0.4	0.3	16.0	0.0	0.0	0.8
5860.50	7.8	0.6	3.8	0.0	0.4	0.3	24.2	0.0	0.0	0.6
5860.67	6.9	0.6	4.0	0.1	0.4	0.3	23.9	0.0	0.0	0.6
5860.83	4.9	0.3	3.5	0.0	0.4	0.2	21.7	0.0	0.0	0.7
5861.00	4.0	0.1	3.0	0.0	0.4	0.2	23.2	0.0	0.0	0.7
5861.17	6.3	0.5	4.2	0.0	0.4	0.3	22.4	0.0	0.0	0.7
5861.33	6.8	0.6	4.1	0.0	0.4	0.3	23.3	0.0	0.0	0.7
5861.50	6.1	0.7	4.3	0.0	0.4	0.3	22.9	0.1	0.0	0.6
5861.67	7.5	0.7	4.5	0.1	0.4	0.3	23.1	0.0	0.0	0.7
5861.83	5.7	0.5	4.4	0.1	0.4	0.3	22.6	0.0	0.0	0.7
5862.00	5.2	0.5	4.1	0.0	0.4	0.3	21.3	0.0	0.0	0.7
5863.50	3.2	0.2	4.4	0.0	0.3	0.2	20.0	0.0	0.0	0.6
5863.67	5.7	0.7	4.9	0.1	0.4	0.3	22.4	0.0	0.0	0.7
5863.83	6.6	0.8	5.1	0.1	0.4	0.4	21.9	0.1	0.0	0.7
5864.00	6.1	1.0	6.0	0.1	0.5	0.4	21.9	0.1	0.0	0.8
5864.17	5.4	0.9	5.6	0.1	0.4	0.4	21.4	0.1	0.0	0.7

5864.33	6.0	1.1	6.6	0.1	0.4	0.4	21.9	0.1	0.0	0.8
5864.50	3.4	1.0	5.9	0.0	0.5	0.5	17.6	0.1	0.0	0.8
5864.67	6.0	1.0	6.3	0.2	0.7	0.5	21.0	0.1	0.0	0.9
5864.83	5.7	1.0	6.2	0.1	0.6	0.5	21.7	0.1	0.0	0.7
5865.00	6.5	1.0	6.0	0.1	0.5	0.5	22.8	0.1	0.0	0.7
5865.17	3.8	1.2	6.9	0.1	0.6	0.7	18.5	0.1	0.0	0.9
5865.33	5.0	1.1	6.7	0.1	0.7	0.5	21.0	0.1	0.0	0.7
5865.50	5.8	1.1	7.5	0.1	1.2	0.6	20.2	0.1	0.0	0.8
5865.67	5.7	1.3	6.3	0.1	0.8	0.7	20.3	0.1	0.0	0.9
5865.83	4.7	1.3	13.3	0.1	0.6	0.6	15.5	0.1	0.0	0.7
5866.00	4.3	1.3	7.3	0.1	0.6	0.7	18.5	0.1	0.0	0.8
5866.08	0.3	0.5	33.3	0.1	0.4	0.2	3.9	0.0	0.0	0.0
5866.17	5.9	1.5	6.1	0.1	2.0	0.8	21.5	0.1	0.0	0.8
5866.33	6.1	1.4	7.3	0.0	0.5	0.7	21.5	0.1	0.0	0.7
5866.50	5.5	1.4	7.1	0.0	0.4	0.7	21.4	0.1	0.0	0.6
5866.67	0.2	0.6	33.1	0.1	0.3	0.2	1.7	0.0	0.0	0.0
5866.83	5.2	1.7	7.7	0.1	1.3	0.8	20.7	0.1	0.0	0.8
5867.00	2.1	0.5	2.2	0.0	0.3	0.1	43.5	0.1	0.0	0.6
5867.17	5.7	1.2	8.2	0.1	1.7	0.5	20.2	0.1	0.0	0.7
5867.33	4.3	1.4	8.3	0.1	0.5	0.7	16.3	0.1	0.0	1.0
5867.50	3.3	1.5	13.7	0.1	0.4	0.7	13.5	0.1	0.0	0.7
5867.67	3.0	1.0	5.7	0.0	0.4	0.6	16.6	0.1	0.0	0.9
5867.83	2.4	0.6	3.8	0.0	0.6	0.2	11.9	0.0	0.0	1.0
5868.00	3.1	0.8	4.9	0.0	0.8	0.4	13.8	0.1	0.0	1.1

Table 3.1: Elemental concentrations of major elements, reported in weight percentage. Negative values recorded were changed to a value of zero, due to the readings being below the detection limits of the machine.

	Co	Ni	Cu	Zn	Ga	As	Pb	Th	Rb	U	Sr	Y	Zr	Nb	Mo
5808	4.69	0.00	2.71	4.21	2.44	4.93	7.57	2.43	27.58	0.00	111.28	22.96	51.35	5.29	0.00
5808.5	5.08	0.00	1.37	5.69	2.41	2.24	7.22	2.48	33.96	0.00	105.56	16.45	43.19	5.51	0.00
5809	5.56	0.00	2.86	6.91	1.70	2.13	6.46	2.08	24.27	0.00	104.66	19.86	48.65	5.27	0.00
5809.5	6.23	15.20	7.92	6.76	4.34	20.67	13.33	3.35	20.61	24.36	184.17	67.75	44.60	10.35	0.00
5810	5.51	2.81	3.96	4.28	0.82	7.11	8.67	1.74	19.13	0.49	127.50	38.54	37.60	5.98	0.00
5810.5	5.35	0.04	2.53	13.96	0.40	4.76	7.47	1.97	23.66	0.00	118.42	18.46	36.87	4.69	0.00
5811	5.95	0.00	1.18	2.48	0.00	2.25	5.52	1.24	15.04	0.00	110.46	3.76	32.30	2.94	0.00
5811.5	5.83	0.00	0.00	0.00	0.00	5.60	6.35	0.80	17.04	1.41	34.09	0.00	32.08	4.69	0.00
5812	8.49	15.56	7.46	2.13	3.85	53.81	21.59	1.45	14.28	0.00	98.82	5.83	36.30	3.66	0.00
5812.5	5.36	0.00	3.33	0.00	0.01	0.52	6.11	1.39	13.19	0.46	135.04	5.70	31.64	2.63	0.00
5813	4.75	0.00	4.87	18.51	0.00	3.05	5.86	1.64	17.90	0.00	105.74	7.91	37.48	3.12	0.00
5813.5	4.96	0.00	3.67	42.44	1.07	0.00	4.92	1.59	22.50	1.93	89.75	2.36	34.25	3.77	0.00
5814	5.62	0.00	0.00	0.00	0.00	0.20	5.44	1.05	22.66	0.00	39.94	0.00	34.12	5.32	0.00
5814.5	5.35	0.00	0.00	0.00	0.00	0.00	3.88	1.30	20.66	2.10	50.02	0.00	37.12	4.61	0.00
5815	5.33	0.00	0.61	0.00	0.00	0.00	5.15	1.13	15.39	0.00	116.93	5.03	30.68	2.92	0.00
5815.6	4.80	0.00	0.00	0.00	0.00	0.00	4.49	1.73	22.95	0.94	155.64	1.95	26.87	6.84	0.00
5816.1	5.73	0.00	0.22	0.00	0.00	1.43	5.68	1.70	24.15	1.27	136.42	4.62	32.90	5.29	0.00
5816.6	5.33	0.00	0.00	0.00	0.00	0.00	4.18	1.77	26.73	0.08	125.05	4.60	32.83	4.21	0.00
5818.5	5.29	0.00	0.00	0.00	0.00	0.00	4.65	1.72	24.86	0.00	106.81	1.45	34.78	4.92	0.00
5819	4.82	0.00	0.00	0.00	0.00	0.00	3.50	1.69	24.65	2.57	112.46	0.00	30.50	5.25	0.00
5819.5	5.16	0.00	0.68	0.00	0.06	0.00	5.23	1.41	17.19	0.00	116.76	5.34	31.78	3.48	0.00
5820	6.09	0.00	0.46	0.00	0.00	0.00	2.93	1.38	25.18	0.00	115.34	0.00	32.34	3.52	2.27
5820.5	5.19	0.00	0.00	0.00	0.00	0.00	4.30	1.61	25.79	0.00	123.45	3.02	30.50	5.62	0.00
5821	5.08	0.00	0.68	0.00	0.00	0.00	4.69	1.27	16.97	0.00	77.06	0.89	31.93	3.81	0.00
5821.5	5.32	0.00	0.00	0.00	0.00	0.00	4.63	1.73	22.69	4.12	104.46	0.49	33.21	5.04	0.00
5822	6.08	0.00	0.00	0.00	0.00	1.27	5.78	1.32	20.23	0.00	49.69	0.00	32.65	5.47	0.00
5822.5	5.63	0.00	1.70	0.78	0.52	0.62	7.35	1.81	21.28	0.00	131.16	3.56	35.31	2.99	0.00
5823	5.53	0.61	2.20	2.23	0.00	0.76	5.17	1.52	16.75	0.00	88.38	7.43	38.15	3.35	0.00
5823.5	5.53	11.03	3.68	2.93	3.13	16.49	11.41	2.42	24.69	0.00	168.15	5.72	40.48	3.31	0.00
5824	5.20	0.00	0.00	0.00	0.00	0.00	3.73	1.27	24.83	0.00	49.92	0.00	34.88	5.77	0.00
5824.5	5.38	1.32	2.54	0.56	0.60	0.52	6.56	1.99	24.86	2.09	79.22	12.57	38.75	4.81	0.00
5825	5.07	2.98	0.00	0.00	0.21	15.14	11.34	1.50	18.53	4.75	54.24	0.70	38.95	5.48	0.00
5825.5	5.43	13.79	3.75	5.14	0.00	13.15	9.92	1.96	22.67	0.31	105.98	5.33	37.49	4.20	0.00
5826	5.47	1.62	1.93	0.41	0.13	4.92	7.46	1.24	16.59	0.00	91.32	1.28	34.57	2.88	0.00
5826.5	5.43	15.50	5.77	1.28	2.56	43.75	18.95	2.16	24.58	0.00	123.85	15.46	39.62	4.28	0.00
5827	4.89	0.00	0.00	0.00	1.50	9.86	9.97	2.66	37.05	0.00	72.23	8.28	44.62	6.36	0.00
5827.5	5.55	5.76	2.61	0.70	2.75	10.00	10.11	3.06	34.97	4.65	139.11	8.36	45.54	5.12	0.00
5828	5.58	4.81	7.42	2.90	2.33	10.74	9.20	1.66	22.13	0.00	52.60	9.34	44.34	1.89	0.00
5828.5	5.73	4.30	3.07	0.40	1.18	21.88	12.96	1.75	19.67	0.00	114.33	14.68	36.55	4.07	0.00
5829	5.07	0.88	1.98	0.00	2.09	2.28	7.77	2.26	31.02	0.00	107.46	8.73	38.98	4.46	0.00
5829.5	4.25	2.84	2.55	0.45	0.48	5.31	6.99	1.96	22.44	0.00	104.74	6.85	38.39	2.59	0.00
5830	5.46	8.35	6.14	3.57	2.08	19.98	13.08	1.72	15.09	1.30	104.31	12.89	37.85	3.33	0.00
5830.5	5.59	2.43	3.16	0.00	1.98	5.01	7.19	2.14	27.04	0.00	129.90	3.66	39.94	3.55	0.00
5831	4.82	0.00	0.35	0.00	0.00	2.92	6.43	1.46	16.68	2.11	115.15	0.89	33.82	3.71	0.00
5831.5	5.20	0.00	4.58	0.00	1.67	7.04	8.17	2.05	22.86	0.00	114.52	5.83	39.83	2.60	0.00
5832	6.03	4.28	4.44	8.27	2.26	7.12	8.49	2.66	31.63	0.00	105.45	9.08	47.72	3.47	0.00
5832.5	4.91	3.87	3.34	3.63	0.42	5.47	7.11	2.03	24.64	0.00	96.28	7.02	40.72	3.17	0.00
5833	5.28	0.00	0.00	0.00	0.00	3.57	6.05	1.33	24.16	3.62	47.88	0.00	35.63	4.66	0.00
5833.5	5.83	0.00	0.00	2.09	0.00	0.00	6.07	1.06	20.68	0.00	37.88	0.00	35.47	4.57	0.00
5834	5.75	0.00	0.00	0.00	0.00	0.83	5.31	1.43	23.53	2.24	43.95	0.00	34.06	4.99	0.00
5834.5	5.41	9.65	5.26	1.49	3.36	16.83	12.77	2.44	28.96	0.00	107.08	8.42	45.04	2.73	0.00
5835	5.14	1.93	2.14	1.83	1.47	3.54	8.32	3.20	40.36	1.52	117.83	7.98	47.29	3.54	0.00
5835.5	6.38	4.29	2.43	1.36	1.00	11.45	9.86	2.60	34.91	0.00	89.32	9.91	43.14	4.81	0.00
5836	5.38	0.04	3.12	0.00	1.39	6.94	8.12	1.66	18.67	0.00	101.96	4.37	38.30	2.66	0.00
5836.5	5.24	2.30	2.11	4.80	2.22	9.41	9.38	2.40	27.94	0.00	112.70	4.39	45.38	3.91	0.00
5837	6.51	8.08	3.58	2.38	2.17	16.01	11.01	2.60	30.34	2.69	126.42	8.23	47.08	3.72	0.00
5837.5	5.34	7.52	3.50	0.02	2.69	14.60	11.30	1.84	24.32	0.00	100.12	12.71	38.34	2.52	0.00
5838	5.26	13.06	3.41	3.72	2.98	19.80	12.22	2.65	29.87	0.00	117.89	7.36	46.42	3.14	0.00
5838.5	5.35	0.00	0.00	0.00	0.00	0.00	5.67	0.82	17.11	3.18	45.49	0.00	29.83	5.68	0.00
5839	5.47	14.82	8.48	12.54	5.93	45.56	20.18	2.35	23.31	0.69	115.11	34.23	43.16	5.44	0.00
5839.5	4.12	3.03	3.16	4.10	1.69	6.65	8.90	1.70	22.47	0.00	102.71	8.36	39.38	3.36	0.00
5840	5.40	5.94	2.78	0.00	0.26	17.39	11.49	1.58	18.30	0.00	105.10	11.25	35.75	2.58	0.00
5840.5	5.79	4.02	3.78	10.03	2.37	10.04	8.81	1.98	19.60	3.97	103.30	8.56	38.77	3.33	0.00
5841	5.66	5.08	4.25	0.55	2.71	10.06	10.53	2.58	32.10	0.00	121.36	10.52	41.71	3.48	0.00
5841.5	5.77	1.50	2.67	0.00	1.10	5.51	9.13	1.82	22.75	0.00	107.25	4.83	37.52	3.27	0.00
5842	5.52	0.00	1.45	0.77	0.00	5.77	7.39	1.49	19.56	0.00	90.80	9.67	34.54	3.24	0.00
5842.5	4.24	2.41	4.24	0.00	1.03	16.53	12.03	1.31	12.97	0.00	90.20	29.24	35.33	4.41	0.00
5843	4.74	0.85	3.52	0.00	0.64	12.48	9.47	1.18	13.76	0.00	89.89	7.88	35.28	3.52	0.00
5843.5	5.57	5.55	4.40	2.39	2.21	14.63	11.72	1.71	17.39	1.71	103.57	10.18	35.84	3.02	0.00
5844	6.28	5.55	4.09	4.60	2.60	12.19	11.07	2.39	30.20	0.00	116.66	9.33	41.27	2.53	0.00
5844.5	3.84	3.34	4.35	1.50	0.26	8.17	9.93	1.37	14.02	1.76	98.34	2.38	35.53	2.34	0.00
5845	5.12	4.02	5.48	9.85	0.82	8.55	9.29	2.48	33.92	0.00	115.51	9.70	41.32	3.27	0.33
5845.5	5.07	5.65	3.80	4.11	1.38	11.92	9.80	1.61	18.47	1.16	98.36	3.30	38.62	3.10	0.00
5846	5.88	2.36	3.91	2.63	0.43	14.41	10.19	1.80	25.38	0.00	95.87	5.10	37.19	3.38	0.00
5846.5	5.41	2.00	2.90	9.92	0.00	6.07	8.61	1.55	19.11	0.00	87.06	2.25	35.06	2.33	0.00
5847	4.91	7.70	5.33	6.80	1.64	8.46	8.92	2.45	29.21	0.00	108.17	8.77	44.64	2.95	0.00
5847.5	5.55	0.00	0.00	0.00	0.00	2.29	6.76	1.05	20.81	0.00	61.60	0.00	30.83	3.44	0.00
5848	5.57	0.00	2.31	0.00	0.77	0.00	6.13	2.25	29.32	0.00	126.25	7.34	38.97	3.45	0.00
5848.5	5.59	0.00	0.00	0.00	0.07	1.81	5.81	2.10	33.82	0.00	81.82	8.04	39.75	4.59	0.00
5849	5.21	0.00	2.93	0.20	0.66	0.11	6.15	2.21	26.62	0.00	126.67	9.65	39.71	3.73	0.00
5852.5	5.52	1.53	2.39	0.00	0.82	6.72	9.43	1.91	25.19	0.00	92.49	3.25	37.87	3.19	0.00
5853	4.62	0.35	0.08	0.00	0.00	8.11	6.60	1.52	25.20	0.00	87.22	1.00	33.81	4.36	0.00
5853.5	5.04	0.00	2.47	1.84	0.94	6.59	9.28	2.45	35.86	0.00	74.90	7.51	43.37	2.92	0.00
5854	5.40	1.19	2.77	1.40	2.76	10.86	8.93	2.65	34.89	0.00	87.64	6.67	45.72	3.17	0.00

Depth	Co	Ni	Cu	Zn	Ga	As	Pb	Th	Rb	U	Sr	Y	Zr	Nb	Mo
5854.5	5.50	0.00	0.85	0.00	0.00	3.86	7.87	1.74	25.93	0.00	69.36	3.88	38.46	3.29	0.00
5856.5	5.80	1.33	3.38	1.67	2.28	8.27	9.37	2.56	33.70	0.00	87.60	6.94	44.57	4.09	0.00
5857	4.46	5.58	4.51	0.12	3.77	11.88	11.43	2.47	30.26	0.00	94.44	7.06	44.56	4.14	0.00
5857.5	5.76	0.00	2.07	0.00	0.27	9.79	8.84	2.16	31.42	0.00	95.82	3.20	41.42	4.26	0.00
5858	4.42	2.77	3.90	3.10	1.87	7.69	8.24	2.34	32.49	0.00	92.93	5.83	41.91	3.27	0.00
5858.5	4.87	4.49	4.54	29.05	2.33	10.95	10.02	2.09	25.05	0.00	111.99	13.16	39.98	3.50	0.00
5859	5.38	0.00	9.99	171.37	1.23	8.56	9.83	2.47	34.90	0.00	104.84	8.10	41.89	3.87	0.00
5859.5	5.78	6.84	37.13	885.57	4.60	8.27	9.35	2.36	29.72	0.00	105.00	6.23	41.24	3.25	0.00
5860	7.72	28.60	9.23	14.43	6.19	48.99	22.04	4.70	56.26	0.00	91.73	24.03	76.62	6.34	0.00
5860.5	5.73	1.42	2.16	1.54	1.61	10.24	9.37	1.89	22.70	0.00	107.82	6.33	39.25	3.08	0.00
5861	5.52	2.17	2.37	0.02	0.24	10.06	8.98	1.73	20.00	0.00	105.52	4.89	35.55	3.37	0.00
5861.5	5.40	0.50	2.56	1.09	1.78	6.63	7.67	1.66	19.60	0.00	99.66	4.10	39.03	2.76	0.00
5862	5.71	2.64	4.17	6.01	0.83	8.11	9.45	1.92	22.75	0.00	111.48	7.36	37.85	2.98	0.00
5863.5	5.52	0.76	2.98	1.47	1.30	7.63	9.39	1.85	25.43	0.00	99.77	11.88	39.74	3.74	0.00
5864	4.52	4.65	2.85	6.93	1.50	11.57	10.47	2.20	25.79	0.32	104.51	5.36	40.78	3.04	0.00
5864.5	5.90	3.97	4.57	6.12	2.59	8.67	10.00	3.13	39.52	1.72	117.25	9.85	51.11	4.11	0.00
5865	5.75	0.00	1.66	74.62	0.56	7.31	8.58	1.65	24.23	0.59	59.61	0.00	38.74	4.65	0.00
5865.5	5.12	8.79	5.07	2.66	1.38	11.51	10.22	3.02	38.70	0.00	108.82	9.23	51.15	4.09	0.00
5866	7.53	7.24	2.78	1.12	2.77	14.63	10.67	2.65	37.06	0.00	89.49	7.08	46.25	4.15	0.00
5866.5	6.11	10.33	4.90	14.53	3.55	8.30	9.86	3.29	43.09	0.00	115.04	15.89	50.91	4.12	0.00
5867	5.53	3.45	8.12	3.34	2.77	6.22	8.87	1.56	14.03	0.00	75.22	9.66	39.30	2.22	0.00
5867.5	6.48	1.25	1.82	0.67	2.23	8.39	9.14	2.69	36.57	0.03	77.95	6.63	46.93	4.19	0.00
5868	7.12	12.97	6.02	3.27	3.60	17.18	12.26	3.82	47.64	0.00	119.32	14.85	58.04	4.67	0.00

Table 3.2: Elemental concentrations of trace elements, reported in ppm. Negative values recorded were changed to a value of zero, due to the readings being below the detection limits of the machine.

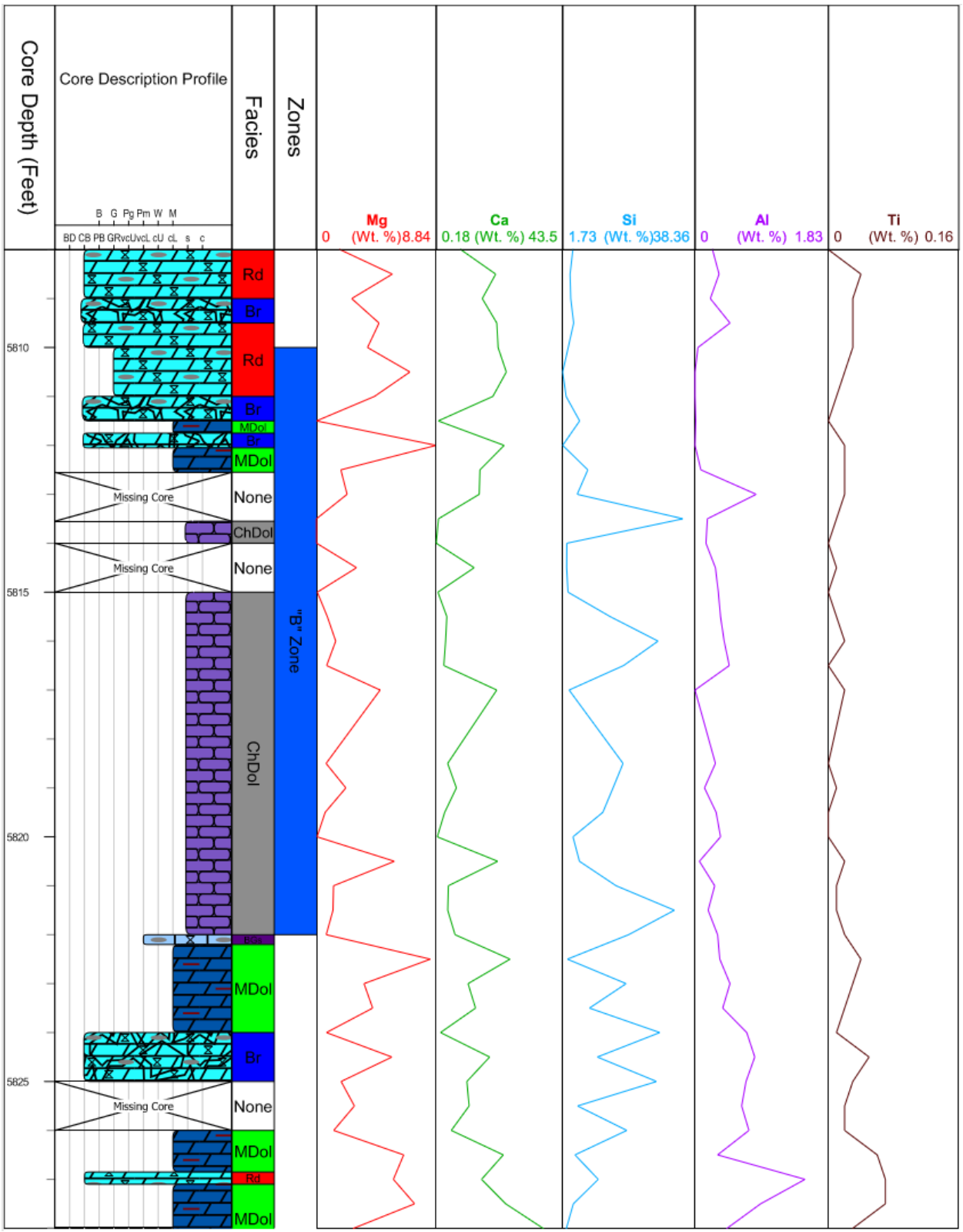
Core Depth (Feet)
Core Description Profile
Facies
Zones
Mg
0 (Wt. %)8.84
Ca
0.18 (Wt. %) 43.5
Si
1.73 (Wt. %)38.36
Al
0 (Wt. %) 1.83
Ti
0 (Wt. %) 0.16
B G Pg Pm W M
BD CB PB GRvcUvcL cU cL s c
5810
5815
5820
5825
Rd
Br
Rd
Br
MDol
Br
MDol
Missing Core
None
ChDol
Missing Core
None
"B" Zone
ChDol
Bios
MDol
Br
Missing Core
None
MDol
Rd
MDol

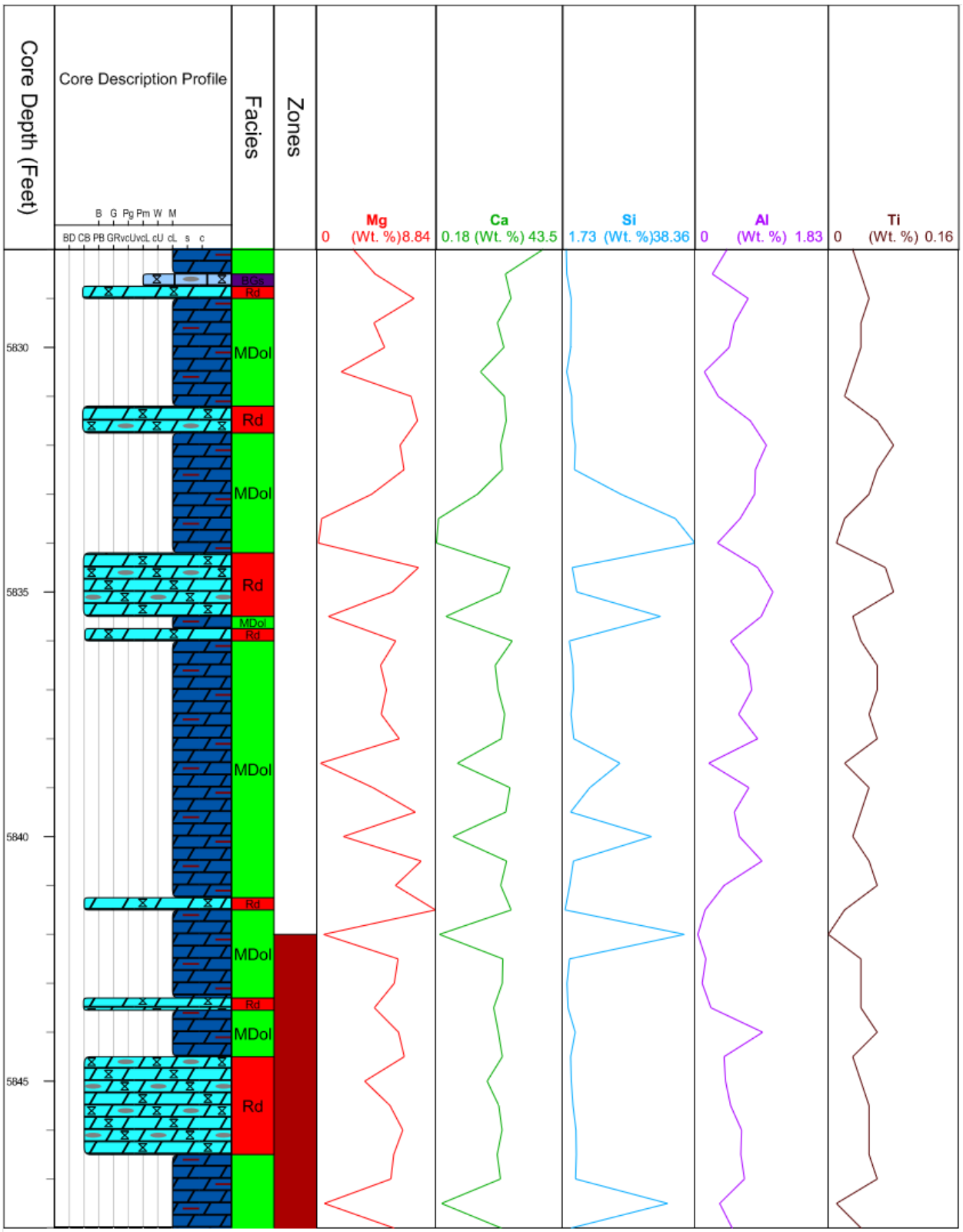
Core Depth (Feet)
Core Description Profile
B G Pg Pm W M
BD CB PB GR vcU vcL cU cL s c
Facies
Zones
Mg
0 (Wt. %) 8.84
Ca
0.18 (Wt. %) 43.5
Si
1.73 (Wt. %) 38.36
Al
0 (Wt. %) 1.83
Ti
0 (Wt. %) 0.16
5830
5835
5840
5845
BGs
Rd
MDol

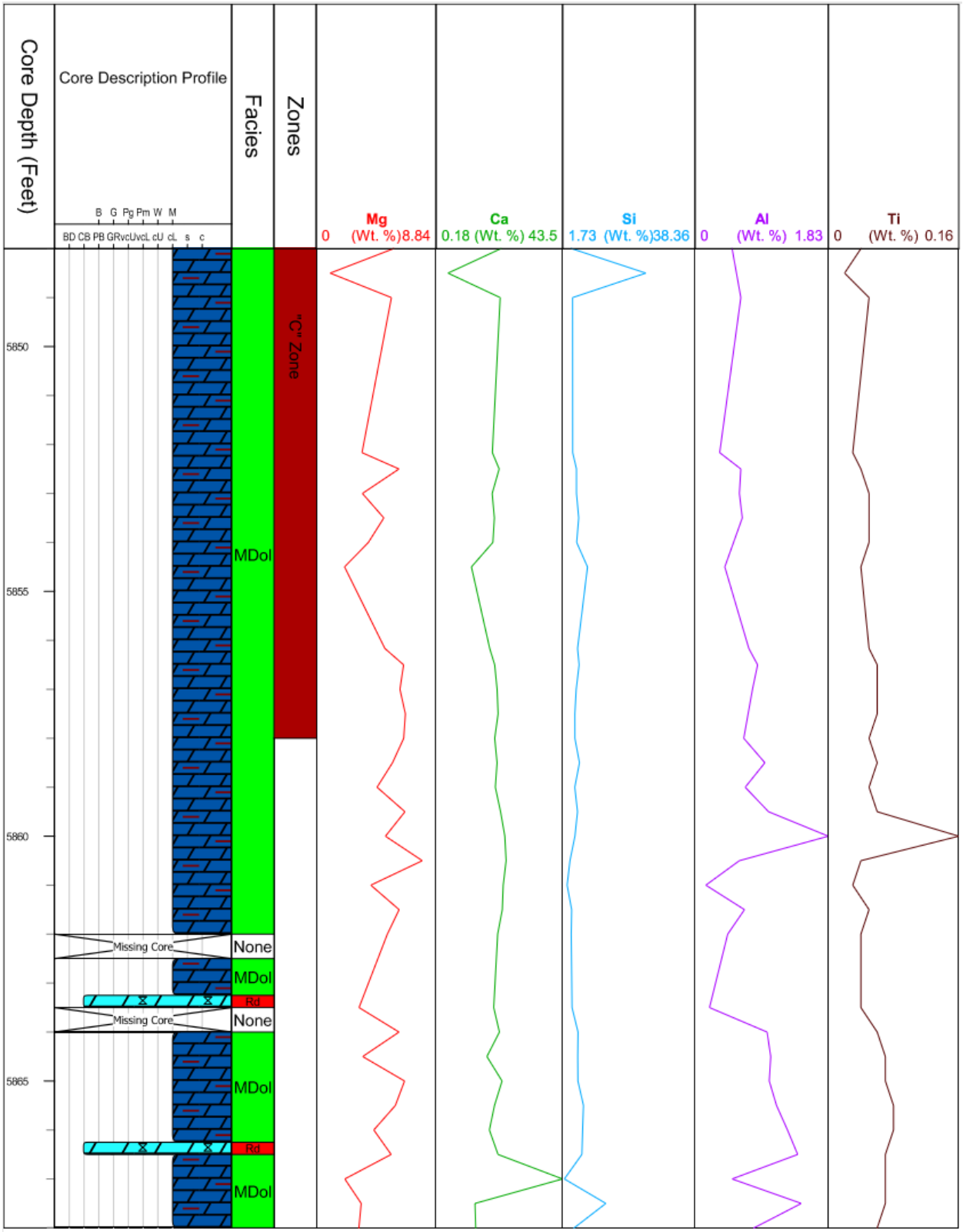
Core Depth (Feet)
Core Description Profile
B G Pg Pm W M
BD CB PB GR vcL UvcL cU cL s c
Facies
Zones
Mg
0 (Wt. %) 8.84
Ca
0.18 (Wt. %) 43.5
Si
1.73 (Wt. %) 38.36
Al
0 (Wt. %) 1.83
Ti
0 (Wt. %) 0.16
5850
5855
5860
5865
"C" Zone
MDol
Missing Core
None
MDol
Rd
Missing Core
None
MDol
Rd
MDol

Figure 3.20: Core description profile of Rich C-7 displaying well log facies, described facies from core, and six-inch HHXRF chemical data from Mg, Ca, Si, Al, and Ti.

Chapter 4 - Discussion

4.1 Depositional Environment of Facies

The depositional environments of facies were interpreted based on examination of core and petrographic analysis. Features including rock texture, abundance of intraclasts, shape of intraclasts, lithology of intraclasts, presence of specific carbonates, and type of fossils with the rock were used to determine the environment of deposition.

Cherty Dolomite

The depositional environment of the cherty dolomite is interpreted to be a shallow, low-energy marine environment with an abundance of siliceous organisms, potentially in a higher abundance compared to the amount of carbonate organisms in the environment. This interpretation was made based on the smooth textures of the rock, lack of intraclasts, abundance of sponge spicule-rich chert, and presence of dolomite, which was previously micrite. Smooth textures, lack of intraclasts, and abundance of fine-grained mud matrix indicate the environment was low energy, with little transport (Nelson, 2013). The abundance of sponge spicule-rich chert is indicative of a shallow environment (Boggs, 2006), although it can also be present in a deep-water environment (Carr et al., 1999). The shallow water environment interpretation is preferred due to lack of calcareous plankton in the Paleozoic (Martin, 2016), which could have allowed a sponge-rich environment to deposit silica without being diluted by calcium carbonate. A Mississippian-age analog with similar properties was interpreted to have formed by similar processes. The Schaben field in Ness County, Kansas, has a primary reservoir consisting of spiculitic wackstone-packstone. The abundance of sponge spicules, reduced faunal diversity, lack of echinoderms, and presence of evaporites suggest the facies was deposited in a restricted environment, like a lagoon, or ramp or supratidal environment (Montgomery et al., 2000).

Although this reservoir is similar with its abundance of shallow marine chert and dolomitic limestone (Bhattacharya et al., 2005), the Schaben field contains evaporites, which are not present in the cherty dolomite facies of the Rich C #7 study well. The lack of evaporites in a shallow environment can potentially be explained by examples of ancient tidal flats that formed during humid periods of Earth's history (Shinn, 1983), or due to salinities being far short of the concentration necessary for the onset of evaporite precipitation, as seen in semi-humid, sub-tropical areas of the Bahamas (Enos, 1983). In addition to a restricted environment being in place, low energy environments often occur in epeiric seas from the broad expanses of shallow water dampening out tidal and wave energy (Enos, 1983). The dolomite was interpreted to have previously been micrite, due to the fine, similar grain sizes and smooth textures.

Intraclastic Breccia

The depositional environment of the intraclastic breccia is interpreted to be a shallow, high-energy marine environment with intense reworking of shallow sediments by currents or waves and no significant transport. Diagenetic replacement occurred locally by Ca-Mg-rich fluids. This interpretation was made based on the rough, mixed textures of the rock, abundance of intraclasts, different lithologies of intraclasts, and angular shape of intraclasts. A rock comprised of intraclasts of different microfacies is indicative of a high energy environment, while the angular shape of the intraclasts suggests there was no significant transport due to the small amount or lack of rounding the intraclasts have undergone (Flügel, 2004)**.** Rocks falling under the depositional breccia category can also indicate high energy conditions (Flügel, 2004). For intraclasts to be formed, rock must be eroded from original location, which typically occurs by storm waves in a shallow water-carbonate environment (Flügel, 2004). The dolomitic mud

intraclasts were interpreted to have previously been micritic mud, due to the fine and similar grain sizes.

Intraclastic Rudstone

The depositional environment of the intraclastic rudstone is interpreted to be a shallow, high-energy marine environment with intense reworking and transport of shallow water sediments by currents or waves. Fluidization and burrowing by organisms occurred locally, along with extensive diagenetic replacement by silica and Ca-Mg-rich fluids. This interpretation was made based on the rough, mixed textures of the rock, abundance of intraclasts, different lithologies of intraclasts, rounded shape of intraclasts, and presence of dolomitic mud intraclasts. Erosion and transport are required for the formation of intraclastic rudstones, which can occur from storm waves in a shallow water-carbonate environment. The rounded shape of the intraclasts suggests significant transport occurred due to the amount of weathering the intraclasts have undergone (Flügel, 2004), while a rock comprising of intraclasts of different microfacies is indicative of a high energy environment (Flügel, 2004). The dolomitic mud intraclasts were interpreted to have previously been micritic mud, due to the fine and similar grain sizes.

Bioclastic Grainstone

The depositional environment of the bioclastic grainstone is interpreted to be a shallow, high-energy marine environment with reworking of shallow-water sediments by currents. The grainstone was formed into flat beds under the upper flow regime and had extensive diagenetic replacement by silica-rich fluids. This interpretation was made based on the rough, mixed texture of the rock, different lithologies of intraclasts, and fossils within the rock. The different lithologies of intraclasts within the rock suggest a high energy environment (Flügel, 2004), and the presence of carbonates with bryozoan bioclasts suggests a shallow water environment.

Bryozoans typically existed in a shallow, tropical environment during the Paleozoic (Scholle, 2003).

Muddy Dolostone

The depositional environment of the muddy dolostone is interpreted to be a more open, deeper-water marine environment undergoing gravitational settling from suspension under low energy with periodic higher energy events that supplied reworked clasts and bioclasts from waves. Fluidization and burrowing by organisms occurred locally, along with extensive diagenetic replacement by Ca-Mg-rich fluids. This interpretation was made based on smooth textures and a mostly homogenous crystal size in the rock texture. The smooth and muddy fabric of the rock indicate deposition in a low-energy environment in open and deeper water (Enos, 1983), with occasional slightly rougher textures and bioclast inclusions suggesting periodic higher energy events. Orientation of the bioclasts inclusions is also an indicator of low-energy and periods of moderate energy conditions by the parallel orientation of platy bioclasts found in some areas of the core (Flügel, 2004). The muddy dolostone is interpreted to have previously been micritic mud, due to the fine and similar grain sizes.

4.2 Ties between Core and Well Log Facies

Reservoir quality and potential were analyzed on the Rich C #7 study well. Well logs with the interpreted stratigraphic column and petrophysical data were constructed. Porosity values from NPHI and DPHI and Delta-T (DT) values from the sonic log were plotted into 2-D and 3-D cross plots to discriminate well log facies and lithofacies. The productive areas of Rich C #7 are the "A" and "B" zones, however, the "A" zone section of this core was not recovered, so the particular reservoir rock of the "A" zone in Rich C #7 was not described. The "B" zone mainly consists of cherty dolomite. The top of the "B" zone contains about a foot of rudstone, with

alternating thin beds of breccia and muddy dolostone underneath, and the bottom of the "B" zone is marked by the transition of the cherty dolomite petrofacies to a thin layer of muddy dolostone (Figure 4.1). The "C" zone consists primarily of the muddy dolostone petrofacies, with the top of the "C" Zone being marked by a thin layer of rudstone. There is a two-foot thick layer of rudstone underneath the top of the "C" zone, as well. The bioclastic grainstone only appears twice, in two to three-inch layers, making it too thin to be seen by log resolution. Additional stacked-thin facies can be observed in the core, below the thin grainstone at 5822', for example, but were ultimately not described due to their thickness being too thin to appear in log resolution. The measured core depths on the logs had four feet added to their depths, due to the Driller Total Depth (TD) being recorded four feet above the Logger TD (KGS, 2018). Refer to Appendix A to view the core description profile with well log facies and well log traces, and a longer, 10 feet-per-inch (ftpi) well log.

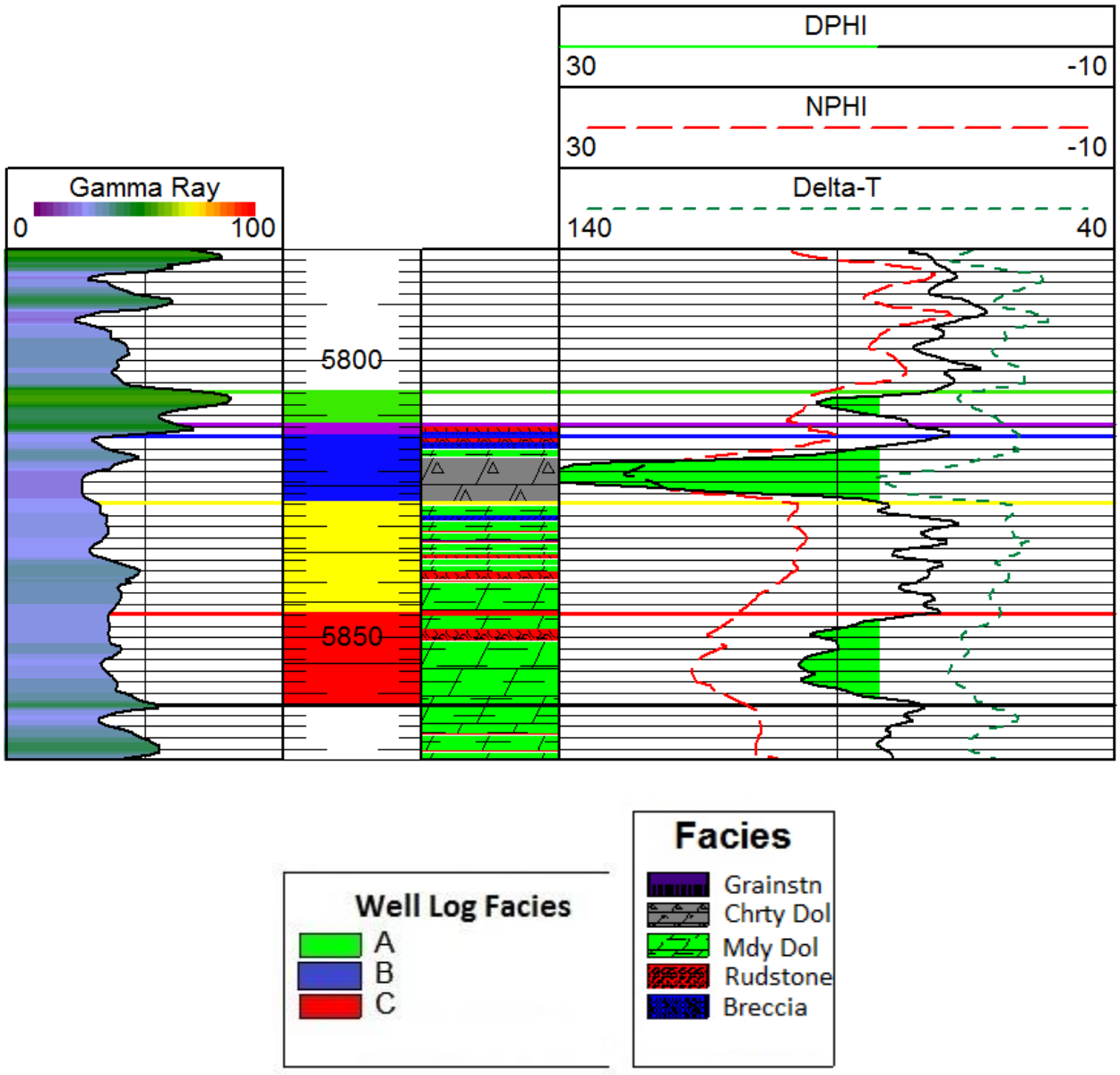

Figure 4.1: 50 ftpi well log with well log facies, interpreted lithofacies, and petrophysical data from the Rich C #7 well. This well log illustrates the cherty dolomite as the primary reservoir facies of the "B" zone. Due to the resolution of this log, the grainstone facies cannot be seen.

The "A", "B", and "C" zones and cherty dolomite lithofacies discriminate well in 2-D and 3-D cross plots, further illustrating the primary reservoir zones, signature well log facies, and

lithofacies. When plotting DPHI against NPHI, the “A”, “B”, and “C” zone well log facies, areas between zones, and the area above the “A” zone is discriminated from this cross plot (Figure 4.2).

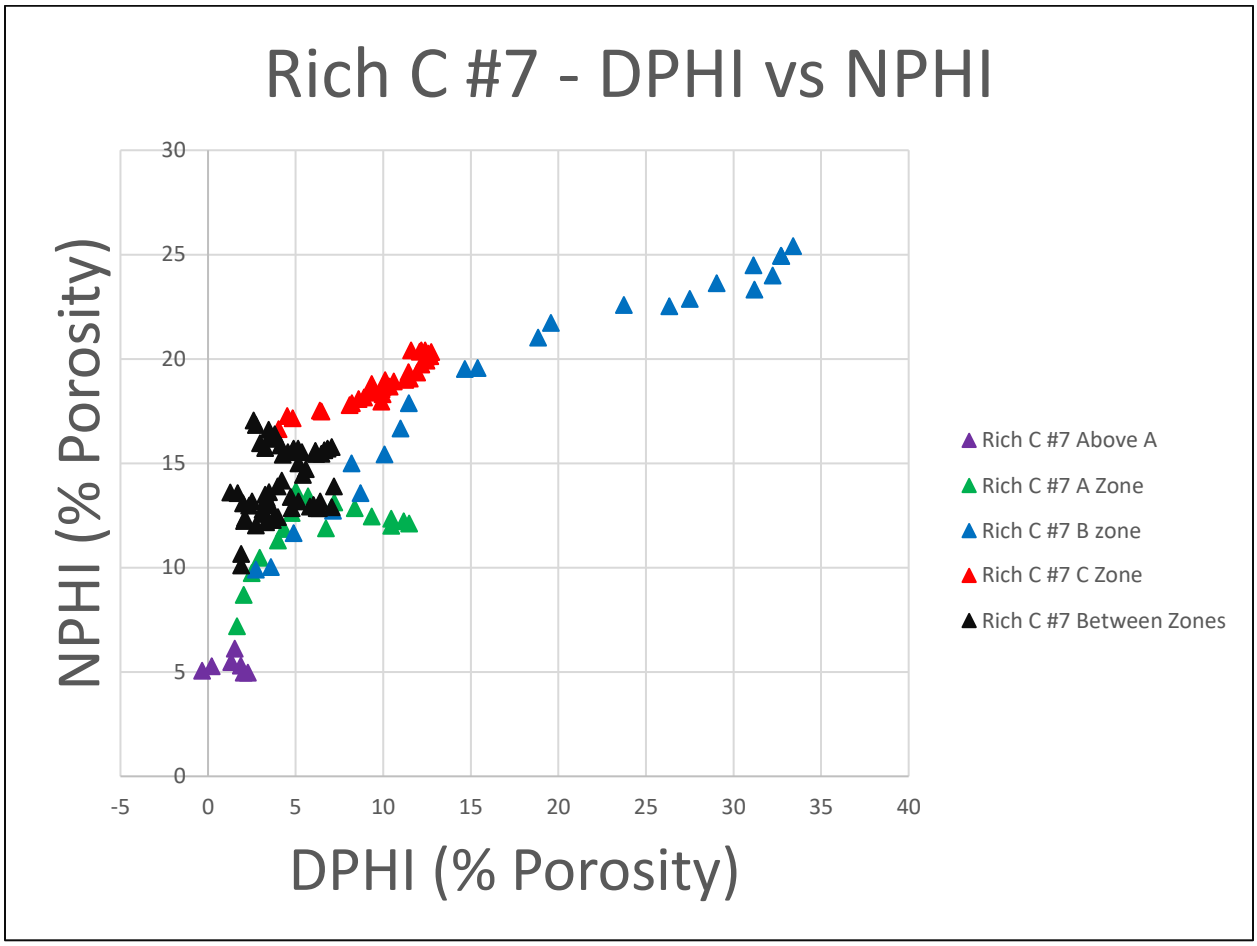

Figure 4.2: 2-D cross plot displaying the NPHI (%) and DPHI (%) log values of the Rich C #7 well log facies. The productive “A” (green) and “B” (blue) zones and the non-productive “C” zone (red) is discriminated from this cross plot, further illustrating the productive zones of Rich C #7. The areas between the signature well log facies, in black, as well as the area above the “A” zone, in purple, also discriminate well from this cross plot.

By plotting DPHI against NPHI, some of the interpreted lithofacies were discriminated from the cross plot. The cherty dolomite, the primary reservoir facies of the productive “B” zone,

is discriminated from this cross plot, further illustrating one of the productive facies in Rich C #7. The muddy dolostone is discriminated, to a degree, and the rudstone is slightly discriminated, due to being split into two different clusters. There are too few data points of the breccia and grainstone to show any kind of relationship (Figure 4.3).

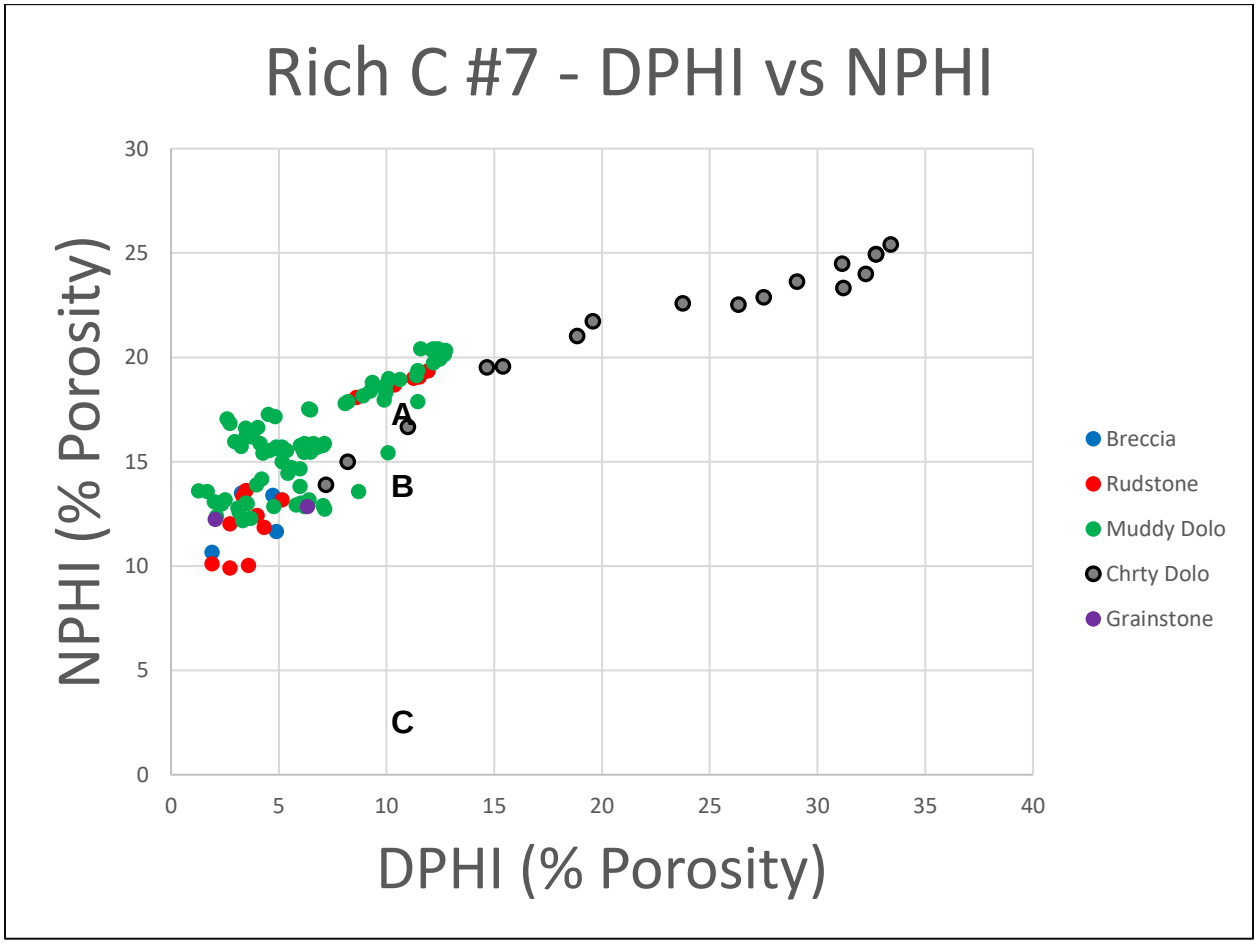

Figure 4.3: 2-D cross plot displaying the NPHI (%) and DPHI (%) log values of the Rich C #7 lithofacies. The cherty dolomite (gray and black), in the productive "B" zone, is discriminated from this cross plot, further illustrating one of the productive facies in Rich C #7. The muddy dolostone, in green, is discriminated, to a degree, and the rudstone, in red, is slightly discriminated, due to being split into two different clusters. There are too

few data points of the breccia, in blue, and grainstone, in purple, to show any kind of relationship.

When using a 3-D cross plot to display DHPI vs DT vs NPHI, the "A", "B", and "C" zone well log facies are also well-discriminated. The non-productive areas, between zones and above the "A" zone, are slightly discriminated from this method (Figure 4.4).

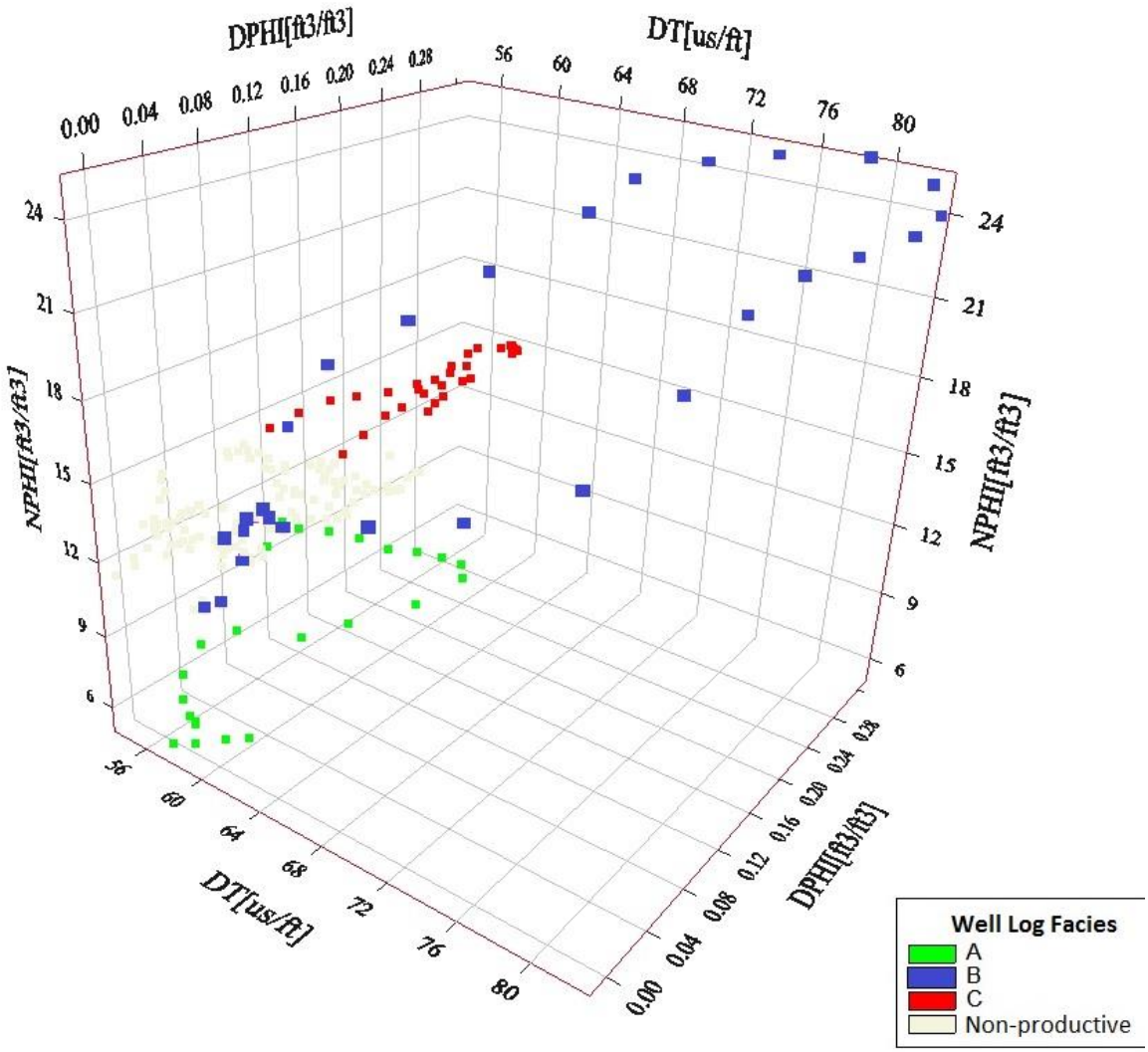

Figure 4.4: 3-D cross plot displaying the NPHI (%), DPHI (%), and DT (µs/ft) log values of the Rich C #7 well log facies. The productive "A" (green) and "B" (blue) zones and the non-

productive "C" zone (red) is discriminated from this cross plot, further illustrating the productive zones of Rich C #7. The areas between zones, and above the "A" zone, labeled as "Non-productive" (cream), are slightly discriminated, as the data points are grouped into two large clusters adjacent to one another.

Similar well log signatures from the Viola Limestone facilitates exploration for the productive paleotopographic traps. Productive wells in the Viola Limestone of south-central Kansas have correlating well log signatures, as seen between Rich C #7 and Herd 1 (Figure 4.6). These two wells are just a couple, amongst others with correlating well log signatures.

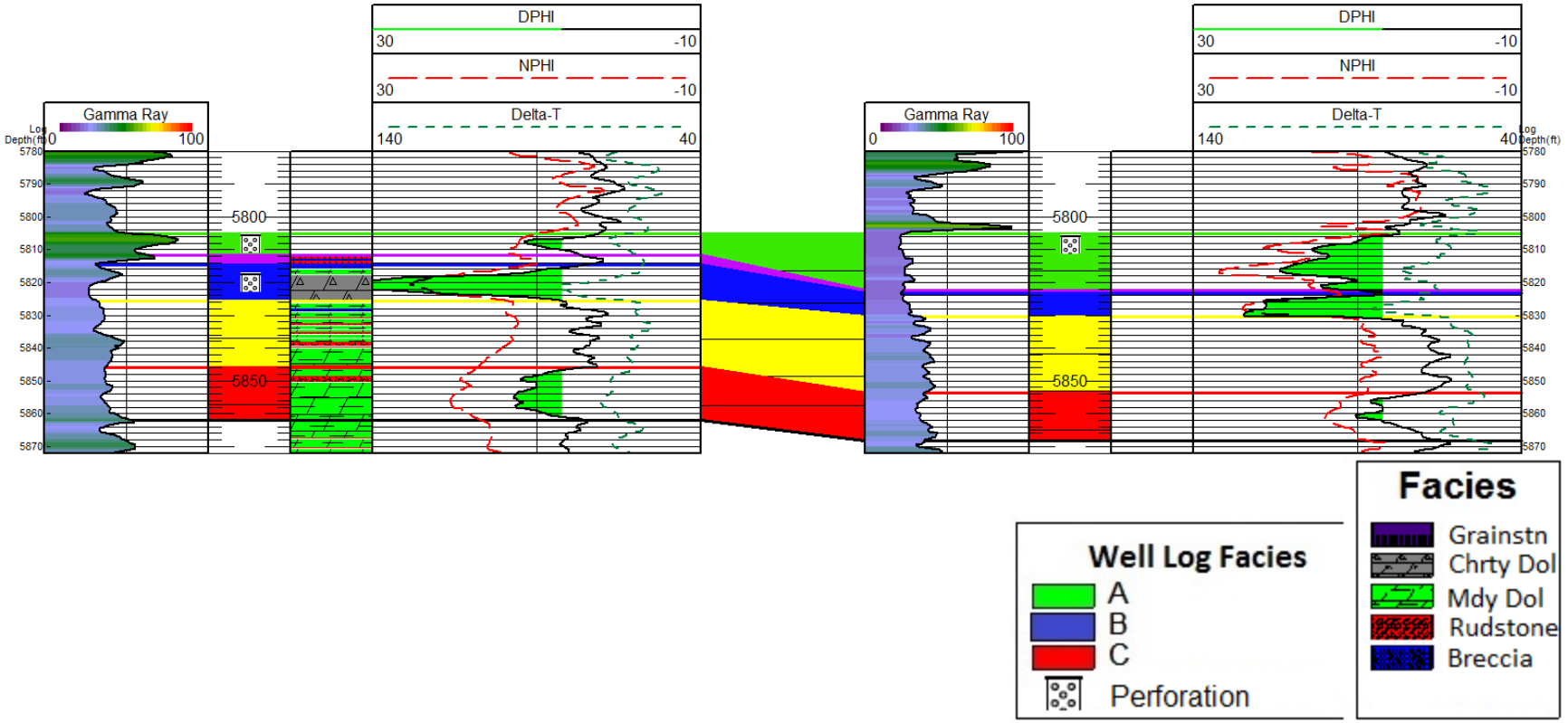
DPHI
30
-10
NPHI
30
-10
Delta-T
140
40
Gamma Ray
0
100
Log Depth(ft)
5780
5790
5800
5810
5820
5830
5840
5850
5860
5870
5800
5850
Well Log Facies
A
B
C
Perforation
Facies
Grainstn
Chrty Dol
Mdy Dol
Rudstone
Breccia

Figure 4.5: 50 ftpi well logs from Rich C #7 and Herd 1 displaying the correlation between the "A", "B", and "C" zones. Due to the resolution of this log, the grainstone facies cannot be seen here in Rich C #7.

The petrophysical data from the Herd 1 well discriminates the productive zones in a similar manner to Rich C #7. By using the same method of plotting DPHI against NPHI, the productive "A" and "B" zones and the non-productive "C" zone is discriminated from this cross plot, further illustrating the productive zones of Herd 1. The areas above the "A" zone and between zones are also discriminated from this cross plot (Figure 4.7).

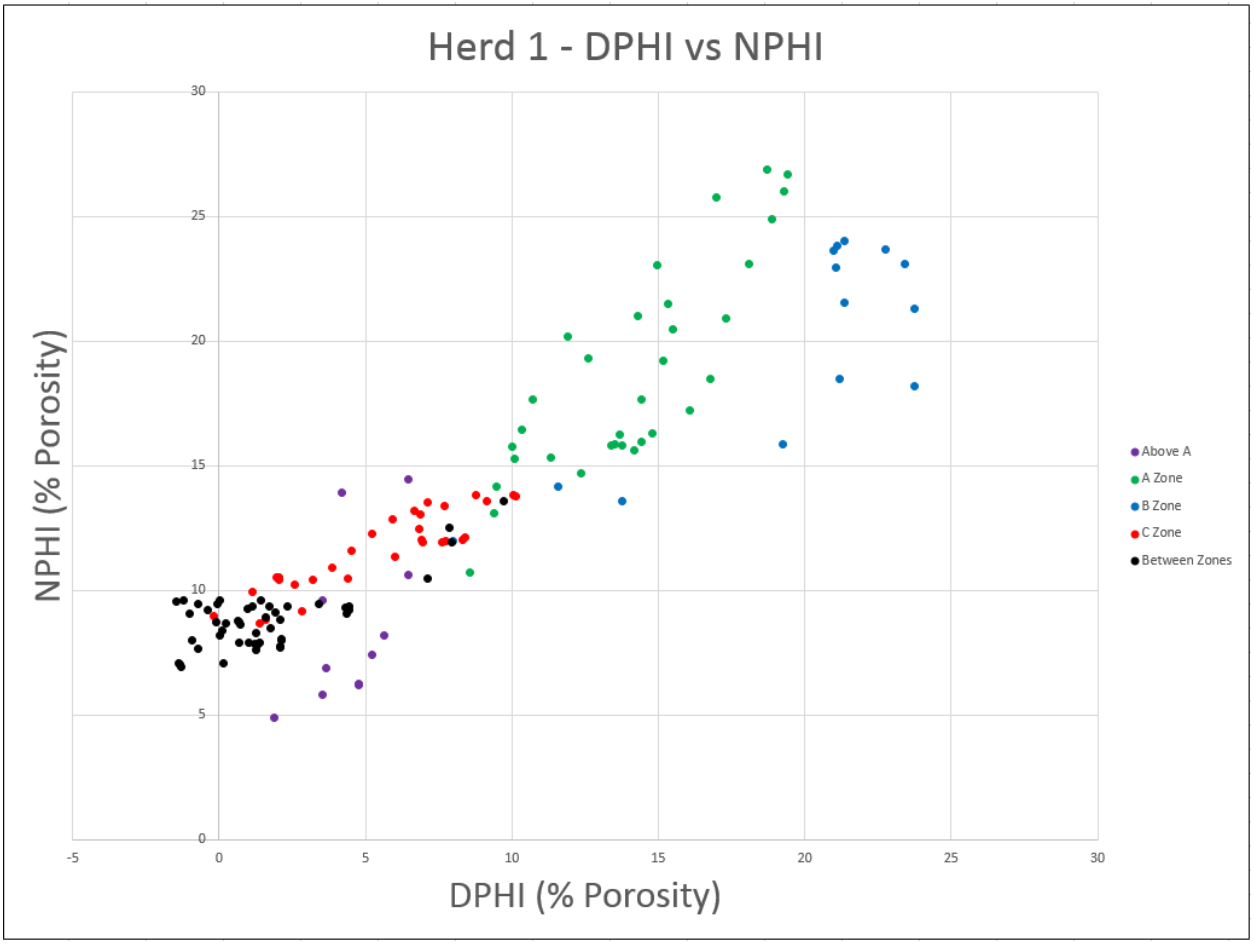

Figure 4.6: 2-D cross plot displaying the NPHI (%) and DPHI (%) log values of the Herd 1 well log facies. The productive "A" (green) and "B" (blue) zones and the non-productive

"C" zone (red) is discriminated from this cross plot, further illustrating the productive zones of Herd 1. The areas between the zones, in black, and the area above the "A" zone, in purple, are also discriminated from this cross plot.

When comparing petrophysical data between Rich C #7 and the Herd 1, similar trends in data can be observed. By plotting DPHI against NPHI, the "A", "B", and "C" zones display similar trends between the two wells. The areas above the "A" zone and between zones also exhibit similar trends between the two wells (Figure 4.8). These similar well log signatures provide an analog for an exploration workflow.

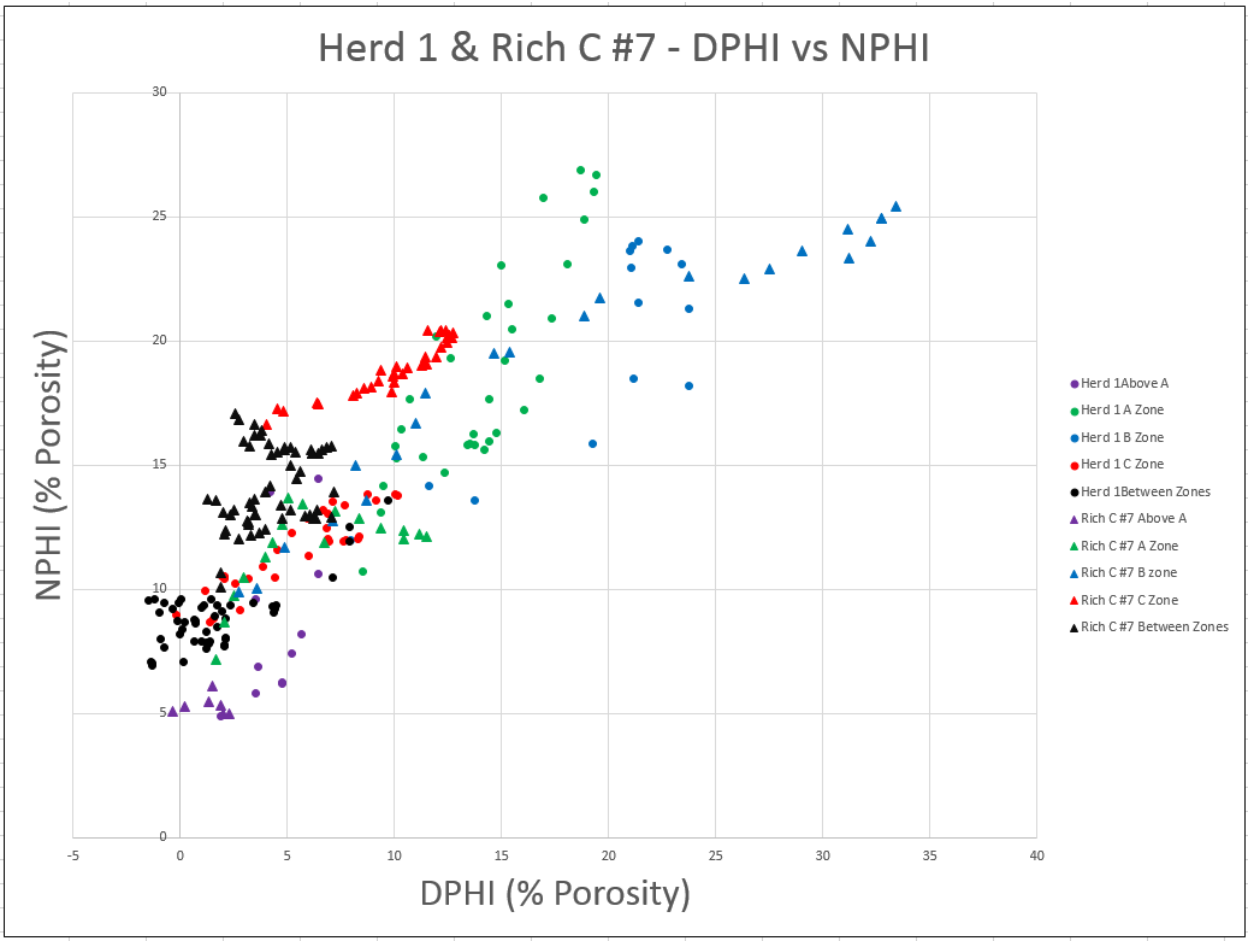

Figure 4.7: 2-D cross plot displaying the NPHI (%) and DPHI (%) log values of the Herd 1 and Rich C #7 well log facies. The data points from the Rich C #7 well are represented by a

triangle symbol, and the data points from the Herd 1 well are represented by a dot symbol. The productive "A" (green) and "B" (blue) zones and the non-productive "C" zone (red) exhibit similar trends between the two wells. The areas between the zones, in black, and the area above the "A" zone, in purple, also exhibit similar trends between the two wells. These similar signatures provide an analogue for an exploration workflow.

4.3 Ties between Elastic Properties and Core and Well Log Facies

Wells in the Herd field with similar well log signatures, like Herd 1 and Rich C #7, could have correlations to the ultrasonic velocities and elastic properties. A similar study may be replicated within the Herd field with objectives of identifying production potential within the Viola Limestone for hydrocarbon exploration. Correlating facies of the core sample to well log characteristics provides a potential work-flow to explore Viola targets.

Production from the Viola Limestone in south-central Kansas comes from regions of preserved dolomite on paleo-topographic highs. Areas where the overlying-non-porous Maquoketa shale are thinnest typically have thicker paleotopographic traps of Viola dolomite (Richardson, 2013). These paleotopographic reservoirs may not necessarily have lateral continuity because of erosional highs and lows, which could present challenges for exploration. Due to the thinness of the reservoir zones, as observed in Rich C #7, the resolution of seismic wavelets could potentially not detect these traps. In a companion study (Cimino, in prep), ultrasonic velocity measurements were taken from the Rich C #7 study core to determine the relationship between P-Wave velocity and the productive zones and formations of the Viola Limestone. This study revealed that P-Wave velocities strongly correlate with the DPHI, NPHI, and DT well log traces of the study core (Hagood et al., 2018). The P-wave velocity of the "B" zone discriminates the zone and its productive facies (Figure 4.9).

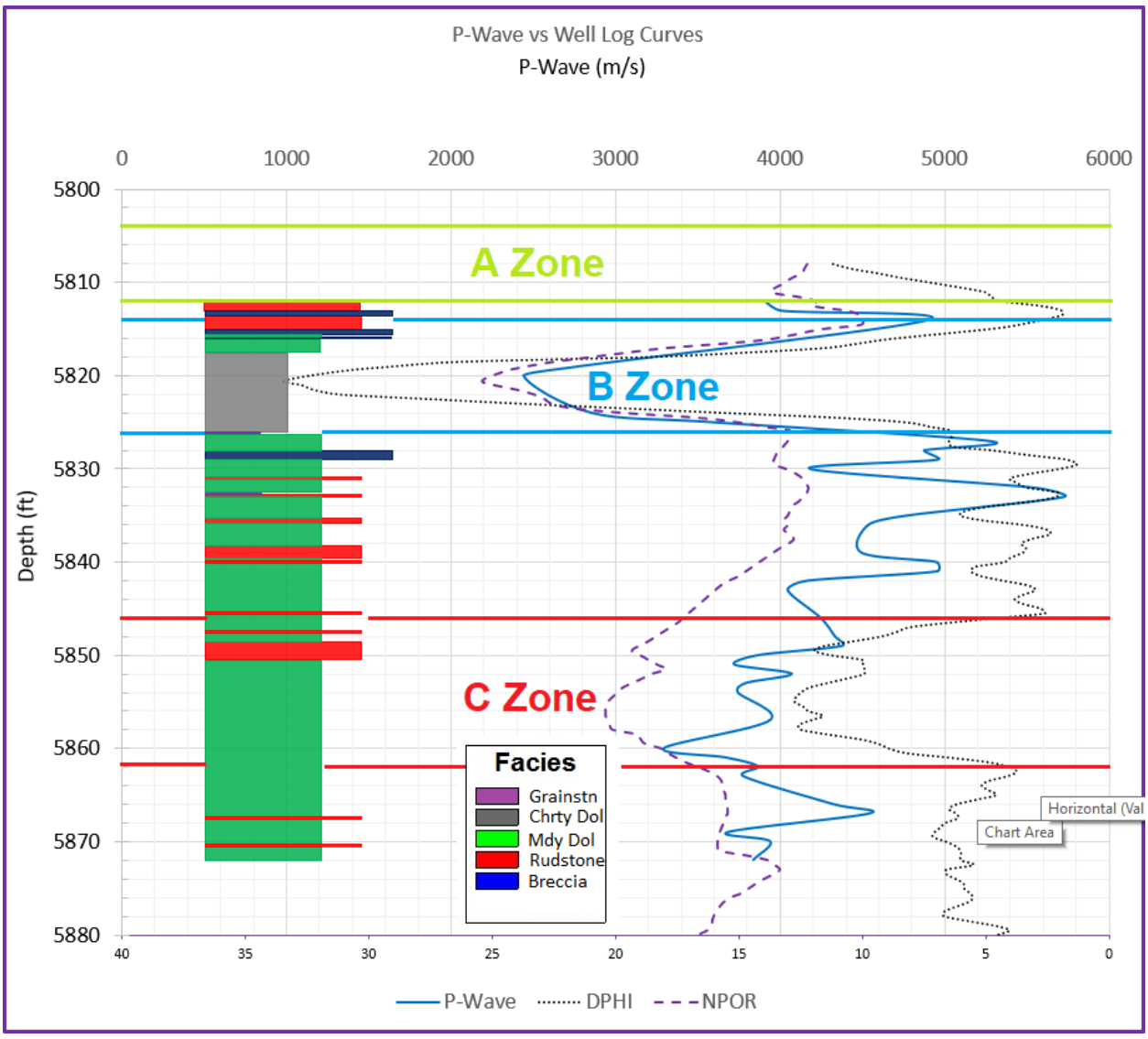

Figure 4.8: Well log with well log facies, interpreted lithofacies, NPHI (NPOR, %), DPHI (%), and ultrasonic velocity measurements (P-Wave, m/s) (Hagood et al., 2018) from the Rich C #7 core. P-Wave velocities correlate directly with the "B" zone's DPHI and NPHI well log signatures and with the productive cherty dolomite facies. This further illustrates the productive facies of Rich C #7.

4.4 Chemical Variations within Core Described Facies

The elemental concentrations and ratios of multiple elements were plotted into cross plots in attempt to correlate productive well log facies and described facies with chemical signatures. Elemental ratios were preferred to minimize the error within concentrations due to the calculations being calibrated using a shale standard, while taking measurements on carbonate rocks. XRF is a comparative analytical method, requiring matching of matrices to produce calibrations that yield accurate results. If a shale matrix calibration is being applied to measurements on a limestone matrix rock, error can be introduced. Readings taken at six-inch intervals were used to compare to log data, because those readings are taken in six-inch intervals.

The potential of chemostratigraphic data correlating to stratigraphy was assessed and was concluded that data from the Bruker HHXRF could discriminate well log facies and some of the described facies from the Rich C #7 well, with certain elemental signatures. Silicon (Si) can be found in biogenic quartz, detrital quartz, clays, and feldspars. For this study, it is beneficial to use a silicon to aluminum (Al) ratio to provide a rough estimate of biogenic quartz in a section. A high Si/Al ratio could indicate the quartz is mainly biogenic, due to the low Al component. Detrital marine sediments typically contain some amount of clay and feldspar, which have higher concentrations of Al, thus exhibiting a lower Si/Al ratio (Turner, 2015). The “B” zone, “C” zone, and “Between Zones” well log facies are discminated by plotting Si against Al (Figure 4.10), while the cherty dolomite facies, rudstone, and muddy dolostone petrofacies are discriminated from this cross plot (Figure 4.11).

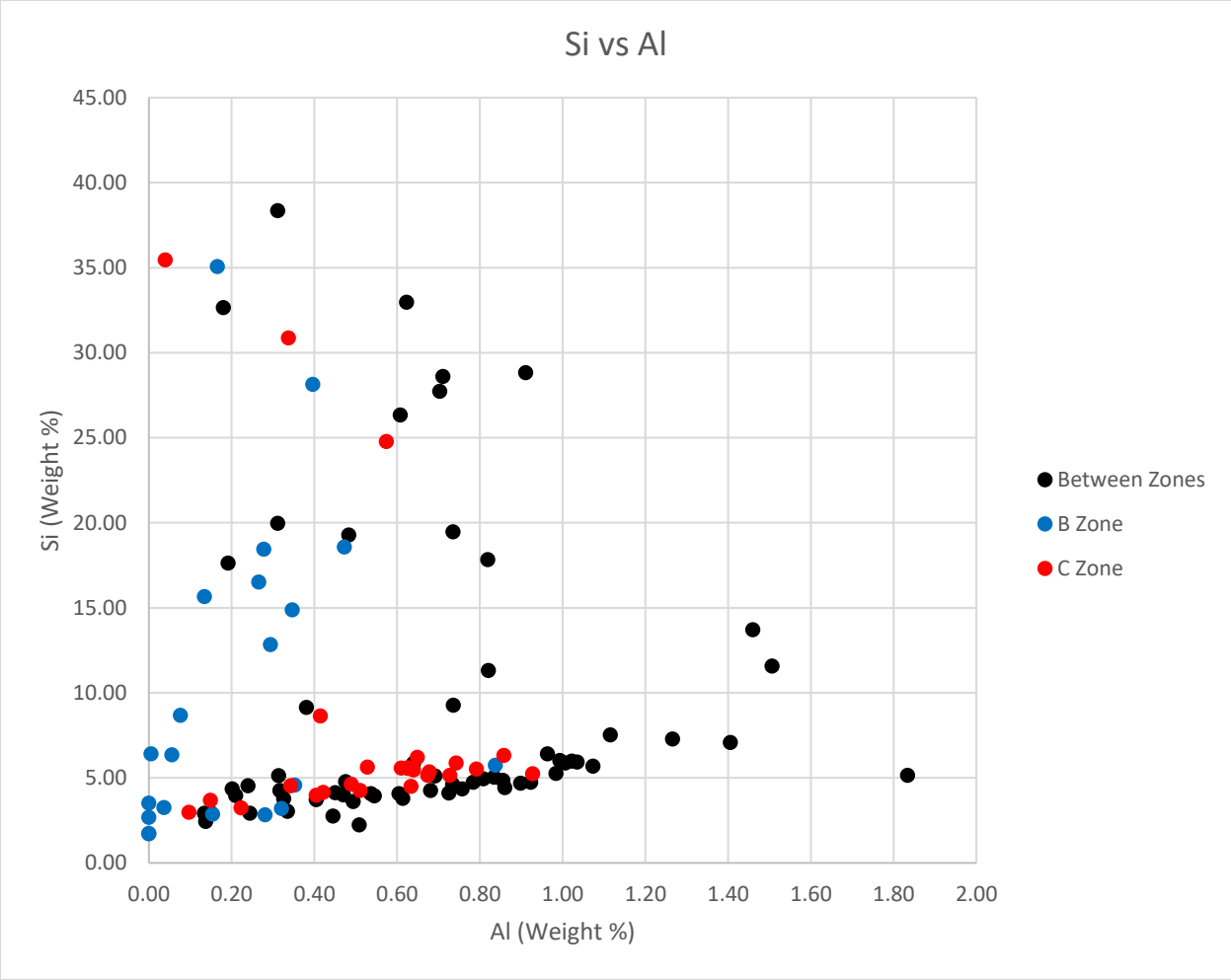

Figure 4.9: Cross plot of HHXRF major elemental data, Si and Al, with well log facies. The "B" zone is in blue, "C" zone is in red, and the areas between zones is black. The well log facies were mostly discriminated from this cross plot, as seen from their groupings.

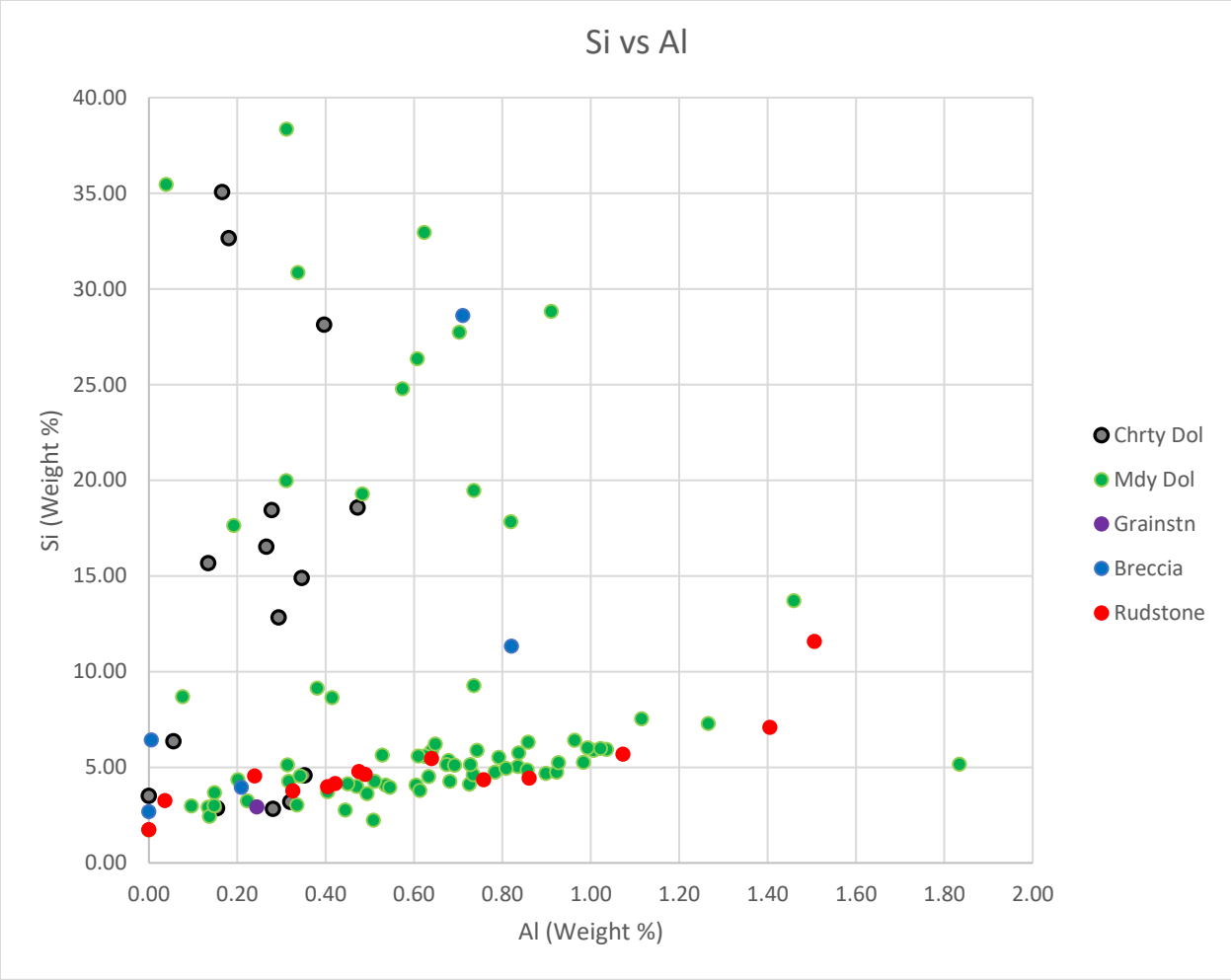

Figure 4.10: Cross plot of HHXRF major elemental data, Si and Al, with described facies. The rudstone (red), muddy dolostone (green), and cherty dolomite (gray and black) facies were mostly discriminated from this cross plot, as seen from their groupings. There are not enough data points of the breccia, in blue, and the grainstone, in purple, to see any significant relationships.

These same well log facies and described facies are also discriminated by the Si/Al versus titanium (Ti) cross plots (Figures 4.12 and 4.13) and the Si/Al versus zirconium (Zr) cross plots (Figures 4.14 and 4.15). The high weight percentage of Si and low weight percentage of Al in the "B" zone and cherty dolomite petrofacies is due to the rock being mainly comprised of

sponge spicule-rich chert, which is biogenic. Comparing the Si/Al ratio to the amount of Ti and Zr within the sample can indicate the amount of detrital influence imposed on the rock during deposition. Ti and Zr are associated with sediment of continental provenance (Turner, 2015). The high Si/Al ratios and low Ti and Zr concentrations exhibited by the "B" zone and cherty dolomite petrofacies is indicative of an environment with very little continental influence upon deposition. The cherty dolomite petrofacies is interpreted to be a shallow, low-energy, and somewhat restricted depositional environment. Ocean currents restricted by a barrier reef, or conditions found in an epeiric sea, from broad expanses of water dampening out tidal energy could inhibit the transportation of continentally derived sediments (Enos, 1983). The low Si/Al ratios and higher Ti and Zr concentrations exhibited by the "C" zone and "Between Zones" well log facies, as well as the rudstone and muddy dolostone petrofacies is indicative of an environment where some degree of continental influence can be observed. The Si/Al ratios are also low due to small amount of biogenic quartz found within these petrofacies (Turner, 2015). These well log facies and petrofacies formed in less restricted environments, where storm waves and ocean bottom currents could transport continentally derived sediment. Clay minerals and aeolian quartz can be transported large distances by winds, and furthermore by ocean currents (Scholle, 1983).

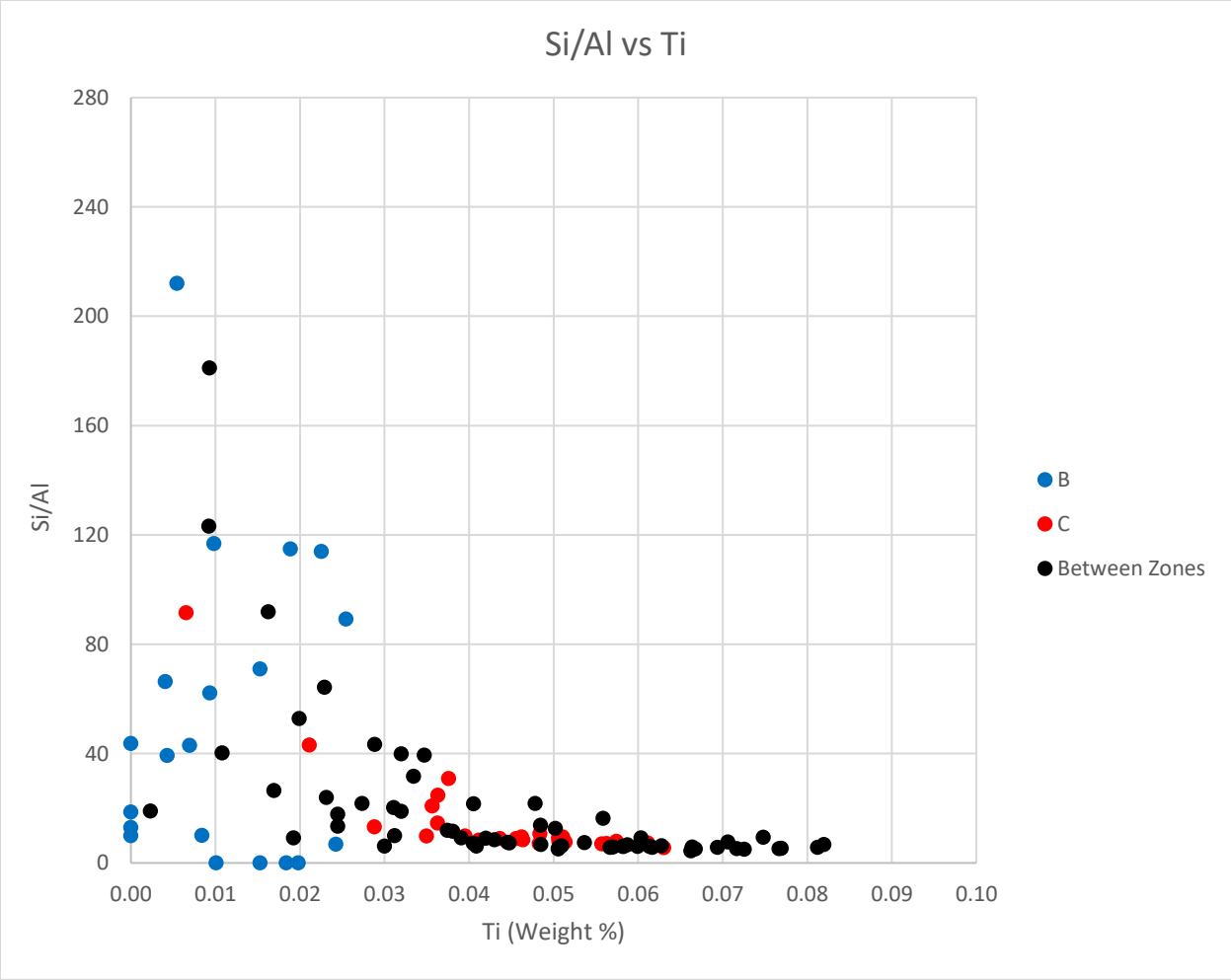

Figure 4.11: Cross plot of HHXRF major elemental data, Si/Al and Ti, with well log facies. The "B" zone is in blue, "C" zone is in red, and the areas between zones is black. The well log facies were discriminated from this cross plot, as seen from their groupings.

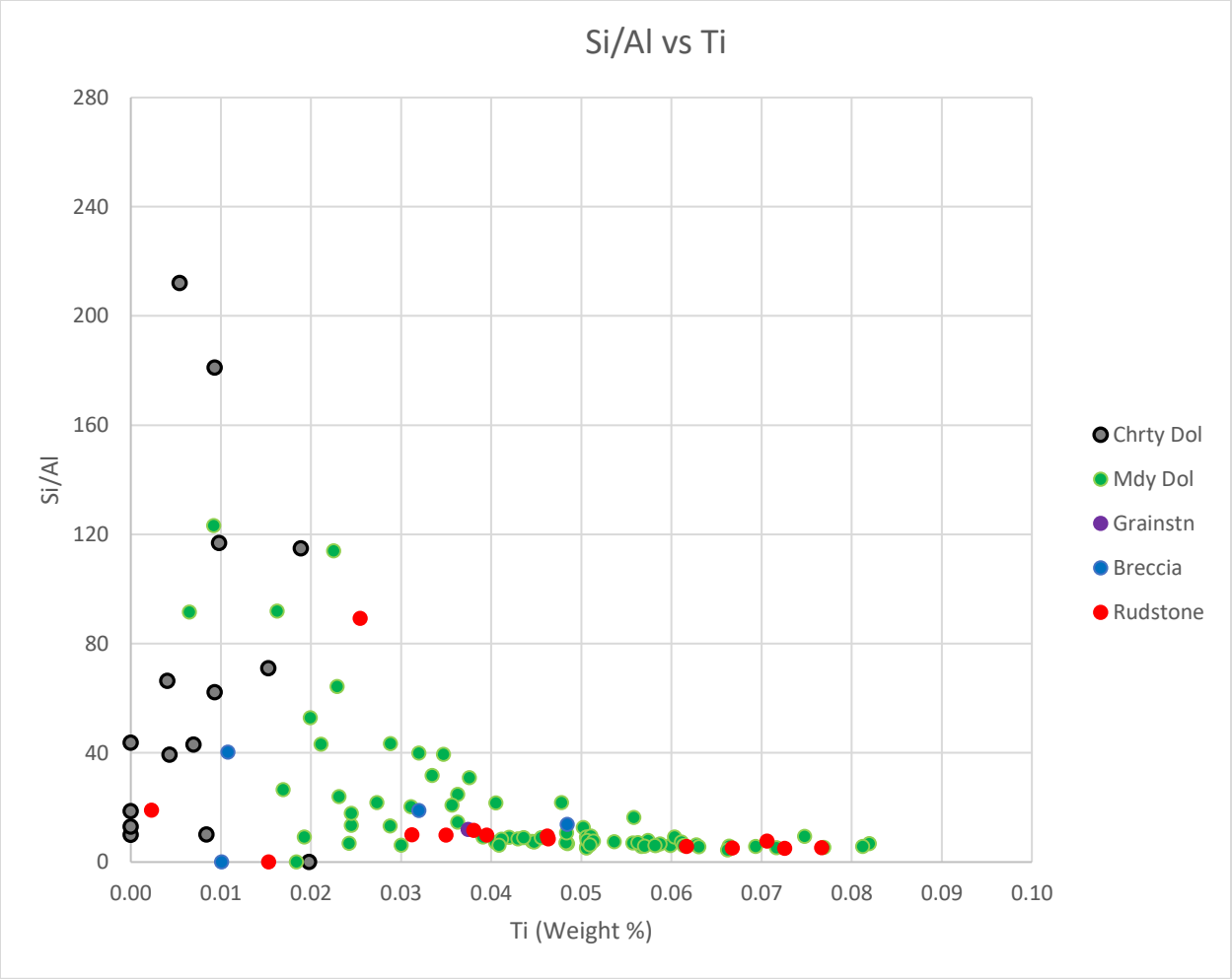

Figure 4.12: Cross plot of HHXRF major elemental data, Si/Al and Ti, with described facies. The rudstone (red), muddy dolostone (green), and cherty dolomite (gray and black) facies were mostly discriminated from this cross plot, as seen from their groupings. There are not enough data points of the breccia, in blue, and the grainstone, in purple, to see any significant relationships.

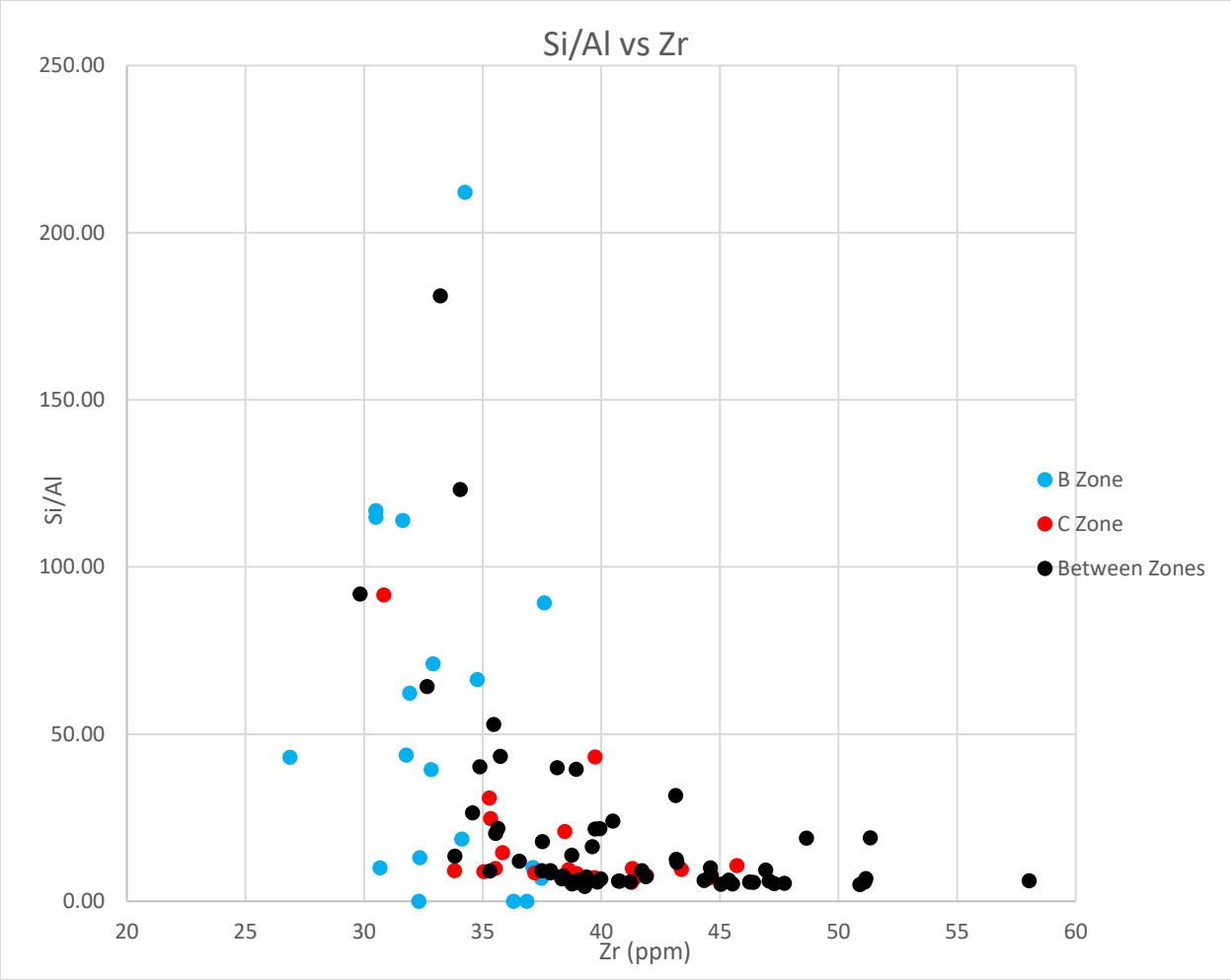

Figure 4.13: Cross plot of HHXRF major elemental data (Si/Al) versus trace elemental data (Zr) with well log facies. The "B" zone is in blue, "C" zone is in red, and the areas between zones is black. The well log facies were discriminated from this cross plot, as seen from their groupings.

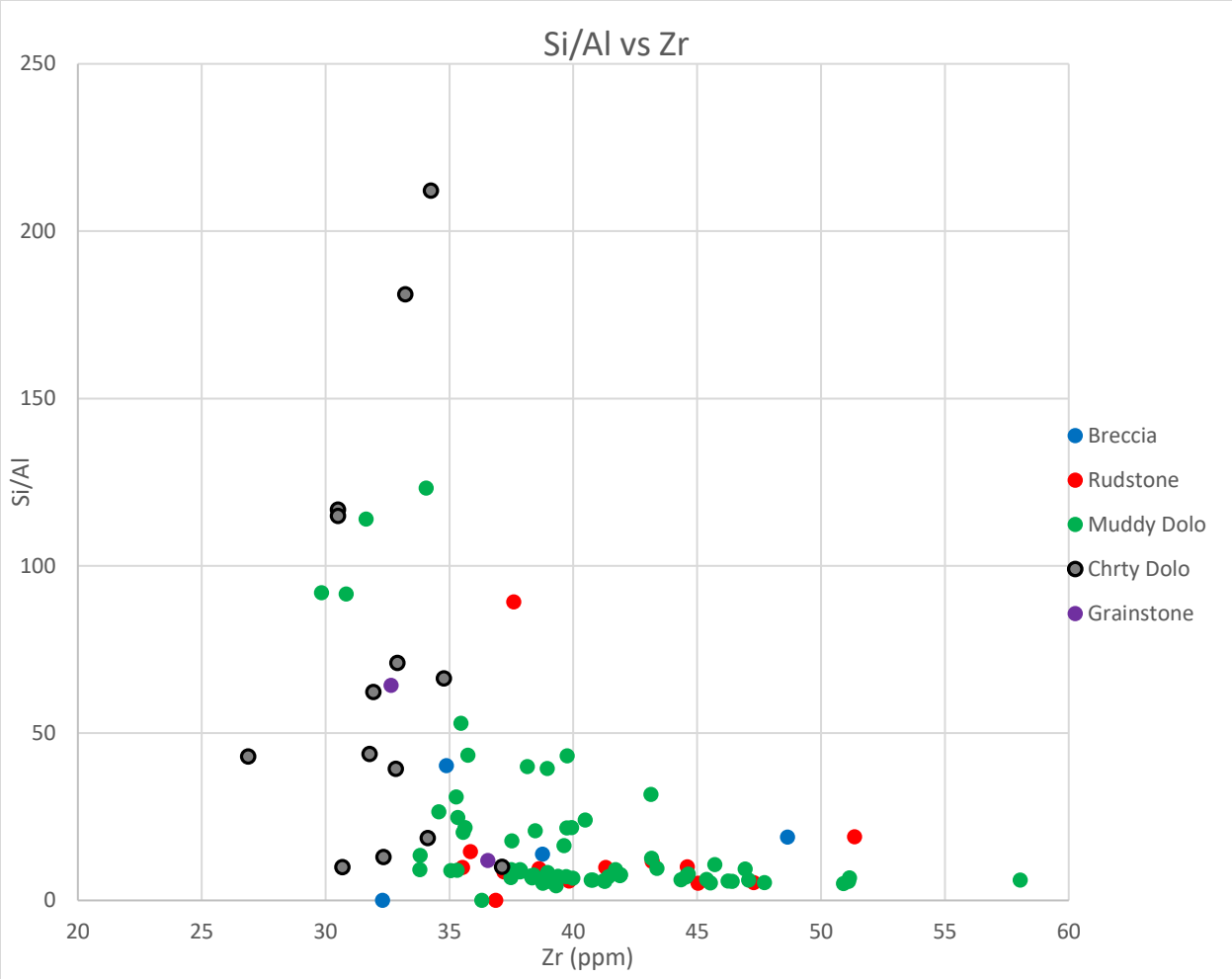

Figure 4.14: Cross plot of HHXRF major elemental data (Si/Al) versus trace elemental data (Zr) with described facies. The rudstone (red), muddy dolostone (green), and cherty dolomite (gray and black) facies were mostly discriminated from this cross plot, as seen from their groupings. There are not enough data points of the breccia, in blue, and the grainstone, in purple, to see any significant relationships.

Additional evidence for continental influence can be derived from the Zr vs Ti cross plots (Figures 4.16 and 4.17). The cherty dolomite petrofacies and "B" zone well log facies, which is comprised primarily of cherty dolomite, exhibits low concentrations of Zr and Ti. Again, this is

due to the facies restricted depositional environment inhibiting continental influence upon deposition.

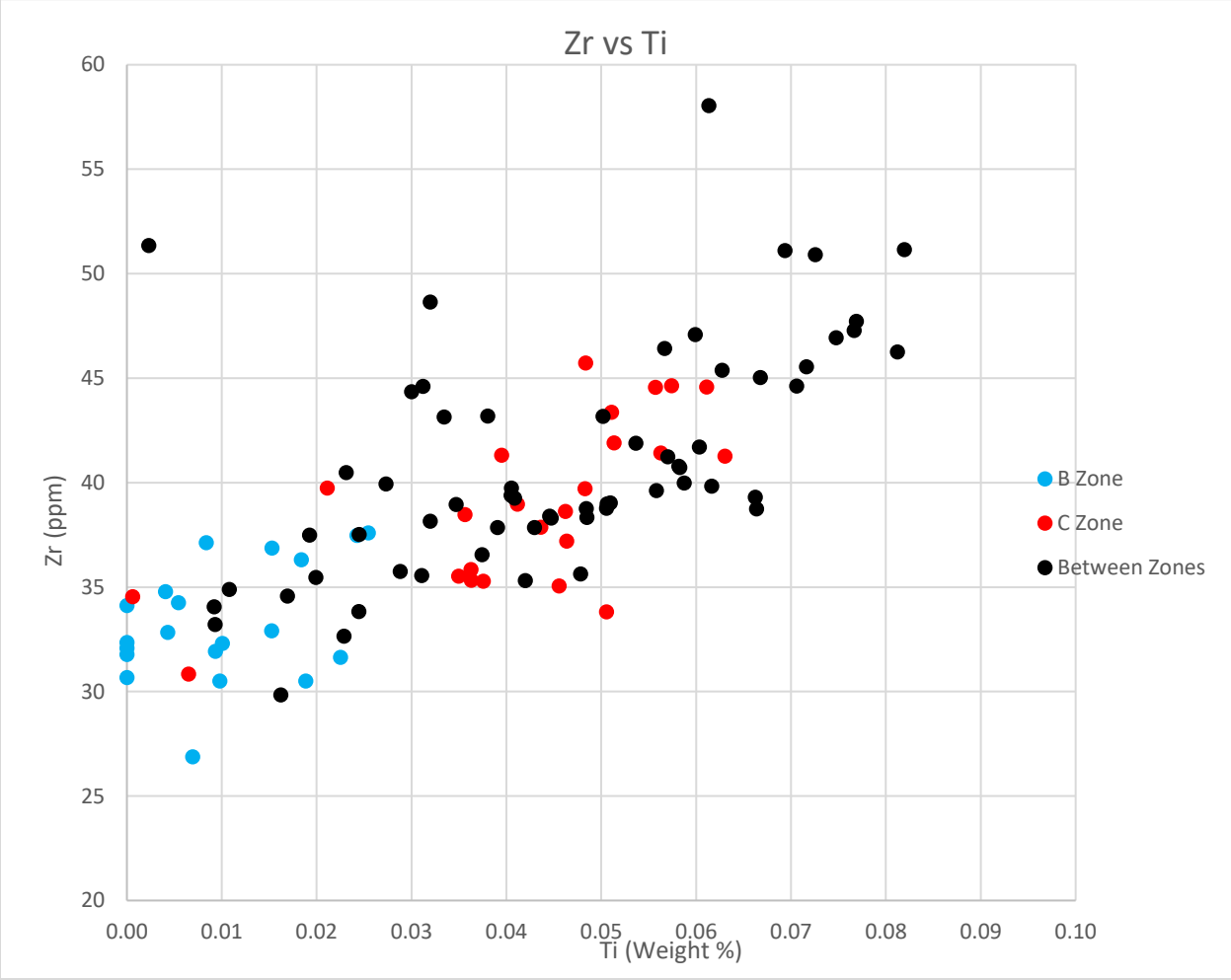

Figure 4.15: Cross plot of HHXRF major elemental data (Ti) versus trace elemental data (Zr) with well log facies. The "B" zone, in blue, was discriminated by this cross plot. The "C" zone, in red, and areas between zones, in black, were not discriminated by this cross plot, but display higher concentrations of Zr and Ti, which are indicative of environments influenced, if not very slightly, by continental sediment.

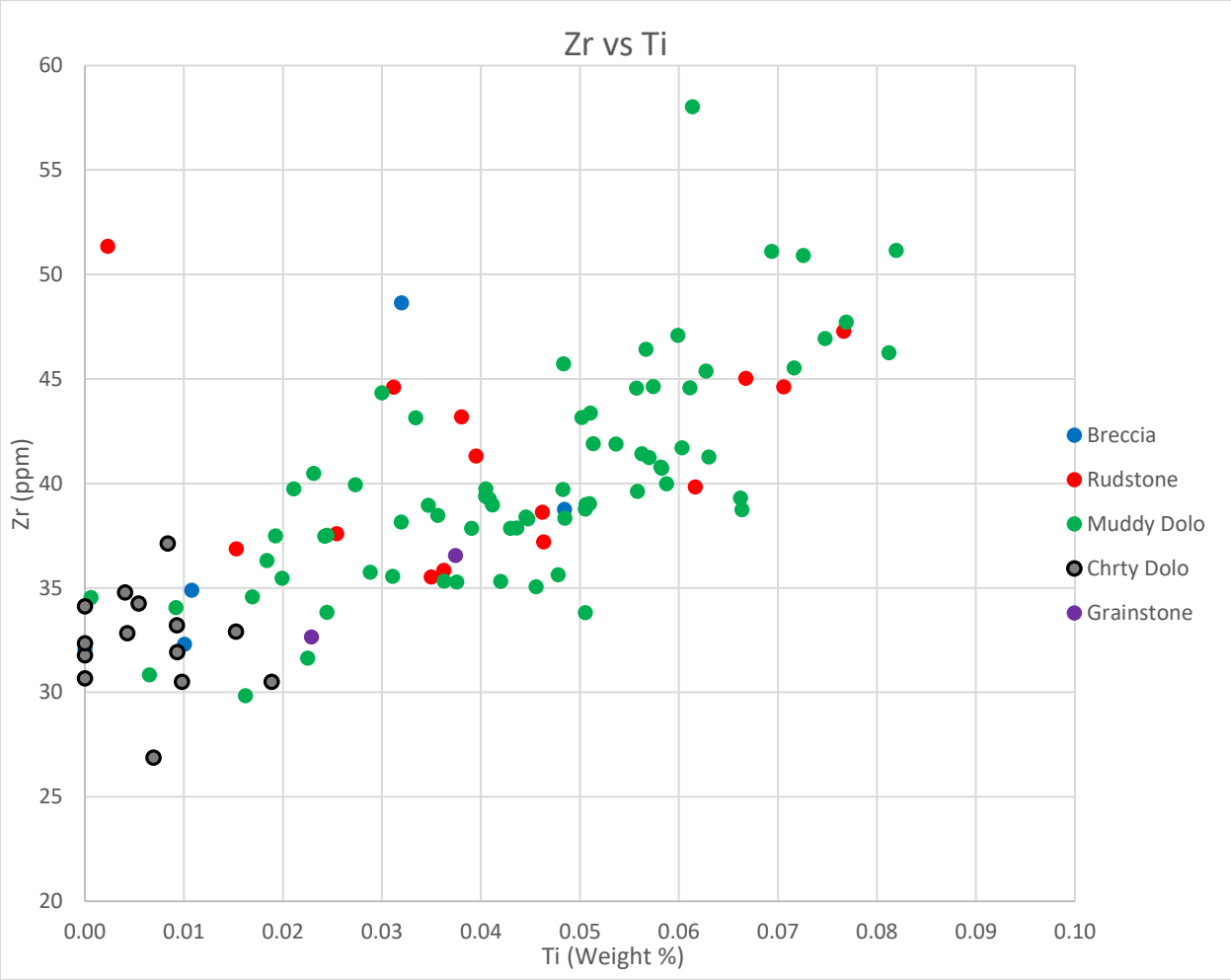

Figure 4.16: Cross plot of HHXRF major elemental data (Ti) versus trace elemental data (Zr) with described facies. The cherty dolomite petrofaci, in gray and black, was discriminated by this cross plot. The rudstone (red), muddy dolostone (green), breccia (blue), and grainstone (purple) facies were not discriminated by this cross plot, but display higher concentrations of Zr and Ti, which are indicative of environments influenced, if not very slightly, by continental sediment.

Some caveats should be mentioned when evaluating the handheld XRF data. The first is the potential loss of accuracy which originated from using a shale standard on carbonate rocks for calibration of the machine and the vast differences of readings between rock textures. The

machine's calibration on a shale standard could compromise the accuracy of individual elemental readings on a carbonate core. Differences in rock texture also gave erratic readings, particularly in sections of the core with bands of chert and dolomite in close proximity. A single reading could record high concentrations of silicon in the white cherty part of the rock, and then right next to that could be gray dolomite, which would have a completely different chemical composition. Differences in particle size can also affect the intensities of XRF readings (Wheeler, 1999). Taking readings along an intact core with different particle sizes could show variations in readings when compared to readings taken from a powder grounded in a controlled process. The surface where the reading is going to be taken also needs to be a smooth and flat surface, otherwise the HHXRF cannot take an accurate reading at that point. Areas where the core were not slabbed to a flat surface were skipped for readings. A potentially better method for this analysis would be a device that constantly moved the core, taking constant readings and converting them into sliding averages. Wireline log data is measured from sliding averages and can discriminate well log facies and described facies. This method could potentially correlate better with wireline log data.

Chapter 5 - Conclusion

This study illustrates the advantages of correlating depositional facies with reservoir quality and linking specific reservoir petrofacies with well log signatures, ultimately to create a greater understanding of the controls on reservoir quality to aid in predicting new areas of exploration. Collectively, this multifaceted study concludes the following;

1. Five lithofacies were identified in the Rich C #7 cored interval: 1) cherty dolomite, 2) intraclastic breccia, 3) intraclastic rudstone, 4) bioclastic grainstone, and 5) muddy dolostone.
2. The depositional environments were interpreted to be a shallow marine environment, ranging from low to high energy: 1) cherty dolomite & muddy dolostone – low energy, and 2) intraclastic breccia, intraclastic rudstone, & bioclastic grainstone – high energy.
3. Cherty dolomite is the only observed reservoir quality facies, due to the "A" zone not being recovered from coring. The cherty dolomite has density porosity values up to 34% and appears once, in the "B" zone of the core, with a thickness of roughly 8ft (2.4m). The "A" and "B" zones are the chief producers of the Viola Limestone in south-central Kansas.
4. The chemical data from the handheld XRF machine was able to partly discriminate well log facies and some of the described facies using specific elemental signatures and ratios. All of the well log facies and the cherty dolomite, rudstone, and muddy dolostone petrofacies were discriminated from plotting Si versus Al, Si/Al versus Ti, and Si/Al versus Zr. The Zr vs Ti cross plot was only able to discriminate the "B" zone and the cherty dolomite petrofacies.

5. The “B” zone well log facies was determined to be comprised mainly of the cherty dolomite petrofacies after examination of the core. This petrofacies only occurs within the “B” zone. In the Rich C #7 core, the “B” zone is capped by alternating thin beds of rudstone and breccia petrofacies, along with a thin layer of breccia near the bottom of the “B” zone. Muddy dolostone with thin layers of rudstone mainly comprise the area between the “B” and “C” zone and below the “C” zone. The “C” zone well log facies consists of mainly muddy dolostone, with a thin layer of rudstone marking the top of the zone in the Rich C #7 core. An almost two-foot-thick layer of rudstone is located a couple feet below the top of the “C” zone.
6. Wire-line log signatures differentiated the “A”, “B”, and “C” zones and cherty dolomite facies in Rich C #7 and correlate easily with other Viola-producing wells in south-central Kansas, like Herd 1. The productive well log facies can be identified from NPHI, DPHI, and sonic log signatures.
7. P-Wave velocity measurements (Hagood et al., 2018) exhibited correlations to the NPHI, DPHI, and sonic log values of Rich C #7. The “B” zone correlates exactly with the P-Wave velocities, with the cherty dolomite facies being discriminated by the velocities.

Chapter 6 - Future Work

The recent development of Viola production in Comanche and Clark Counties would be greatly enhanced by similar work to this study. Coring of the entire Upper Viola, including the A zone, followed by logging with a complete suite of modern well logs would allow comparison to the results of this study. With multiple cores available, a sequence stratigraphic analysis could be performed to identify higher-order sea level changes. This would facilitate in predicting and correlating successive facies to aid in exploration. Specific sequences could also be predicted and tracked by the neural networks using this workflow.

P-wave velocities and elastic properties discriminate each zone, including the cherty dolomite of the “B” zone, and perhaps the A zone, respectively. Further analysis with Gassmann’s fluid replacement modeling could potentially enable hydrocarbon presence to be identified within seismic surveys. These elastic properties provide a workflow to create a wavelet using seismic inversion, to ultimately be used in detecting the thin bed frequencies of the productive paleotopographic traps in seismic exploration. A 3-D seismic survey of the Herd field would need to be performed or obtained to continue this study. Seismic exploration is key to efficiently exploiting the Viola Limestone in south-central Kansas due to the paleotopographic reservoirs not having lateral continuity because of erosional highs and lows.

References

Adkison, W.L., 1972, Stratigraphy and structure of Middle and Upper Ordovician rocks in the Sedgwick Basin and adjacent areas, south-central Kansas: U.S. Geol. Survey, Prof. Paper 702, 33 p.

Bhattacharya, S., Doveton, J. H., Carr, T. R., Guy, W. R., and Gerlach, P. M., 2005, Integrated core-log petrofacies analysis in the construction of a reservoir geomodel: A case study of a mature Mississippian carbonate reservoir using limited data: AAPG Bulletin, v. 89, p. 1257–1274.

Blakey, R., 2016, *Paleogeography Maps- Teaching Material Images:* Professor Emeritus, Northern Arizona University, NAU.edu

Bornemann, E., Doveton, J. H., and. St. Clair, P. N., 1982 *Lithofacies Analysis of the Viola Limestone in South-central Kansas.* Kansas Geological Survey.

Boggs, Jr., S. (Ed.). (2006). Other Chemical/Biochemical and Carbonaceous Sedimentary Rocks. In *Principles of Sedimentology and Stratigraphy* (pp. 197-240). Upper Saddle River, NJ: Pearson Prentice Hall.

Bruker Corp, 2015, "Handheld XRF: How It Works", <https://www.bruker.com/products/x-ray-diffraction-and-elemental-analysis/handheld-xrf/how-xrf-works.html>, February 2017.

Carr, T. R., D. W. Green, and G. P. Willhite, 1999, Improved oil recovery in Mississippian carbonate reservoirs of Kansas, Near Term-Class 2 annual report, January 1, 1998 to December 31, 1998: National Petroleum Technology Office, U.S. Department of Energy, Tulsa, Oklahoma, 57 p.

Cimino, V., 2018, M.S. Thesis, Kansas State University, Personal communication.

Cone, M. P., and Kersey, D. G., 1992, ME 10: Development Geology Reference Manual, 209 pp.

Embry, A.F., and Klovan, J.E., 1971**,** A Late Devonian reef tract on Northeastern Banks Island, NWT: Canadian Petroleum Geology Bulletin, v. 19, p. 730-781.

Enos, P. 1983, Shelf Environment, in Scholle, P. A., Bebout, D. G., and Moore, C. H., eds., Carbonate Depositional Environments: American Association of Petroleum Geologists Memoir 33, p. 268-295.

Flügel, E. (Ed.). (2004). *Microfacies of Carbonate Rocks: Analysis, Interpretation and Application*. New York, NY: Springer-Verlag Berlin Heidelberg.

Harries, P. J., 2009, *Epeiric Seas: A Continental Extension of Shelf Biotas*: Encyclopedia of Life Support Systems, v. 4., 1-6 pp.

Hagood, W. K., Cimino, V., Totten, M., and Raef, A., 2018, *Analysis and Integration of Well Logs and Ultrasonic Velocities of Productive Facies in the Upper Viola Formation in Southwestern Kansas*: AAPG Search and Discovery Article #11110.

James, N.P., 1984**,** Shallowing-upward sequences in carbonates, in Walker, R.G., ed., Facies Models: Geological Association of Canada, Geoscience Canada, Reprint Series 1, p. 213–228.

Kansas Geological Survey, 2018, <http://www.kgs.ku.edu>, October 2018.

Linares, A., 2016, *Petrographic Analysis and Diagenetic History of the Viola Limestone at Stephen's Ranch, in the Morrison Northeast Field of Clark County, Kansas*, M. S. Thesis, Kansas State University, 63 pp.

Martin, R. (Ed.). (2016). Mesozoic Era. In *Earth's Evolving Systems: The History of Planet Earth* (pp. 364-420). Burlington, MA: Jones & Bartlett Learning.

Merriam, D.F., 1963, Geologic History of Kansas: Kansas Geol. Survey Bulletin, v. 162, 317 pp.

Montgomery, S. L., Franseen, E. K., Bhattacharya, S., Gerlach, P. M., Brynes, A., and Guy, W. L., 2000, Schaben field, Kansas: Improving performance in a Mississippian shallow-shelf carbonate: AAPG Bulletin, v. 84, p. 1069–1086.

Nelson, S.A., 2013, "Carbonates & Other Rocks", <https://www.tulane.edu/~sanelson/eens212/carbonates.htm>, February 2019.

Newell, K. D., Watney, W. L., Cheng, S. W. L., Brownrigg, R. L., 1987, Stratigraphic and Spatial Distribution of Oil and Gas Production in Kansas: Kansas Geological Survey Series, v. 9, 86 pp.

Richardson, L. J., 2013, *The Herd Viola Trend, Comanche County, Kansas*: AAPG Mid-Continent Section Meeting 20220th ser., 1-32 pp.

Scholle, P. A. and Ulmer-Scholle, D. S., 2003, A Color Guide to the Petrography of Carbonate Rocks: AAPG Memoir 77, 474 pp.

Shinn, E. A., 1983, Tidal Flat Environment, in Scholle, P. A., Bebout, D. G., and Moore, C. H., eds., Carbonate Depositional Environments: American Association of Petroleum Geologists Memoir 33, p. 172-210.

Scholle, P. A., Arthur, M. A., Ekdale, A. A., 1983, Pelagic Environment, in Scholle, P. A., Bebout, D. G., and Moore, C. H., eds., Carbonate Depositional Environments: American Association of Petroleum Geologists Memoir 33, p. 620-691.

Scholle, Peter A., Don G. Bebout, and Clyde H. Moore, eds. 1983. AAPG Memoir. Vol. 33, Carbonate Depositional Environments. Tulsa, Okla., U.S.A.: American Association of Petroleum Geologists.

St. Clair, P. N., 1985, *Core studies of the Viola Limestone in Barber and Pratt counties, south-central Kansas; in, Core Studies in Kansas; Sedimentology and Diagenesis of*

Economically Important Rock Strata in Kansas, W. L. Watney, J. H. Doveton, and A. W. Walton, comps.: Kansas Geological Survey, Subsurface Geology Series 6, 8-16 pp.

Turner, B. W., Tréanton, J. A., Slatt, R. M., 2015, *The Use of Chemostratigraphy to Refine Ambiguous Sequence Stratigraphic Correlations in Marine Shales: An Example From the Woodford Shale, Oklahoma*: AAPG Search and Discovery Article #90216.

Vohs, A B., 2016, *3D seismic attributes analysis in reservoir characterization: The Morrison NE field & Morrison field, Clark County Kansas*, M.S. Thesis, Kansas State University, 91 pp.

Wheeler, B. D., 1999, Analysis of Limestones and Dolomites by X-Ray Fluorescence, The Rigaku Journal, v. 16, p. 16-25.

Zeller, D.E., 1968, The Stratigraphic Succession of Kansas,

Kansas: Geol. Survey Bulletin, v. 189, 81 pp.

Appendix A - Description Profiles and Logs

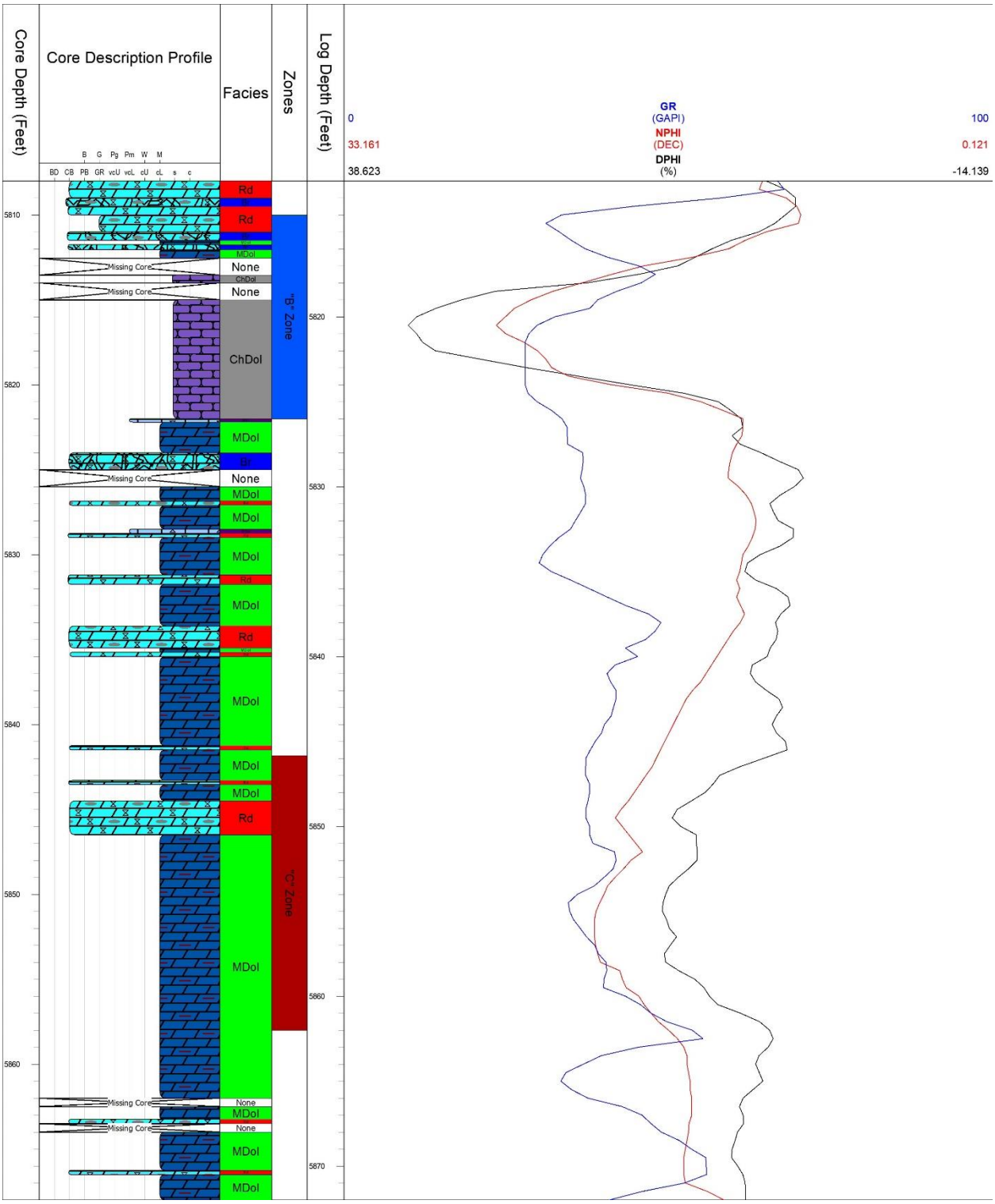

Figure A.1: Core description profile of Rich C-7 displaying well log facies, described facies from core, gamma ray (GR), density porosity (DPHI), and neutron porosity (NPHI).

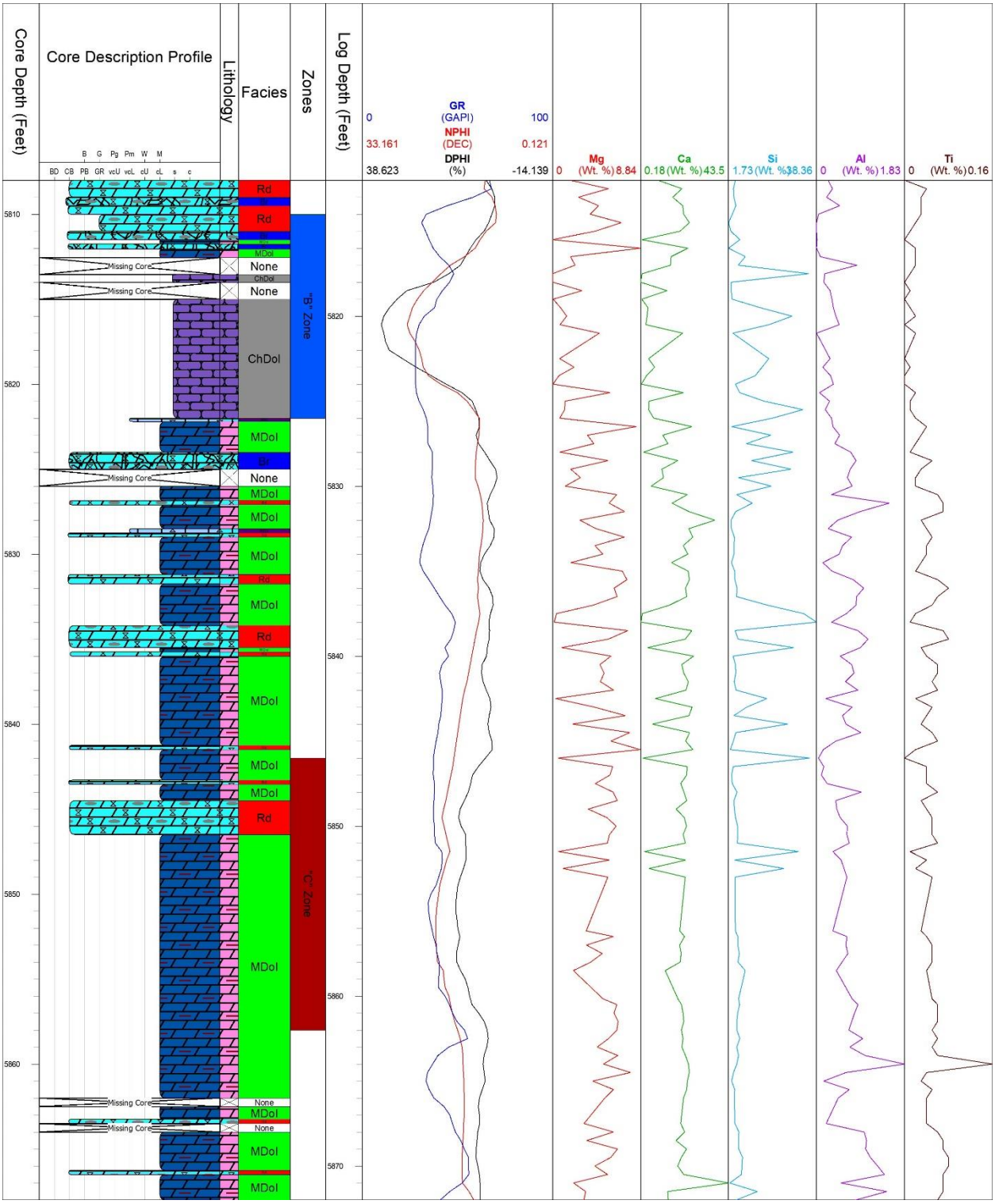

Figure A.2: Core description profile of Rich C-7 displaying well log facies, described facies from core, GR, DPHI, NPHI, and HHXRF chemical data from Mg, Ca, Si, Al, and Ti.

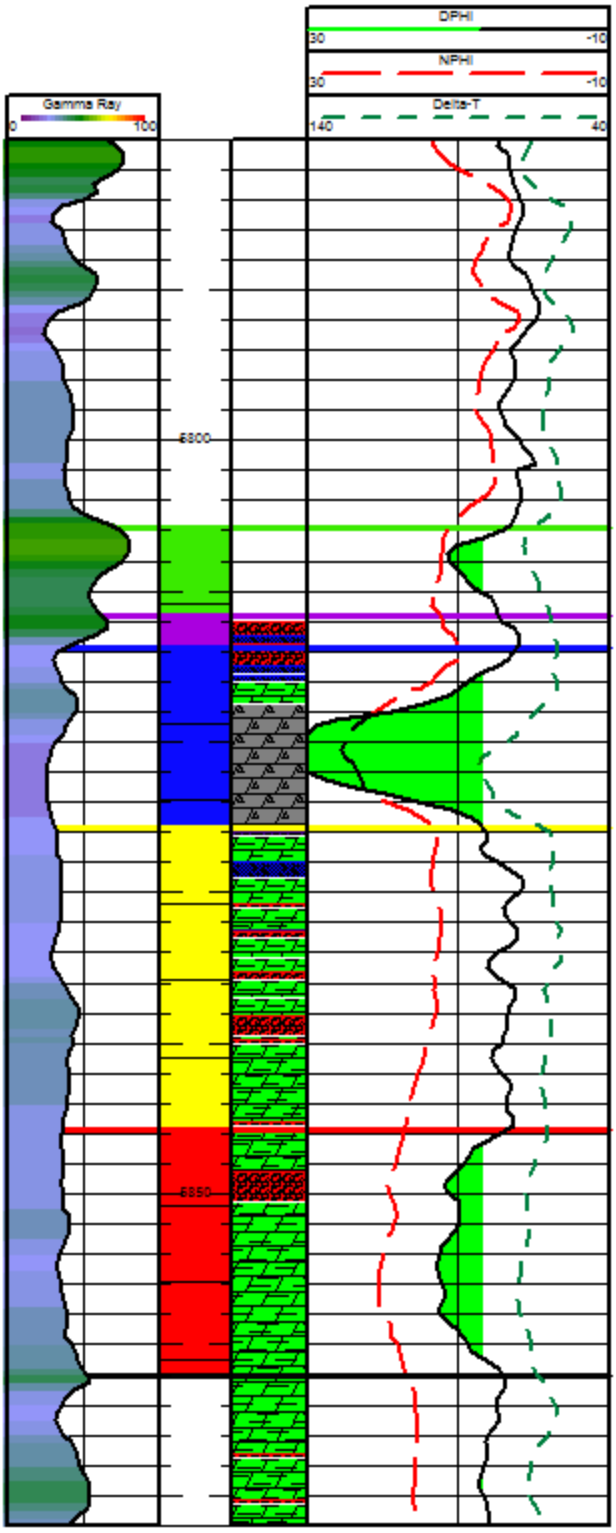

Figure A.3: Well log of Rich C-7 displaying GR, DPHI, NPHI, Sonic in Delta-T (DT), well log facies, and described facies from core.

Appendix B - Thin Section Descriptions

5808’-5814.9’

Figure B.1: Box: 1-3; Depth: 5808’-5814.9’.

5808’:

Lithofacies: Intraclastic Rudstone
Primary Constituents: Dolomitic, siliceous, and mud intraclasts, detrital quartz grains, sparse echinoderms, rare phosphate grains
Porosity Type: Intergranular, Interparticle
Porosity %: 5

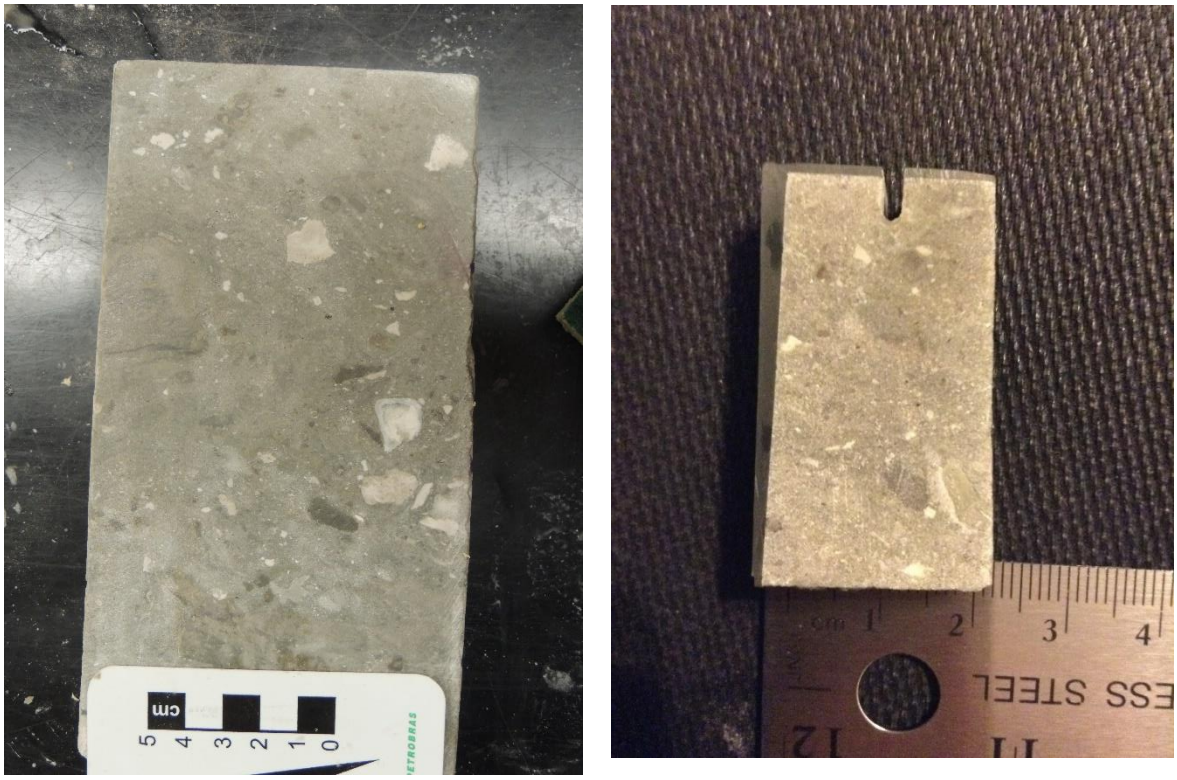

Figure B.2: Cored section of Intraclastic rudstone in the Viola Ls. from Rich C #7 (left) and thin section plug of this core piece taken at 5808’(right).

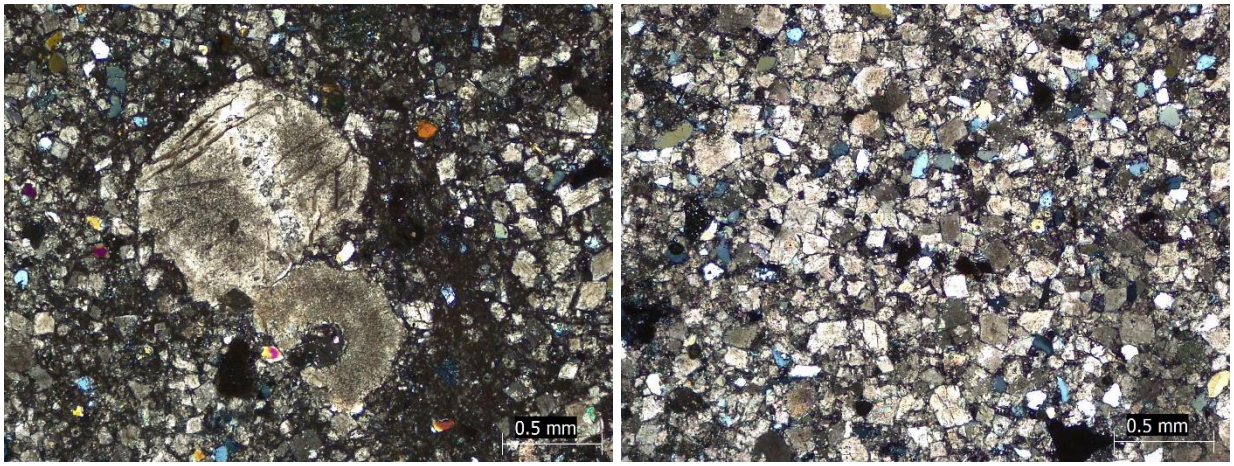

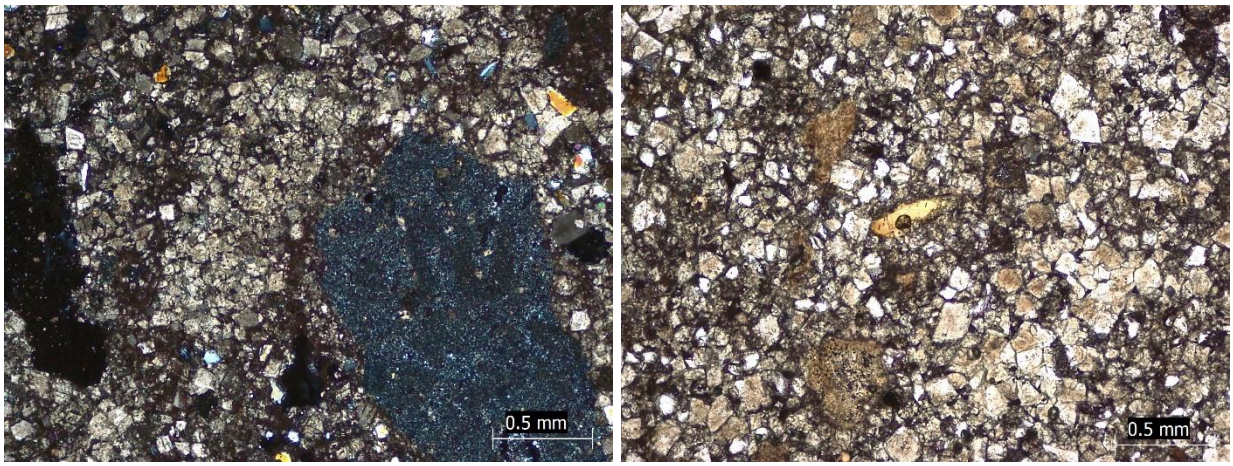

Figure B.3: Thin section photomicrographs of Rudstone at 5808' from the Rich C #7 well. From left to right, the photomicrographs are in XPL, XPL, XPL, and PPL.

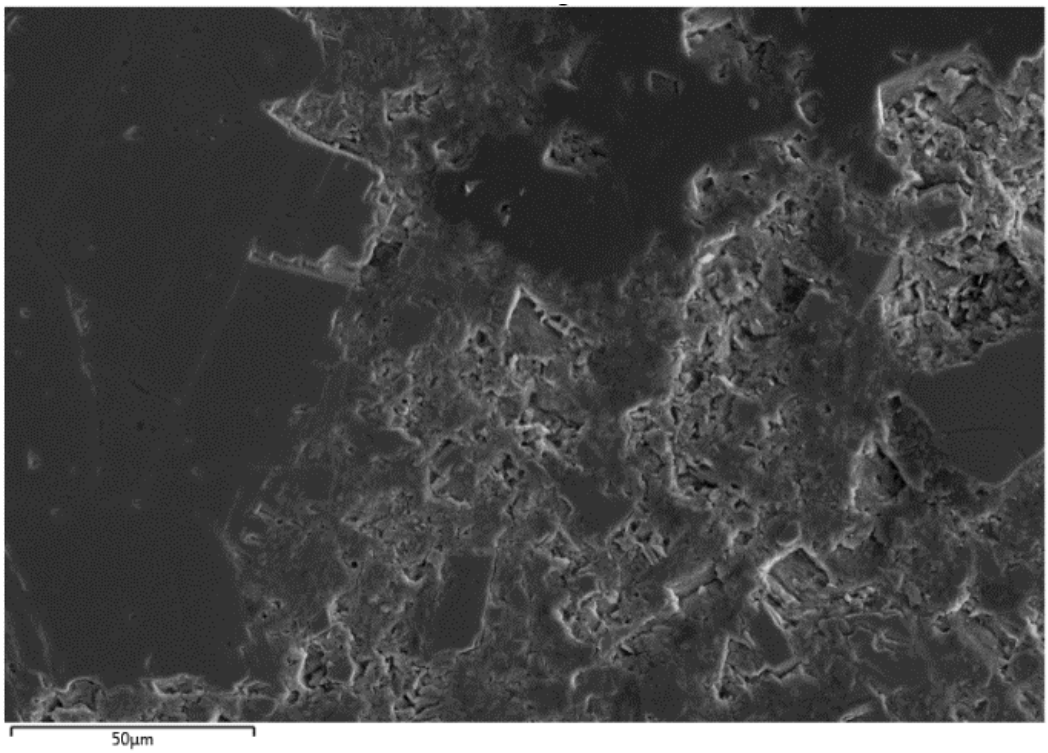

Figure B.4: SEM image at 50µm of the Rudstone thin section at 5808' from the Rich C #7 well. This thin section was coated with a 10 nm thick gold coating.

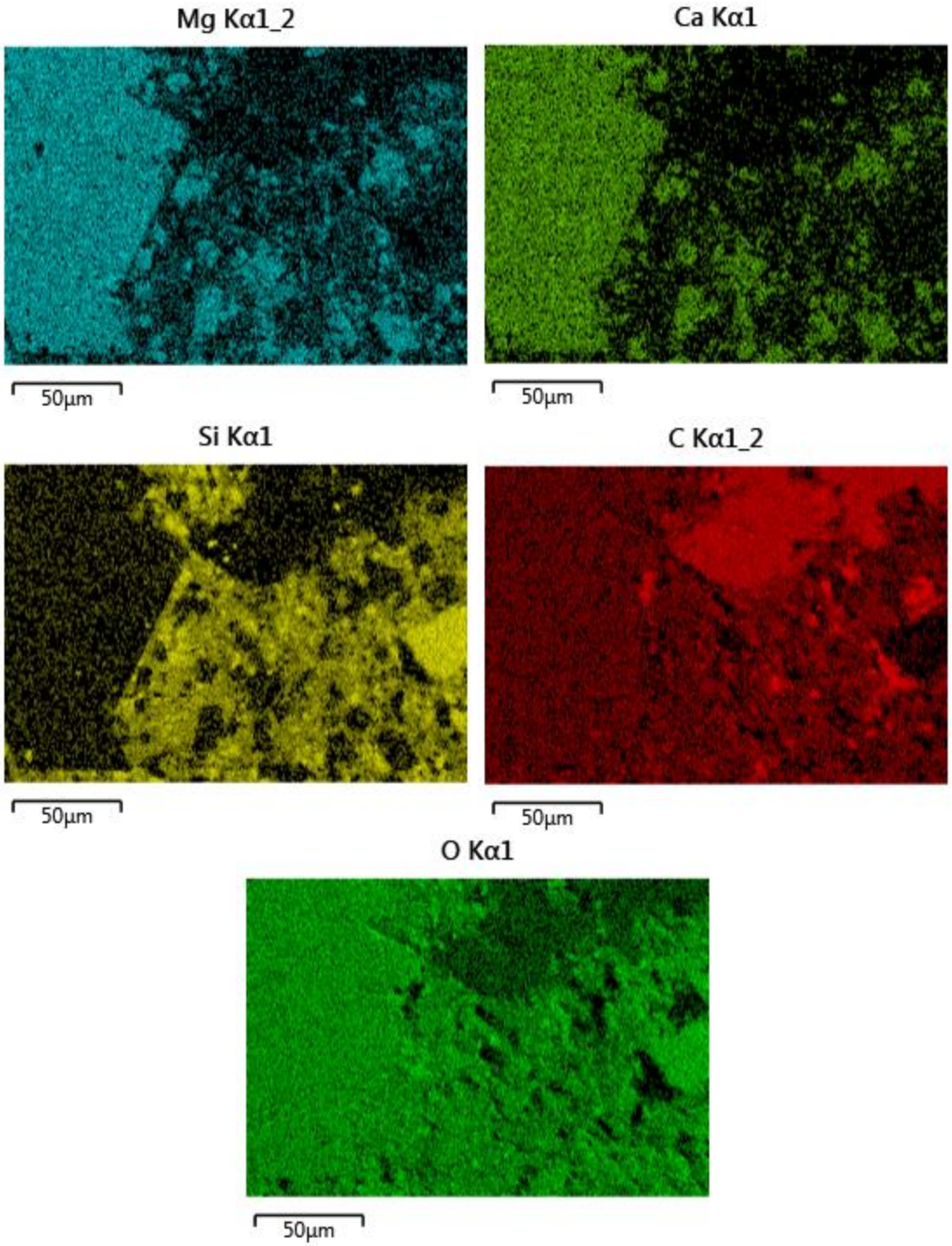

Figure B.5: From left to right, EDS map images showing the distribution of dolomite (Mg), calcite (Ca), silicates (Si), carbon, and oxygen from the previous SEM image at 5808'.

5811.66':

Lithofacies: Intraclastic Breccia
Primary Constituents: Angular chert intraclasts, cemented by dolomite, rare pyrite

Porosity Type: Intergranular, Interparticle
Porosity %: 10

Figure B.6: Cored section of Intraclastic breccia in the Viola Ls. from Rich C #7 (left) and thin section plug of this core piece taken at 5811.66'(right).

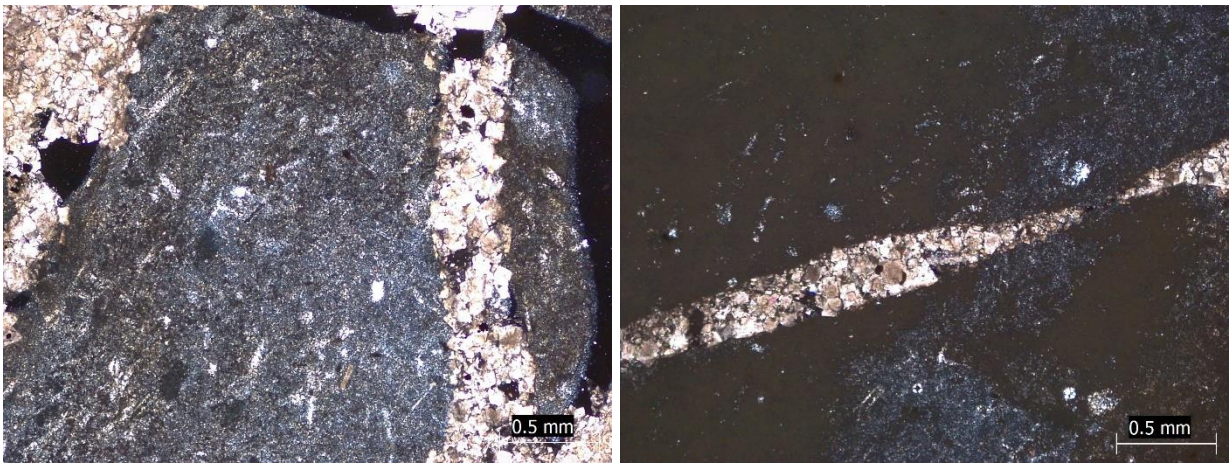

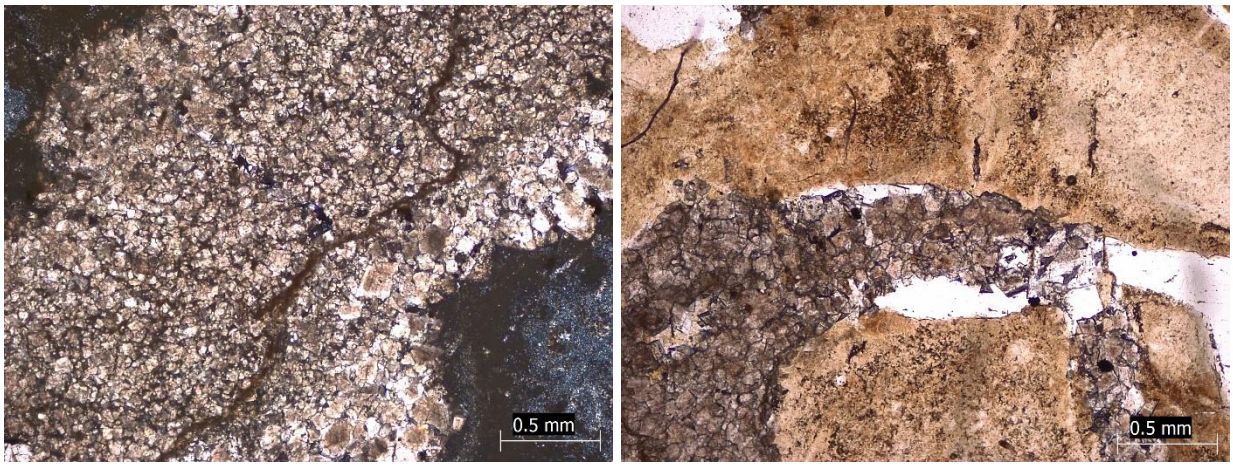

Figure B.7: Thin section photomicrographs of Breccia at 5811.6' from the Rich C #7 well. From left to right, the photomicrographs are in XPL, XPL, XPL, and PPL.

5812':

Lithofacies: Intraclastic Breccia
Primary Constituents: Dolomitic, siliceous, chert, and mud intraclasts, rare pyrite
Porosity Type: Intergranular, Vuggy
Porosity %: 7

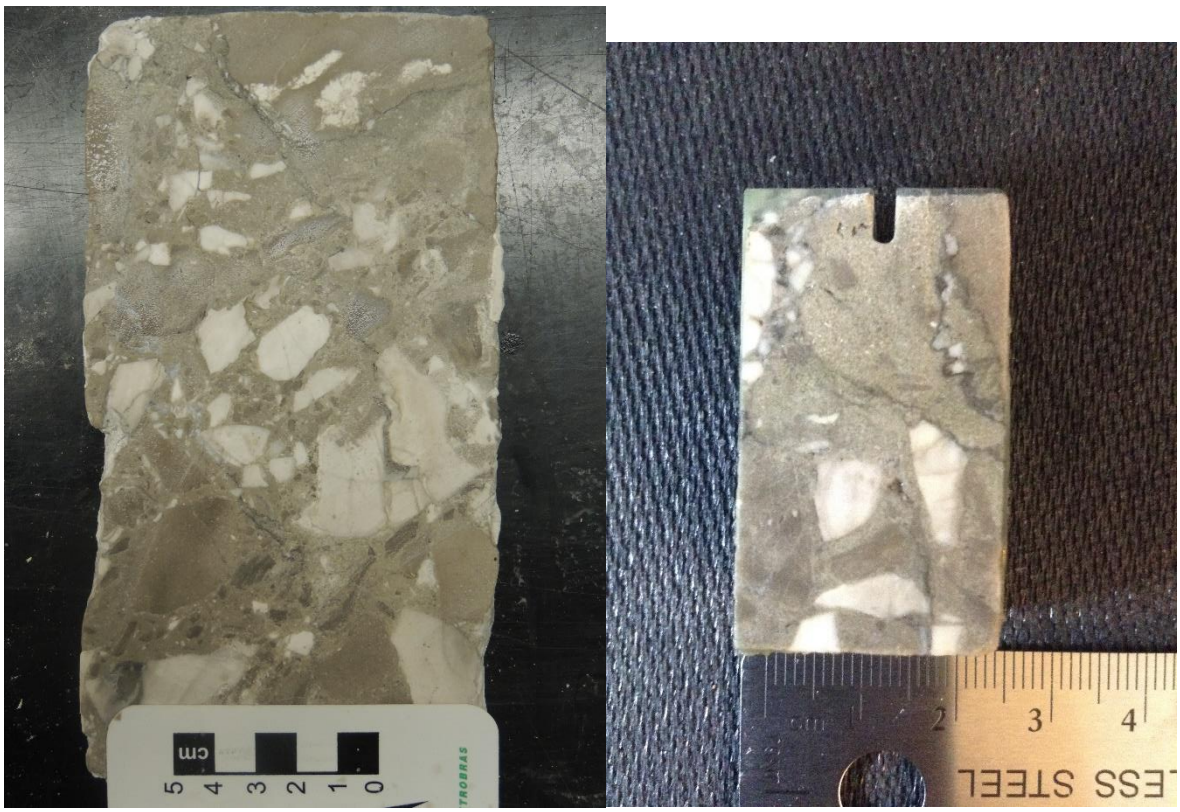

Figure B.8: Cored section of Intraclastic breccia in the Viola Ls. from Rich C #7 (left) and thin section plug of this core piece taken at 5812'(right).

Figure B.9: Thin section photomicrographs of Breccia at 5812' from the Rich C #7 well. From left to right, the photomicrographs are in XPL, XPL, PPL, and PPL.

5815’-5825.5’

Figure B.10: Box: 4-7; Depth: 5815’-5825.5’.

5818.5':

Lithofacies: Cherty Dolomite
Primary Constituents: Chert, dolomite rhombs
Porosity Type: Intergranular
Porosity %: 30

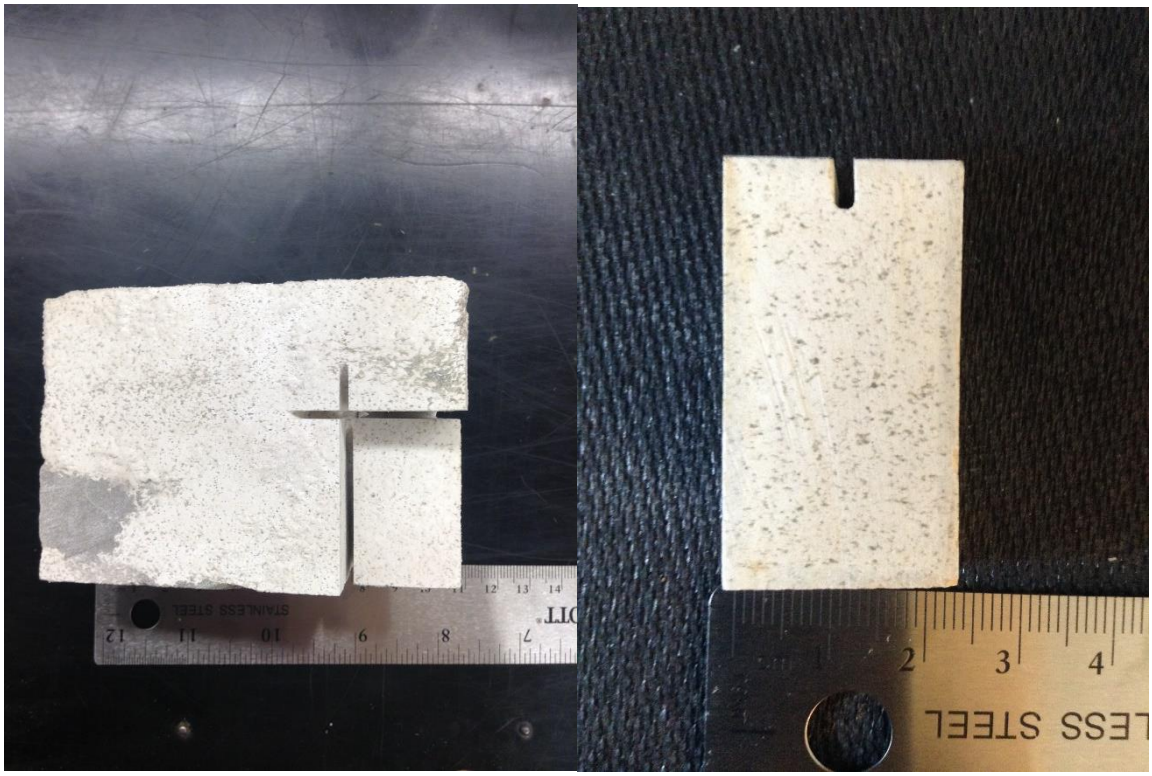

Figure B.11: Cored section of Cherty dolomite in the Viola Ls. from Rich C #7 (left) and thin section plug of this core piece taken at 5818.5'(right).

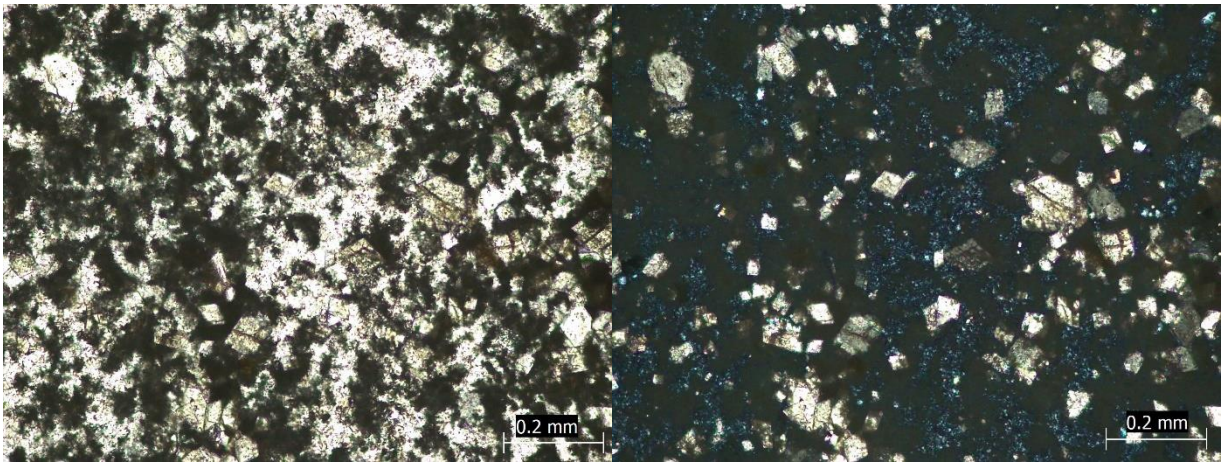

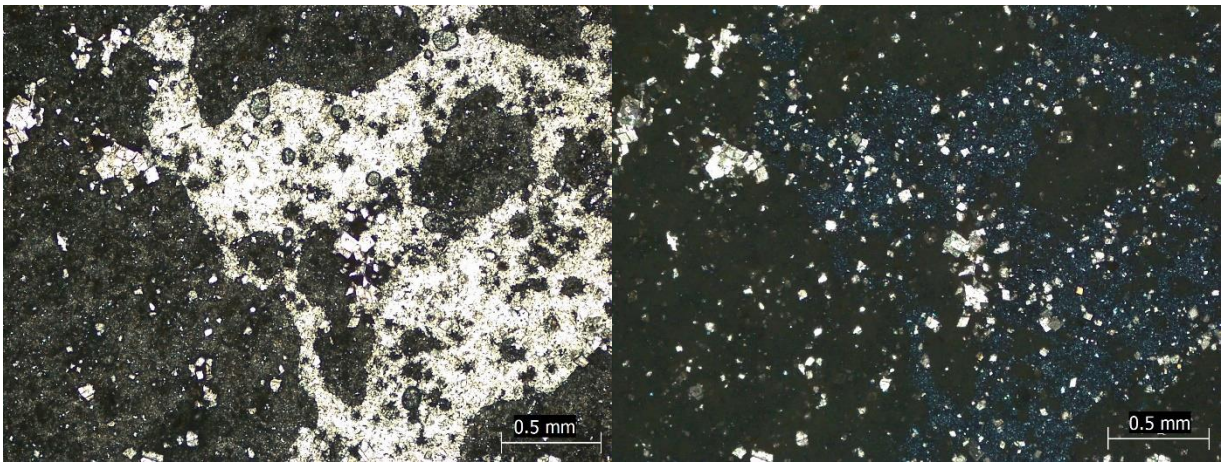

Figure B.12: Thin section photomicrographs of Cherty dolomite at 5818.5' from the Rich C #7 well. From left to right, the photomicrographs are in PPL, XPL (same microscope location as previous image), PPL, and XPL (same microscope location as previous image).

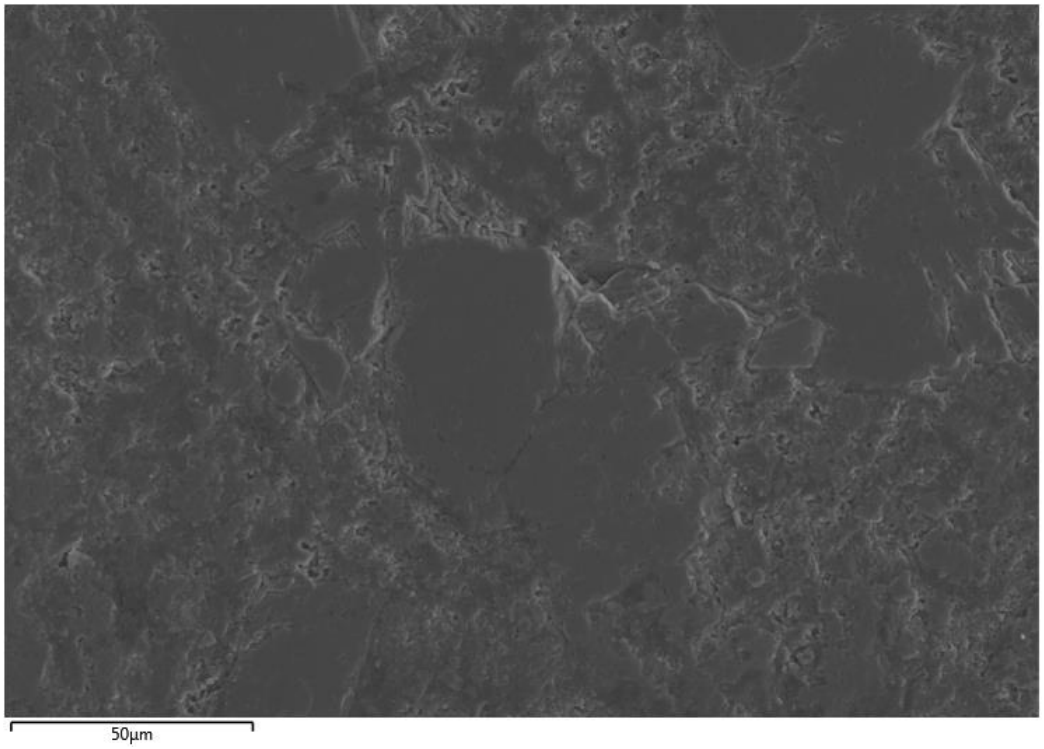

Figure B.13: SEM image at 50µm of the Cherty dolomite thin section at 5818.5' from the Rich C #7 well. This thin section was coated with a 10 nm thick gold coating.

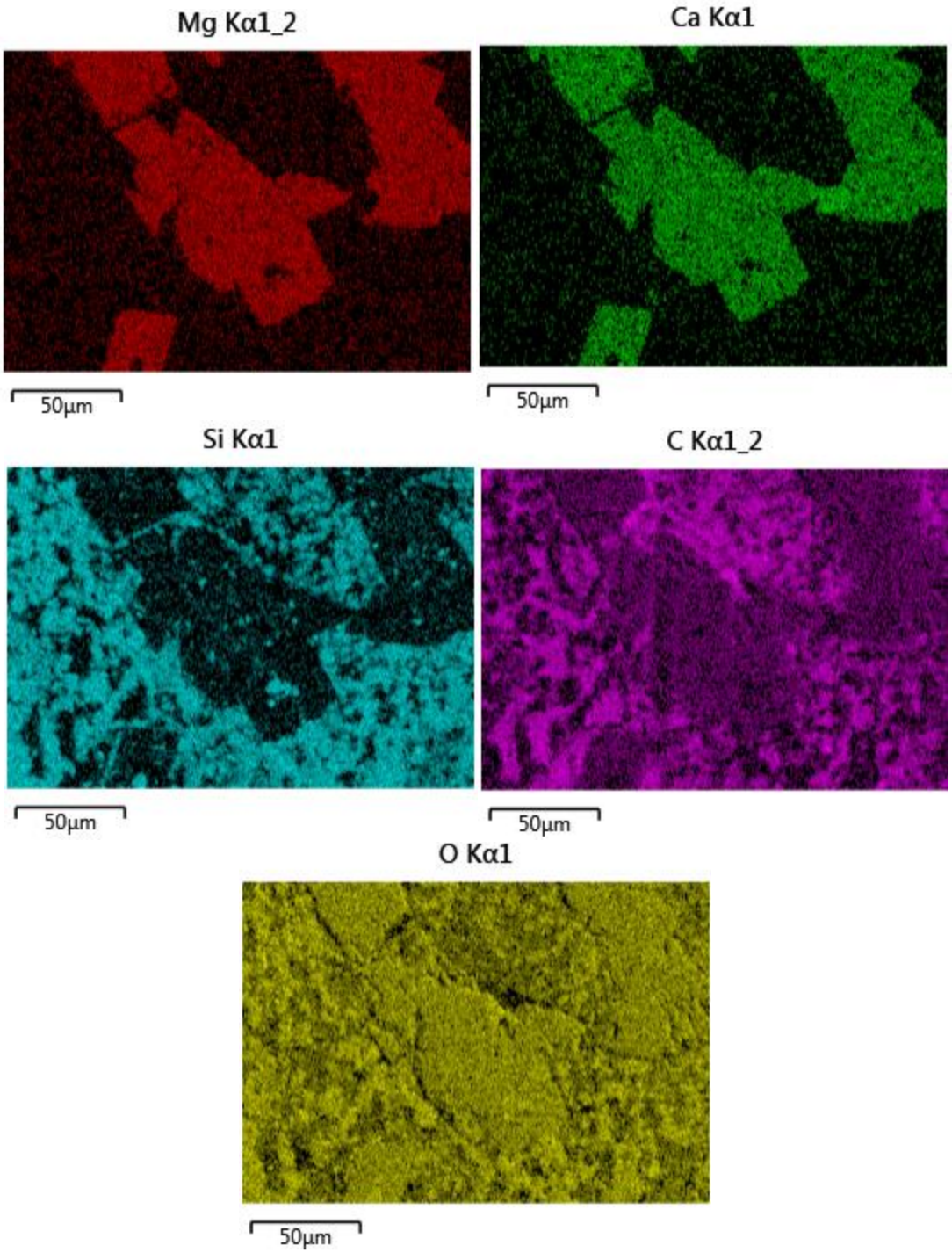

Figure B.14: From left to right, EDS map images showing the distribution of dolomite (Mg), calcite (Ca), silicates (Si), carbon, and oxygen from the previous SEM image at 5818.5'.

5822':

Lithofacies: Cherty Dolomite

Primary Constituents: Chert, sponge spicules, dolomite rhombs
Porosity Type: Intergranular, Vuggy
Porosity %: 20

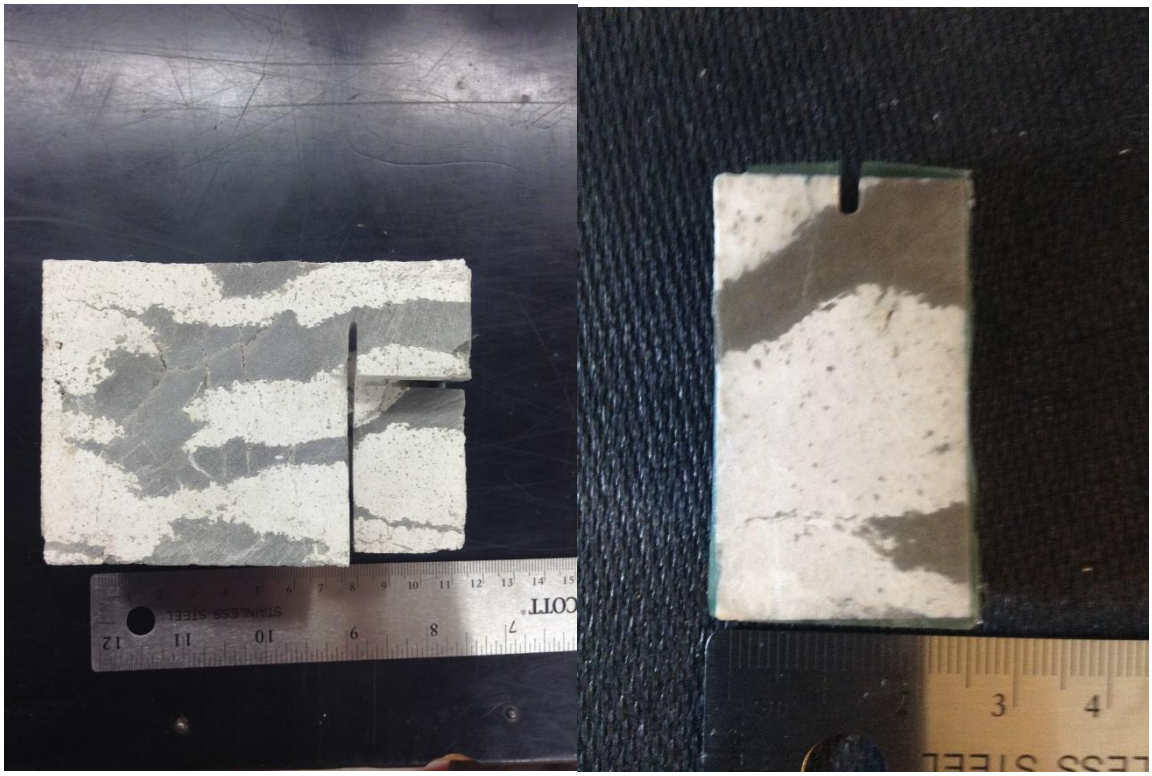

Figure B.15: Cored section of Cherty dolomite in the Viola Ls. from Rich C #7 (left) and thin section plug of this core piece taken at 5822'(right).

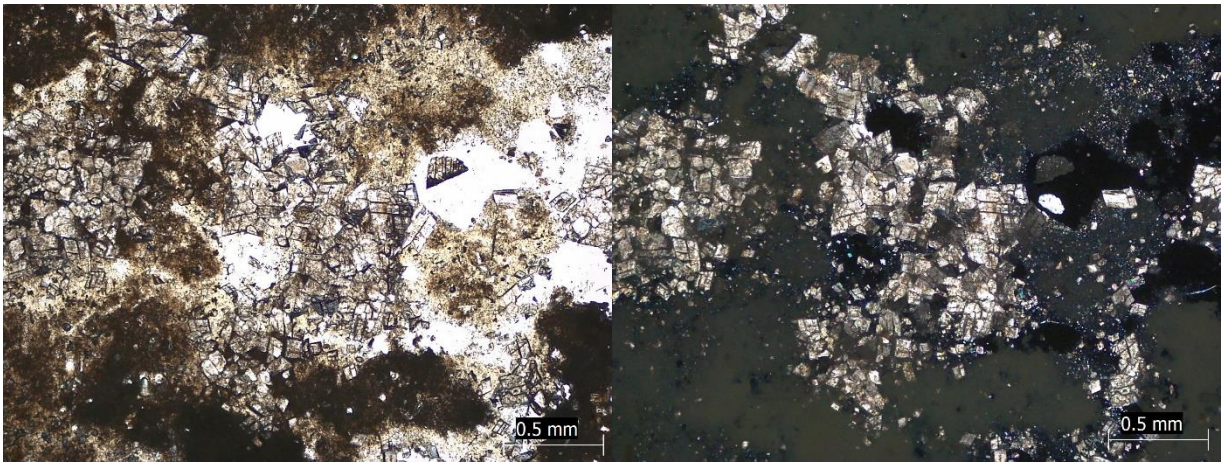

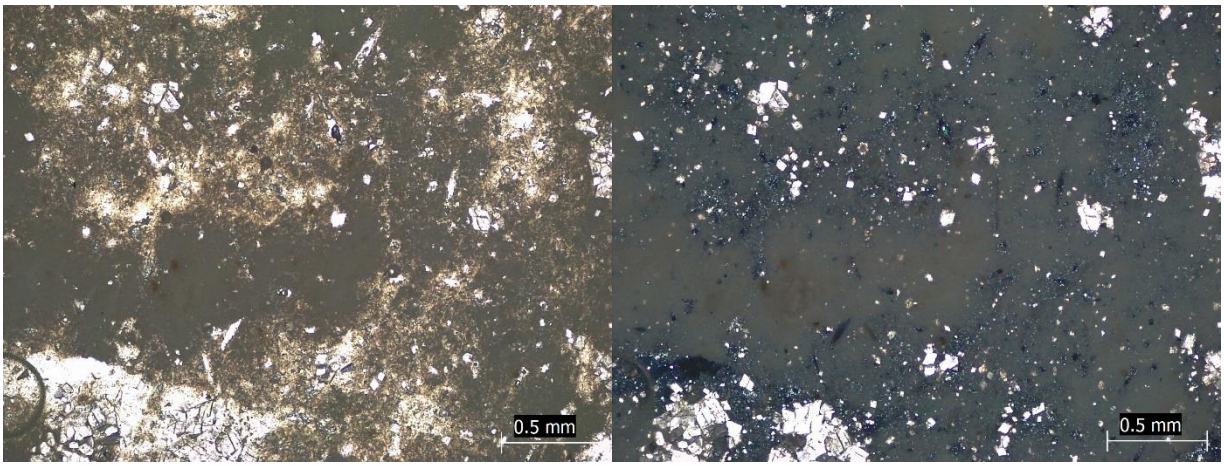

Figure B.16: Thin section photomicrographs of Cherty dolomite at 5822' from the Rich C #7 well. From left to right, the photomicrographs are in PPL, XPL (same microscope location as previous image), PPL, and XPL (same microscope location as previous image).

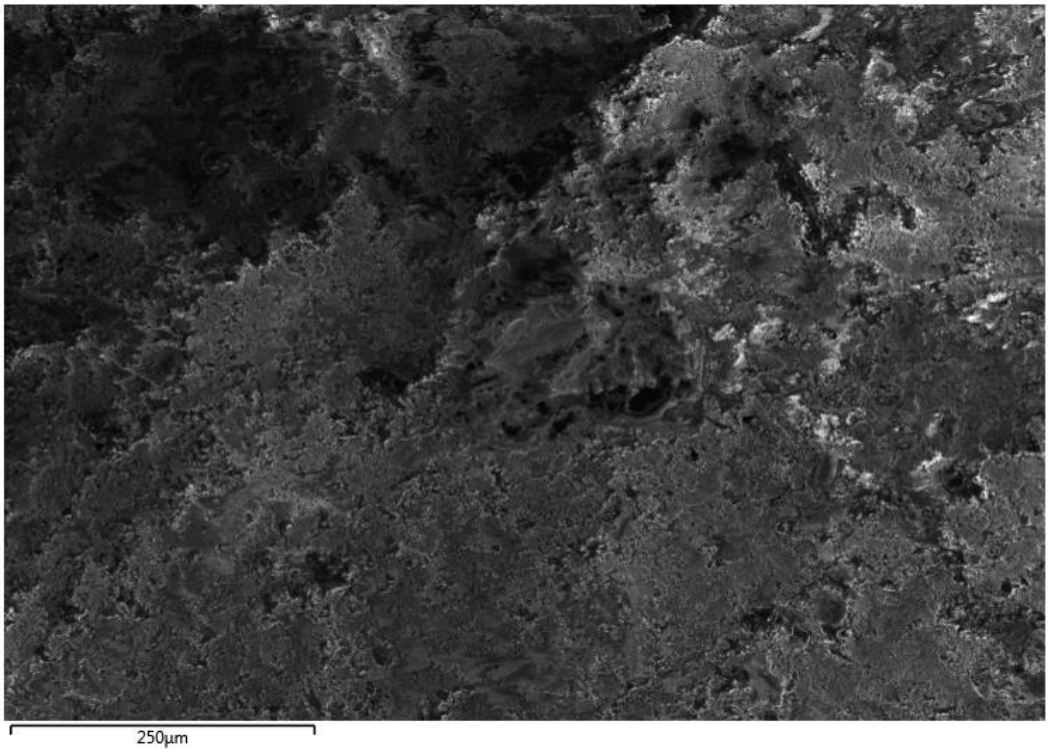

Figure B.17: SEM image at 250µm of the Cherty dolomite thin section at 5822' from the Rich C #7 well. This thin section was not coated with gold.

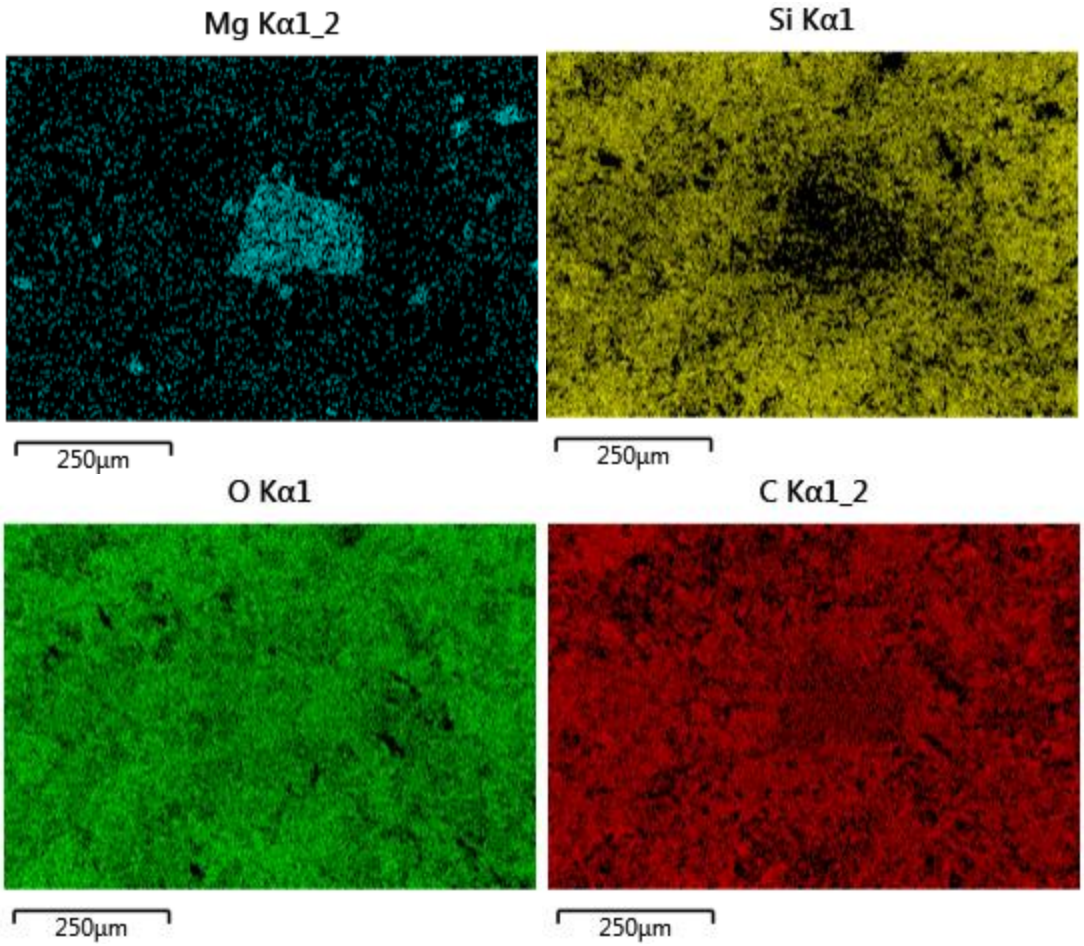

Figure B.18: From left to right, EDS map images showing the distribution of dolomite (Mg), silicates (Si), oxygen, and carbon from the previous SEM image at 5822'.

5822.5':

Lithofacies: Muddy Dolostone
Primary Constituents: Dolomite, pyrite, siliceous grains, calcite in fracture
Porosity Type: Intergranular, vug, fracture
Porosity %: 3

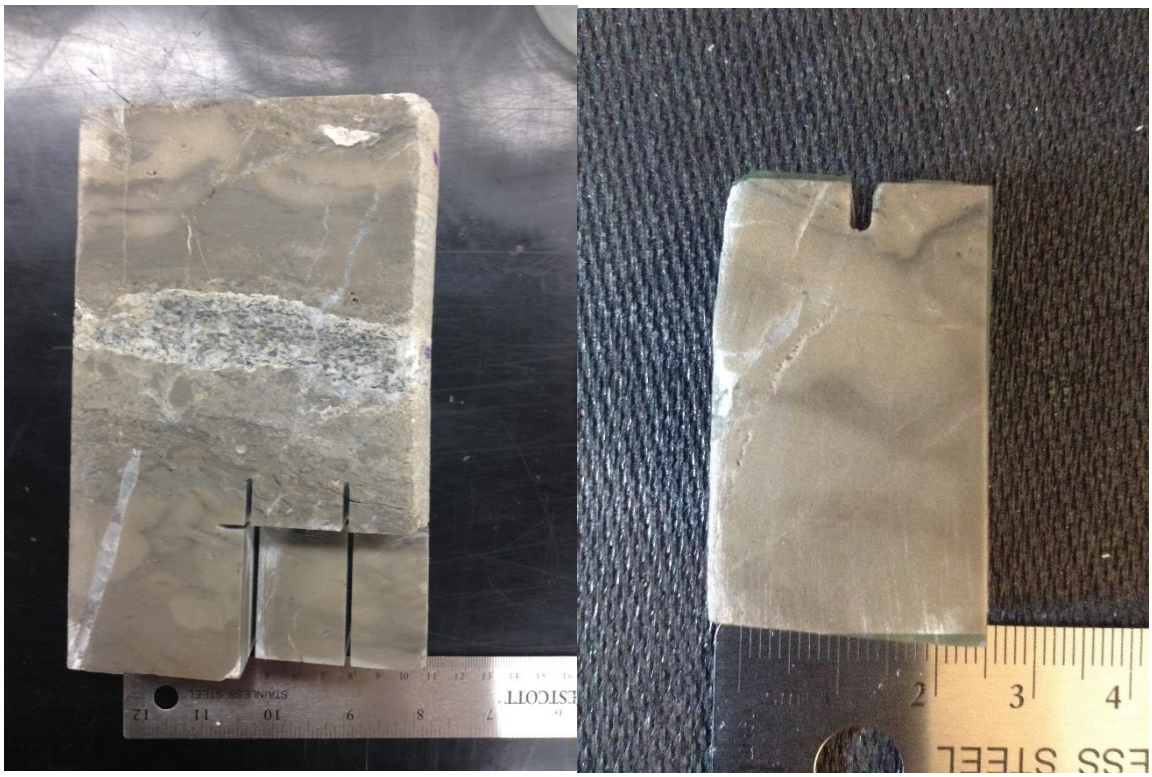

Figure B.19: Cored section of Muddy dolostone in the Viola Ls. from Rich C #7 (left) and thin section plug of this core piece taken at 5822.5'(right).

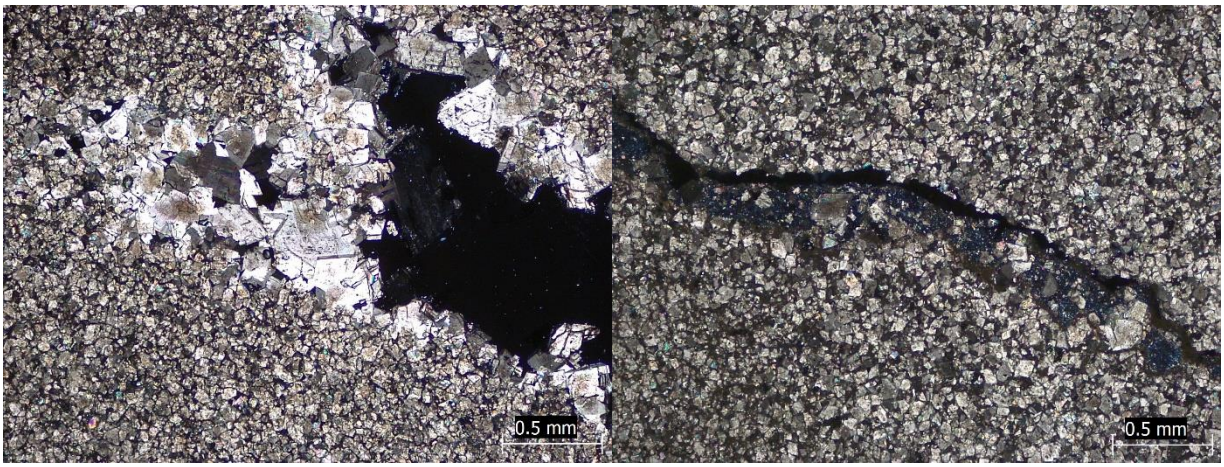

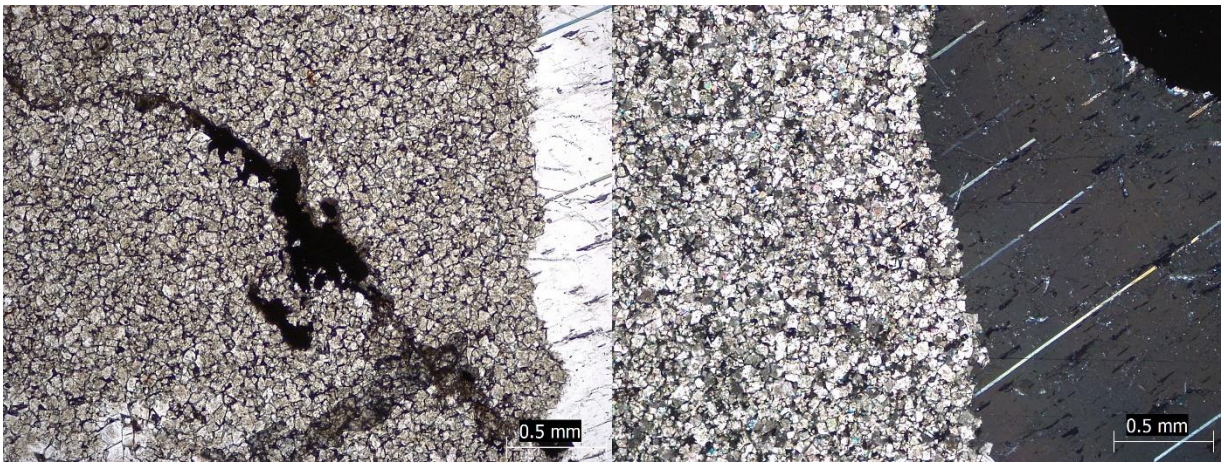

Figure B.20: Thin section photomicrographs of Muddy dolostone at 5822.5' from the Rich C #7 well. From left to right, the photomicrographs are in XPL, XPL, PPL, and XPL.

5824.66':

Lithofacies: Intraclastic Breccia
Primary Constituents: Angular dolomitic and siliceous intraclasts, fragments of chert with sponge spicules, bioclastic grainstone fragment with bryozoans and bivlaves, detrital quartz grains
Porosity Type: Intergranular, Interparticle
Porosity %: 3

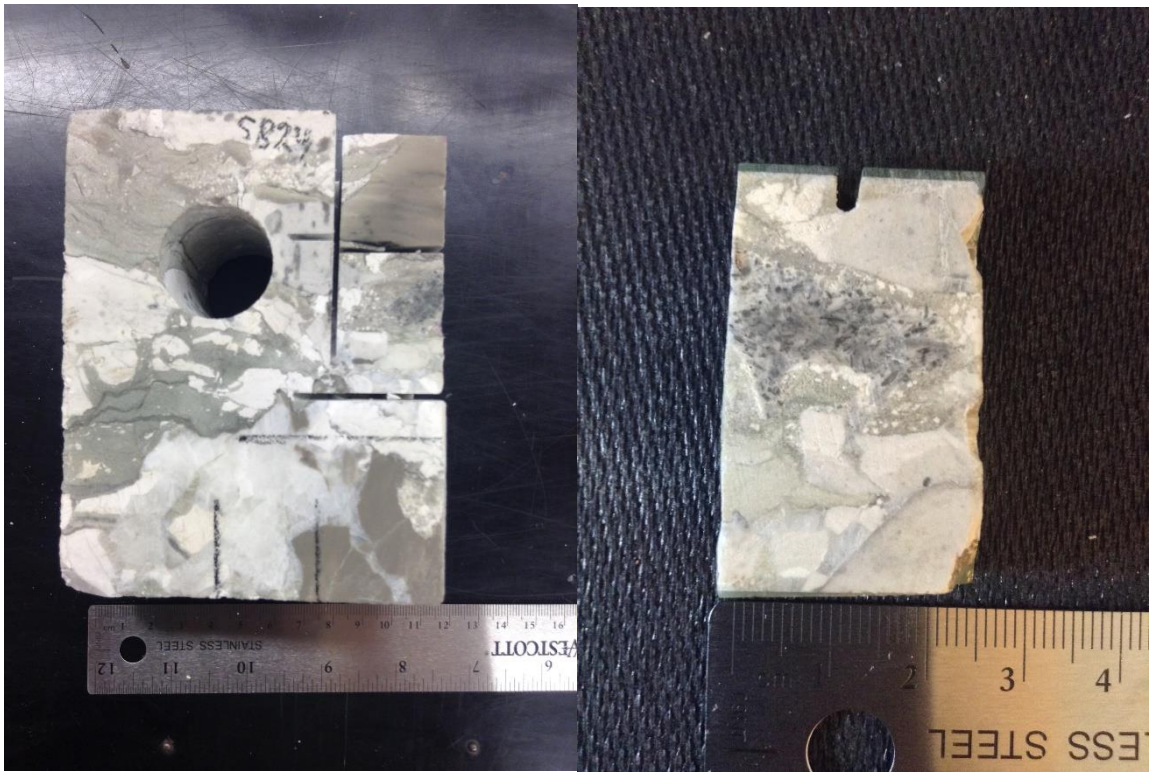

Figure B.21: Cored section of Intraclastic breccia in the Viola Ls. from Rich C #7 (left) and thin section plug of this core piece taken at 5824.66'(right).

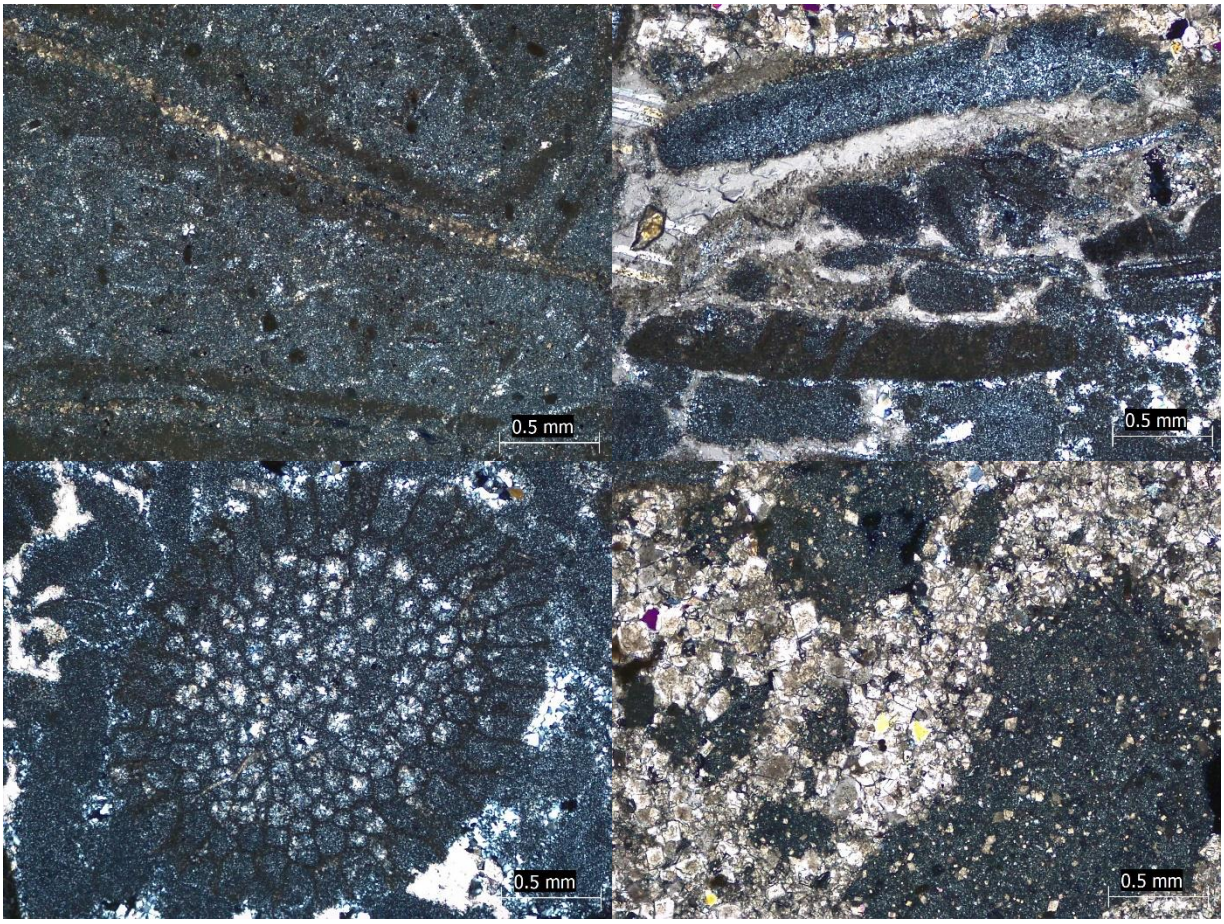

Figure B.22: Thin section XPL photomicrographs of Breccia at 5824.66' from the Rich C #7 well.

5825.83’-5836.5’

Figure B.23: Box: 8-11; Depth: 5825.83’-5836.5’.

5828.5':

Lithofacies: Bioclastic-intraclastic Grainstone
Primary Constituents: Silicified echinoderms, bryozoans, crinoids, and ooids, silica nodules, dolomitic intraclasts
Porosity Type: Intergranular
Porosity %: 3

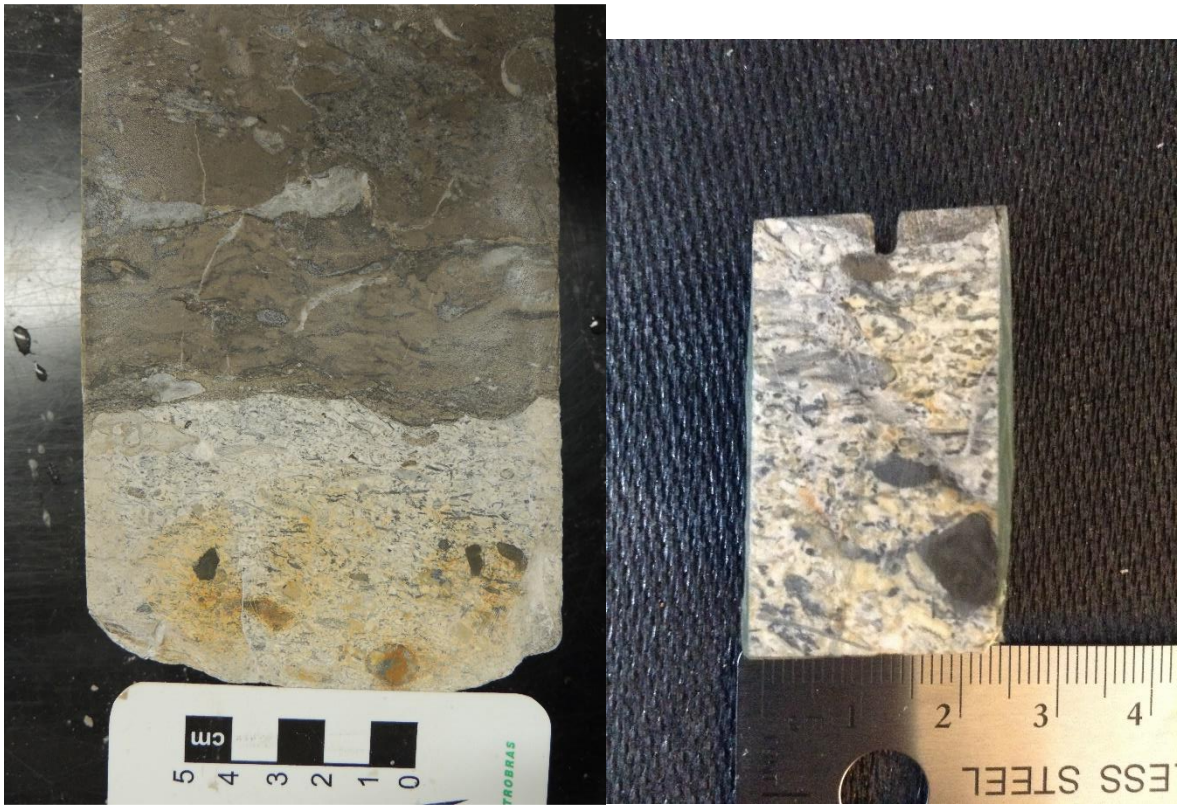

Figure B.24: Cored section of Bioclastic-intraclastic grainstone in the Viola Ls. from Rich C #7 (left) and thin section plug of this core piece taken at 5828.5'(right).

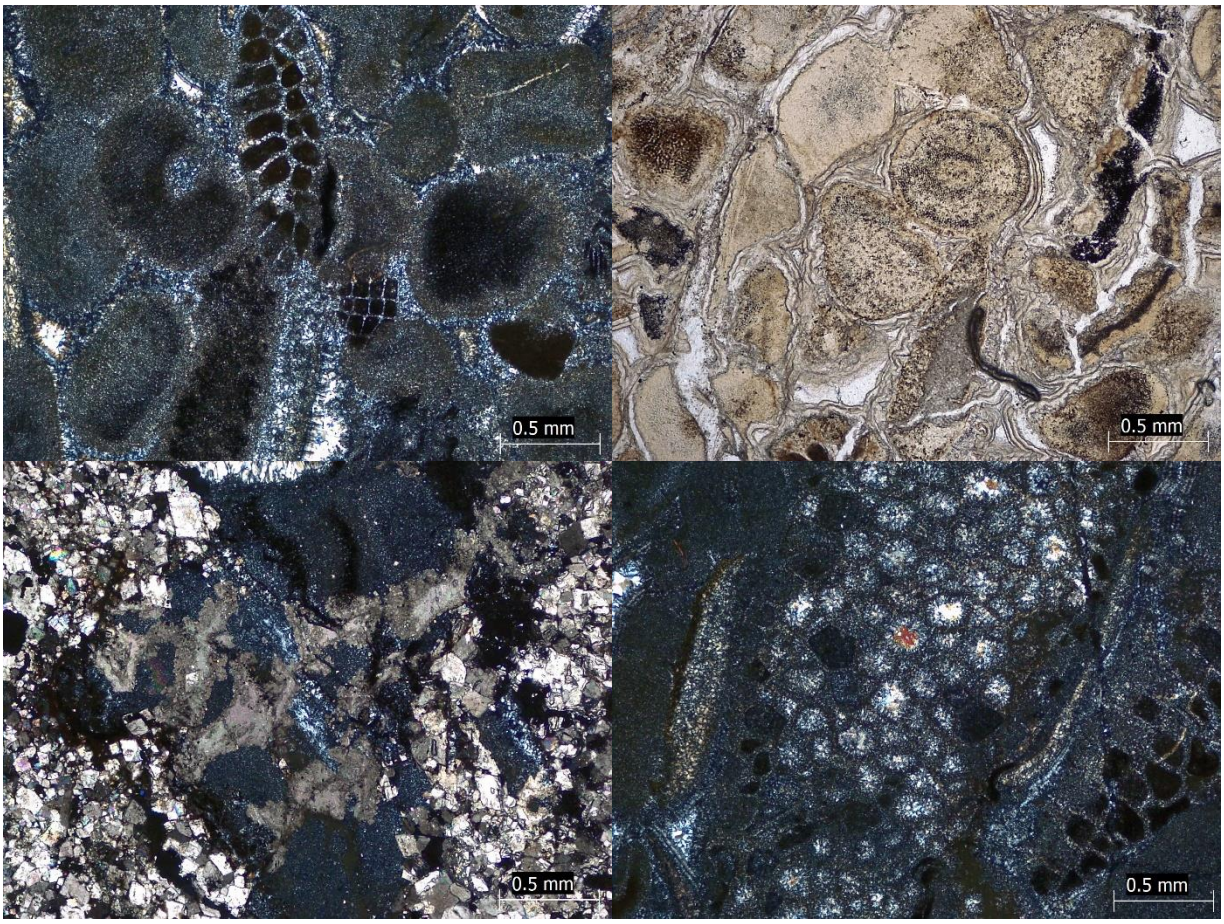

Figure B.25: Thin section photomicrographs of Grainstone at 5828.5' from the Rich C #7 well. From left to right, the photomicrographs are in XPL, PPL, XPL, and XPL.

5828.6':

Lithofacies: Intraclastic Rudstone
Primary Constituents: Dolomitic and siliceous intraclasts, rare pyrite
Porosity Type: Intergranular
Porosity %: 3

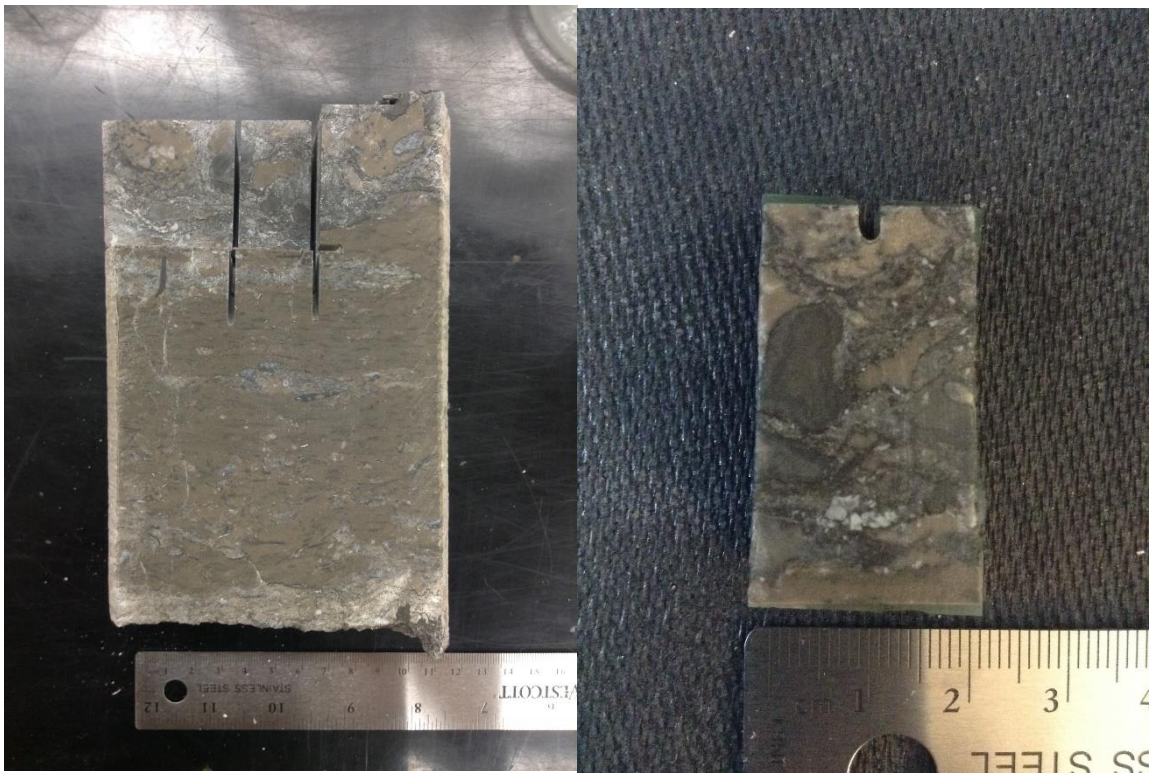

Figure B.26: Cored section of Intraclastic rudstone in the Viola Ls. from Rich C #7 (left) and thin section plug of this core piece taken at 5828.6'(right).

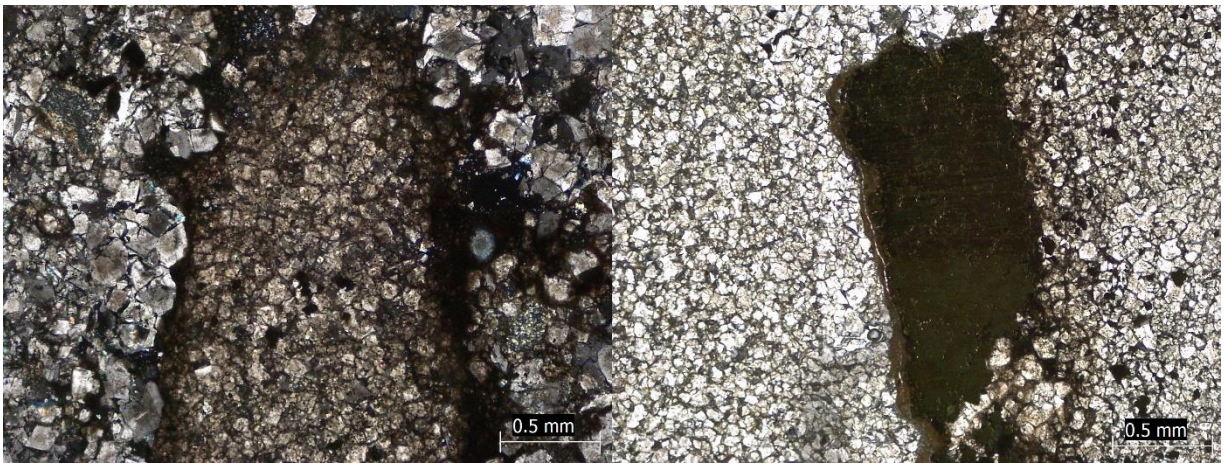

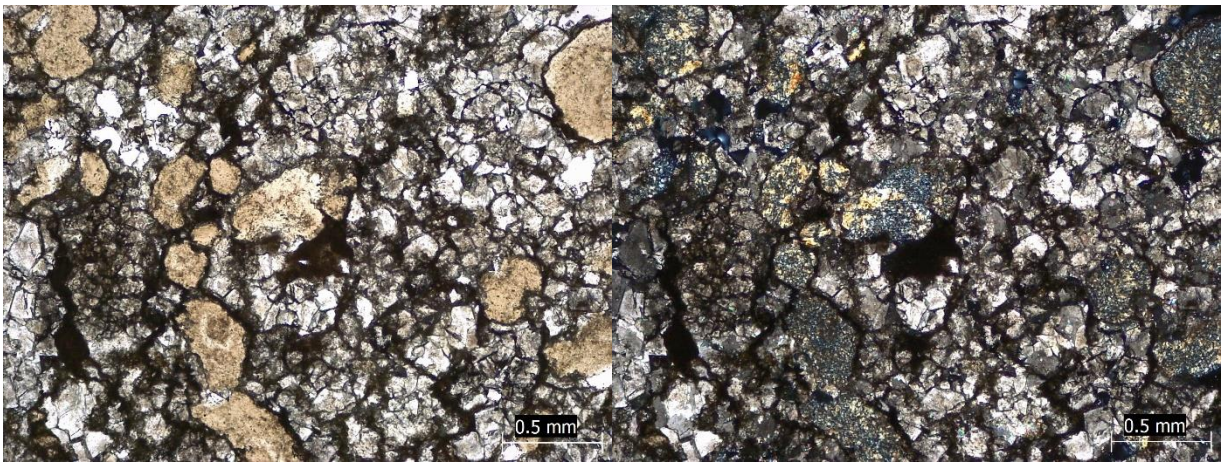

Figure B.27: Thin section photomicrographs of Rudstone at 5828.6' from the Rich C #7 well. From left to right, the photomicrographs are in XPL, PPL, PPL, and XPL (same microscope location as previous image).

5831.5':

Lithofacies: Intraclastic Rudstone
Primary Constituents: Dolomitic, siliceous, and dolomitic mud intraclasts
Porosity Type: Intergranular
Porosity %: 5

Figure B.28: Cored section of Intraclastic rudstone in the Viola Ls. from Rich C #7 (left) and thin section plug of this core piece taken at 5831.5'(right).

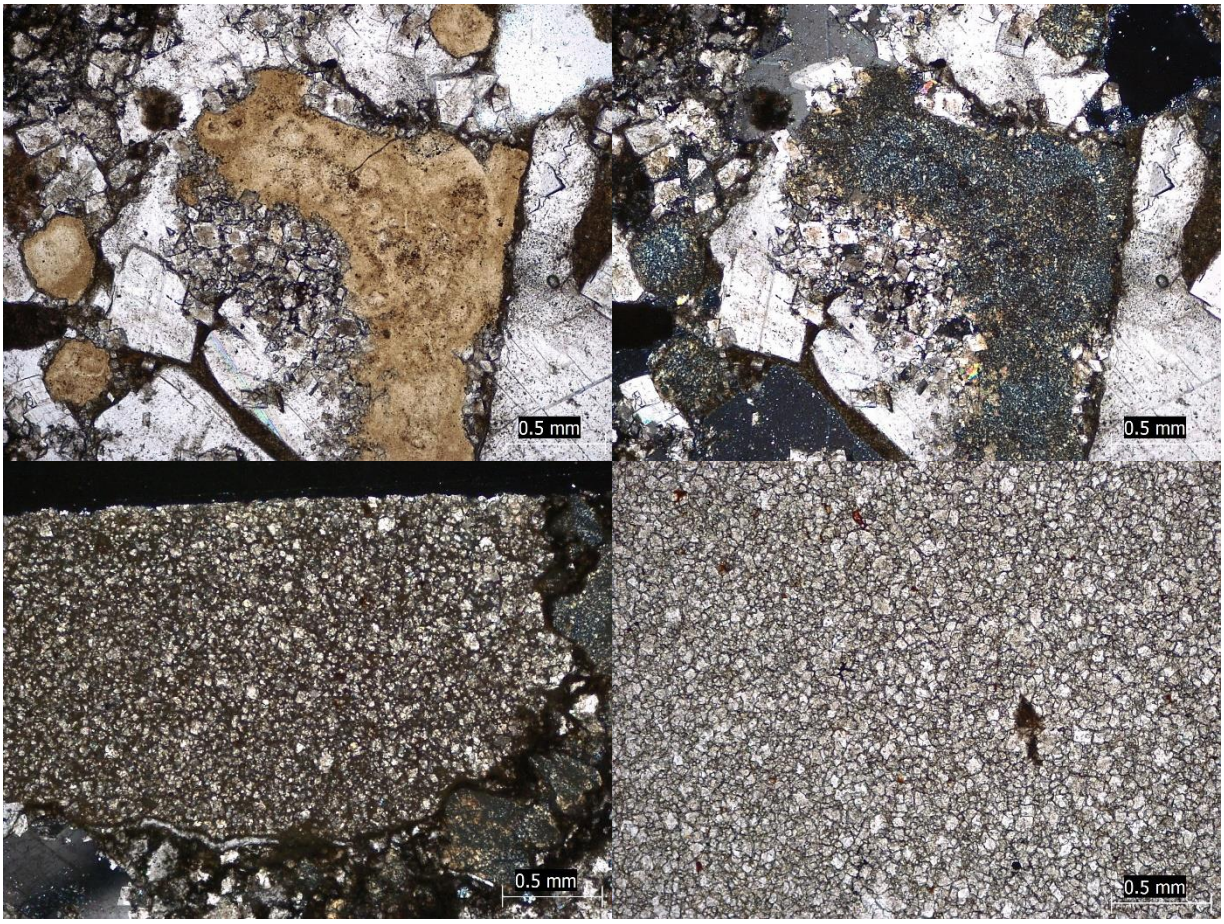

Figure B.29: Thin section photomicrographs of Rudstone at 5831.5' from the Rich C #7 well. From left to right, the photomicrographs are in PPL, XPL, XPL, and PPL.

5834':

Lithofacies: Muddy Dolostone
Primary Constituents: Laminated dolomite, chert with sponge spicules
Porosity Type: Intergranular
Porosity %: 10

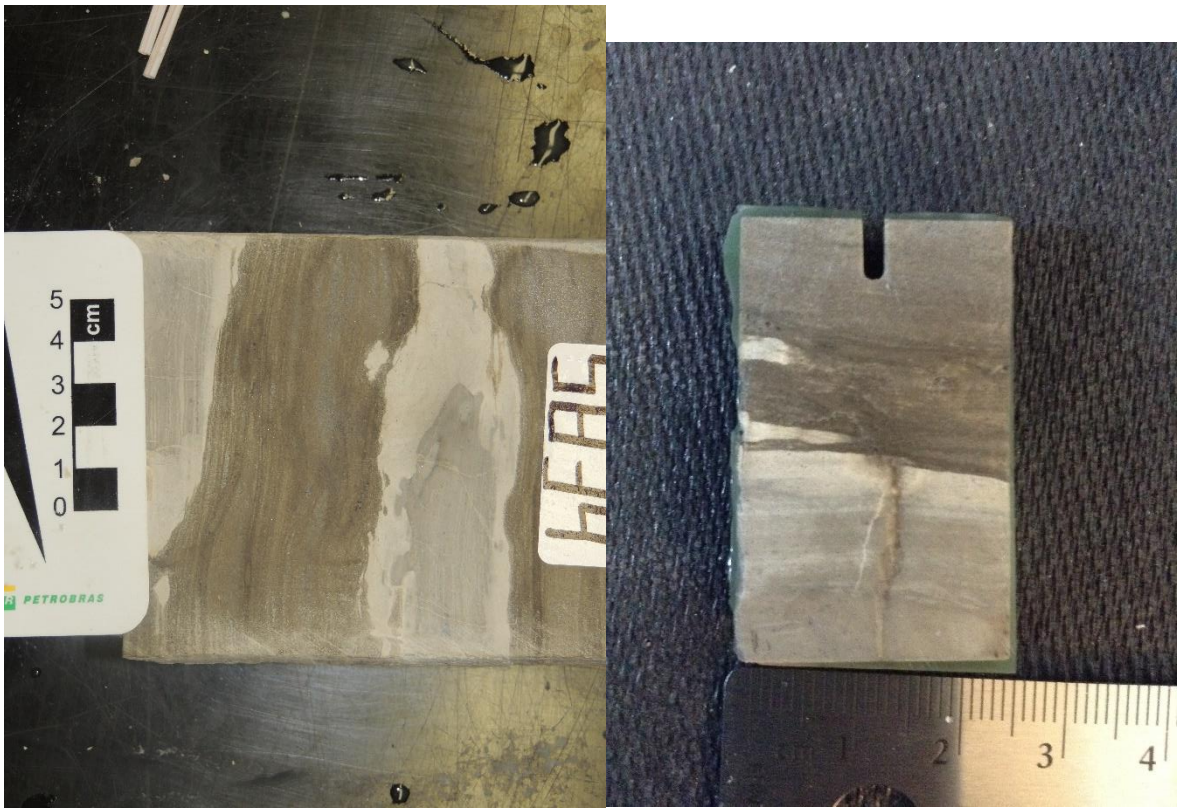

Figure B.30: Cored section of Muddy dolostone in the Viola Ls. from Rich C #7 (left) and thin section plug of this core piece taken at 5834'(right).

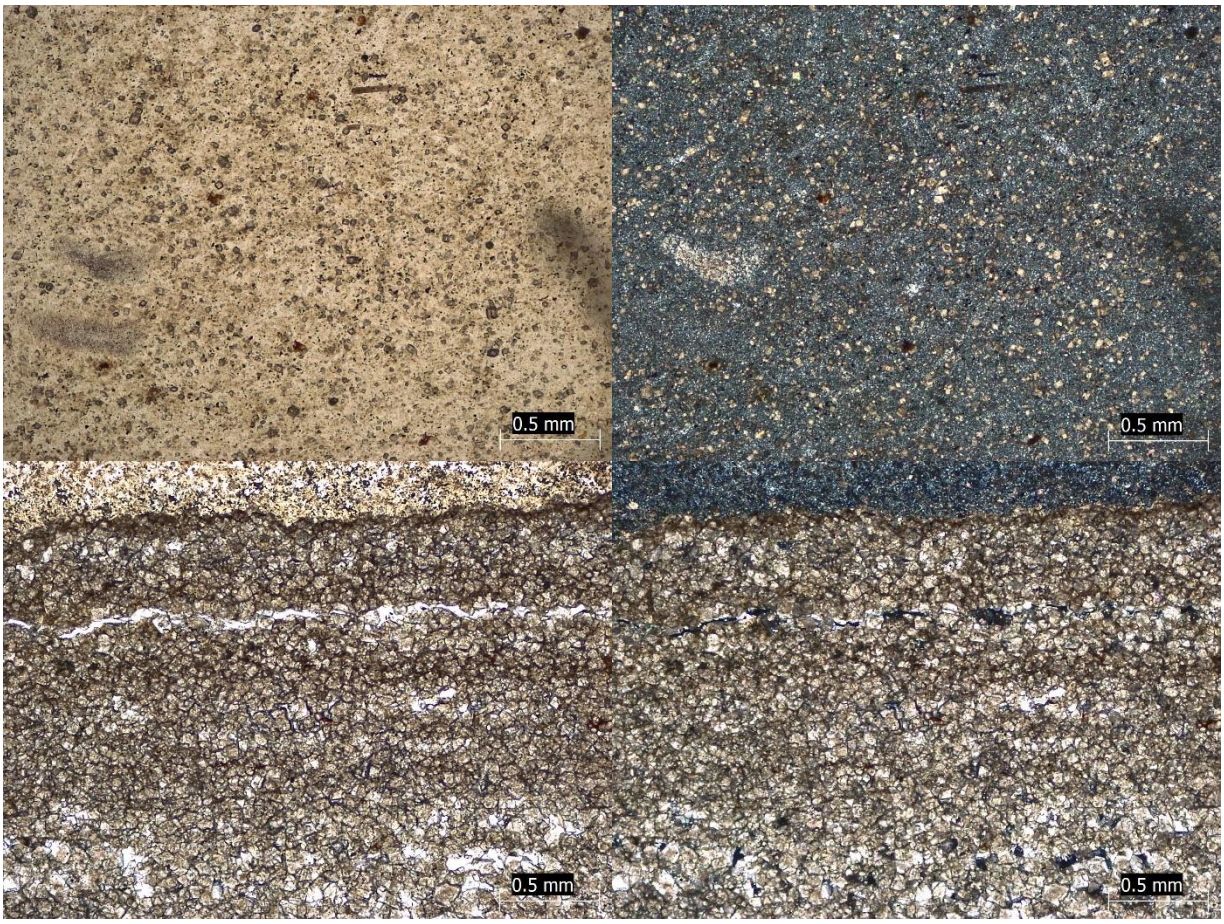

Figure B.31: Thin section photomicrographs of Muddy dolostone at 5834' from the Rich C #7 well. From left to right, the photomicrographs are in PPL, XPL (same microscope location as previous image), PPL, and XPL (same microscope location as previous image).

5835.33':

Lithofacies: Intraclastic Rudstone
Primary Constituents: Finely-crystalline dolomite, dolomitic and siliceous intraclasts, coarsely-crystalline calcite
Porosity Type: Intergranular
Porosity %: 10

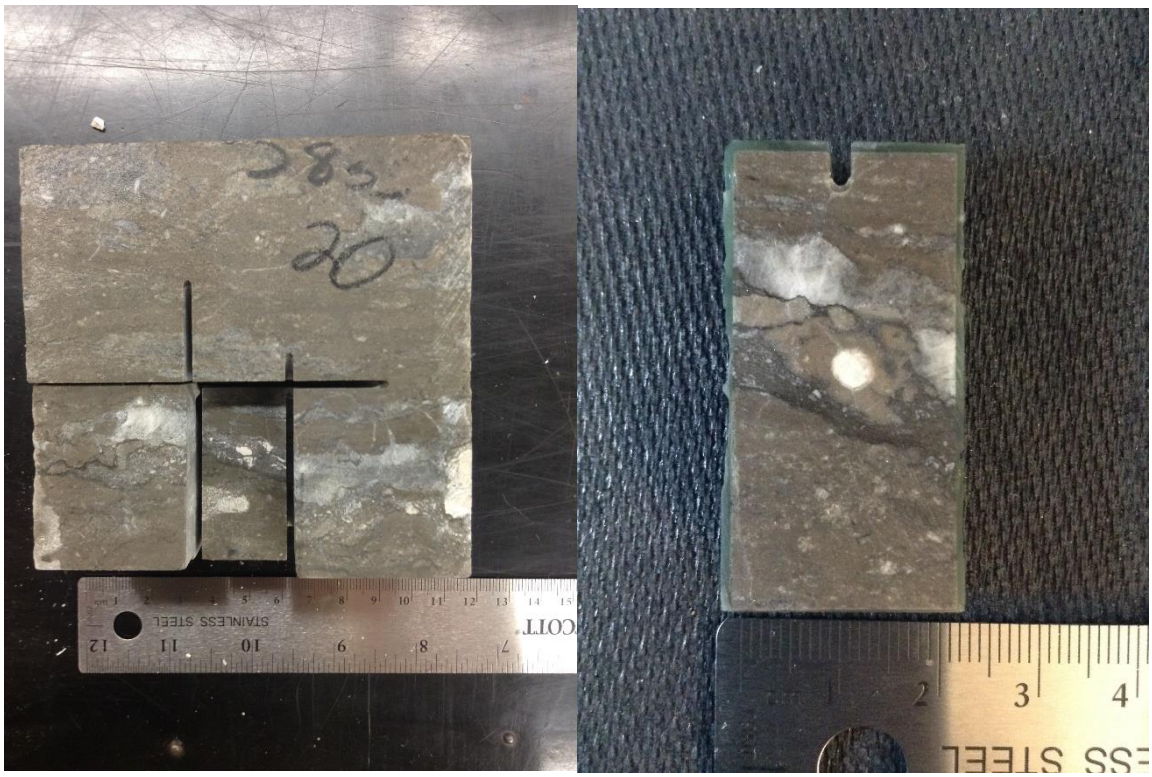

Figure B.32: Cored section of Intraclastic rudstone in the Viola Ls. from Rich C #7 (left) and thin section plug of this core piece taken at 5835.33'(right).

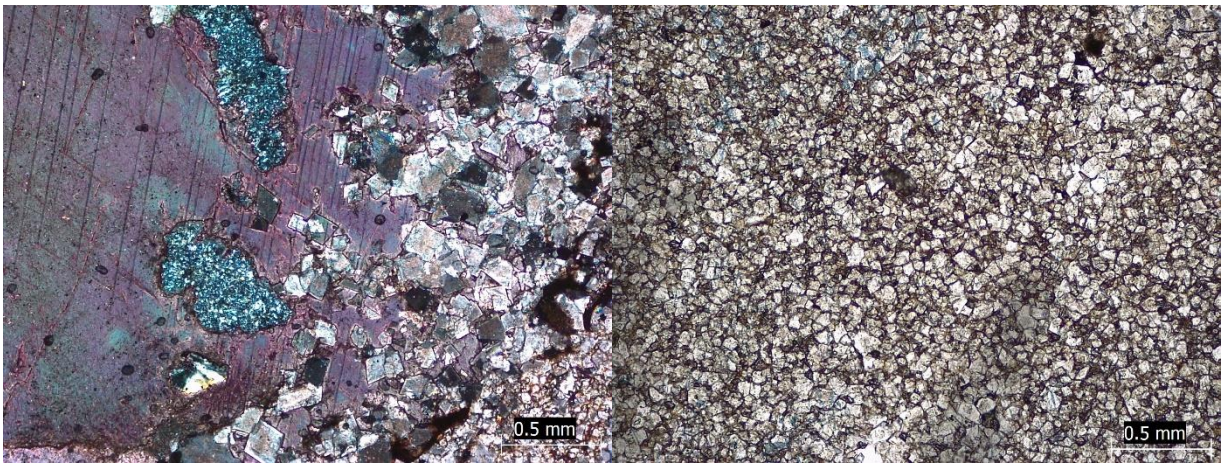

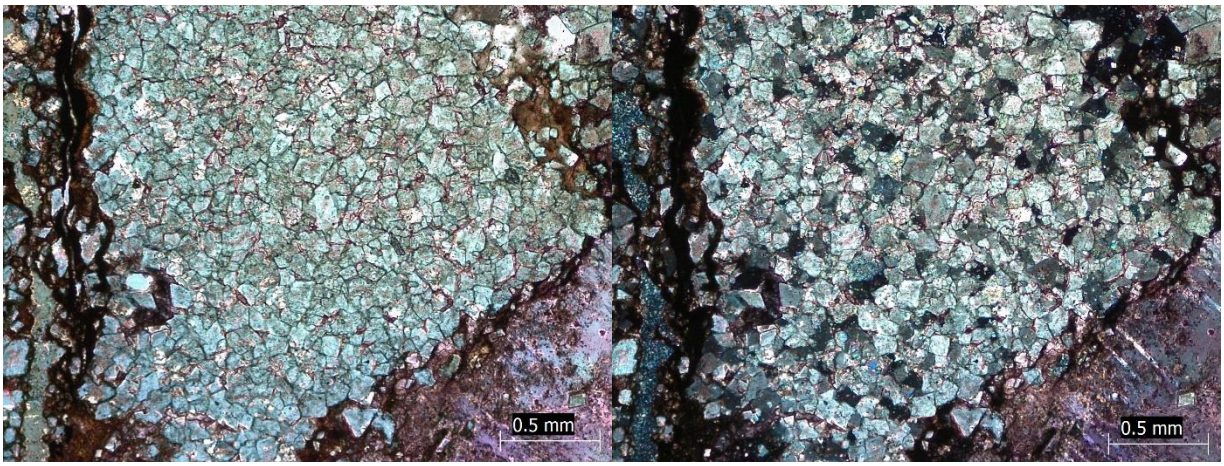

Figure B.33: Thin section photomicrographs of Rudstone at 5835.33' from the Rich C #7 well. From left to right, the photomicrographs are in XPL, PPL, PPL, and XPL (same microscope location as previous image).

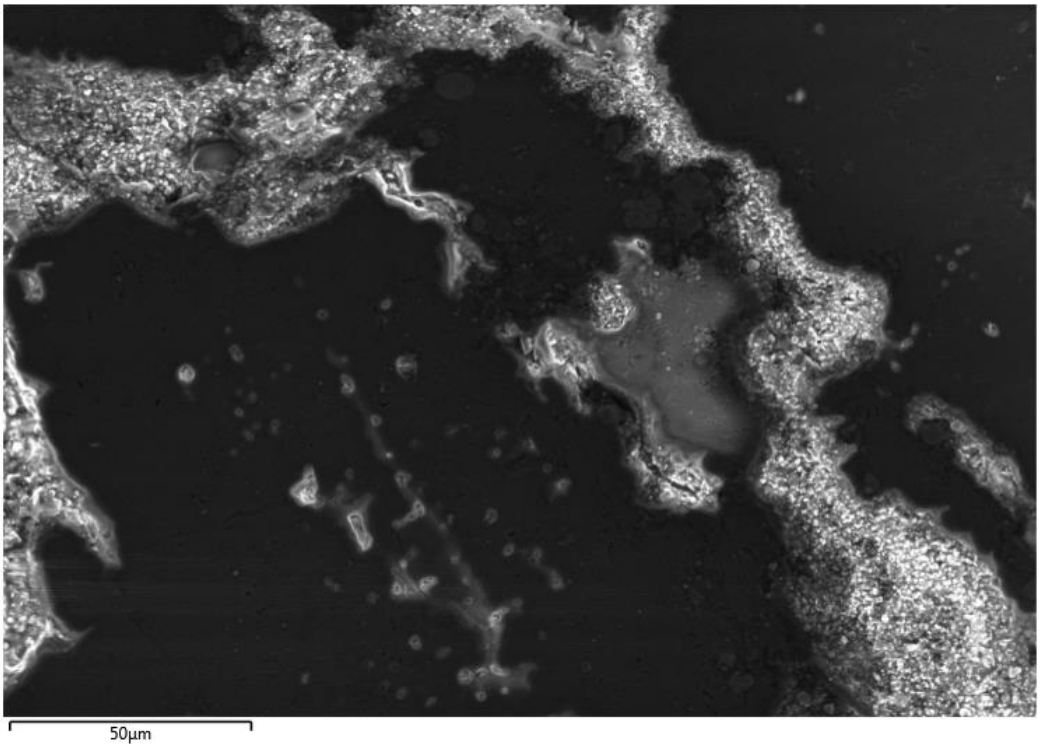

Figure B.34: SEM image at 50µm of the Rudstone thin section at 5835.33' from the Rich C #7 well. This thin section was coated with a 10 nm thick gold coating.

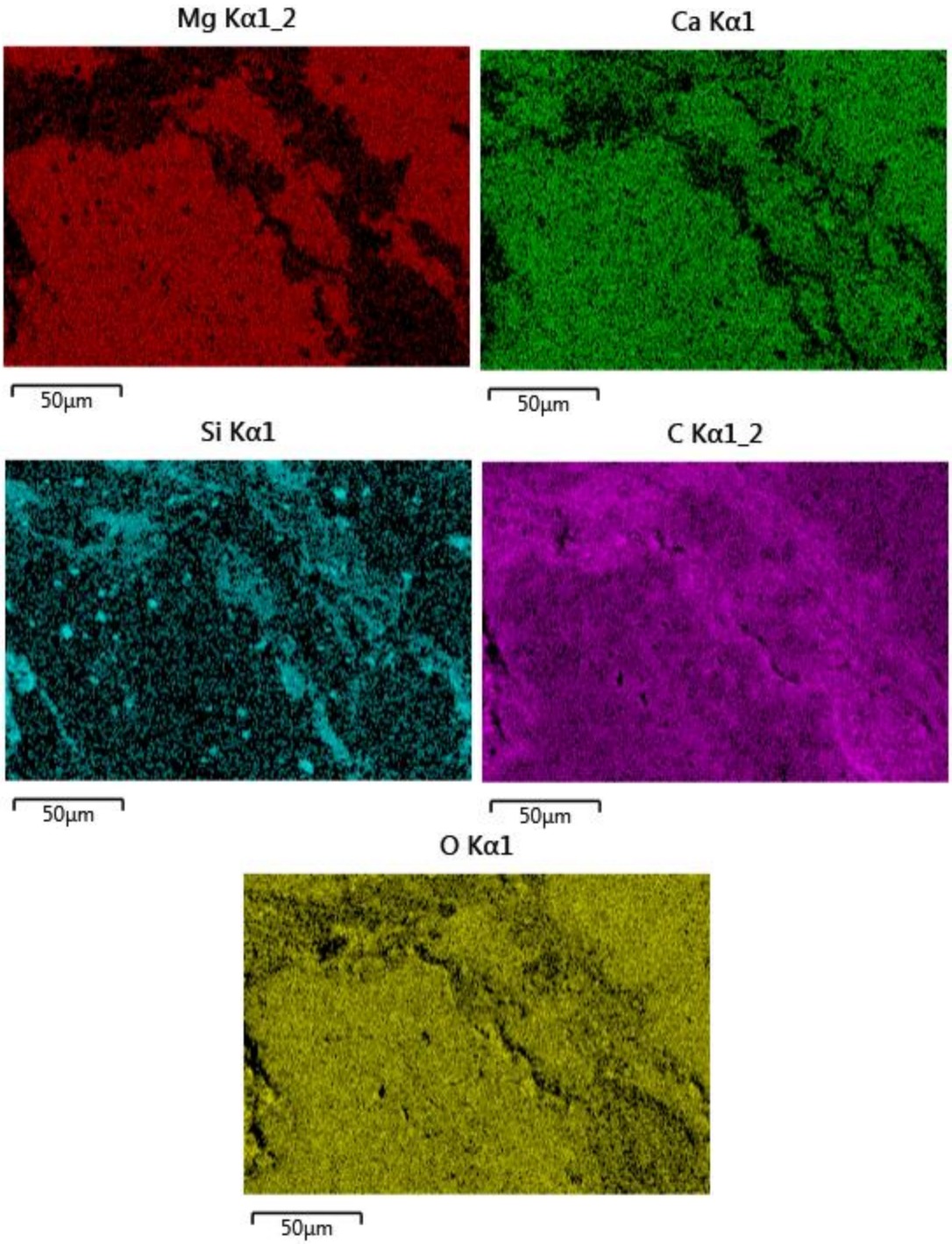

Figure B.35: From left to right, EDS map images showing the distribution of dolomite (Mg), calcite (Ca), silicates (Si), carbon, and oxygen from the previous SEM image at 5835.33'.

5836.66’-5847.83’

Figure B.36: Box: 12-15; Depth: 5836.66’-5847.83’.

5837':

Lithofacies: Muddy Dolostone
Primary Constituents: Finely-crystalline dolomite, coarse dolomite inside vugs
Porosity Type: Vuggy
Porosity %: 5

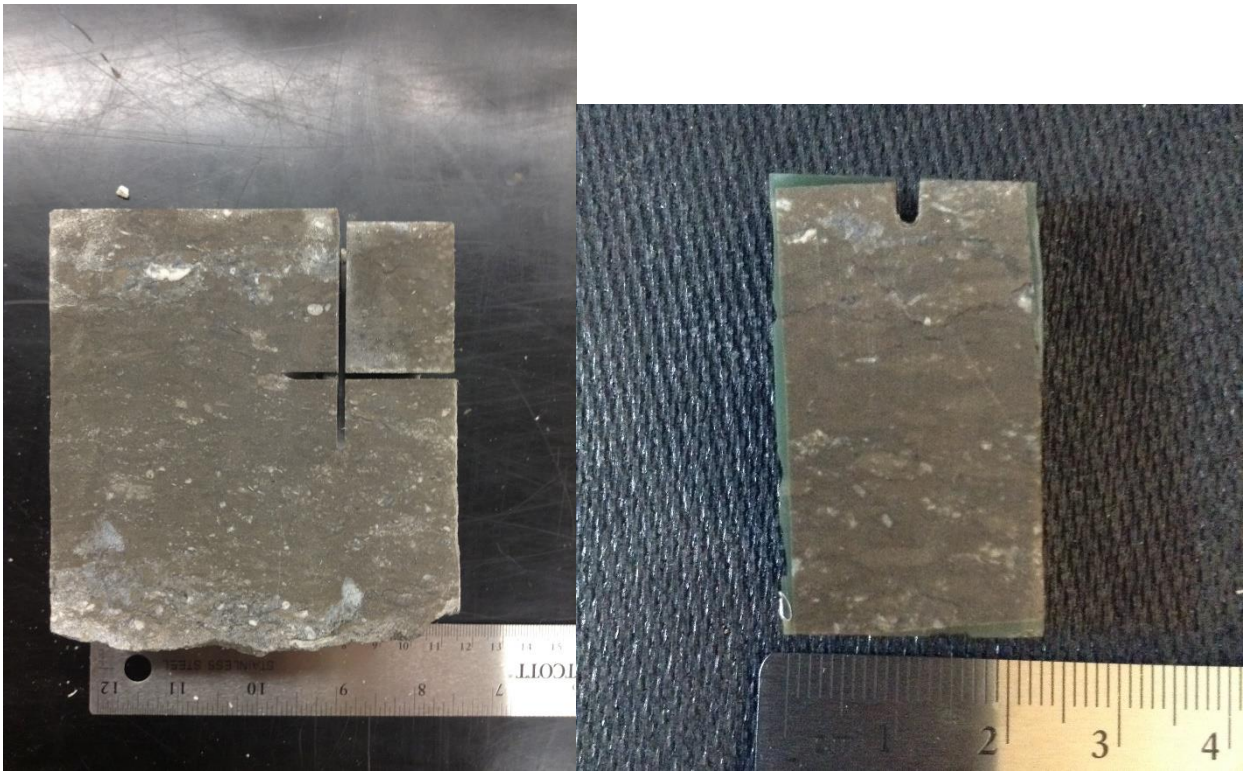

Figure B.37: Cored section of Muddy dolostone in the Viola Ls. from Rich C #7 (left) and thin section plug of this core piece taken at 5837'(right).

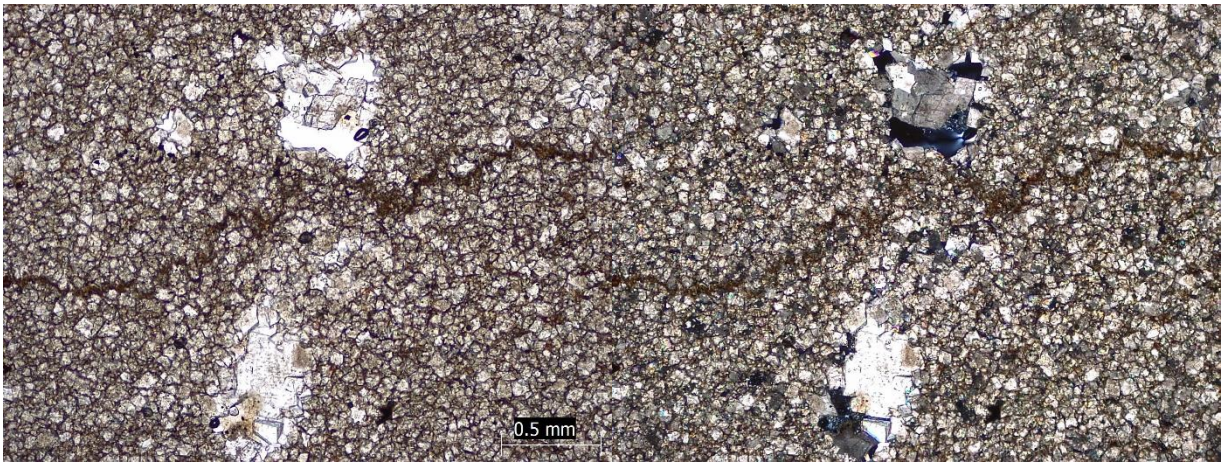

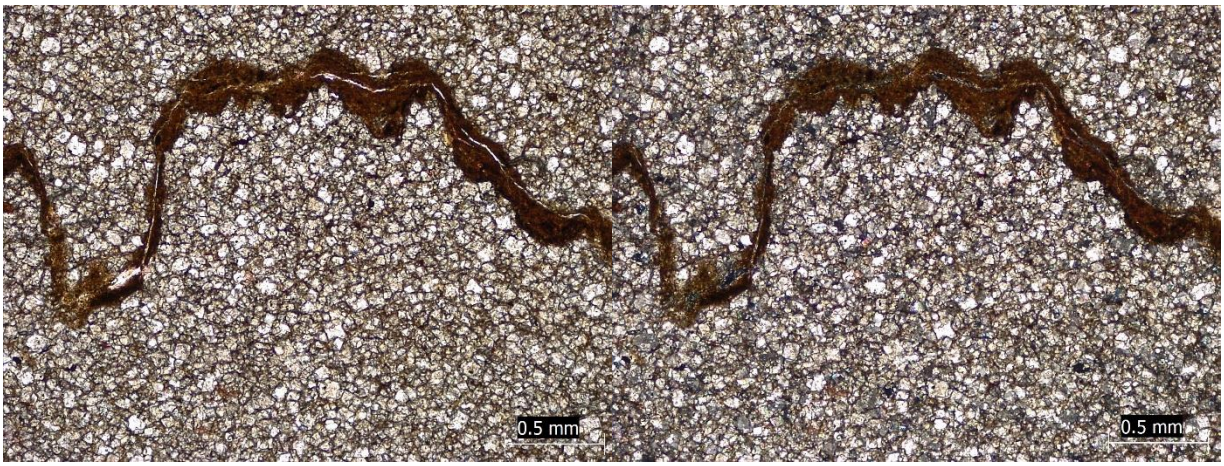

Figure B.38: Thin section photomicrographs of Muddy dolostone at 5837' from the Rich C #7 well. From left to right, the photomicrographs are in PPL, XPL (same microscope location as previous image), PPL, and XPL (same microscope location as previous image).

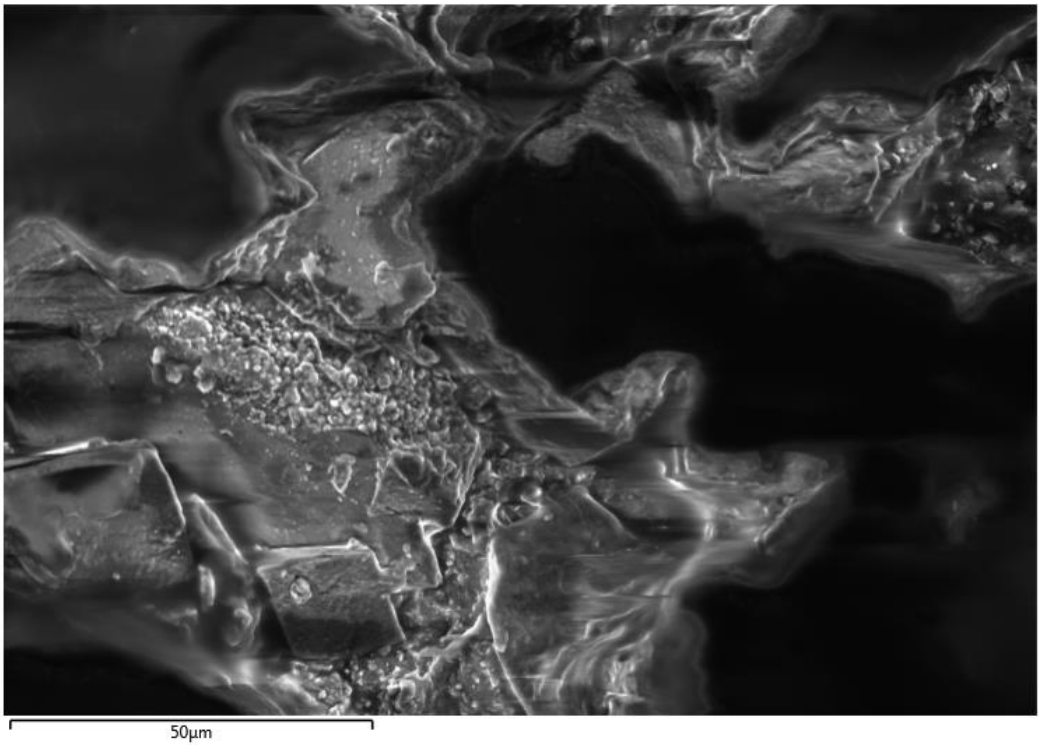

Figure B.39: SEM image at 50µm of the Muddy dolostone thin section at 5837' from the Rich C #7 well. This thin section was coated with a 10 nm thick gold coating.

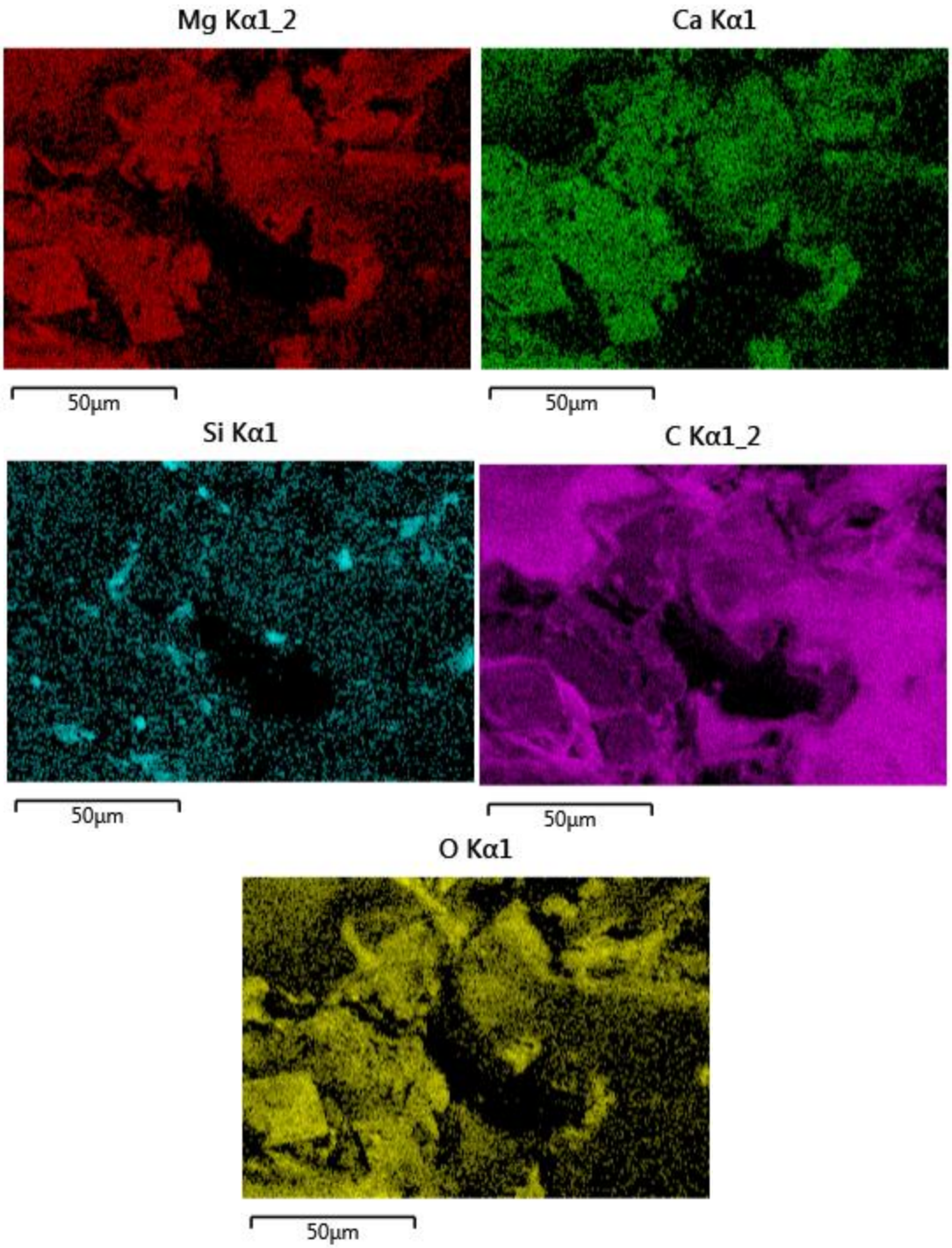

Figure B.40: From left to right, EDS map images showing the distribution of dolomite (Mg), calcite (Ca), silicates (Si), carbon, and oxygen from the previous SEM image at 5837'.

5841.33':

Lithofacies: Intraclastic Rudstone
Primary Constituents: Dolomitic and siliceous intraclasts, silica inside vugs

Porosity Type: Intergranular, Vuggy
Porosity %: 3

Figure B.41: Cored section of Intraclastic rudstone in the Viola Ls. from Rich C #7 (left) and thin section plugs of this core piece taken at 5841.33'(right).

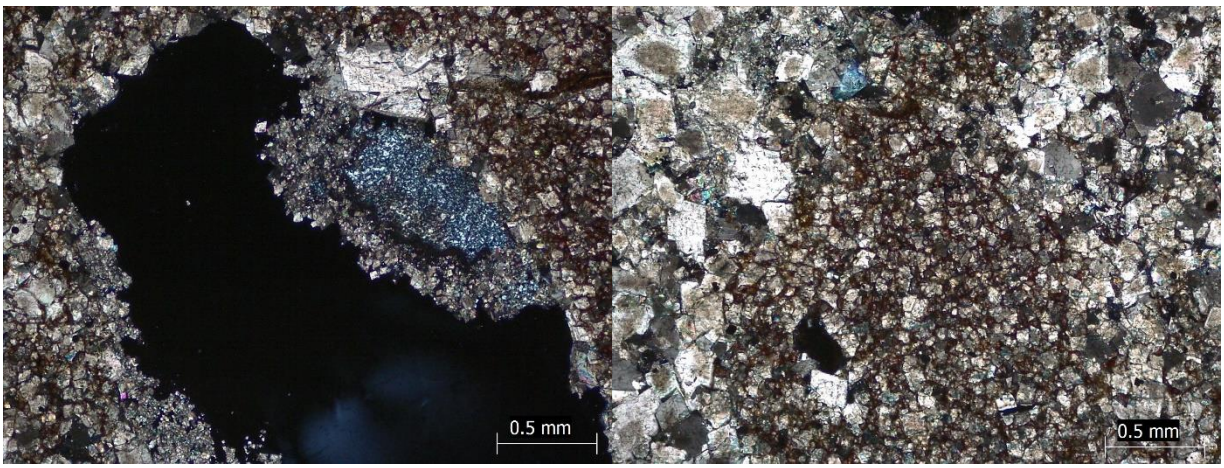

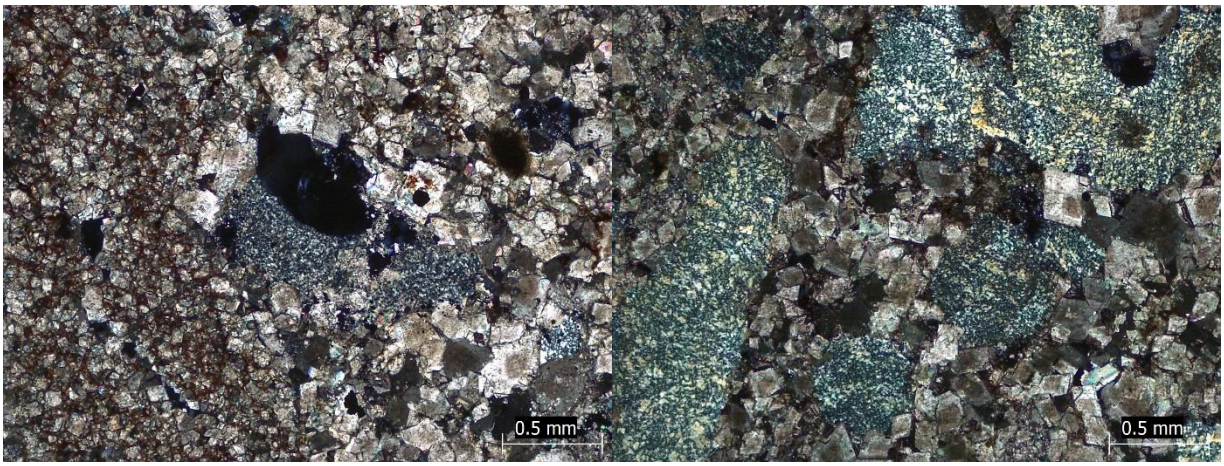

Figure B.42: Thin section XPL photomicrographs of Rudstone at 5841.33' from the Rich C #7 well.

5841.83':

Lithofacies: Muddy Dolostone
Primary Constituents: Laminated, finely-crystalline dolomite
Porosity Type: Intergranular
Porosity %: 1

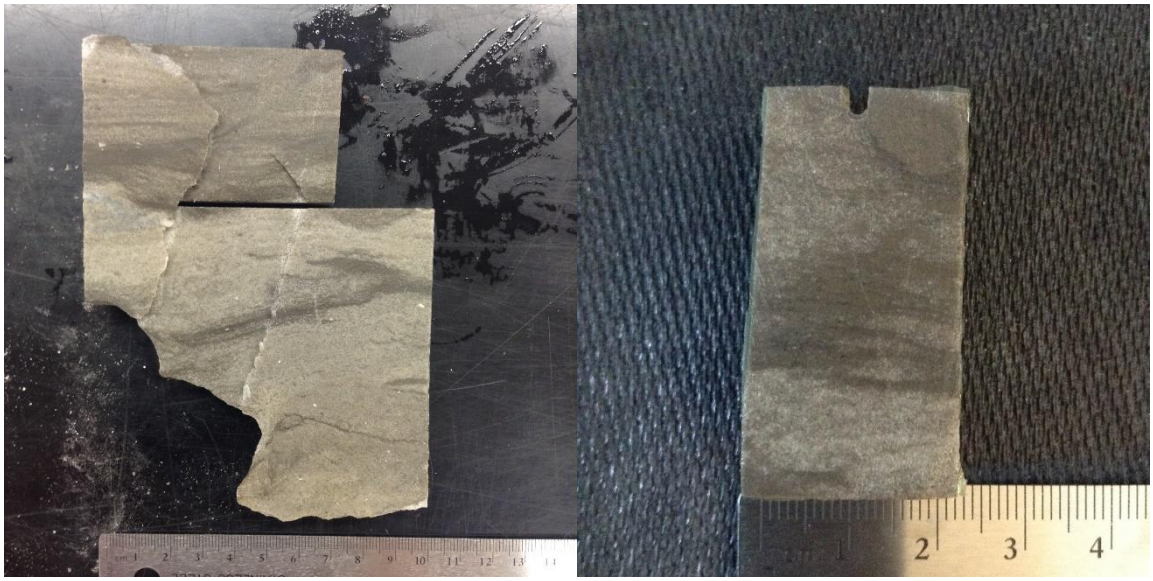

Figure B.43: Cored section of Muddy dolostone in the Viola Ls. from Rich C #7 (left) and thin section plug of this core piece taken at 5841.83'(right).

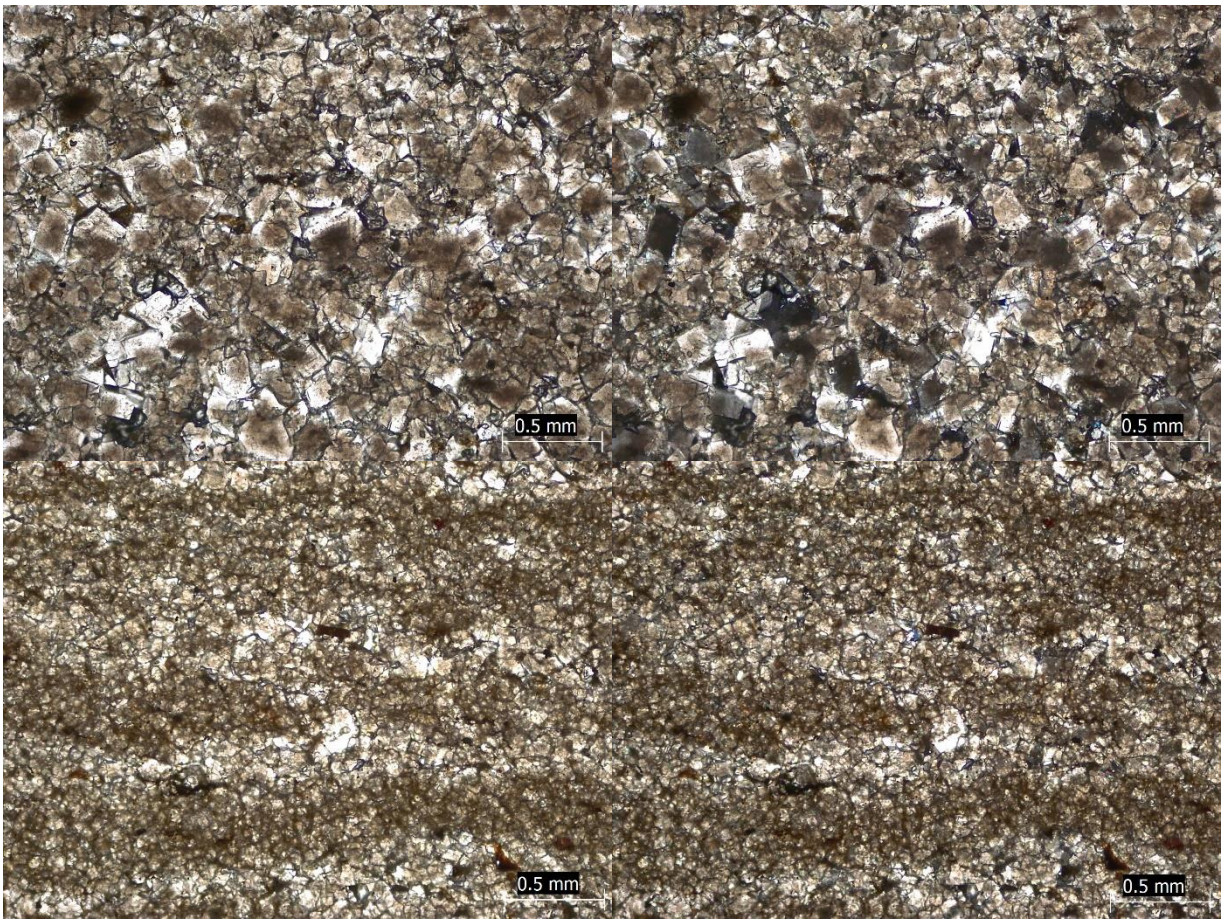

Figure B.44: Thin section photomicrographs of Muddy dolostone at 5841.83' from the Rich C #7 well. From left to right, the photomicrographs are in PPL, XPL (same microscope location as previous image), PPL, and XPL (same microscope location as previous image).

5843.83':

Lithofacies: Muddy Dolostone
Primary Constituents: Finely-crystalline dolomite, dolomitic mud and siliceous intraclasts
Porosity Type: Vuggy
Porosity %: 10

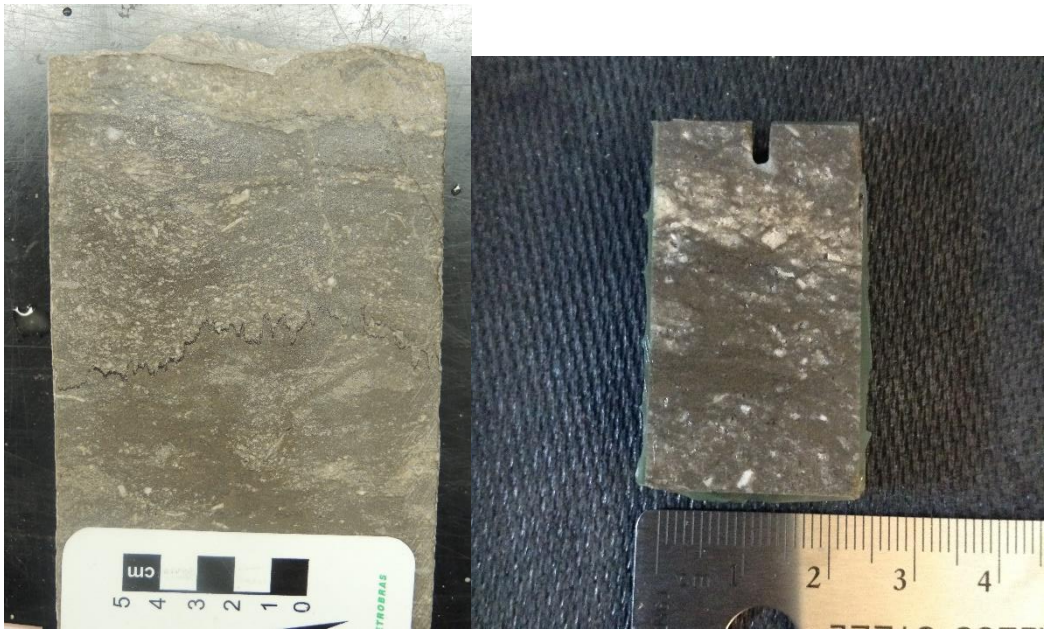

Figure B.45: Cored section of Muddy dolostone in the Viola Ls. from Rich C #7 (left) and thin section plug of this core piece taken at 5843.83'(right).

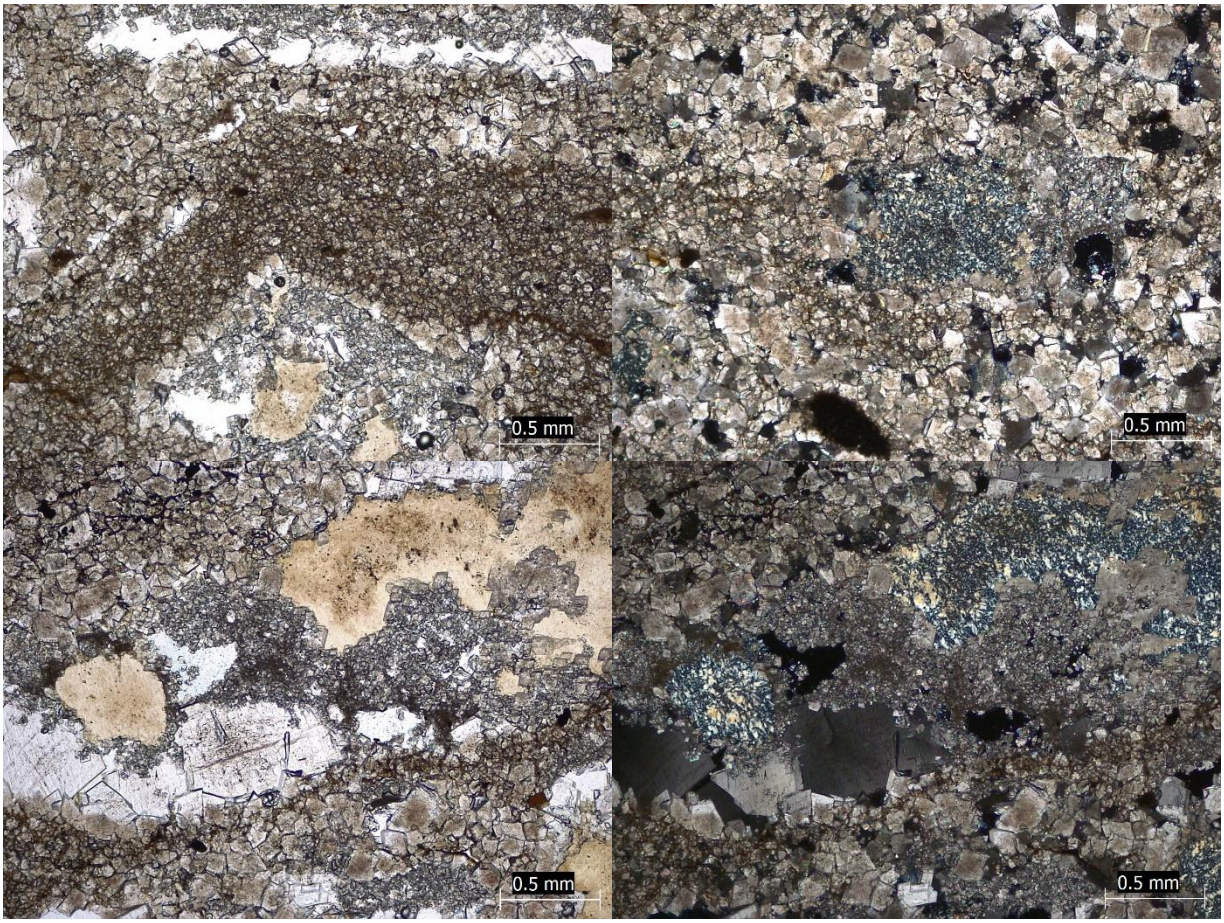

Figure B.46: Thin section photomicrographs of Muddy dolostone at 5843.83' from the Rich C #7 well. From left to right, the photomicrographs are in PPL, XPL, PPL, and XPL (same microscope location as previous image).

5848’-5859’

Figure B.47: Box: 16-19; Depth: 5848’-5859’.

5852.66':

Lithofacies: Muddy Dolostone
Primary Constituents: Very finely-crystalline muddy dolomite, chert with sponge spicules
Porosity Type: Intergranular
Porosity %: 3

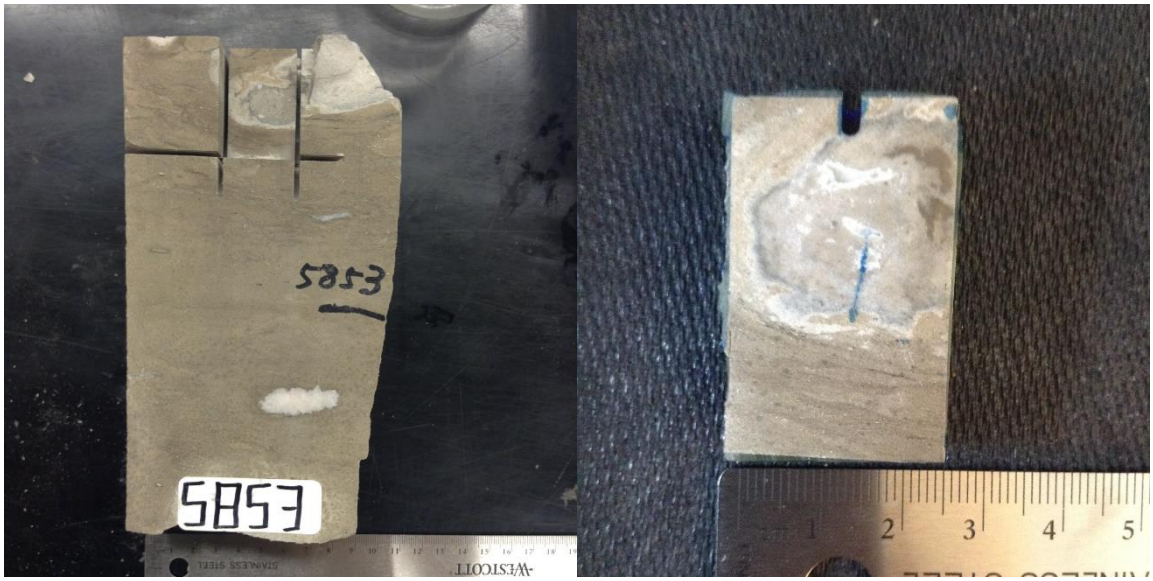

Figure B.48: Cored section of Muddy dolostone in the Viola Ls. from Rich C #7 (left) and thin section plug of this core piece taken at 5852.66'(right).

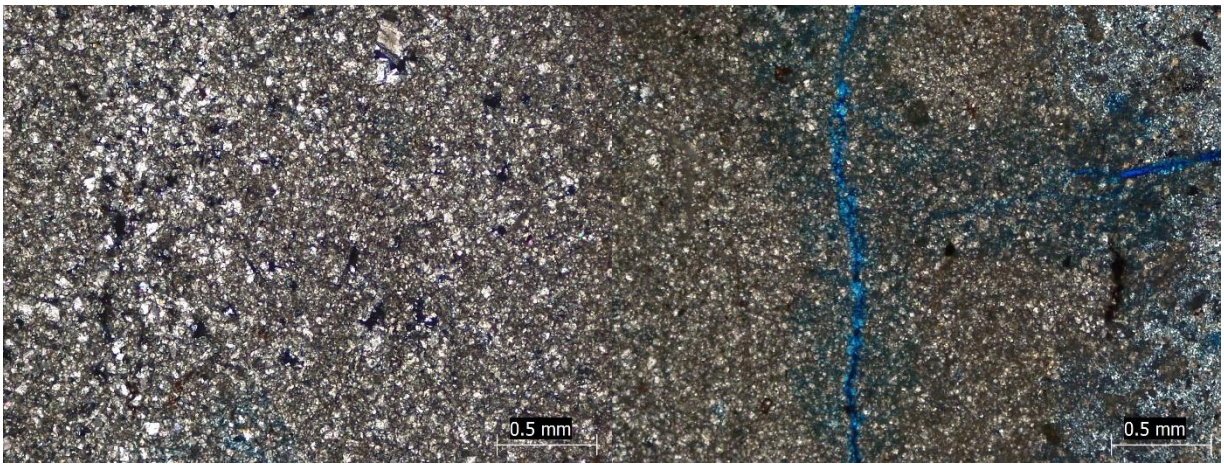

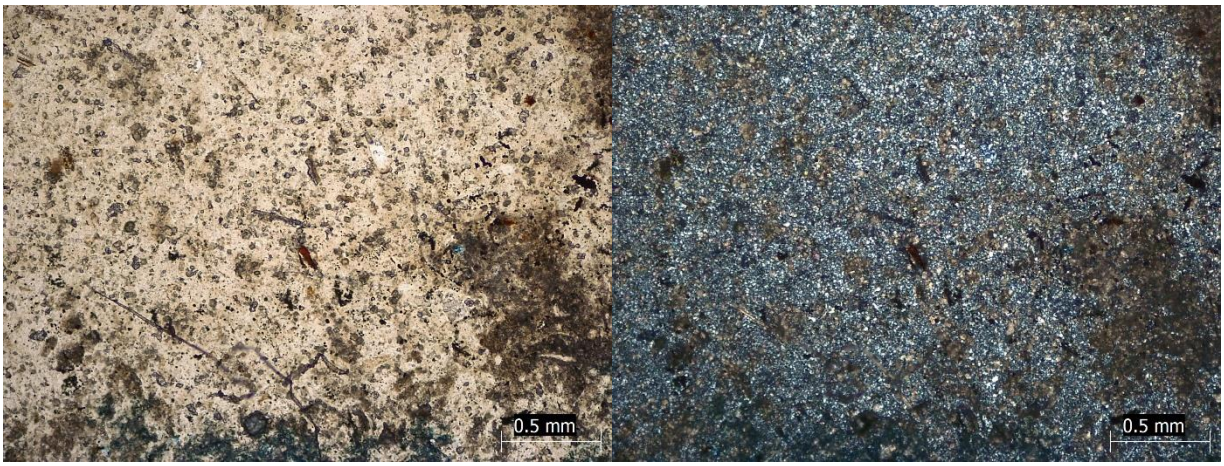

Figure B.49: Thin section photomicrographs of Muddy dolostone at 5852.66' from the Rich C #7 well. From left to right, the photomicrographs are in XPL, XPL, PPL, and XPL (same microscope location as previous image).

5853.5:

Lithofacies: Muddy Dolostone
Primary Constituents: Very finely-crystalline muddy dolomite
Porosity Type: Vuggy
Porosity %: 3

Figure B.50: Cored section of Muddy dolostone in the Viola Ls. from Rich C #7 (left) and thin section plug of this core piece taken at 5853.5'(right).

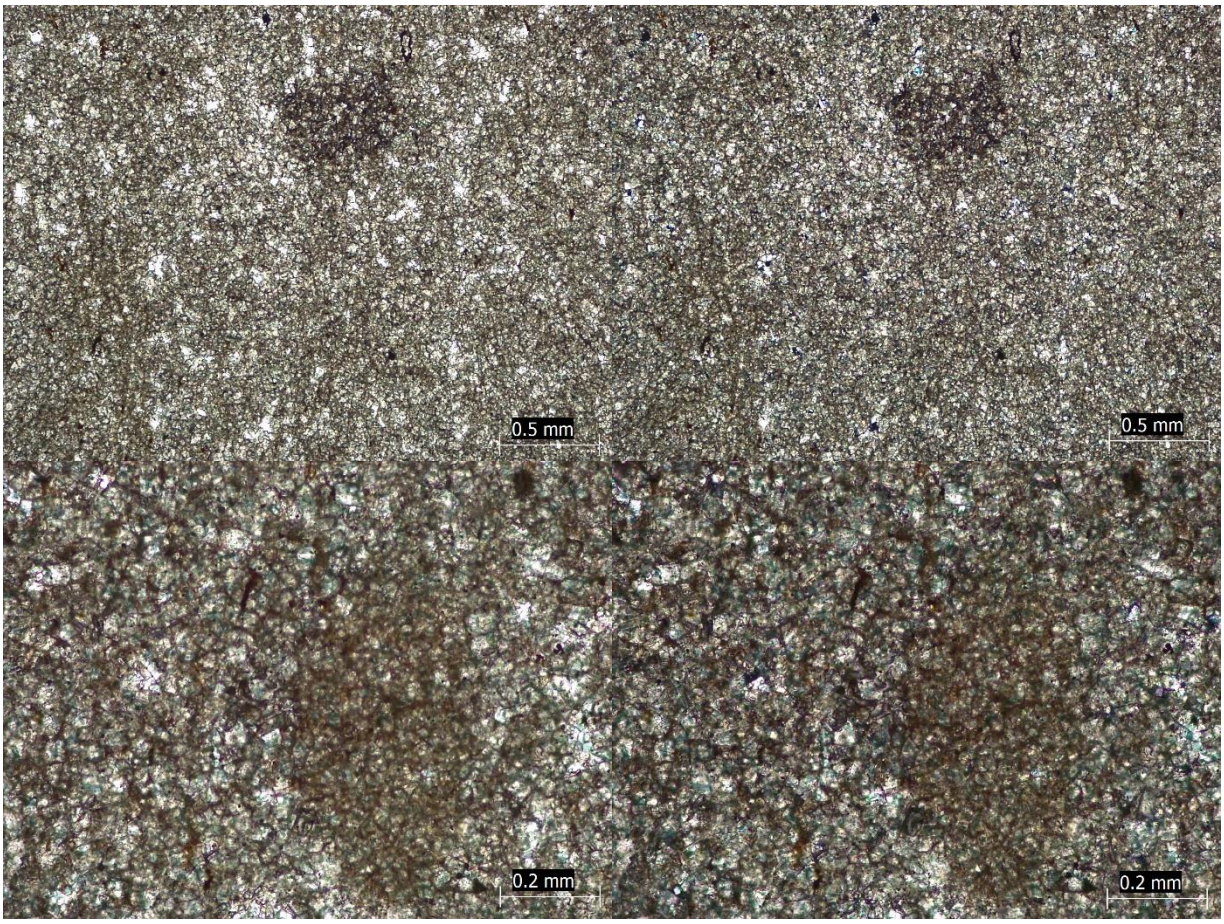

Figure B.51: Thin section photomicrographs of Muddy dolostone at 5853.5' from the Rich C #7 well. From left to right, the photomicrographs are in PPL, XPL (same microscope location as previous image), PPL, and XPL (same microscope location as previous image).

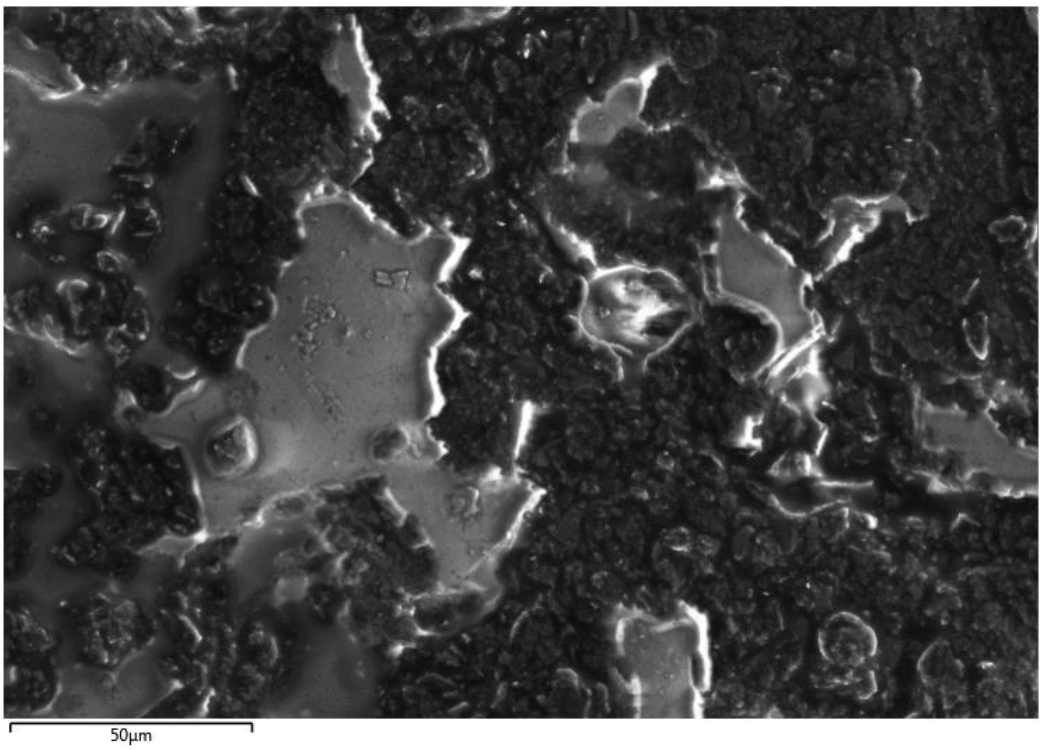

Figure B.52: SEM image at 50µm of the Muddy dolostone thin section at 5853.5' from the Rich C #7 well. This thin section was coated with a 10 nm thick gold coating.

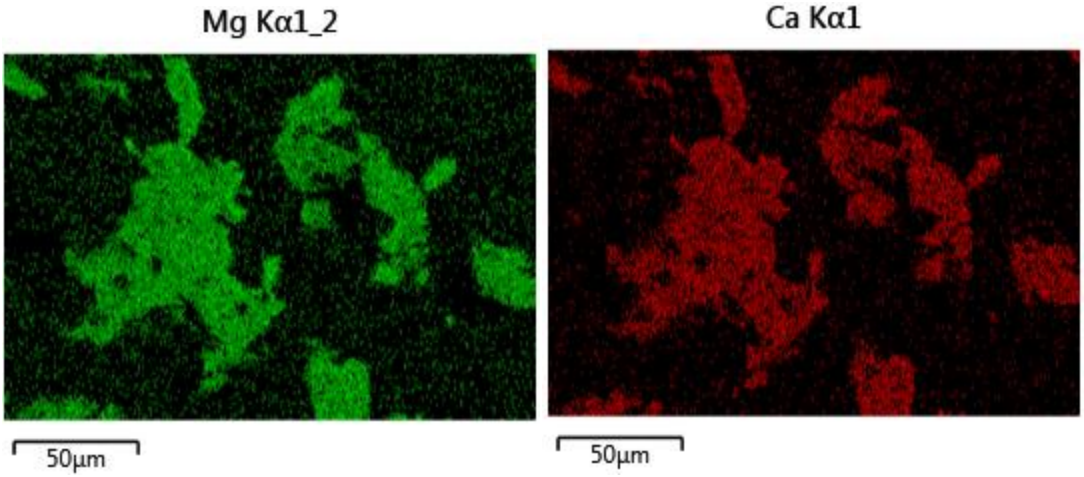

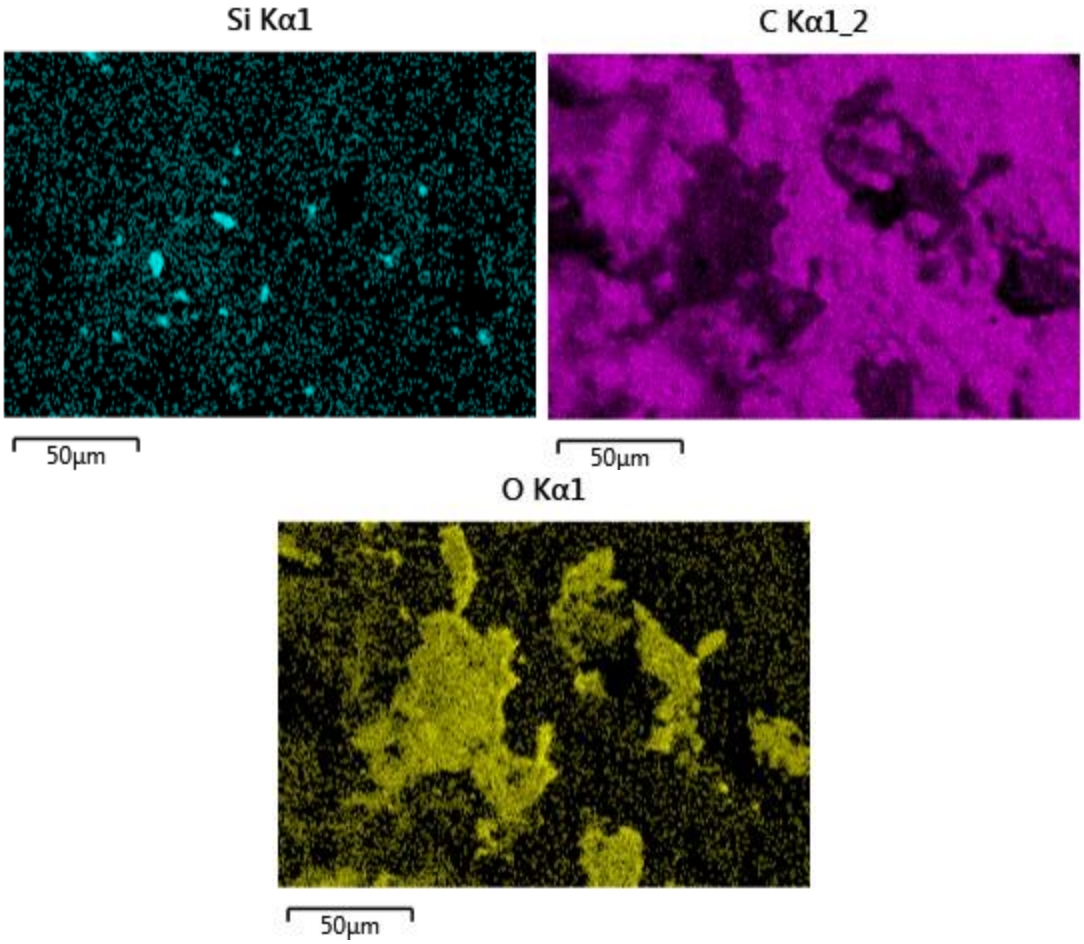

Figure B.53: From left to right, EDS map images showing the distribution of dolomite (Mg), calcite (Ca), silicates (Si), carbon, and oxygen from the previous SEM image at 5853.5'.

5857.66':

Lithofacies: Muddy Dolostone
Primary Constituents: Very muddy, very finely-crystalline dolomite, silica and dolomite rhombs inside fractures, rare phosphate grains
Porosity Type: Vuggy
Porosity %: 1

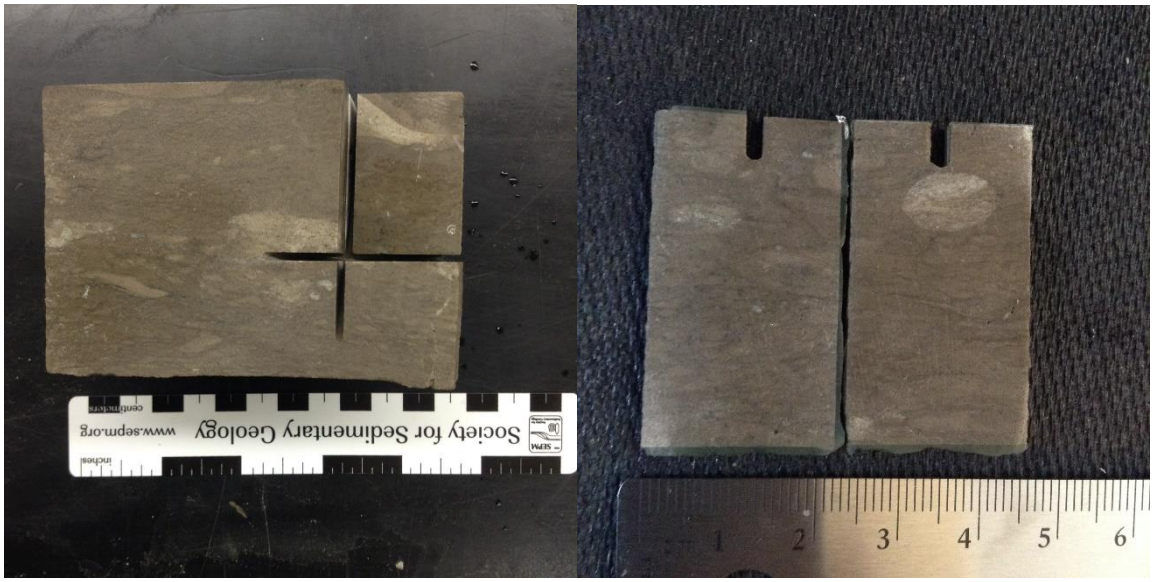

Figure B.54: Cored section of Muddy dolostone in the Viola Ls. from Rich C #7 (left) and thin section plugs of this core piece taken at 5857.66'(right).

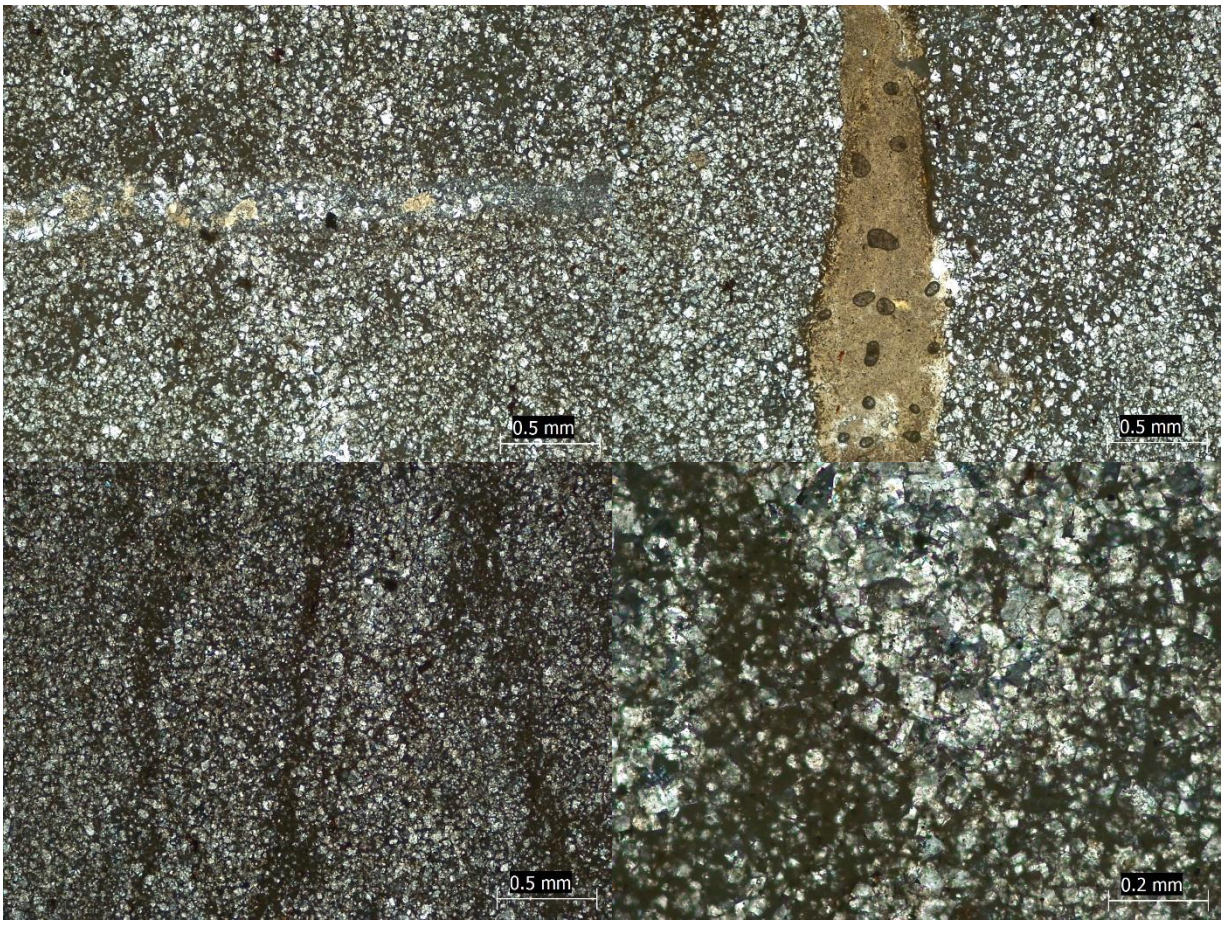

Figure B.55: Thin section photomicrographs of Muddy dolostone at 5857.66' from the Rich C #7 well. From left to right, the photomicrographs are in PPL, PPL, XPL, and XPL.

5859.17'-5868'

Figure B.56: Box: 20-23; Depth: 5859.17'-5868'.

5860.5':

Lithofacies: Muddy Dolostone
Primary Constituents: Finely-crystalline muddy dolomite, silica, coarse dolomite and calcite in fractures and vugs
Porosity Type: Vuggy, intergranular
Porosity %: 4

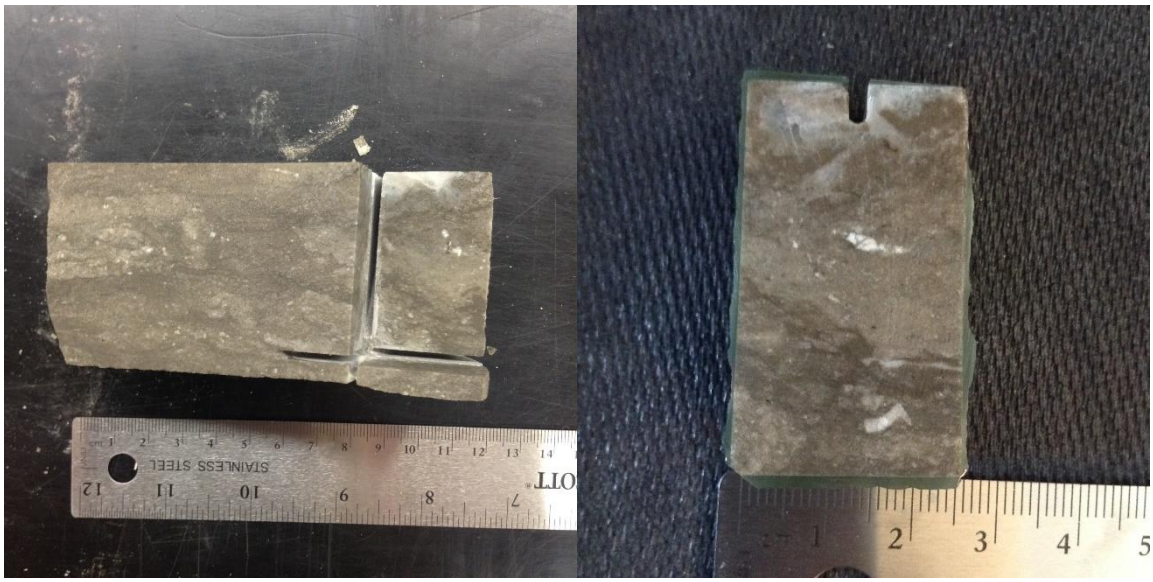

Figure B.57: Cored section of Muddy dolostone in the Viola Ls. from Rich C #7 (left) and thin section plugs of this core piece taken at 5860.5'(right).

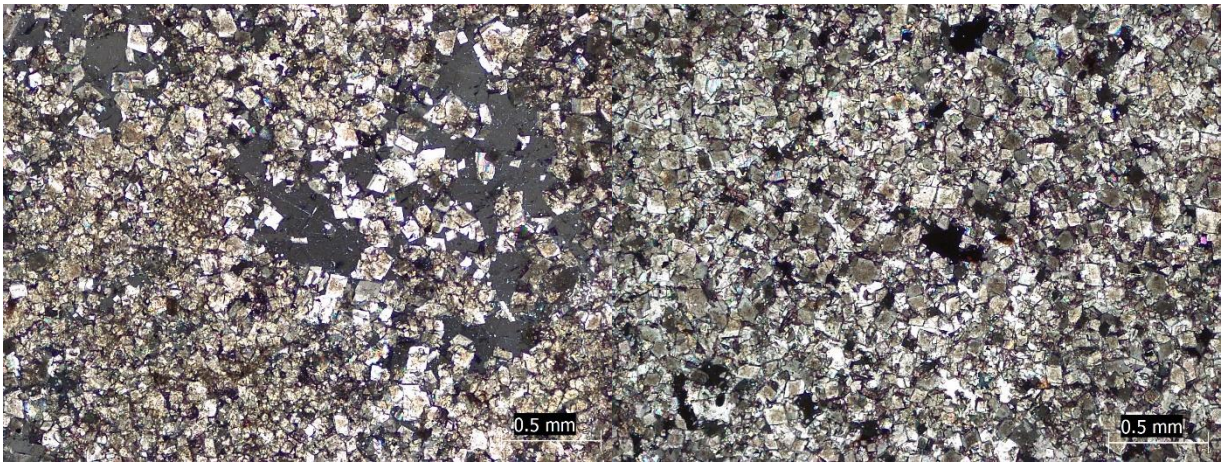

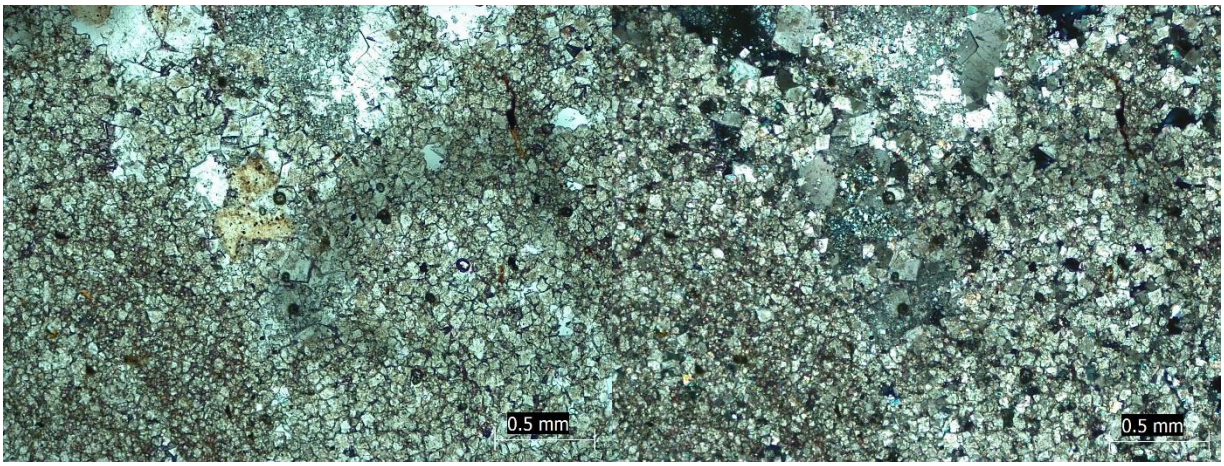

Figure B.58: Thin section photomicrographs of Muddy dolostone at 5860.5' from the Rich C #7 well. From left to right, the photomicrographs are in XPL, XPL, PPL, and XPL (same microscope location as previous image).

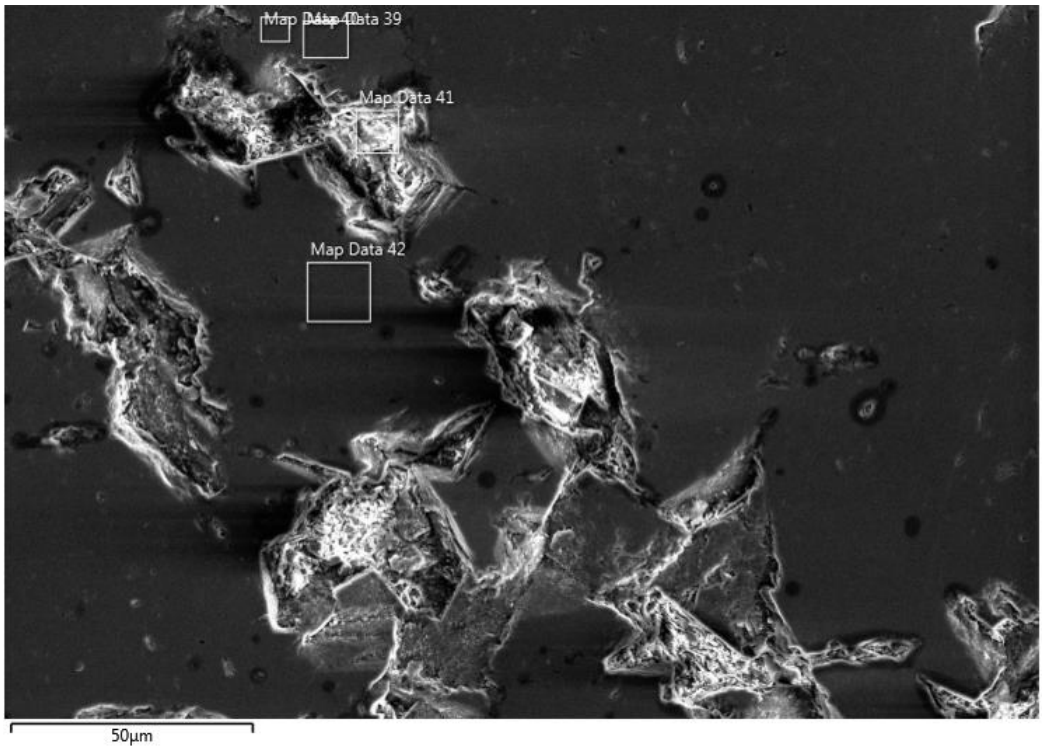

Figure B.59: SEM image at 50µm of the Muddy dolostone thin section at 5860.5' from the Rich C #7 well. This thin section was coated with a 10 nm thick gold coating.

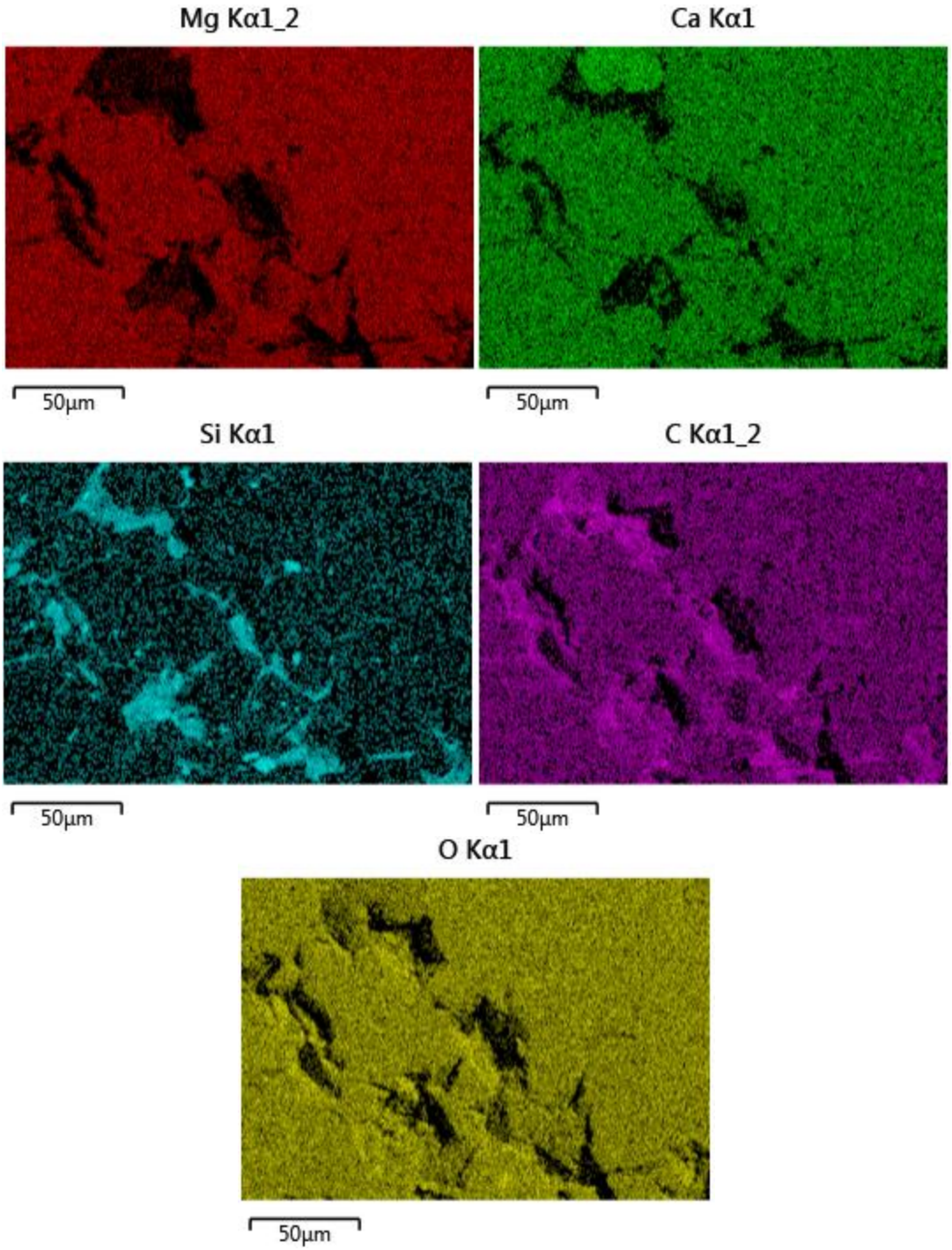

Figure B.60: From left to right, EDS map images showing the distribution of dolomite (Mg), calcite (Ca), silicates (Si), carbon, and oxygen from the previous SEM image at 5860.5'.

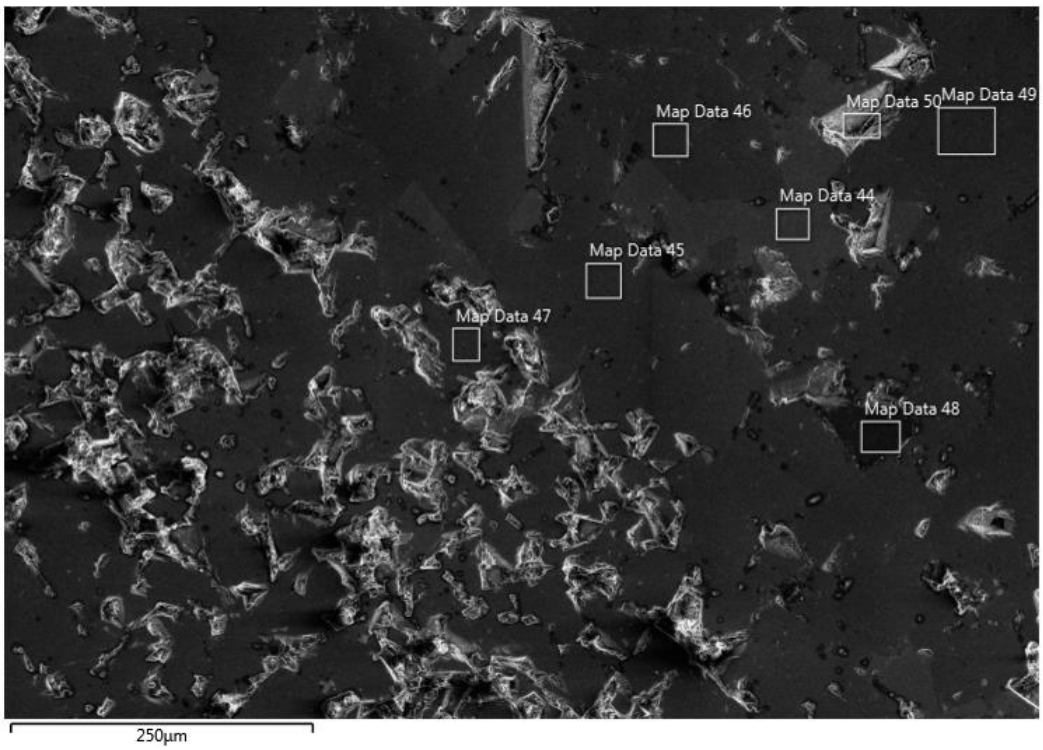

Figure B.61: High-field-of-view SEM image at 250µm of the Muddy dolostone thin section at 5860.5' from the Rich C #7 well. This thin section was coated with a 10 nm thick gold coating.

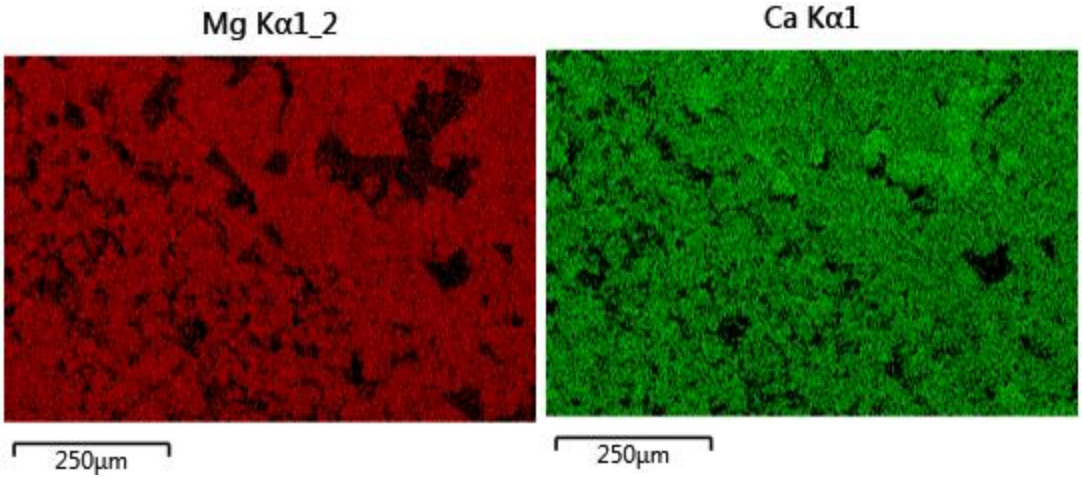

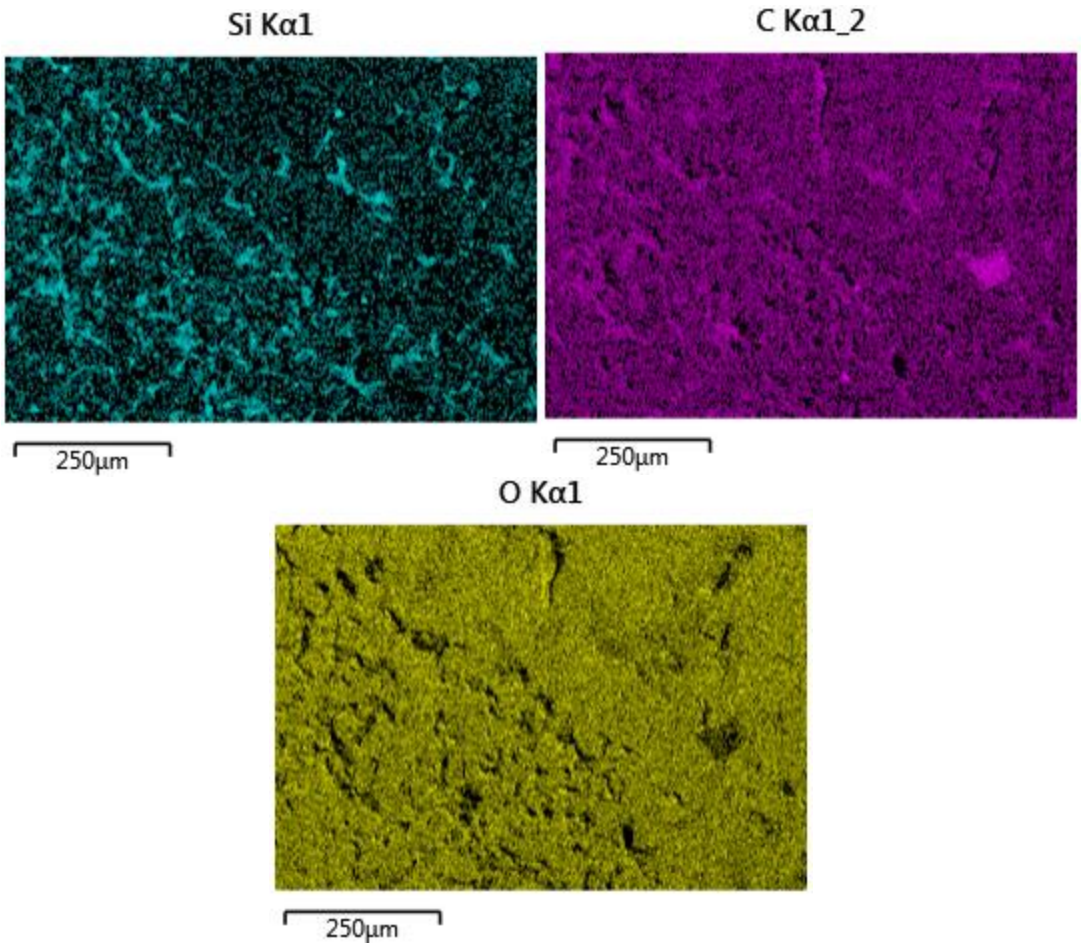

Figure B.62: From left to right, EDS map images showing the distribution of dolomite (Mg), calcite (Ca), silicates (Si), carbon, and oxygen from the previous high field of view SEM image at 5860.5'.

5863':

Lithofacies: Muddy Dolostone
Primary Constituents: Finely-crystalline muddy dolomite, silica and coarse dolomite in vugs
Porosity Type: Vuggy, intergranular
Porosity %: 7

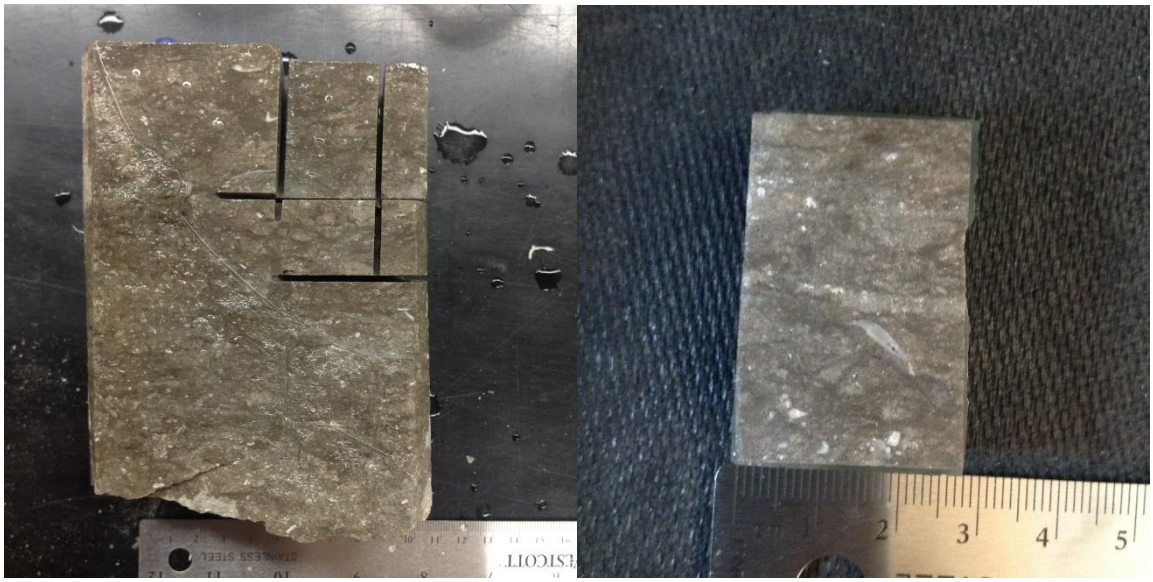

Figure B.63: Cored section of Muddy dolostone in the Viola Ls. from Rich C #7 (left) and thin section plugs of this core piece taken at 5863'(right).

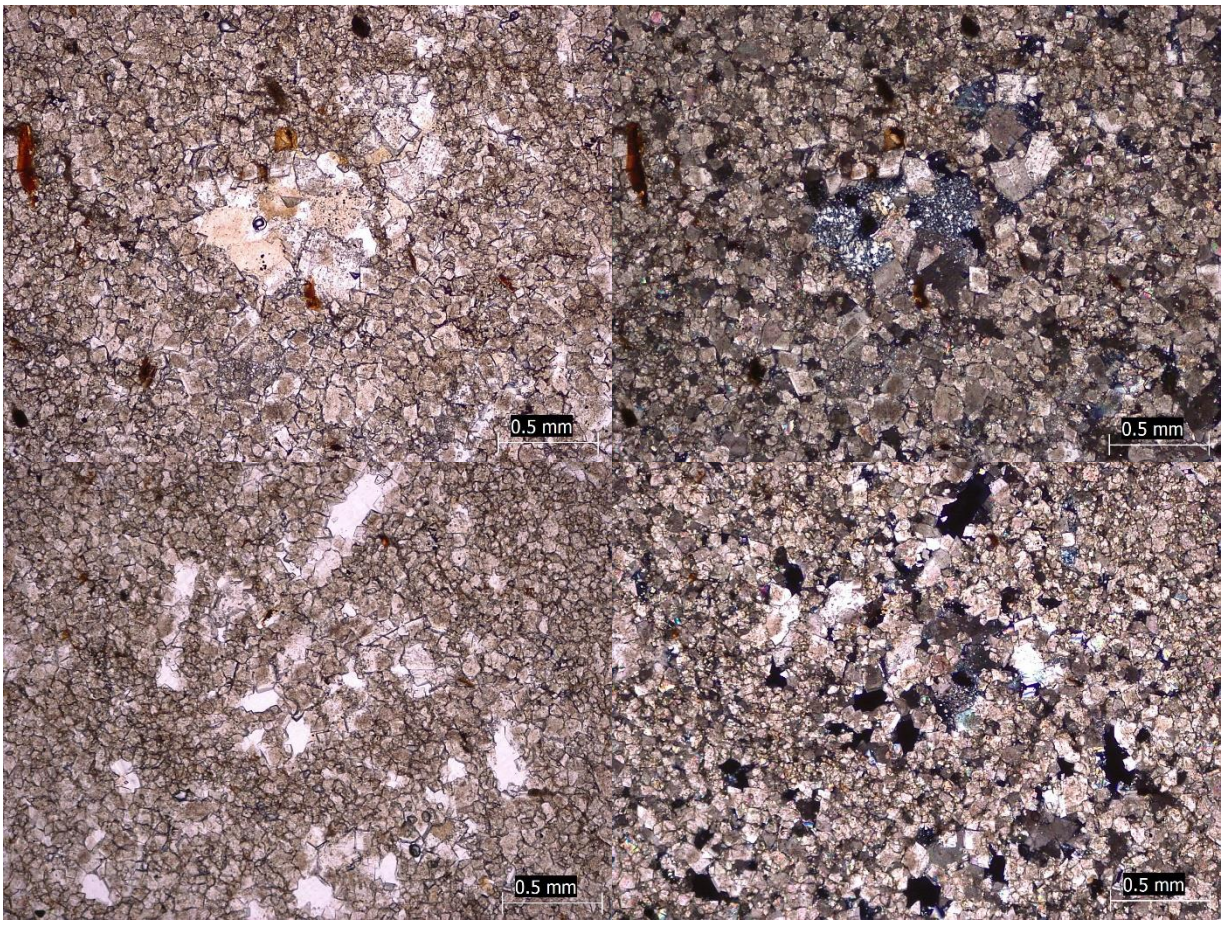

Figure B.64: Thin section photomicrographs of Muddy dolostone at 5863' from the Rich C #7 well. From left to right, the photomicrographs are in PPL, XPL (same microscope location as previous image), PPL, and XPL (same microscope location as previous image).

5864':

Lithofacies: Muddy Dolostone
Primary Constituents: Finely-crystalline muddy dolomite, silica and coarse dolomite in vugs, phosphate grains
Porosity Type: Vuggy, intergranular
Porosity %: 5

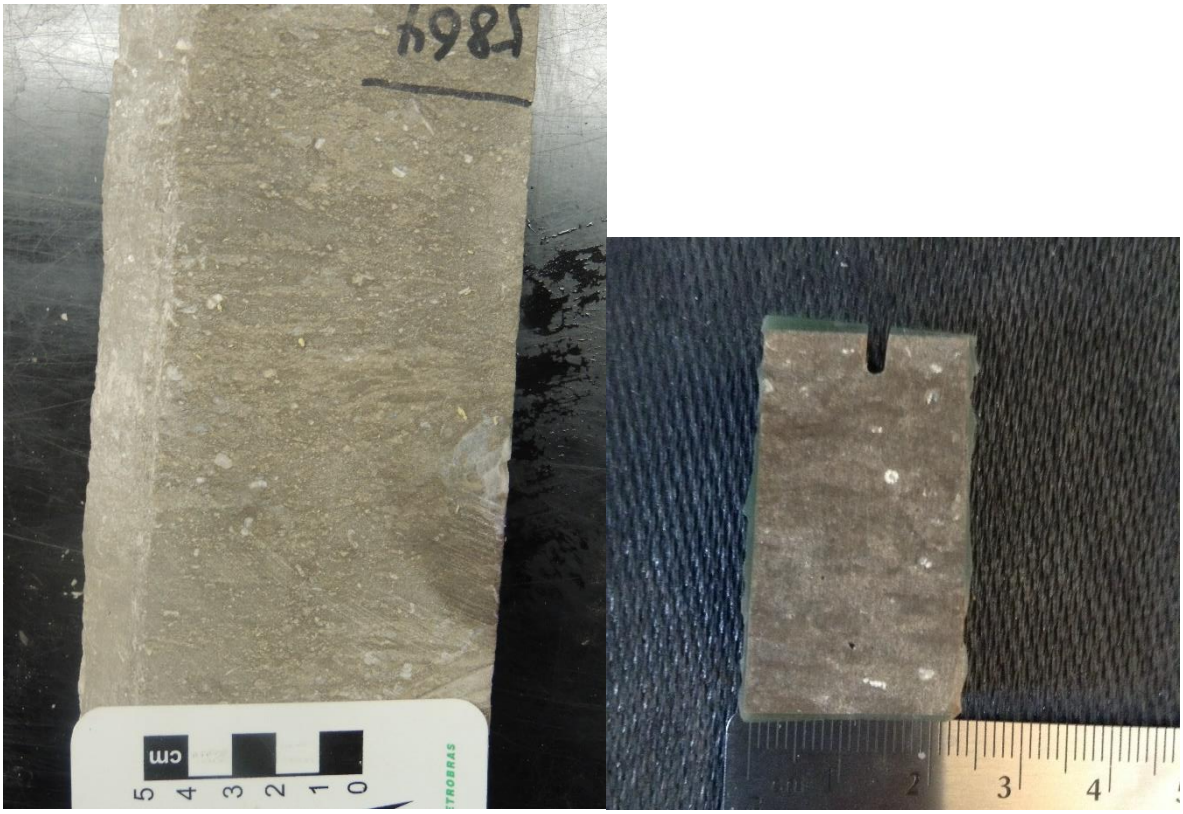

Figure B.65: Cored section of Muddy dolostone in the Viola Ls. from Rich C #7 (left) and thin section plugs of this core piece taken at 5864'(right).

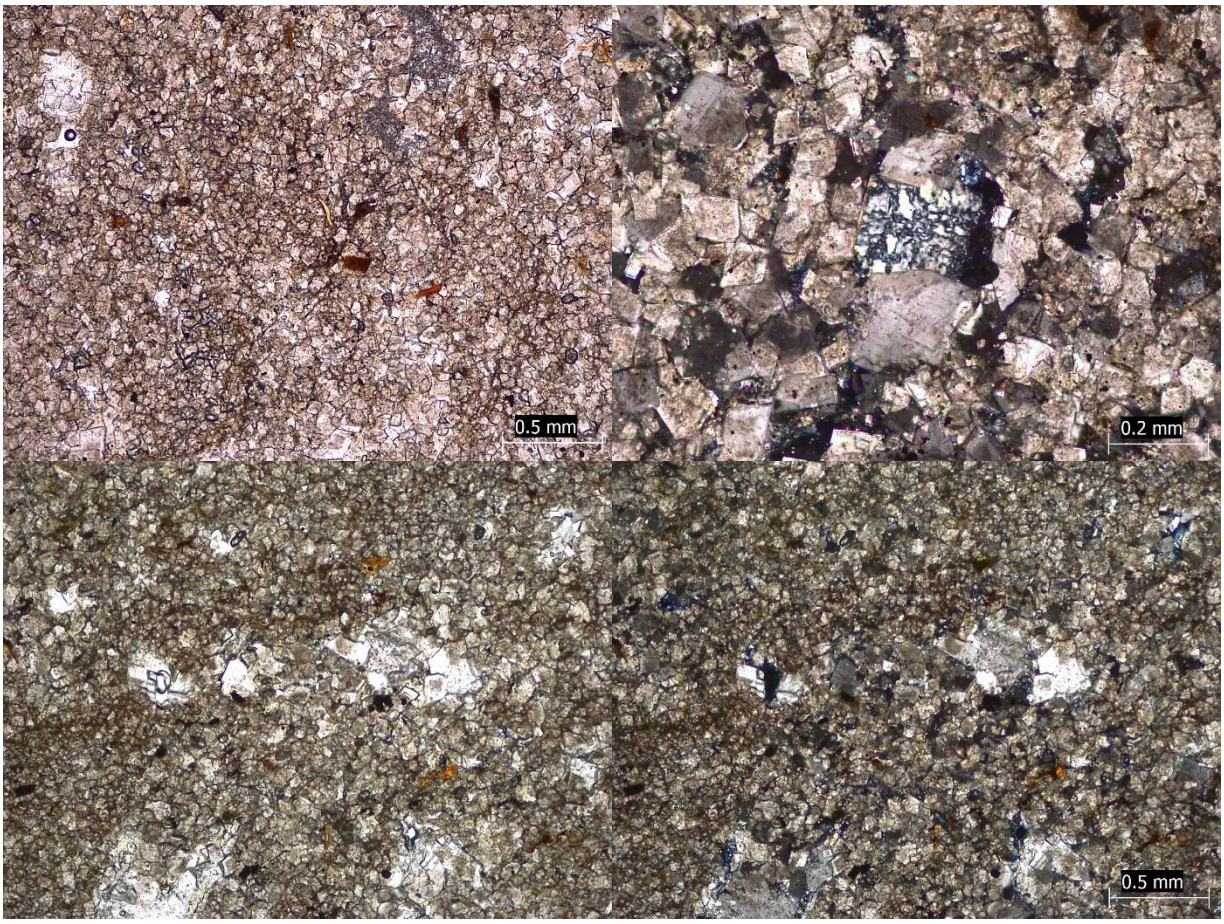

Figure B.66: Thin section photomicrographs of Muddy dolostone at 5864' from the Rich C #7 well. From left to right, the photomicrographs are in PPL, XPL, PPL, and XPL (same microscope location as previous image).

5865.5':

Lithofacies: Muddy Dolostone
Primary Constituents: Very finely-crystalline, laminated muddy dolomite, phosphate grains, rare silica in interparticle pores
Porosity Type: Intergranular
Porosity %: 1

Figure B.67: Cored section of Muddy dolostone in the Viola Ls. from Rich C #7 (left) and thin section plugs of this core piece taken at 5865.5'(right).

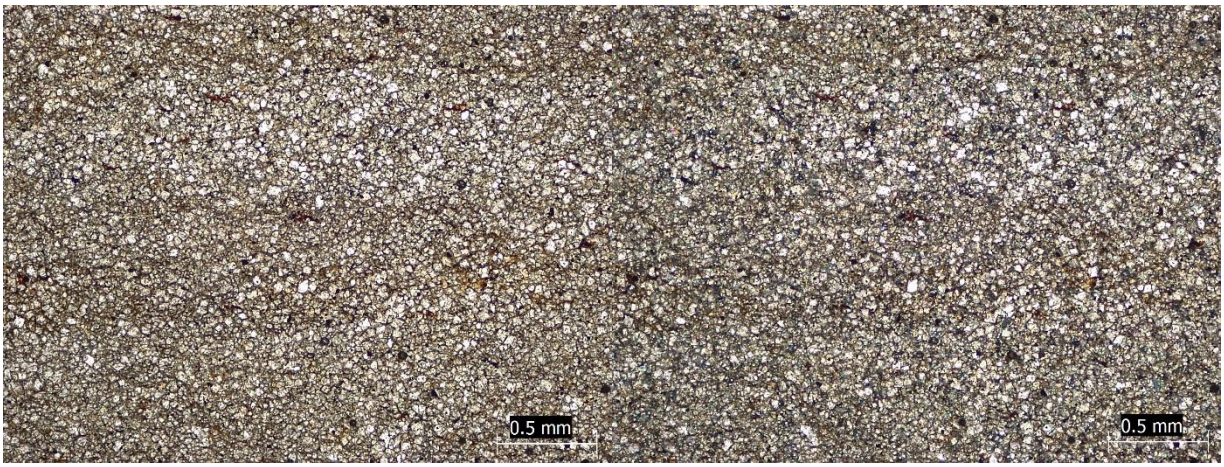

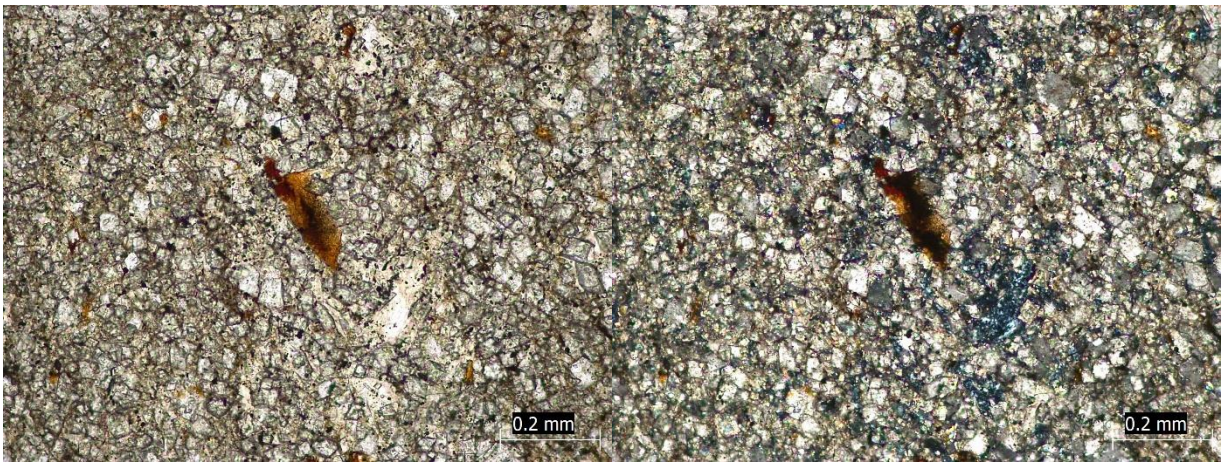

Figure B.68: Thin section photomicrographs of Muddy dolostone at 5865.5' from the Rich C #7 well. From left to right, the photomicrographs are in PPL, XPL (same microscope location as previous image), PPL, and XPL (same microscope location as previous image).

5866.66':

Lithofacies: Intraclastic Rudstone
Primary Constituents: Siliceous and Sponge spicule-rich chert intraclasts, rare dolomitic mud intraclasts, calcite between fragments
Porosity Type: Vuggy, interparticle
Porosity %: 1

Figure B.69: Cored section of Intraclastic rudstone in the Viola Ls. from Rich C #7 (left) and thin section plugs of this core piece taken at 5865.5'(right).

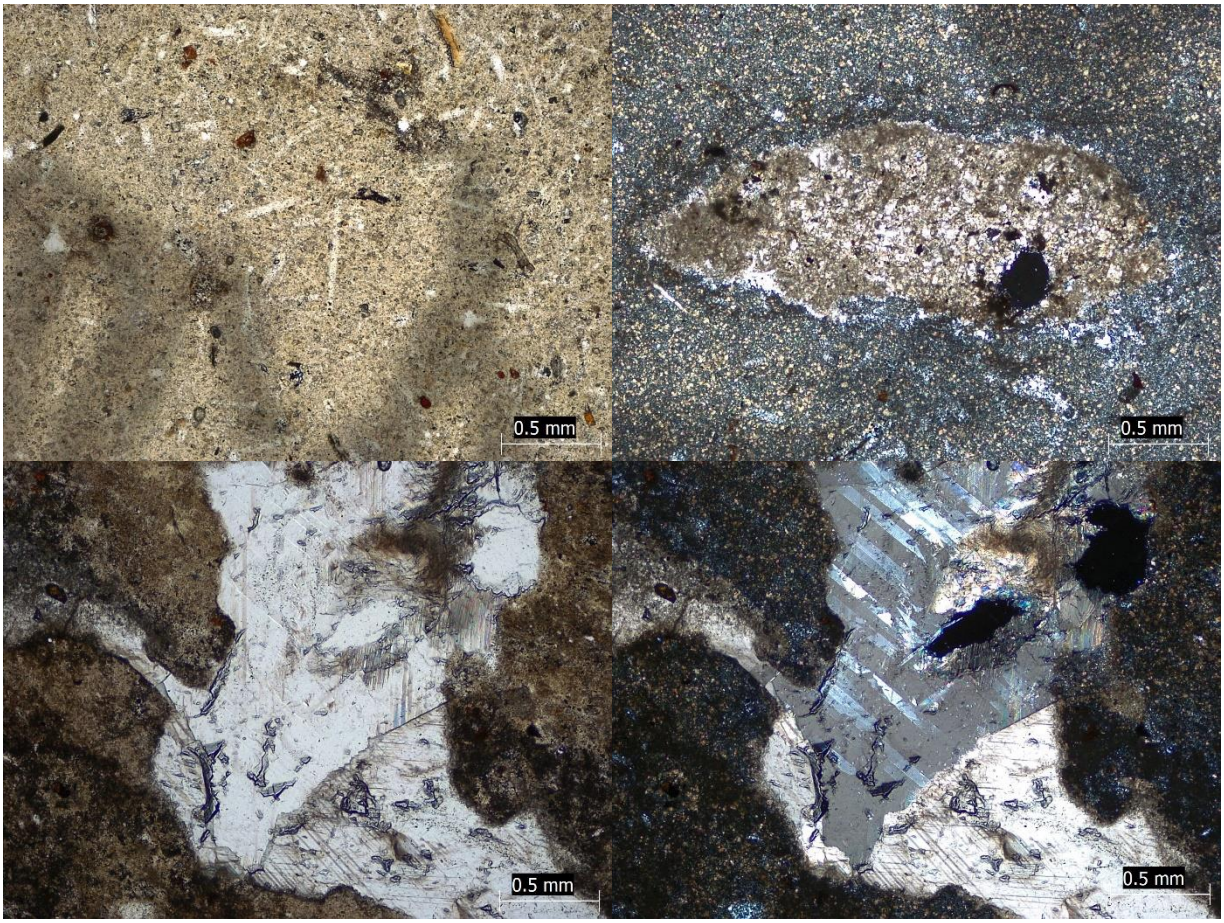

Figure B.70: Thin section photomicrographs of Intraclastic rudstone at 5866.66' from the Rich C #7 well. From left to right, the photomicrographs are in PPL, XPL, PPL, and XPL (same microscope location as previous image).